ASEAN
Journal of Scientific and Technological Reports
Online ISSN:2773-8752

Vol. 27 No. 1, January - February 2024

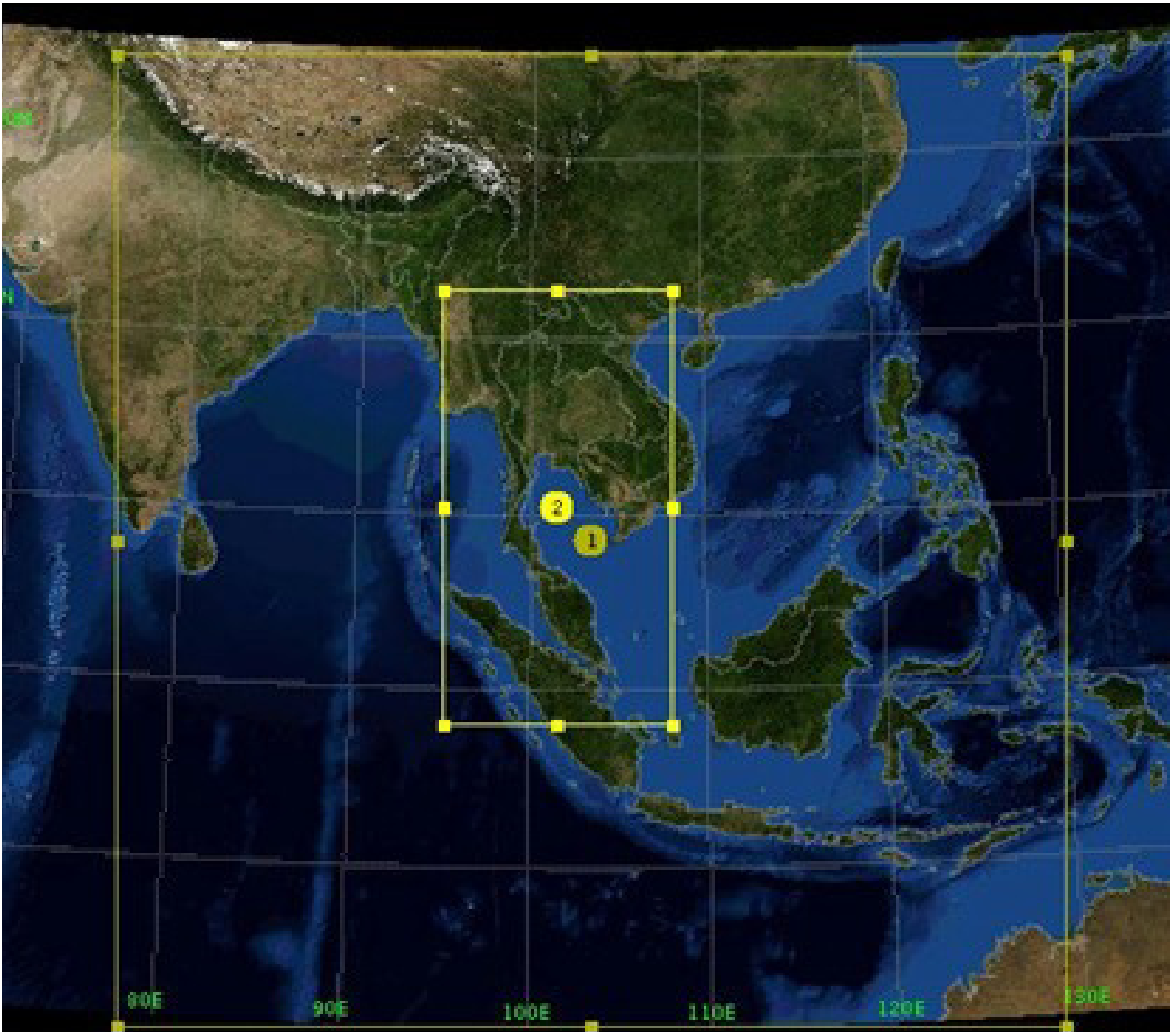

ISSN 2773-8752 (online)
https://ph02.tci-thaijo.org/index.php/tsujournal/issue/view/17076

ASEAN
Journal of Scientific and Technological Reports
Online ISSN:2773-8752

ASEAN Journal of Scientific and Technological Reports (AJSTR)

Contact Us Institute of Research and Innovation, Thaksin University
222 M. 2 Ban-Prao sub-district, Pa-Pra-Yom district, Phatthalung province, Thailand
Tel. 0 7460 9600 # 7242 , E-mail: aseanjstr@tsu.ac.th

List of Contents

ASEAN
Journal of Scientific and Technological Reports
Online ISSN:2773-8752

ASEAN
Journal of Scientific and Technological Reports
Online ISSN:2773-8752

Research article

Influence of Inhibitors from Microwave Pretreatment of Oil Palm Frond Pulping (OPFP) on Bioethanol Production

Tussanee Srimachai[1,2] and Kiattisak Rattanadilok Na Phuket[1, 2*]

[1] College of Innovation and Management, Songkhla Rajabhat University, Songkhla, Thailand, 90000; College of Innovation and Management, Songkhla Rajabhat University, Songkhla, Thailand, 90000; Tussnee.sr@skru.ac.th
[2] College of Innovation and Management, Songkhla Rajabhat University, Songkhla, Thailand, 90000; Community Innovation Learning and Transfer Center "Thung Yai Sarapee Model" Songkhla Rajabhat University, Satun, 91100, Thailand; Kiattisak.pa@skru.ac.th
* Correspondence: panpong1@hotmail.com

Citation:
Srimachai, T.; Rattanadilok Na Phuket, K. Influence of inhibitors from microwave pretreatment of oil palm frond pulping (OPFP) on bioethanol production. *ASEAN J. Sci. Tech. Report.* **2024**, *27*(1), 1-15. https://doi.org/10.55164/ajstr.v27i1.249524.

Article history:
Received: May 17, 2023
Revised: August 25, 2023
Accepted: August 31, 2023
Available online: December 28, 2023

Abstract: This research aims to analyze the influence of inhibitors from microwave pretreatment of oil palm frond pulping (OPFP) on the efficiency of bioethanol fermentation by *S.cerevisiae* in the simultaneous saccharification and fermentation (SSF) processes. OPFPs were achieved at different ages: 3-4, 4-7, 7-10, 10-20, and 20-25 years old. OPFP was pretreated with a microwave and sulfuric acid (MW/SF), microwave and hydrogen sulfide (MW/HP), and microwave and water (MW/W). The results showed that the main inhibitors formed during the pretreatment process of OPFP were acetic acid, furfural, 5-hydroxymethylfurfural (HMF), furfural, formic acid, and phenol. The pretreatment of OPFP with MW/W had the lowest concentrations of inhibitors compared to the other pretreatment methods. The highest bioethanol yields at all ages of OPFP were in the range of 0.41-0.42 g-bioethanol/g-glucose, corresponding to more than 80% fermentation efficiency. At these conditions, the concentrations of the acetic acid were 0.09-0.19 g/l, HMF =0, furfural =0, formic acid 0.05-0.28 g/l, and phenol 0.22-0.47 g/l. The MW/W was the suitable pretreatment of OPFP for bioethanol production due to the lowest to generate the inhibitor and high ethanol production yield.

Keywords: Bioethanol production; Oil palm frond pulping; Inhibitors; Microwave pretreatment

1. Introduction

It is generally known that fossil resources decrease continuously, and fossil-based fuels cause environmental problems. An alternative way to solve these issues is using alternative energy, such as ethanol. Ethanol is particularly important as a liquid biofuel, which can be mixed with gasoline with different ratios (e.g., E10, E20, E85). Ethanol has been produced from sugar or starch-based raw materials on the industrial scale. However, using starch and sugar for ethanol production has led to a "food vs. fuels" conflict due to the increasing global population [1]. Therefore, using lignocellulosic raw materials is attractive due to the large quantity, low prices, and no rapacious land for the plantation of humans.

Biomass resources are organic materials containing carbon, hydrogen, and oxygen atoms in their structure [2]. The process of biofuel production and consumption results in zero net CO_2 emissions because the amount of CO_2 released during combustion equals the amount of CO_2 absorbed by trees and plants through photosynthesis [2]. In Thailand, an oil palm frond (OPF) is a

sustainable agricultural waste obtained from the harvest of fresh fruit bunch. OPF contains many carbohydrates in the form of simple sugars, which could certainly be used as a raw material for producing bioethanol. However, using lignocellulosic materials to produce bioethanol requires a pretreatment process. The pretreatment step aims to open up the structure and decrease the crystal structure of lignocelluloses via the solubilization of hemicellulose and lignin [3]. On the other hand, access to the cellulose surface area increased for the following saccharification and fermentation processes. The pretreatment process is a key step in the biochemical conversion of lignocellulose to produce bioethanol [4]. During pretreatment, inhibitors are somewhat generated depending on the pretreatment method. Inhibitors in lignocellulosic hydrolysates consist of aliphatic acids (i.e., acetic, formic, and levulinic acid), furaldehydes (i.e., 5-hydroxymethylfurfural (HMF), and furfural), aromatic compounds (i.e.phenolics) and extractives; all of which affect bioethanol fermentation [5]. Jonsson and Matin [6] reported that the disadvantage of using sulfuric acid pretreatment was the formation of inhibitory by-products. Additionally, the advantage of hydrothermal pretreatment by controlling the pH around neutral values was the decreased amount of fermentation inhibitors [7]. Microwave pretreatment is a potential alternative to conventional heating due to its efficiency and ease of use. Energy consumption is reduced as treatment time is 10 times shorter than other heating systems [2]. Additionally, the combined method (microwave-assisted) can improve enzymatic hydrolysis and effectively remove lignin and hemicellulose, which is the maximum utilization of lignocellulosic components [8]. Biomass pretreatment provides a practical and clean process to increase surface area and improve access to enzyme binding sites. [9].

This research analyzes the influence of inhibitors formed during the different methods in the pretreatment of oil palm frond pulping (OPFP). These included microwave treatment with sulfuric acid (MW/SF), microwave treatment with hydrogen peroxide (MW/HP), and microwave treatment with water (MW/W). The research focuses on the effect of inhibitors (acetic acid, furfural, 5-hydroxymethylfurfural (HMF), formic acid, and phenol) on the efficiency of the bioethanol fermentation by *S.cerevisiae* in the following simultaneous saccharification and fermentation (SSF) processes.

2. Materials and Methods

2.1 Preparation of oil palm frond

The fresh oil palm frond (OPF) without leaves was cut to 1.0 m in length. The OPF was selected from oil palm trees having different ages: 3-4, 4-7, 7-10, 10-20, and 20-25 years old as shown in Figure 1A. The oil palm frond juice was removed from OPF by pressing OPF with a conventional sugarcane press machine. The remaining OPF solid, oil palm frond pulping (OPFP), was then cut into small pieces and dried at 103^{0}C for 24 hours to remove the moisture. After that, it was ground to 0.2 - 2 mm in size and put in a plastic bag at room temperature to protect the sample from moisture before use (Figure 1B). The initial chemical components in OPFP are shown in Table 1.

Figure 1. Raw material, (A) the fresh oil palm frond (OPF) without leaves used in the experiment, (B) Preparation of oil palm frond pulping (OPFP)

Table 1. The initial chemical components in OPFP

Oil palm age (years)	Components %(w/w)				
	Cellulose	**Hemicellulose**	**Holocellulose**	**Lignin**	**Ash**
3-4	38.84	34.68	73.52	24.74	1.74
4-7	39.82	33.58	73.40	25.56	1.04
7-10	40.44	31.06	71.50	26.94	1.56
10-20	42.38	28.68	71.06	27.52	1.42
20-25	43.50	26.34	69.84	29.44	1.24

2.2 Pretreatment of oil palm frond pulping

In this study, there are 3 types of pretreatments of OPFP:(i) using microwave and sulfuric acid (97%, Merck)(MW/SF),(ii)using microwave and hydrogen peroxide(37%, Merck) (MW/HP), and (iii) using microwave and water (MW/W). All pretreatments were carried out in 100 ml solutions (sulfuric acid, hydrogen peroxide, or aqueous solutions) in which 10% w/v of OPFP was loaded (fixed amount of OPFP at 10 g). Different sulfuric acid and hydrogen peroxide concentrations were studied at 0, 1, 2, 3, and 4 vol.%. The microwave was generated by the Samsung Home Model (frequency 2.45 GHz multimode cavity and largest 800 W) by putting the samples in the microwave and setting it up at 500 W for 15 minutes to study the effect of different pretreatment processes.

2.3 Enzyme hydrolysis and bioethanol production

The pretreated OPFP was forwarded to the hydrolysis and bioethanol production by simultaneous saccharification and fermentation (SSF). Bioethanol production from OPFP cellulose by SSF was tested in a batch mode. The enzymatic hydrolysis was done in 250 ml volumetric flasks using 10% (w/v) of OPFP. 5 ml of 5 M citrate buffer solution (pH 4.8) and 85 ml of distilled water were added to the flasks. Afterward, the flasks were sterilized in an autoclave (Model SA 300 VL Brand sturdy) at 121 ^{0}C for 15 min. The cellulosic enzyme used in this study was Cellic^R CTec2 (Cellulase + β-glucosidase). The enzymatic loading was 3% w/w (g-enzyme/g-cellulose). The mixtures were incubated at 55 ^{0}C with shaking (Shaking Incubator Model BJPX Series)at 150 rpm for 96 hours. Then, 10% (v/v) of *S. cerevisiae* and 1% (v/v) yeast extract were added. Finally, the mixtures were incubated at 37 ^{0}C with shaking at 150 rpm for 24 hours. Samples were collected at 0, 24, 48, 72, and 96 hours to determine the amounts of reducing sugar and bioethanol. Bioethanol yield and fermentation efficiency (%) were calculated using Eq. (1) and (2), respectively [10].

$$\text{Ethanol yield } (\text{g}-\text{ethanol}/\text{g}-\text{glucose}) = \frac{\text{Maximum ethanol concentration}\,(\text{g}/\text{l})}{\text{Utilized glucose } (\text{g}/\text{l})} \quad (1)$$

$$\text{Fermentation efficiency } (\%) = \frac{\text{Actual ethanol yield } (\text{g}/\text{l})}{\text{Theoretical ethanol yield}\,(\text{g}/\text{l})} x100 \quad (2)$$

2.4 Analytical methods

The total sugars were analyzed by high-performance liquid chromatography (HPLC) with a refractive index detector at 50 ^{0}C. 5.0 µl of samples were injected into a column (SH1011, 8.0x300 nm, Shodex) with 0.04 N H_2SO_4 as the mobile phase (flow rate 0.8 ml/min). The running time of the samples was 20 min. The dichromate reagent method determined the bioethanol concentration [11]. Formic acid, acetic acid, HMF, and furfural were determined by HPLC using a Bio-Rad HOX-87P ion-exclusion column, a Waters 2414 refractive index detector, and 0.01 N H_2SO_4 as the mobile phase at a flow rate of 0.6 ml/min and 60 ^{0}C. The phenolic compounds in samples were determined by the Folin-Cio-Cateu method [12].

3. Results and Discussion

3.1 Effect of microwave-hydrogen peroxide pretreatment (MW/HP) on the formation of inhibitors

The effect of microwave-hydrogen peroxide (MW/HP) pretreatment of OPFP obtained from different oil palm ages (3-4, 4-7, 7-10, 10-20, and 20-25 years) on the formation of inhibitors in OPFP hydrolysates after 96 hr of enzyme hydrolysis is shown in Figure 2. Compared with microwave-water (MW/W) pretreatment, the pretreatment of OPFP with MW/HP promoted the formation of inhibitors. Increasing the concentration of HP combined with microwave resulted in the increased concentrations of inhibitors found in hydrolysate at all oil palm ages. The inhibitors found with MW/HP were formic acid, acetic acid, and phenol. All of these compounds inevitably occurred even with water pretreatment. Matin and Jonsson [15] reported that the main inhibitors in lignocellulosic hydrolysates were formic acid, acetic acid, 5-hydroxymethylfurfural (HMF), furfural and phenol, which could be produced in different concentrations depending on the pretreatment methods. Indeed, the concentration of the inhibitors significantly affected enzyme digestion and the fermentation process, which will be discussed later. Additionally, Table 2 shows the concentration of inhibitors found in this study with other experiments [13].

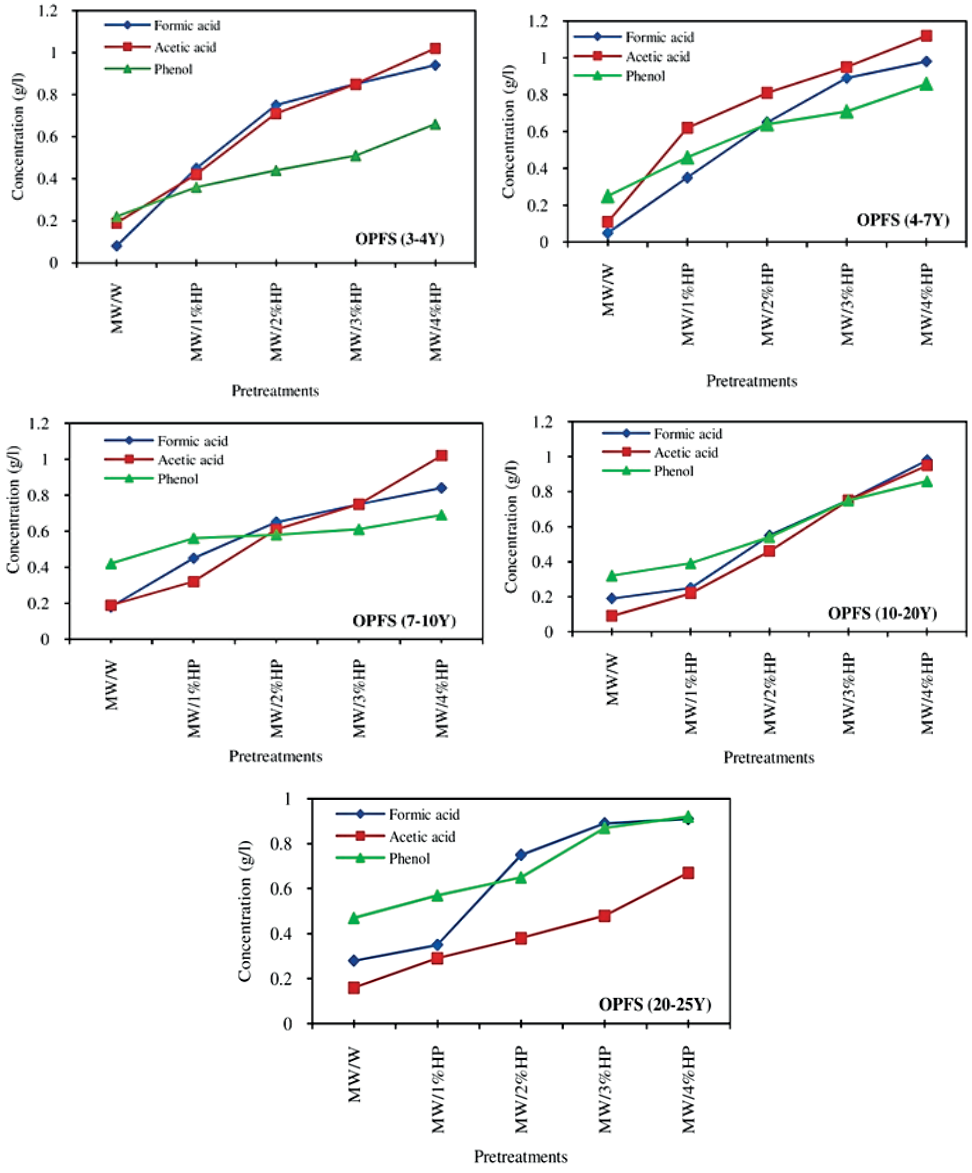

Figure 2. Inhibitors concentrations in hydrolysates of OPFP aged 3-4, 4-7, 7-10, 10-20, and 20-25 years using the different OPFP pretreatment methods with MW/HP.

Table 2. Comparison inhibitors concentration between all palm age of OPFP and other experiments

Sample	Pretreatment	Inhibitors concentration (g/l)					Reference
		Formic acid	Acetic acid	HMF	Furfural	Phenol	
OPFP (3-4 Y)	MW+W (15 min)	0.08	0.19	0.00	0.00	0.22	This study
	MW+4%HP (15 min)	0.94	1.02	0.00	0.00	0.66	This study
	MW+4%SF (15 min)	1.56	2.75	0.45	3.50	1.85	This study
OPFP (4-7 Y)	MW+W (15 min)	0.05	0.11	0.00	0.00	0.25	This study
	MW+4%HP (15 min)	0.98	1.12	0.00	0.00	0.86	This study
	MW+4%SF (15 min)	1.66	2.65	0.75	3.65	1.75	This study
OPFP (7-10Y)	MW+W (15 min)	0.18	0.19	0.00	0.00	0.42	This study
	MW+4%HP (15 min)	0.84	1.02	0.00	0.00	0.69	This study
	MW+4%SF (15 min)	1.66	2.45	0.65	3.35	1.75	This study
OPFP (10-20 Y)	MW+W (15 min)	0.19	0.09	0.00	0.00	0.32	This study
	MW+4%HP (15 min)	0.98	0.95	0.00	0.00	0.86	This study
	MW+4%SF (15 min)	1.66	2.65	0.85	3.25	1.67	This study
OPFP (20-25 Y)	MW+W (15 min)	0.28	0.19	0.00	0.00	0.47	This study
	MW+4%HP (15 min)	0.91	0.67	0.00	0.00	0.92	This study
	MW+4%SF (15 min)	1.75	2.85	0.75	3.65	1.77	This study
wheat straw	Thermal autoclaving (60 min)	0.07	1.02	0.00	0.00	0.50	[14]
	1.5%HCL autoclaving (60 min)	0.18	0.82	0.04	0.84	0.96	[14]
	1%NaOH autoclaving (60 min)	2.06	3.59	0.00	0.00	3.24	[14]
	5% H_2O_2 (60 min)	0.62	0.69	0.00	0.00	0.29	[14]
Eucalyptus residue	065%H_2SO_4 (15 min)	0.00	3.10	0.20	1.23	0.00	[15]

3.2 Effect of microwave-sulfuric acid pretreatment (MW/SF) on the formation of inhibitors

The effect of microwave-sulfuric acid (MW/SF) pretreatment of OPFP obtained from different oil palm ages (3-4, 4-7, 7-10, 10-20, and 20-25 years) on the formation of inhibitors in OPFP hydrolysates after 96 hr of enzyme hydrolysis is shown in Figure 3. Compared with microwave-water (MW/W) pretreatment, the pretreatment of OPFP with MW/SF promoted the formation of inhibitors. Increasing the concentration of SF combined with microwave resulted in the increased concentrations of inhibitors found in hydrolysate at all oil palm ages. The inhibitors found with MW/SF were formic acid, acetic acid, phenol, HMF, and furfural. Compared with MW/HP, sulfuric acid promoted more types of inhibitors, such as HMF and furfural. However, HMF and furfural have been reported to be less toxic to *S. cerevisiae* than phenol, acetic acid, and formic [6]. Behera et al. [16] similarly reported that the formation of inhibitors depended on the conditions used in the acid pretreatment process, such as the acid type and concentration.

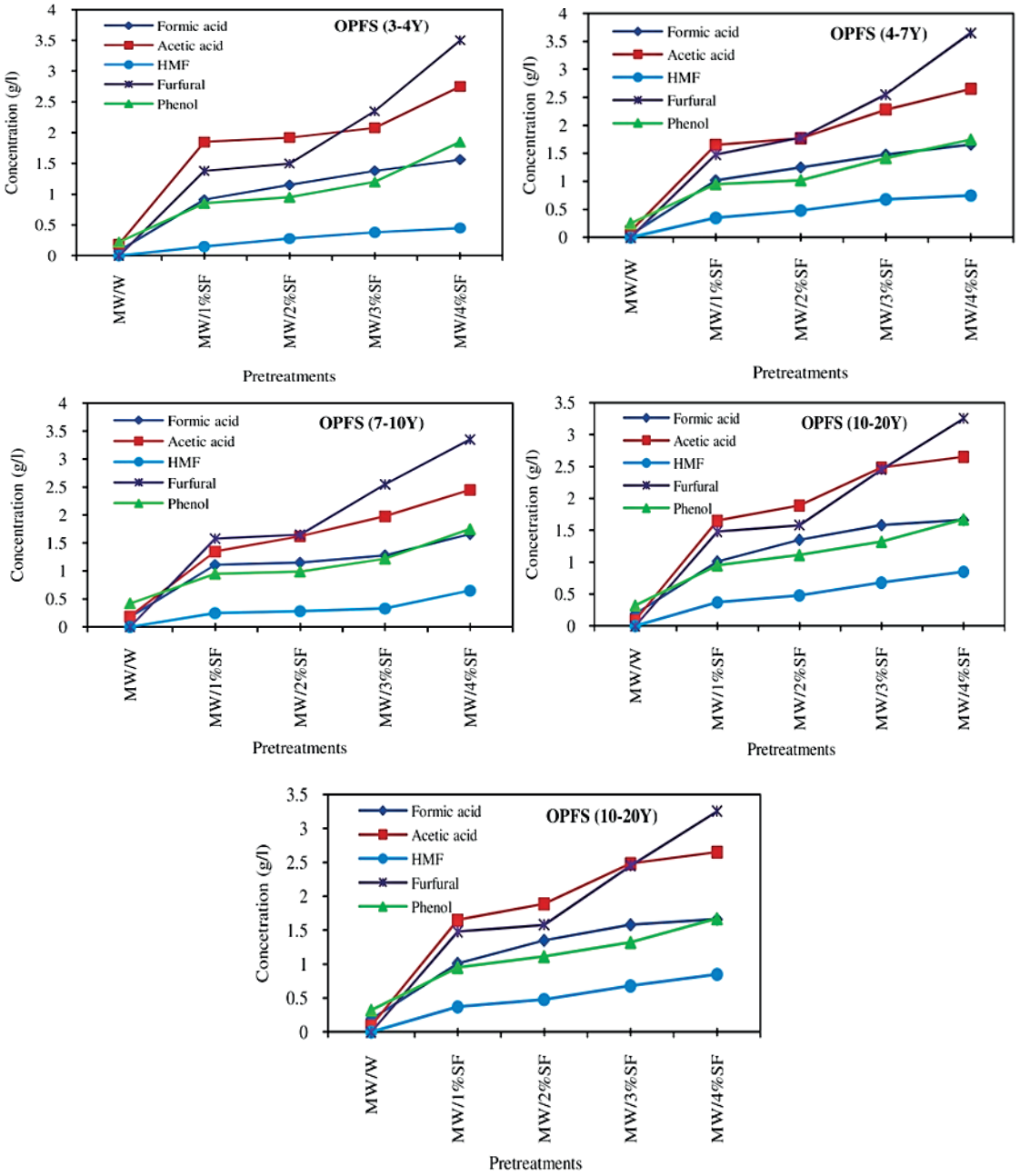

Figure 3. Inhibitors concentration in hydrolysates of OPFP aged 3-4, 4-7, 7-10, 10-20, and 20-25 years using the different OPFP pretreatment methods with MW/SF.

3.2.1 Acetic acid

All the pretreatment methods gave concentrations of acetic acid in the range of 0.09-2.85 g/l at various oil palm ages (Figures. 2 and 3). Therefore, it can be concluded that acetic acid is inevitably generated regardless of the type of pretreatment methods and the age of the oil palm. Compared to the other pretreatment methods, the pretreated OPFP with MW/W generated the lowest concentrations of acetic acid in the range of 0.09-0.19 g/l. The concentrations of acetic acid after the pretreatment of OPFP with MW/HP and MW/SF were in the range of 0.32-1.12 g/l and 1.65-2.84 g/l, respectively. Sulfuric acid generated a greater amount of acetic acid than hydrogen peroxide. The pretreatment of OPFP with MW/SF at the same concentration produced a more severe reaction than MW/HP, which was affected by a higher reaction temperature, resulting in the generation of acetic acid inhibitors than the pretreatment by MW/HP. The nature and concentration of inhibitors depend highly on the amount of solids in the reactor, pretreatment

conditions such as time, pH, temperature, and the concentrations of chemicals and raw materials used [17]. It has been reported that the cellular growth of yeast and ethanol production was inhibited completely when the concentration of acetic acid was about 3.5 g/l [5]. Therefore, the pretreatment of OPFP with MW/W, MW/HP, and MW/SF (concentrations of HP and SF not more than 4%) in this study can be applied to practice.

3.2.2 Furfural

Furfural was formed only by the pretreatment of OPFP with MW/SF. During the thermochemical pretreatment, inhibitors such as furfural and HMF are produced by dehydration of the pentose and hexose(Palmqvist, E., Hahn-Hagerdal, 2000)[17]. The concentrations of furfural were found in the range of 1.38-3.65 g/l for oil palm ages 3-4, 4-7, 7-10, 10-20, and 20-25 years (Figure. 3). The concentration of furfural increased with the acid concentration. This is consistent with the previous study [18]. Furfural harmed the ethanol production rate and such impact increased with concentration [16],[19]. Decreased ethanol production occurred at 2 g/l of furfural and the complete inhibition was reported at 4 g/l [20]. Therefore, furfural generated from MW/SF in this study has a significant effect on the production of bioethanol. Furfural inhibited the growth of *S. cerevisiae*, leading to a slower sugar consumption rate of yeast [21]. This, in turn, reduces the production of bioethanol. The pretreatment with MW/W and MW/HP did not generate furfural (Figure 2). Toquero and Bolado [13] similarly reported that no furfural was formed after the pretreatment of wheat straw with dilute alkali. The pretreatment of rice hulls with alkaline peroxide neither generated furfural [22].

3.2.3 5-hydroxymethylfurfural (HMF)

HMF was formed only with the pretreatment of OPFP with MW/SF; the concentrations of HMF were found in the range of 0.15-0.85 g/l at various oil palm ages (Figure 3). The pretreatment with MW/W and MW/HP generated no HMF (Fig. 2). The generation of HMF is believed to be associated with the formation of furfural when SF was used in the pretreatment. The pretreatment with dilute acids similarly generated furfural and HMF [23]. However, the concentrations of HMF were lower than those of furfural at all oil palm ages. This agrees with a previous study in which furfural was formed more easily than HMF in acid pretreatment at high temperatures [24]. HMF was formed from the degradation of glucose catalyzed by sulfuric acid [25]. The HMF concentrations that have an inhibiting effect on bioethanol production were reported to be higher than 1 g/l [26]. Since the HMF concentrations in this study were lower than 1 g/l, it is not severely toxic compared to furfural. Furfural has more potent toxicity than HMF [19]. However, HMF was reported to have a synergistic effect when combined with other inhibitors [16].

3.2.4 Formic acid

All the pretreatment methods gave concentrations of formic acid in the range of 0.05-1.75 g/l at various oil palm ages (Figures 2 and 3). The lowest concentrations of formic acid were in the 0.05-0.28 g/l range when OPFP was pretreated with MW/W. The concentrations of formic acid after pretreated OPFP with MW/HP and MW/SF were 0.25-0.98 g/l and 0.91-1.75 g/l, higher than the pretreatment with MW/W. Similar to the case of acetic acid, SF generated a greater amount of formic acid than HP. This is partly due to the formation of furfural and HMF. It has been reported that formic acid could occur from the degradation of furfural and HMF and had a more inhibitory effect than acetic acid [16], [27]. The complete inhibitory effect of formic acid on ethanol production was reported to occur at a concentration of 2 g/l [10]. However, if the formic acid concentration was less than 1 g/l, a higher bioethanol yield than fermentation without formic acid was observed [14]. This is consistent with our result. The pretreatment of OPFP with MW/SF, which gave concentrations of formic acid higher than 1 g/l, caused a decrease in the bioethanol yields compared to the pretreatment with MW/HP and MW/W.

3.2.5 Phenol

The phenol concentrations of all pretreatment methods were in the range of 0.22-1.77 g/l for oil palm ages 3-4, 4-7, 7-10, 10-20, and 20-25 years(Figures 2 and 3). The minimum phenol concentrations were in the range of 0.22-0.47 g/l after the pretreatment of OPFP with MW/W. After the pretreatment with MW/HP and MW/SF, the phenol concentrations were in the range of 0.36-0.92 g/l and 0.85-1.77 g/l, respectively, higher than the pretreatment with MW/W. Phenolic compounds were formed during the pretreatment due to the partial breakdown of lignin [16].

In conclusion, the concentrations of inhibitors after all pretreatment conditions in this study were in the range of 0.09-2.85 g/l of acetic acid, 1.38-3.65 g/l of furfural, 0.15-0.85 g/l of HMF, 0.05-1.75 g/l of formic

acid and 0.22-1.77 g/l of phenol. These ranges are consistent with previous research. In diluted acid pretreatment, using 0.65%H_2SO_4 (20 min) to treat the Eucalyptus residue generated 3.10 g/l of acetic acid, 1.23 g/l of furfural and 0.20 g/l of HMF [28]. Interestingly, the increased ages of OPF produced more inhibitors. Increasing the age of OPF increased the initial components in OPFP, which affected the synergism to have the inhibitors after the pretreatment with MW/HP and MW/SF. The pretreatment with MW/W created the lowest inhibitors when compared to the others. Similar to the liquid hot water (LHW) pretreatment, the advantage of the combined pretreatment with water and microwave was to avoid the formation of inhibitors [3], [29]. These inhibitors harm the hydrolytic process by reducing the adsorption of an enzyme [30].

3.3 Glucose concentration

The OPFP from different pretreatment methods was subjected to enzymatic hydrolysis and bioethanol production by simultaneous saccharification and fermentation (SSF), and the glucose concentrations were measured after 96 hours of enzymatic hydrolysis. The results are shown in Figure 4. It was found that OPFP from the pretreatment with MW/HP (4%)gave the highest glucose concentrations, which were 13.35, 19.61, 21.73, 25.07, and 28.67 g/l for oil palm aged 3-4, 4-7, 7-10, 10-20 and 20-25 years, respectively. Regardless of the age of the oil palm, the glucose concentration was enhanced with the increased concentration of hydrogen peroxide used in the pretreatment. The pretreatment with HP gave higher concentrations of glucose than the pretreatments with MW/W, which were 11.10, 15.10, 16.75, 19.56, and 22.30 g/l for oil palm aged 3-4, 4-7, 7-10, 10-20 and 20-25 years, respectively.

For OPFP with MW/SF pretreatment, the highest glucose concentrations were found with 4% SF that was 11.91, 18.27, 19.07, 23.46, and 24.76 g/l for oil palm aged 3-4, 4-7, 7-10, 10-20 and 20-25 years, respectively. Increasing the sulfuric acid concentration from 1-4% for the combined microwave and chemical pretreatment process positively affected the glucose concentration. The pretreatment with SF gave lower glucose concentrations than with HP at the same concentrations as the pretreating agent. This is because the lignin that inhibited the enzymatic hydrolysis was removed with acid pretreatment but to a lesser extent than the alkali treatment [31]. When the lignocellulose structure is destroyed with the pretreatment process, the enzyme will work more effectively. Using hydrogen peroxide in the pretreatment was found to have more effect on the enzymatic digestibility than using sulfuric acid in the pretreatment [29]. Moreover, the pretreatment with MW/SF at some concentrations was better than that with water in terms of glucose concentrations released from enzymatic hydrolysis.

All types of pretreatment methods gave higher glucose concentrations than without pretreatment. This is because the high energy radiation of microwave pretreatment leads to more change in cellulosic materials by increasing specific surface area and decreasing the degree of polymerization of cellulose [32]. Taherzadeh and Karimi [3] reported that the pretreated bagasse with microwave radiation resulted in a double glucose concentration compared to the untreated bagasse, corresponding to this study's result (Figures 4 and 5).

3.4 Bioethanol production from the SSF process

Production of bioethanol from cellulose hydrolysate by *S. cerevisiae* in the combination of pretreated OPFP with MW/W gave the most significant bioethanol concentrations: 4.55, 6.28, 6.95, 8.02, and 9.17 g/l at different oil palm ages of 3-4, 4-7, 7-10, 10-20 and 20-25 years, respectively (Figures 4 and 5). The bioethanol yields based on the amount of glucose are also shown. The pretreatment of OPFP with MW/W gave the highest bioethanol yields in the range of 0.41-0.42 g-bioethanol/g-glucose regardless of the ages of OPFP. Similarly, the studies of Kaparaju et al. [33] and Kadar et al. [34] reported that the ethanol yields from rice straw and industrial wastes using *S. Cerevisiae* in simultaneous saccharification and fermentation (SSF) were 0.41 and 0.31-0.36 g-bioethanol/g-glucose. The bioethanol yield obtained from sago pith waste using microwave hydrothermal hydrolysis was 0.47 g-bioethanol/g-glucose [10].

The pretreated OPFP with MW/W gave the highest bioethanol yield compared to MW/HP and MW/SF pretreatments. Although the MW/HP and MW/SF pretreatments showed higher glucose concentrations than the MW/W pretreatment in enzymatic hydrolysis, they generated greater amounts of inhibitors. These inhibitors significantly affected the efficiency of enzymatic hydrolysis, as seen from the higher glucose concentrations in the pretreatments with MW/HP and MW/SF. However, the inhibitors harmed the growth of yeast in fermentation. As a result, increasing the concentrations of hydrogen peroxide

and sulfuric acid decreased bioethanol yield. The combined pretreatment with MW/HP and MW/SF could increase the amount of cellulose. Still, it inevitably generated more toxicity (furfural, HMF, formic acid, acetic acid, phenol, etc.), negatively affecting the SSF's yeast activity. Inhibitory components such as acetic acid, furfural, HMF, formic acid, and phenolic compounds caused a lag phase in the cell growth of *S. cerevisiae*, resulting in a slow sugar consumption rate [35]. Therefore, the combined pretreatment of OPFP with MW/W is attractive. Furthermore, this type of pretreatment could save the cost of chemicals.

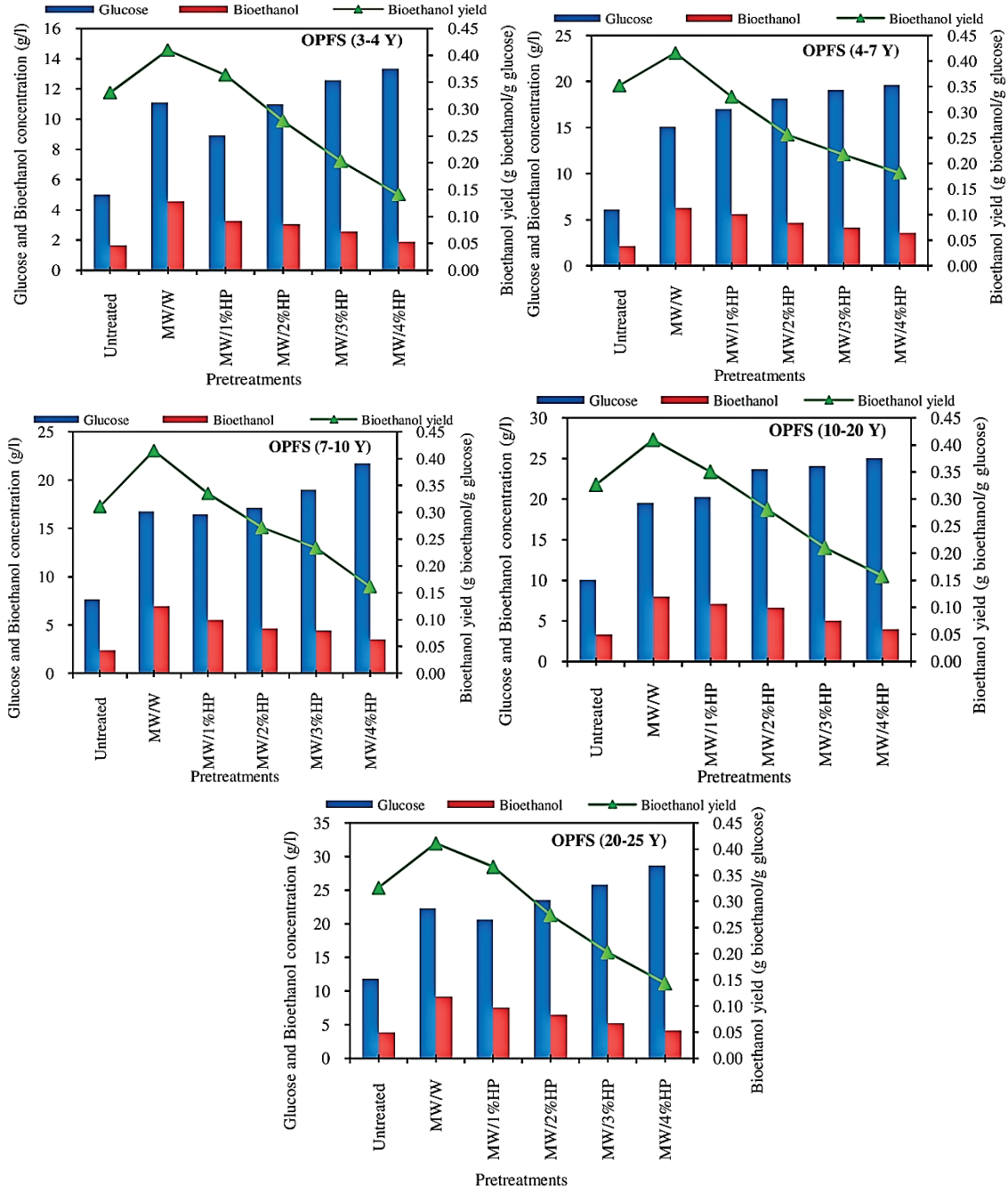

Figure 4. Glucose, bioethanol concentration, and bioethanol yield in SSF process of OPFP at oil palm aged 3-4, 4-7, 7-10, 10-20, and 20-25 years using the different OPFP pretreatment methods with MW/HP.

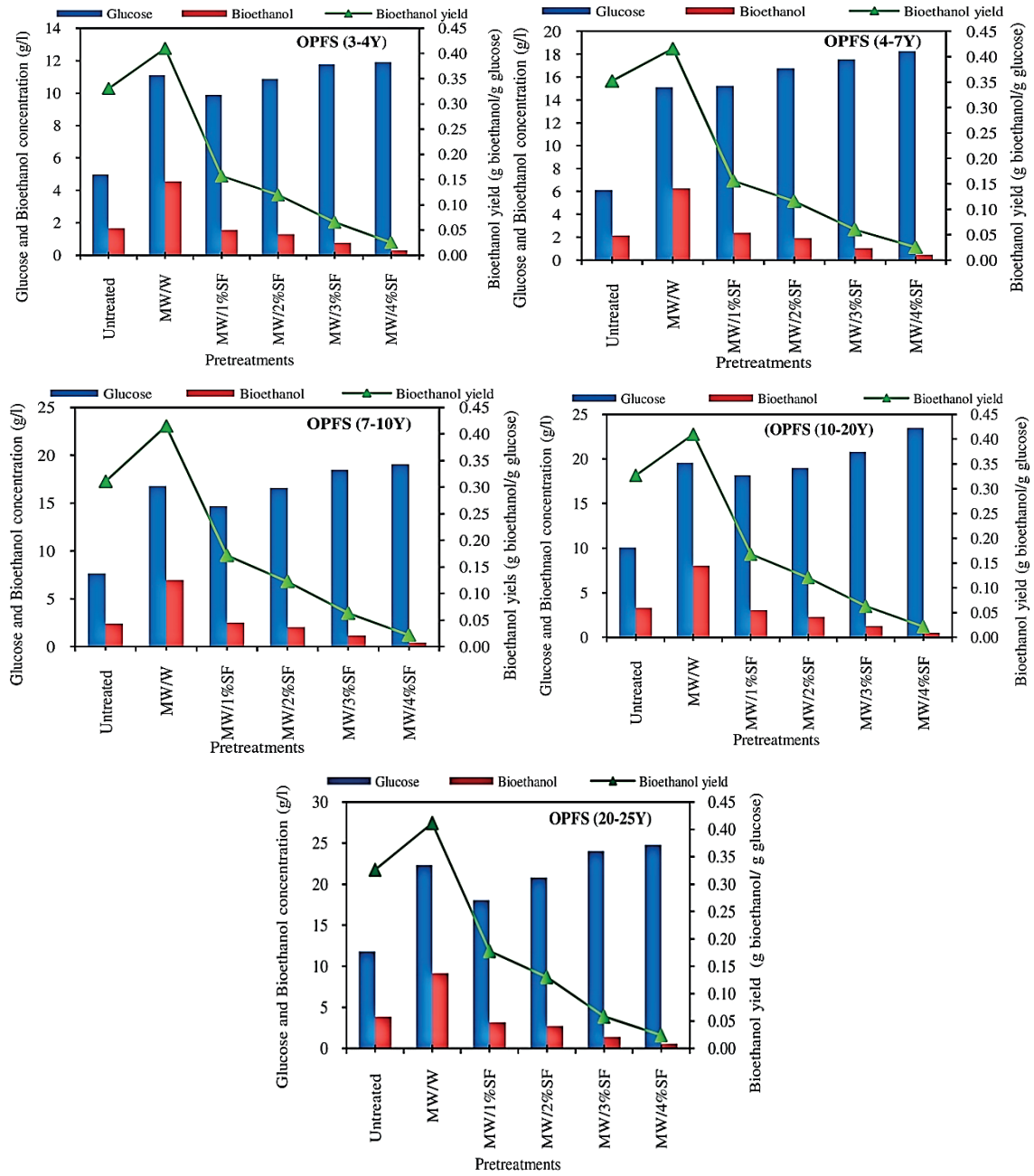

Figure 5. Glucose, bioethanol concentration, and bioethanol yield in the SSF process of OPFP aged 3-4, 4-7, 7-10, 10-20, and 20-25 years using the different OPFP pretreatment methods with MW/SF.

Comparisons between the concentrations of bioethanol from the experiment with the theoretical values were made and shown in Figures 6 and 7. The fermentation efficiency (%) is also included. The results showed that combining the pretreated OPFP with MW/W gave the highest efficiencies, about 82% of the theoretical bioethanol yield (0.51g-bioethanol/g-glucose), regardless of the ages of OPFP. Jung et al. [21] reported that the combined pretreatment with 1% (w/v) sulfuric acid and microwave at 1,200W and a heating time of 3 min resulted in 52.5% of theoretical ethanol yield after 72 hr of SSF.

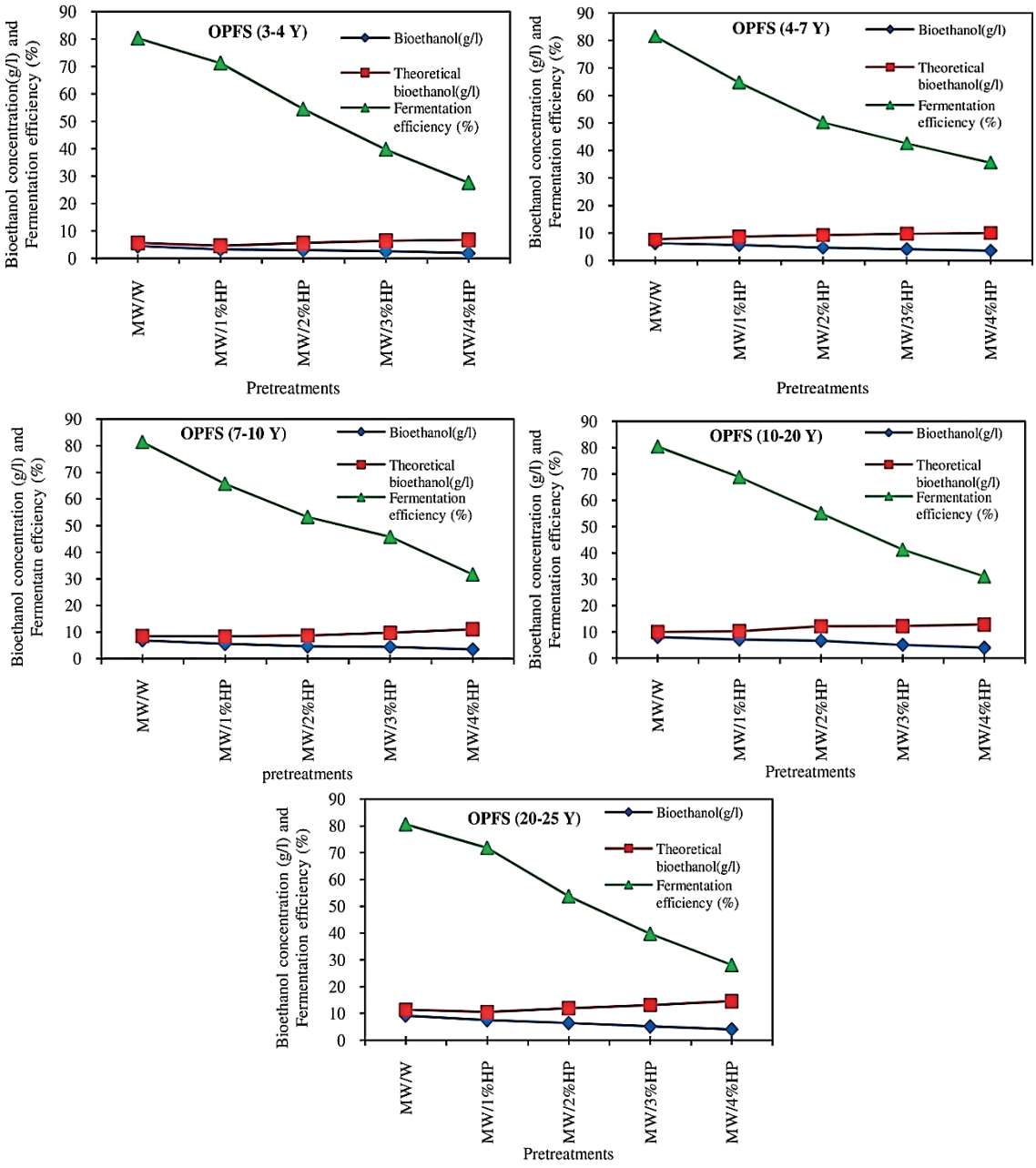

Figure 6. Comparison of experimental and theoretical concentrations of ethanol and fermentation efficiency (%) at different oil palm ages: 3-4, 4-7, 7-10, 10-20, and 20-25 years using the different OPFP pretreatment methods with MW/HP.

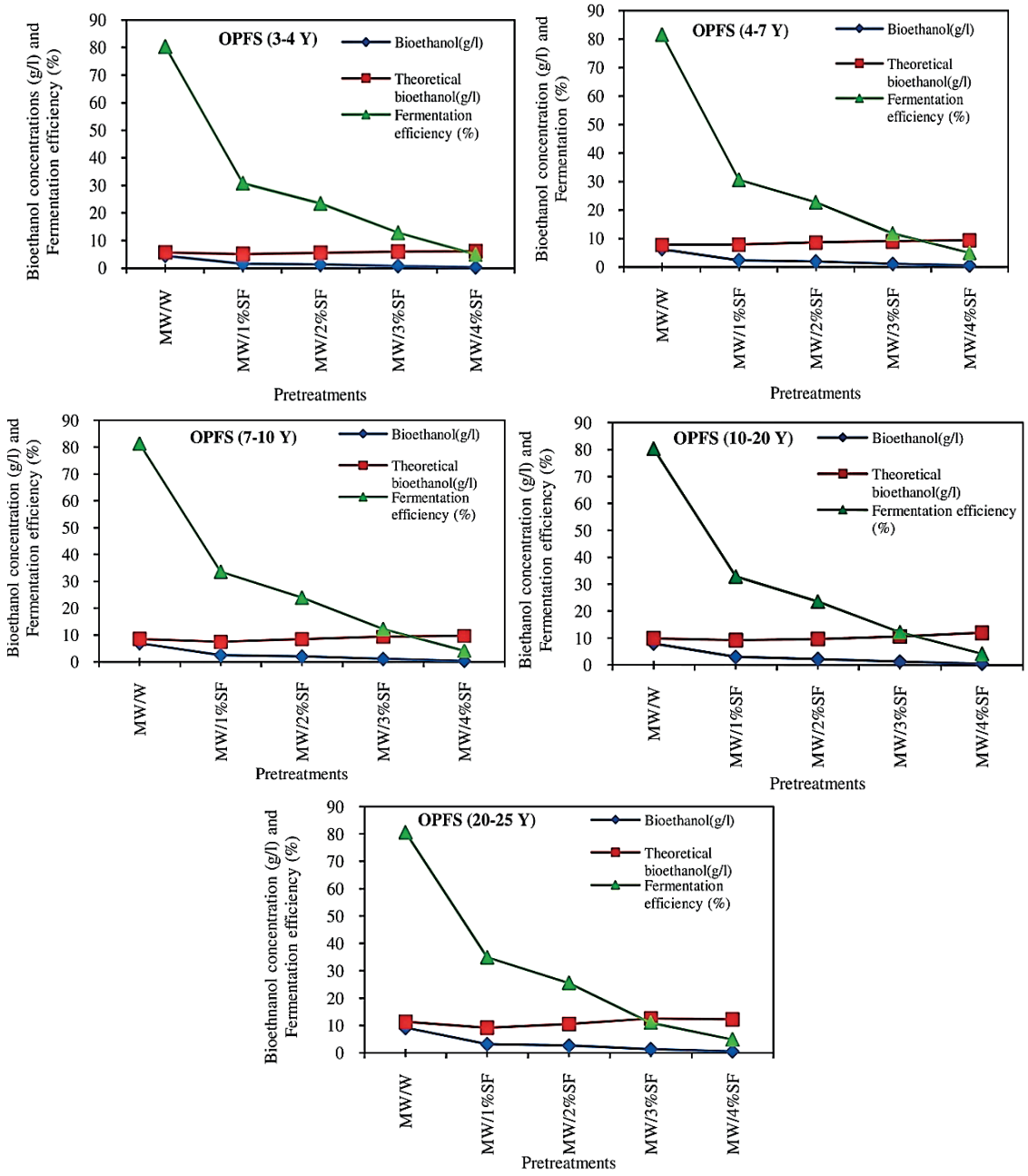

Figure 7. Comparison of experimental and theoretical concentrations of ethanol and fermentation efficiency (%) at different oil palm ages: 3-4, 4-7, 7-10, 10-20, and 20-25 years using the different OPFP pretreatment methods with MW/SF

4. Conclusions

OPFP pretreated with MW/W showed the highest bioethanol yield compared to MW/HP and MW/SF pretreatments. MW/HP and MW/SF pretreatments yielded higher glucose concentrations during enzymatic hydrolysis than MW/W pretreatments but produced large amounts of inhibitor. These inhibitors significantly affected the efficiency of enzymatic hydrolysis, as evidenced by the high glucose concentrations in the MW/HP and MW/SF pretreatments. However, the inhibitor adversely affected yeast growth during fermentation. As a result, bioethanol yield decreased with increasing hydrogen peroxide and sulfuric acid concentrations. Combined MW/HP and MW/SF pretreatments can increase the amount of cellulose but inevitably produce more toxic substances (furfural, HMF, formic acid, acetic acid, phenol, etc.) and reduce yeast activity in the SSF.

5. Acknowledgements

The authors would like to thank the Microbial Resource and Management (MRM) Research Unit staff, Faculty of Science, Thaksin University, Thailand.

Author Contributions: Conceptualization, K.R.; methodology, T.S., and K.R.; formal analysis, T.S.; investigation, K.R., and T.S.; writing—original draft preparation, K.R.; writing—review and editing, K.R.

Funding: The Higher Education Commission (HEC) for funding this research.

Conflicts of Interest: The authors declare no conflict of interest.

References

[1] Shafiel, M.; Kabir, M.M.; Zilouei, H.; Horvath, I.H.; Karimi, K. Techno-economical study of biogas production improved by steam explosion pretreatment. *Bioresource Technology*. **2013**, *148*, 53–60.
[2] Hoang, A.T.; Nižetić, S.; Ong, H.C. c, Mofijur, M.; Ahmed, S.F.; B. Ashok, B.; Bui, V.T.V.; Chau, Q.M. Insight into the recent advances of microwave pretreatment technologies for the conversion of lignocellulosic biomass into sustainable biofuel. *Chemosphere*. **2021**, *281*, 130878.
[3] Taherzadeh, M.; Karimi, K. Pretreatment of lignocellulosic wastes to improve ethanol and biogas production: a review. *International Journal of Molecular Sciences*. **2008**, *9*, 1621–1651.
[4] Yang, B.; Wyman, C.E. Pretreatment: the key to unlocking low-cost cellulosic ethanol Biofuels, Bioproducts and Biorefining. **2008**, *2*, 26–40.
[5] Bellido, C.; Bolado, S.; Coca, M.; Lucas, S.; Gonzalez-Benito, G.; Garcia-Cubero, M.T. Effect of inhibitors formed during wheat straw pretreatment on ethanol fermentation by Pichiastipitis. *Bioresource Technology*. **2011**, *102*, 10868–10874.
[6] Jönsson, L.J.; Matin, C. Pretreatment of lignocellulose: Formation of inhibitory by-products and strategies for minimizing their effects. *Bioresource Technology*. **2016**, *199*, 103–112.
[7] Hu, F.; Ragauskas, A. Pretreatment and lignocellulosic chemistry. *BioEnergy Research*. **2012**, *5*, 1043–1066.
[8] Rezania, S.; Din, M.F.M.; Mohamad, S.E.; Sohaili, J.; Taib, S.M.; Yusof, M.B.M.; Kamyab, H.; Darajeh, N., Amimul, A. Review on pretreatment methods and ethanol production from cellulosic water hyacinth. *Bioresources*. **2017**, *12*(1), 2108–2124.
[9] Karthikeyan, O.P.; Trably, E.; Mehariya, S.; Bernet, N.; Wong, J.W.C.; Carrere, H. Pretreatment of food waste for methane and hydrogen recovery: A review. *Bioresource Technology*. **2018**, *249*, 1025–1039.
[10] Thangavelu, S.K.; Ahmed, A.S.; Ani, F.N. Bioethanol production from sago pith waste using microwave hydrothermal hydrolysis accelerated by carbon dioxide. *Applied Energy*. **2014**, *128*, 277–283.
[11] William, M.B.; Reese, D. Colorimetric determination of ethyl alcohol. *Analytical Chemistry*. 1950, *22*, 1556.
[12] Singleton, V.L.; Orthofer, R.; Lamuela-Raventors, R.M. Analysis of total phenols and other oxidation substrates and antioxidants by means of Folin-Ciocalteu reagent. *Methods in Enzymology*. **1990**, *299*, 152–158.
[13] Toquero, C.; Bolado, S. Effect of four pretreatments on enzymatic hydrolysis and ethanol fermentation of wheat straw, Influence of inhibitors and washing. *Bioresource Technology*. **2014**, *157*, 68–76.
[14] Larsson, S.; Palmqvist, E.; Hahn-Hägerdal, B.; Tengborg, C.; Stenberg, K.; Zacchi, G.; Nilvebrant, N.O.; The generation of fermentation inhibitors during dilute acid hydrolysis of softwood. *Enzyme and Microbial*. **1999**, *24*, 151–159.
[15] Martin, C.; Jonsson, L.J. Comparison of the resistance of industrial and laboratory strains of Saccharomyces and Zygosaccharomyces to lignocelluloses derived fermentation inhibitors. *Enzyme and Microbial Technology*. **2003**, *32*, 386–395.
[16] Behera, S.; Arora, R.; Nandhagopal, N.; Kumar, S. Importance of chemical pretreatment for bioconversion of lignocellulosic biomass. *Renewable and Sustainable Energy Reviews*. **2014**, *36*, 91–106.
[17] Palmqvist, E.; Hahn-Hagerdal, B. Fermentation of lignocellulosic hydrolysates I: inhibition and detoxification, Bioresour. *Technol*. **2000**, *74*(1), 17–24.
[18] Talebnia, F. Optimization study of citrus wastes saccharification by dilute acid hydrolysis. *BioResources*. **2008**, *3*(1), 108–122.
[19] Guo, G.L.; Chen, W.H.; Chen, W.H.; Men, L.C.; Hwang, W.S. Characterization of dilute acid pretreatment of silver grass for ethanol production. *Bioresource Technology*. **2008**, *99*, 6046–6053.

[20] Diaz, M.J.; Ruiz, E.; Romero, I.; Cara, C.; Moya, M.; Castro, E. Inhibition of Pichiastipitis fermentation of hydrolysates from olive tree cuttings. *World Journal of Microbiology and Biotechnology*. **2009**, *25*, 891–899.
[21] Klinke, H.B.; Thomsen, A.B.; Ahring, B.K. Inhibition of ethanol-producing yeast and bacteria by degradation products produced during pre-treatment of biomass. *Applied Microbiology and Biotechnology*. **2004**, 66(1), 10–26.
[22] Diaz, A.; Le Toulle, J.; Blandino, A.; De Ory, I.; Caro, I. Pretreatment of rice hills with alkaline peroxide to enhance enzyme hydrolysis for ethanol production. *Chemical Engineering Transactions*. **2013**, *32*, 949–954.
[23] Agbor, V. B.; Cicek, N.; Sparling, R.; Berlin, A.; Levin, D.B. Biomass pretreatment: Fundamentals toward application. *Biotechnology Advances*. **2011**, *29*, 675–685.
[24] Jonsson, L.; Alriksson, B.; Nilvebrant, N.O. Bioconversion of lignocelluloses: inhibitors and detoxification. *Biotechnology for Biofuels*. **2013**, *6*(16), 1–10.
[25] Jung, Y.H.; Kim, I.J.; Kim, H.K.; Kim, K.H. Dilute acid pretreatment of lignocelluloses for whole slurry ethanol. *Bioresource Technology*. 2013, *132*, 109–114.
[26] Delgenes, J.P.; Moletta, R.; Navarro, J.M. Effects of lignocelluloses degradation products on ethanol fermentation of glucose and xylose by S. cerevisaie, Z. mobilis, Pichiastipitis and Candida shehatae. *Enzyme and Microbial Technology*. **1996**, *19*, 220.
[27] Zheng, Y.; Pan, Z.; Zhang, R. Overview of biomass pretreatment for cellulosic ethanol production. *International Journal of Agricultural and Biological Engineering*. **2009**, *2*, 51–68.
[28] Canettieri, E.V.; Rocha, G.J.M.; Carvalho, J.A.; Silva Jr.; J.B.A. Optimization of acid hydrolysis from the hemicellulosic fraction of Eucalyptus grandis residue using response surface methodology. *Bioresource Technology*. **2007**, 98, 422–8.
[29] Hendriks, A.T.W.M.; Zeeman, G. Pretreatments to enhance the digestibility of lignocellulosic biomass. *Bioresource Technology*. **2009**, *100*, 10–18.
[30] Kont, R. Strong cellulose inhibitors from the hydrothermal pretreatment of wheat straw. *Biotechnology for Biofuels*. **2013**, *6*, 135.
[31] Binod, P.; Satyanagalakshmi, K.; Sindhu, R.; Janu, K.U.; Sukumaran, R.K.; Pandey, A. Short duration microwave assisted pretreatment enhances the enzymatic saccharification and fermentable sugar yield from sugarcane bagasse. *Renewable Energy*. **2012**, *37*, 109–116.
[32] Sarkar, N.; Ghosh, S.K.; Bannerjee, S.; Aikat, K. Bioethanol production from agricultural wastes: An overview. *Journal of Renewable Energy*. **2012**, *37*, 19–27.
[33] Kaparaju, P.; Serrano, M.; Thomsen, A.B.; Kongjan, P.; Angelidaki, I. Bioethanol, biohydrogen and biogas production from wheat straw in a biorefinery concept. *Bioresource Technology*. **2009**, *100*, 2562–2568.
[34] Kadar, Z.S.; Szengyel, Z.S.; Réczey, K. Simultaneous saccharification and fermentation (SSF) of industrial wastes for the production of ethanol. *Industrial Crops and Products*. **2004**, *20*, 103–110.
[35] Tomas-Pejo, E.; Oliva, J.M.; Ballesteros, M.; Olsson, L. Comparison of SHF and SSF process from steam-exploded wheat straw for ethanol production by xylose-fermentation Saccharomyces cerevisiae strains. *Biotechnology and Bioengineering*. **2008**, *100*, 1122–1131.

ASEAN
Journal of Scientific and Technological Reports
Online ISSN:2773-8752

Research article

Silver and Silver Alloy on Carbon-supported Catalysts for Cathodes in Proton Exchange Membrane Fuel Cell and Direct Ethanol Fuel Cell

Siwat Thungprasert[1*], Jennarong Jaikaung[2], Theeraporn Promanan[3], Samroeng Narakaew[4] and Aphiruk Chaisenaand[5]

[1] Faculty of Science, Lampang Rajabhat University, Lampang, 52100, Thailand; siwattawis@g.lpru.ac.th
[2] Faculty of Science, Lampang Rajabhat University, Lampang, 52100, Thailand; cj_jennarong@hotmail.com
[3] Faculty of Science, Lampang Rajabhat University, Lampang, 52100, Thailand; theeraporn.lpru@gmail.com
[4] Faculty of Science, Lampang Rajabhat University, Lampang, 52100, Thailand; krachodnok@lpru.ac.th
[5] Faculty of Science, Lampang Rajabhat University, Lampang, 52100, Thailand; aphiruk@lpru.ac.th
* Correspondence: siwattawis@g.lpru.ac.th

Citation:
Thungprasert, S.; Jaikaung, J.; Promanan, T.; Narakaew, S.; Chaisenaand, A. Silver and Silver Alloy on Carbon-supported Cathode Catalysts in PEMFC and DEFC. *ASEAN J. Sci. Tech. Report.* **2024**, *27*(1), 15-23. https://doi.org/10.55164/ajstr.v27i1.250827.

Article history:
Received: September 5, 2023
Revised: October 20, 2023
Accepted: November, 11 2023
Available online: December 28, 2023

Abstract: This research was focused on the synthesis of 20 %wt silver, silver platinum alloy, and silver-copper alloy catalysts on carbon Vulcan XC-72 supporter for proton exchange membrane fuel cell (PEMFC) and direct ethanol fuel cell (DEFC) cathode using sodium borohydride method. Herein, the ratio of silver and platinum or copper sources was 1:1 by weight. The obtained catalysts were characterized by X-ray diffraction (XRD) and transmission electron microscopy (TEM), and the electro-activity performance was investigated on single-cell testing. XRD and TEM results confirmed the catalytic products of the Ag metal, AgPt alloy, and silver copper oxide ($Ag_xCu_{2-x}O$). Therefore, the particle size of the catalytic 20%wt AgPt/C was observed in the smallest size of about 4.71 ± 1.03 nm. The catalyst was selected for PEMFC and DEFC cathode testing. It showed high power density of 14.68 and 1.26 $W/cm^2.g_{(M)}$, respectively.

Keywords: Silver-based alloy; Cathode catalyst; Proton exchange membrane fuel cell, Direct ethanol fuel cell

1. Introduction

The proton exchange membrane fuel cell (PEMFC) and direct ethanol fuel cell (DEFC) are green technologies developed for continuous clean energy. Platinum supported on carbon catalyst was generally used as anode and cathode materials. Platinum will catalyze the hydrogen or ethanol dissociation into protons and electrons at the anode. After that, protons travel through the polymer electrolyte membrane from the anode to the cathode, where electrons travel along an external load circuit to the cathode side. At the cathode, platinum will catalyze the dissociation of oxygen. The electrons recombine with the protons and oxygen to form pure water as the reaction byproduct. Using a platinum catalyst at the cathode, the oxygen reduction reaction (ORR) was reported to be two electrons, producing hydrogen peroxide and destroying the electrode surface. Moreover, the platinum catalyst is an expensive reagent [1, 2]. Cathode catalysts such as platinum and non-platinum alloys have replaced pure platinum catalysts. This research focuses on silver and silver alloys because catalysts do not agglomerate after a long

operation. It has properties similar to platinum (same group of the periodic table and same face center cubic crystal structure) but at a much lower cost [3, 4]. Silver alloy catalysts such as CuAg/C [5], AgCu/C [6], and PtAg/C [7, 8, 9] have higher electro-activity than platinum catalysts. The catalyst for the cathode fuel cell should have nano-size particles with a good dispersion on the carbon supporter. To obtain a nano-sized product, many processes, such as heat treatment in hydrogen gas and nitrogen gas, are used [10, 11]. However, this method requires high energy and a complicated procedure. This research uses sodium borohydride ($NaBH_4$) to reduce metal ions in solvent to form metal or metal alloy because of its strong reductive ability [12, 13, 14]. Moreover, good dispersion of catalysts on carbon support will be obtained using modified surface carbon with hydrogen peroxide (H_2O_2) [15, 16]. In this research, the functional groups on the carbon surface were modified by being treated with hydrogen peroxide. After that, the Ag, AgCu, and AgPt catalyst supported on treated carbon was synthesized by the $NaBH_4$ method using $AgNO_3$, $Cu(NO_3)_2{\cdot}3H_2O$ and $H_2PtCl_6{\cdot}xH_2O$ as metal sources and ethylene glycol as a solvent

2. Materials and Methods

2.1 Carbon supporter treatment

H_2O_2 was used to modify the carbon surface. First, Carbon Vulcan XC-72 (Fuel Cell Store) was stirred in H_2SO_4 (97.5-98.5%, RCI Labscan). Then, washed with deionized water and stirred in KOH (85.0%, Ajax Finechem). Then, it was washed and stirred in H_2O_2 (50%, World Chemical Group) for 48 hours at room temperature. Finally, it was filtered, washed with deionized water, and dried in the oven. Fourier transform infrared spectroscopy (FTIR, FTIR-8900, Shimadzu) characterized functional groups of the carbon surface.

2.2 Synthesis of silver and silver-alloy

Twenty percent by weights of silver, silver-platinum alloy, and silver-copper alloy catalysts supported on carbon Vulcan XC-72 were prepared using $NaBH_4$ reducing agent. The ratio of silver to other metals was varied as 1:1 by weight. The treated carbon and metal sources ($AgNO_3$ 99.8%, RCI Labscan, $Cu(NO_3)_2{\cdot}3H_2O$ 99.5%, QRëC, and $H_2PtCl_6{\cdot}xH_2O$, Sigma-Aldrich) were added into ethylene glycol (99.5%, LoBa Chemie). The $NaBH_4$ (97.0%, LoBa Chemie) was added to the mix solutions. The reaction was stirred for 24 hours. Finally, the black product was filtered, washed with ethanol (95%, World Chemical Group), and dried in an oven to obtain the catalyst samples (20 %wt Ag/C, 20 %wt AgCu/C, and 20 %wt AgPt/C). The prepared catalysts were characterized by X-ray diffraction (XRD, RigaKu, Cu K_α (λ 1.54)), Scanning Electron Microscopy (SEM, JSM-5910LV, JEOL) equipped with Energy Dispersive Spectroscopy (EDS, The Microanalysis Suite Issue-16, INCA) and Transmission Electron Microscopy (TEM, JEM-2010, JEOL) techniques.

2.3 Single-cell testing

A single-cell testing station investigated the electrochemical performance of all catalysts acting as PEMFC and DEFC cathode (FCED, P200, APFCT). Catalyst-coated membrane (NR-212, Fuel Cell Store, as electrolyte for both fuel cells) was prepared using the commercial 20 %wt Pt/C (Fuel Cell Store, Pt/C_std) for the anode side and prepared catalyst for the cathode side. One membrane side was sprayed with an anode catalyst area of about 3 cm x 3 cm and nearly 0.4 mg/cm^2 for catalyst loading. Another membrane side was sprayed with a cathode catalyst in the same area. A single-cell testing technique was used to compare the electro-catalyst activity of PEMFC and DEFC. The PEMFC used hydrogen gas on the anode side and oxygen gas on the cathode side. The gas flow rate is 0.5 slpm for both sides. The single cell was operated at room temperature and 1 atm pressure. The DEFC used oxygen gas at the cathode side, and the gas flow rate was 0.5 slpm. At the anode side with 10% ethanol solution, the flow rate was 1.0 Lhr^{-1}, and the temperature was 60 °C. The single cell was operated at 60 °C and 1 atm pressure.

3. Results and Discussion

The modified functional groups on the treated carbon surface were compared with untreated carbon. They were characterized by FTIR, as shown in Figure 1. It can be seen that the untreated carbon's peaks at 3155.3 and 1602.9 cm^{-1} correspond to the vibration of -O-H and -C=C-, respectively. However, they were observed with low intensity. The treated carbon with hydrogen peroxide was detected in the bands at 3396.4, 1652.9, and 1558.4 cm^{-1}, corresponding to the vibration of –O-H, -C=O, and –C=C-, respectively. It also detected the bands at 1440-1395, 1320-1210, and 750-650 cm^{-1} corresponding to the vibration of -C-O, -O-H, and -O-H out of the plane, respectively, confirmed carboxylic group (-C(=O)-O-H). Those functional groups appeared due to hydrogen peroxide, which acted as a strong oxidizing agent [17] and can oxidize the carbon-carbon bond on the carbon surface to carboxylic group [18, 19]. This carboxylic group, a negatively charged functional group, induces the formation of metal alloy catalysts on carbon due to electrostatic interaction between a metal ion and carboxylic group. The catalyst on treated carbon surface with a good uniform distribution and smaller nanoscale than catalyst on untreated carbon because nucleation rate was greater than agglomeration rate of particle [20,21].

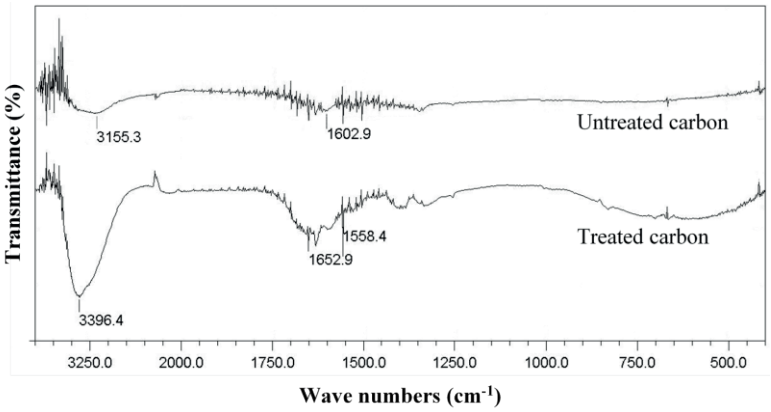

Figure 1. FTIR spectra of treated carbon and untreated carbon

XRD patterns of 20 %wt Ag/C, 20 %wt AgCu/C, and 20 %wt AgPt/C catalysts are shown in Figure 2. All catalysts show the board peak at 2θ ≈ 24° corresponding to the (002) plane of carbon. 20%Ag/C showed the peaks at 2θ = 38.06° (111), 44.21° (200), and 64.45° (220), which corresponded planes of cubic Ag metal with space group *Fm3m* (JCPDS No.00-004-0783). While XRD patterns of the catalytic products from synthetic 20 %wt AgCu/C were identified as $Ag_xCu_{2-x}O$ compound [22, 23], XRD patterns exhibited evidence of the diffraction peaks have shifted to lower 2θ values, the position of (111) plane was closer to silver copper (I) oxide than Ag metal due to copper (I) oxide with the larger hole radius than silver had replaced the silver position with the metals oxide can be oxidized by oxygen in air under $NaBH_4$ solution condition at the ambient temperature is represented in Table 1. The XRD pattern of the catalytic product from 20 %wt AgPt/C, the 2θ position of (111) plane of the sample, was compared with Ag and Pt metals, which were identified as AgPt alloy [8, 24, 25] as shown in Table 1. The characteristic diffraction peaks of AgPt/C catalysts have shifted to higher 2θ values. The position of the (111) plane was closer to Ag alloy than Ag metal because the size of the unit cell from Ag alloy was smaller than that of Ag metal. In addition, platinum had been replaced with a smaller atomic radius than silver at the silver position. After the metals were mixed to form an alloy, the acquired alloy phase provided the different unit cell parameters from the pure metals. In the case of the atomic distance, the distance between the same atomic types appeared further than the distance from the heteroatom by the effect of the atomic force. All XRD patterns are illustrated in Figure 2. The EDS technique confirmed the Ag, Cu, Pt, and O compositions of both silver compound and alloy, as listed in Table 2.

The EDS technique conducted the qualitative and quantitative analyses of elements for all catalysts, as shown in Table 2. The EDS spectra of all catalysts confirmed the presence of respective elements and the amount of carbon, oxygen, and all metals on carbon. The observed oxygen from this technique mostly came from metal oxide. The amount of the observed metals was less than the theoretical metals ratio because of the limitation of this technique and sampling was a small area to use as a representative for all catalysts.

Table 1. Peak positions of the (111) plane between standard and alloy samples

Sample catalysts	2θ for (111) plane
Ag (JCPDS No. 00-004-0783)	38.12
Pt (JCPDS No. 00-004-0802)	39.76
Cu_2O (JCPDS No. 00-005-0667)	36.42
AgPt	38.78
$Ag_xCu_{2-x}O$	37.46

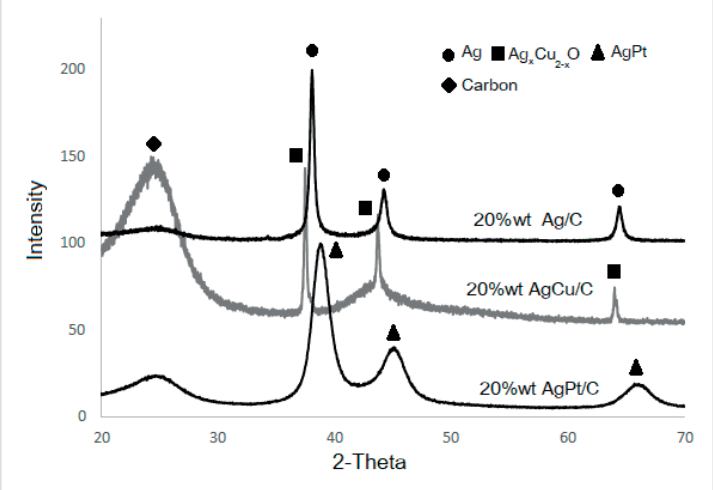

Figure 2. The XRD patterns of silver metal, silver platinum alloy, and silver copper (I) oxide on carbon-supported catalysts

Table 2. Weight percent of silver metal, silver platinum alloy, and silver copper (I) oxide on carbon-supported catalysts from EDS

Synthetic conditions	Element (Wt%)				
	Ag	Cu	Pt	C	O
20 %wt Ag/C	22.71	-	-	77.29	-
20 %wt AgCu/C	10.01	9.15	-	76.92	3.92
20 %wt AgPt/C	15.28	-	2.78	81.94	-

From TEM images of all catalysts shown in Figure 3, the particle sizes of catalysts were observed on the nanoscale with a good dispersion on the carbon surface. The average particle sizes (were used by ImageJ) from Ag/C, AgCu/C, and AgPt/C were 40.67±10.58, 21.99±7.20 and 4.71±1.03 nm, respectively. Figure 3 shows that the smallest particle is the AgPt/C catalyst. The catalyst with the smallest nanoscales will improve the fuel cell performance due to its high surface area [20]. The microstructure of all catalysts was characterized by TEM technique and the phases of products could be confirmed by the selected area electron diffraction (SAED) pattern. In Figure 3, the catalytic products from the synthetic conditions of 20 %wt Ag/C exhibit diffracted ring patterns

of (111), (200), (220), (311), and (222) planes of silver metal. By contrast, the catalytic products from the synthetic condition of 20 %wt AgCu/C exhibit diffracted ring patterns of (111), (200), (220), (311), and (222) planes of silver copper (I) oxide. Moreover, the catalytic products from the synthetic condition of 20 %wt AgPt/C exhibit diffracted ring patterns of (111), (200), (220), and (311) planes of silver platinum alloy. All the SAED results were related to the results from XRD and EDS techniques.

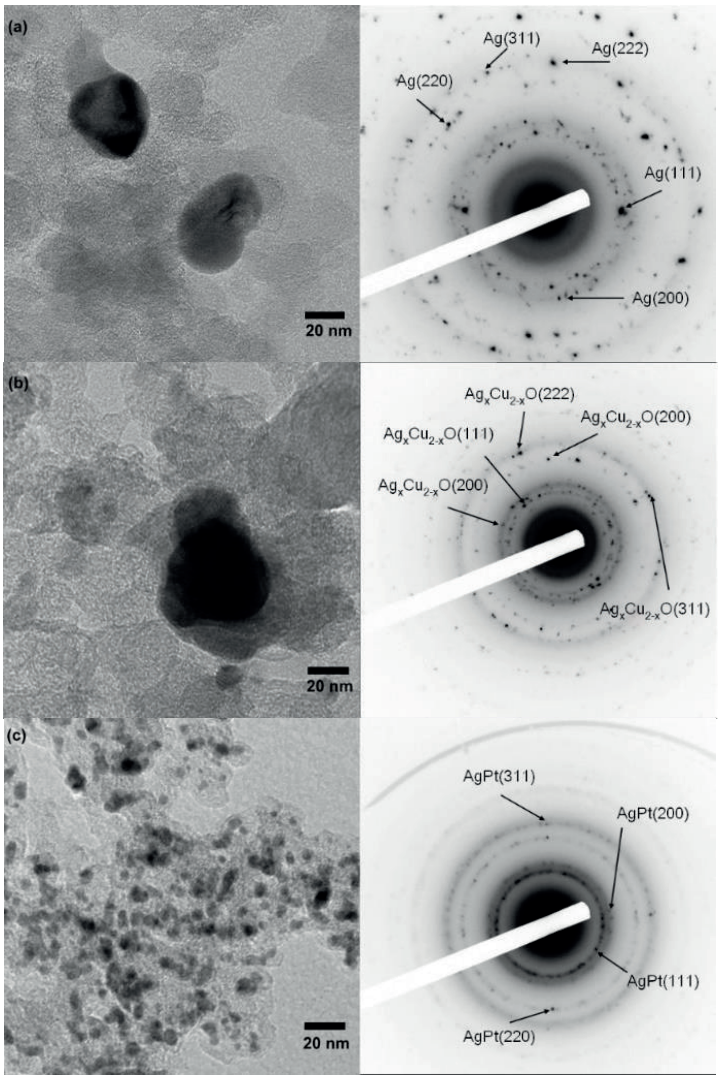

Figure 3. TEM and SADE images of 20 %wt Ag/C (a), 20 %wt AgCu/C (b), and 20 %wt AgPt/C (c) catalysts

Table 3. The power density of silver metal, silver platinum alloy, and silver copper (I) oxide on carbon-supported catalysts

Synthetic onditions	Catalysts at cathode	Particle size (nm)	Power density ($W/cm^2.g_{(M)}$)	
			PEMFC	DEFC
-	Pt/C_std	-	10.32	1.17
20 %wt Ag/C	Ag/C	40.67 ± 10.58	4.99	0.37
20 %wt AgCu/C	$Ag_xCu_{2-x}O$/C	21.99 ± 7.20	5.10	1.19
20 %wt AgPt/C	AgPt/C	4.71 ± 1.03	14.68	1.26

Single cells techniques for PEMFCs and DEFCs (in acidic type) were used to compare the electrocatalysts activity performance between standard and sample cells. The anode catalyst for both cells was commercial 20 %wt Pt/C (Pt/C_std). The cathode catalyst for the standard cell was commercial 20 %wt Pt/C, and sample cells were prepared catalyst (20 %wt Ag/C, 20 %wt AgCu/C, and 20 %wt AgPt/C). The PEMFC was operating at room temperature. The DEFC was operating at 60 °C because a higher temperature lowers the activation loss of the redox reactions, decreases the cell resistance, and enhances the reactant transport [26]. Figures 4(a) and 4(c) show the polarization curve between current density and voltage from single-cell testing of all catalysts for PEMFC and DEFC, respectively. It was found that the 20 %wt AgPt/C catalysts showed higher current density than other catalysts for both testing cells.

The performance curves between current density and power density from PEMFC and DEFC testing of all catalysts are shown in Figure 4b and 4d, respectively. In Table 3, the 20 %wt AgPt/C catalysts showed higher power density than others. The catalysts were 14.68 and 1.26 $W/cm^2.g_{(M)}$ (M as silver or silver alloy catalysts) from PEMFC and DEFC, respectively. The power density of PEMFC was higher than that of DEFC because, on the anode side, PEMFC used hydrogen gas, but DEFC used 10% ethanol solution. Hydrogen gas was faster to decompose with catalyst into positively charged protons and negatively charged electrons than ethanol solution [27,28]. The performance of 20 %wt AgPt/C catalysts was influenced by smaller particles than other catalysts, as confirmed by TEM images. The fine particle catalysts showed better performance because of many active sites on smaller particles compared to catalysts with large particle sizes [29]. In addition, 20 %wt AgPt/C catalysts were reportedly stable after long cell operation with less agglomeration and metals leaching [13]. Therefore, the ORR mechanism of silver platinum alloy formation can break the oxygen bond, leading to completed four-electron reduction without hydrogen-peroxide generation (Eq 1-3) [30,31].

$$AgM + O_2 + e^- \rightarrow AgM\text{-}O\text{-}O^- + H^+ + e^- \rightarrow AgM\text{-}O\text{-}OH^- \quad (1)$$

$$AgM\text{-}O\text{-}OH^- + H^+ + e^- \rightarrow AgM\text{-}O^- + H_2O \quad (2)$$

$$AgM\text{-}O^- + H^+ + e^- \rightarrow AgM\text{-}O\text{-}OH^- + H^+ \rightarrow AgM + H_2O \quad (3)$$

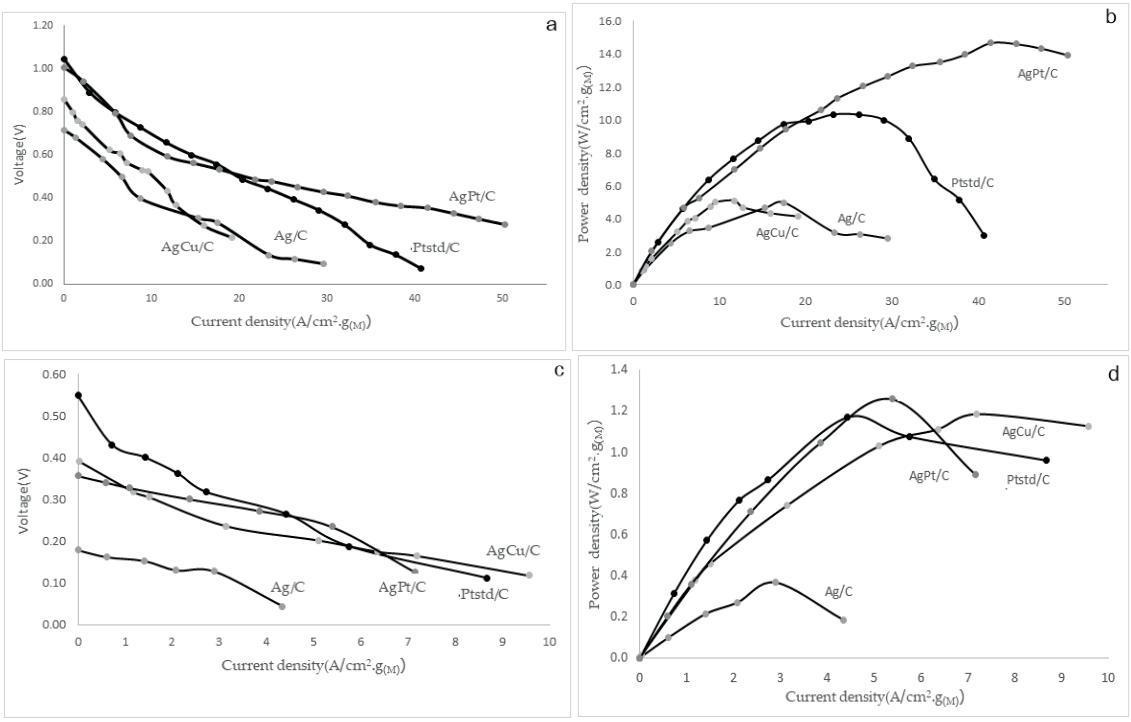

Figure 4. Polarization curves and performance of silver metal, silver platinum alloy, and silver copper (I) oxide on carbon-supported catalysts for PEMFC (a-b) and DEFC (c-d)

4. Conclusions

This research focused on synthesizing 20 %wt silver and silver alloy catalysts on carbon Vulcan XC-72 for PEMFC and DEFC cathode with $NaBH_4$ reduction methods. XRD, TEM, and SAED techniques confirmed the $Ag_xCu_{2-x}O$/C catalyst using equal silver and copper nitrate. Meanwhile, 20 %wt AgPt/C catalyst can easily synthesize due to the high reduction potential of Pt. The particle size of the silver platinum alloy catalyst was observed in a smaller size, around 4.71±1.03 nm. It was selected for the catalytic PEMFC and DEFC cathode testing and showed higher power density than other catalysts. Both testing cells were 14.68 and 1.26 $W/cm^2.g_{@M}$, respectively. This research concluded that 20 %wt AgPt/C catalysts exhibited the highest performance catalyst for PEMFC and DEFC.

5. Acknowledgements

This research was funded by the Center of Excellence for Innovation in Chemistry (PERCH-CIC) and the Department of Chemistry, Faculty of Science, Lampang Rajabhat University are gratefully acknowledged.

Author Contributions: Conceptualization, S.T.; methodology, S.T., J.J. and T.P.; formal analysis, S.T. and T.P; investigation, S.T, S.N.and A.C; writing—original draft preparation, S.T.; writing—review and editing, S.T.; All authors have read and agreed to the published version of the manuscript.

Funding: This research was supported by the Center of Excellence for Innovation in Chemistry (PERCH-CIC) and the Department of Chemistry, Faculty of Science, Lampang Rajabhat University

Conflicts of Interest: The authors declare no conflict of interest.

References

[1] Vielstic, W.; Lamm, A.; Gasteiger, H.A. *Handbook of Fuel Cell Fundamentals Technology and Application*. 2; Wiley: Chichester, **2003**; pp. 468-487.

[2] Mai, Y.l.; Xie, X.S.; Wang, Z.D.; Yan, C.F.; Liu, G.H. Effect of heat treatment temperature on the Pt_3Co binary metal catalysts for oxygen reduced reaction and DFT calculations. *J Fuel Chem Technol.* **2022**, *15*(1), 114-121.

[3] Subramanian, N.P.; Li, X.; Nallathambi, V.; Kumaraguru, S.P.; Colon-Mercado, H.; Wu, G.; Lee, J.W.; Popov, B.N. Nitrogen-modified carbon-based catalysts for oxygen reduction reaction in polymer electrolyte membrane fuel cells. *J Power Sources.* **2009**, *188*(1), 38-44.

[4] Neergat, M.; Shukla, A.K.; Gandhi, K.S.. Platinum-based alloys as oxygen–reduction catalysts for solid–polymer–electrolyte direct methanol fuel cells. *J Appl Electrochem.* **2001**, *31*, 373-378.

[5] Duan, D.; Liu, H.; You, Xi.; Wei, H.; Liu, S. Anodic behavior of carbon supported Cu@Ag core–shell nanocatalysts in direct borohydride fuel cells. *J Power Sources.* **2015**, *293*, 292-300.

[6] Duan, D.; Liu, H.; You, Xi.; Wei, H.; Liu, S. Kinetics of sodium borohydride direct oxidation on carbon supported Cu-Ag bimetallic nanocatalysts. *Electrochim Acta.* **2016**, *198*, 212-219.

[7] Weng, X.; Liu, Q.; Feng, J.J.; Yuan, J.; Wang, A.J. Dendrite-like PtAg alloyed nanocrystals: Highly active and durable advanced electrocatalysts for oxygen reduction and ethylene glycol oxidation reactions. *J Colloid Interface Sci.* **2017**, *504*, 680-687.

[8] Li, J.; Rong, H.; Tong, X.; Wang, P.; Chen, T.; Wang, Z. Platinum–silver alloyed octahedral nanocrystals as electrocatalyst for methanol oxidation reaction. *J Colloid Interface Sci.* **2018**, *513*, 251-257.

[9] Zhao, H.; Lu, Z.; Liu, R.; Li, Z.; Guo, Y. Preparation of platinum-silver alloy nanoparticles and their catalytic performance in methanol electro-oxidation. *J Fuel Chem Technol.* **2020**, *48*(8) ,1015-1024.

[10] Luo, J.; Kariuki, N.; Han, L.; Wang, L.; Zhong, C.J.; He, T. Preparation and characterization of carbon- supported PtVFe electrocatalysts. *Electrochim Acta.* **2006**, *51*, 4821-4827.

[11] Osmieri, L.; Escudero-Cid, R.; Alessandro, H.A.; Videlaa, M.; Ocón, P.; Specchi, L.S. Performance of a Fe-N-C catalyst for the oxygen reduction reaction in direct methanol fuel cell: Cathode formulation optimization and short-term durability. *Appl Catal B: Environ.* **2017**, *201*, 253-265.

[12] Wu, C.; Bai, Y.; Liu, D.X.; Wu, F.; Pang, M.L.; Yi, B.L. Ni–Co–B catalyst-promoted hydrogen generation by hydrolyzing $NaBH_4$ solution for in situ hydrogen supply of portable fuel cells. *Catal Today.* **2011**, *170*, 33-39.

[13] Thungprasert, S.; Sarakonsri, T.; Tunkasiri, T. Electron microscopy study of the formation of dendrite Cu_6Sn_5 powders synthesized by solution route method. *Chiang Mai J Sci.* **2007**, 34(1) ,29-33.

[14] Lima, F.S.; Fontes, E.H.; Nandenha, J.; de Souza, R.F.B.; Neto, A.O. Addition of bismuth to Pt and Pd for electric power generation with selective cogeneration of acetate from ethanol in a fuel cell type reactor. *J Fuel Chem Technol.* **2021**, *49*(10), 1540-1548

[15] Moreno-Castilla, C.; López-Ramón, M. V.; Carrasco-Marín, F. Changes in surface chemistry of activated carbons by wet oxidation. *Carbon.* **2000**, *38*, 1995-2001.

[16] Wang, Y.J.; Fang, B.; Li, H.; Bi, X.T.; Wang, H. Progress in modified carbon support materials for Pt and Pt-alloy cathode catalysts in polymer electrolyte membrane fuel cells. *Prog Mater Sci.* **2016**, *82*, 445-498.

[17] Peng, Y.; Liu, H. Effects of Oxidation by hydrogen peroxide on the structures of multiwalled carbon nanotubes. *Ind Eng Chem Res.* **2006**, *45*, 6483-6488

[18] Chen, W.; Qu, B. Investigation of a platinum catalyst supported on a hydrogen peroxide-treated carbon black. *Int J Hydrog Energy.* **2010**, *35*, 10102-10108.

[19] He, Xi.; Hong, Z.N.; Jiang, J.; Dong, G.; Liu, H.; Xu, R.K. Enhancement of Cd(II) adsorption by rice straw biochar through oxidant and acid modifications. *Environ Sci Pollut Res.* **2021**, *28*, 42787–42797

[20] Thungprasert, S.; Sarakonsri, T.; Klysubun, W.; Vilaithong, T. Preparation of Pt-based ternary catalyst as cathode material for proton exchange membrane fuel cell by solution route method. *J Alloy Compd.* **2011**, *509*, 6812-6815.

[21] Guha, A.; Lu, W.; Zawodzinski Jr., T. A.; Schiraldi, D.A. Surface-modified carbons as platinum catalyst support for PEM fuel cells, *Carbon.* **2007**, *45*, 1506–1517.

[22] Pierson, J. F.; Wiederkehr, D.; Chappe, J. M.; Martin, N. Reactive sputtering: A method to modify the metallic ratio in the novel silver–copper oxides. *Appl Surf Sci.* **2006**, *253*, 1484-1488.

[23] May, C. D.; Vaughey, J.T. New cathode materials for silver-based primary batteries: $AgCuO_2$ and $Ag_2Cu_2O_3$. *Electrochem Commun.* **2004**, *6*, 1075–1079.

[24] Chen, S.S.; Lin, X.X.; Wang, A.J.; Huang, H.; Feng, J.J. Facile synthesis of multi-branched AgPt alloyed nanoflowers and their excellent applications in surface enhanced Raman scattering. Sensor Actuat B-Chem. **2017**, *248*, 214-222.

[25] Shao, F.Q.; Zhu, X.Y.; Wang, A.J.; Fang, K.M.; Yuan, J.; Feng, J.J. One-pot synthesis of hollow AgPt alloyed nanocrystals with enhanced electrocatalytic activity for hydrogen evolution and oxygen reduction reactions, *J. Colloid Interface Sci.* **2017**, *505*, 307-314.

[26] Azam, A.M.I.N.; Lee, S.H.; Masdar, M.S.; Zainoodin, A.M.; Kamarudin, S.K. Parametric study on direct ethanol fuel cell (DEFC) performance and fuel crossover, *International Journal of Hydrogen Energy*. **2019**, 44, 8566-8574.

[27] Spiegel, C. *Designing & Building Fuel Cells*; McGraw-Hill: United States, **2007**

[28] Hoogers, G. *Fuel Cell Technology Handbook*; CRC Press LLC: United States, **2003**

[29] Vielstic, W.; Lamm, A.; Gasteiger, H. G. Handbook of Fuel Cell Fundamentals Technology and Application Vol. 2; Wiley: Chichester, **2003**; pp 503.

[30] Neergat, M.; Shukla, A.K.; Gandhi, K.S. Platinum-Based Alloys as Oxygen Reduction Catalysts for Solid-Polymer-Electrolyte Direct Methanol Fuel Cell. *Journal of Applied Electrochemistry*. **2001**, *31*, 373-378.

[31] Subramanian, N.P.; Kumaraguru, S.P.; Colon-Mercado, H.; Kim, H.; Popov, B.N.; Black, T.; Chen, D.A. Studies on Co-Based Catalysts Supported on Modified Carbon Substrates for PEMFC Cathodes. *Journal of Power Sources*. **2006**, *157*, 56-63.

ASEAN
Journal of Scientific and Technological Reports
Online ISSN:2773-8752

Research article

Developing of Construction Permit Application System by Adopting Agile Methodology

Dolluck Phongphanich[1*], Chutamas Krachangsri[2], Kanjana Phuakkhong[3], Nattayanee Prommuang[4], Amorntip Prayoonwong[5], and Somkid Sinwittayarak[6*]

[1] Faculty of Science and Technology, Suratthani Rajabhat University, Suratthni, 84100, Thailand; dolluckbangsuk@gmail.com
[2] Faculty of Science and Technology, Suratthani Rajabhat University, Suratthni, 84100, Thailand; chutamas.kra@sru.ac.th
[3] Faculty of Science and Technology, Suratthani Rajabhat University, Suratthni, 84100, Thailand; kanjana.phu@sru.ac.th
[4] Faculty of Science and Technology, Suratthani Rajabhat University, Suratthni, 84100, Thailand; nattayanee.pro@sru.ac.th
[5] Faculty of Science and Technology, Suratthani Rajabhat University, Suratthni, 84100, Thailand; aprayoonwong@gmail.com
[6] Faculty of Science and Technology, Suratthani Rajabhat University, Suratthni, 84100, Thailand; somkid@sru.ac.th
* Correspondence: somkid@sru.ac.th; dolluckbangsuk@gmail.com

Citation:
Phongphanich, D., Krachangsri, C., Phuakkhong, K., Prommuang, N., Prayoonwong, A. and Sinwittayarak, S. Developing of construction permit application system by Agile Methodology. *ASEAN J. Sci. Tech. Report.* **2024**, *27*(1), 24-36. https://doi.org/10.55164/ajstr.v27i1.250714.

Article history:
Received: August 28, 2023
Revised: October 30, 2023
Accepted: November 7, 2023
Available online: December 28, 2023

Abstract: Agile methodology is one of the most widely used methodologies in software development in many agencies and organizations thanks to its quick response to user's needs and feedback and high level of user participation in the development process. This research aimed to develop a construction permit application system to enhance local governmental organizations' efficiency in providing services to residents by applying Agile methodology and assessing user satisfaction with the system efficiency. The system was developed in the form of a responsive web application. The research was carried out in 2 parts: 1) System development by applying Agile methodology, and 2) Measuring user satisfaction in the efficiency of construction permit application system using black-box testing with a 5-point scale rating and applying descriptive statistics, namely average and standard deviation. The results from the research indicated that user satisfaction with the efficiency of the construction permit application system by adopting Agile methodology was at a very high level, scoring an average of 4.55 and a standard deviation of 0.57. The developed system using Agile led to the practical construction permit application system, which effectively met user's needs. The system also met the standard criteria, which include the ability to operate according to functionalities designed, user-friendliness, system performance, and satisfaction with security features. Moreover, the system development using Agile also provided quick responses to user needs and thorough, continuous engagements from all users in operations management. This would aid in developing a system that met the users needs and truly addressed current challenges.

Keywords: Agile methodology; Construction permit application; Local government organization; Scrum; Web application

1. Introduction

Thailand's 20-year national strategy ensures it achieves its vision of becoming "a developed country with security, prosperity, and sustainability." The first phase of the strategy focuses on public services and government efficiency to push Thailand to the world's top 60 highly digitalized governments [1]. This will also represent Thailand's success in transforming into a digitalized

government on the global stage. Such transformation is vital to the government's policy on digitalization and meets the needs of the public under the New Normal era, as per the Order of Prime Minister No. 267/2560 dated 15 October 2017, which pursues adaptation of technology under the notion of "smart government service," as a means to drive the country and serve the public by "local governmental organizations," which is one of the government's entities assigned to provide services to residents [2], [3].

Thailand scored a relatively high mark compared with 2018, moving to 57th out of 193 countries and ranking 3rd in ASEAN. Nonetheless, the Local Online Service Index (LOSI), which measures information services, transactions, and participation mechanisms from the local people of the main cities, is down in 2020; therefore, it is important to take into consideration all the measures [4], [5]. Local government organizations play a key role with residents and communities based on their importance. It is also equally important for local government organizations to adopt the policy of digitalization to meet the needs of residents since the policy would be one of the tools to enhance government agencies' capability. Moreover, it is a decisive factor in fully embracing the government's digitalization transformation policy.

"Bureau of Mechanics, Surat Thani City Municipality" is a local organization located in the northernmost province of Southern Thailand or Surat Thani Province. The Bureau holds various responsibilities, such as monitoring, designing, drafting, and keeping records of historical infrastructure, building, and city planning per the Town Planning Act. Building control and inspection per the Act also fall under the Bureau's responsibility. However, data is kept as hard copies and the construction permit application process is outdated. Lack of innovation and digitalization causes negative consequences to operations, management, and service provisions to the public. Information and communication technology are essential in transforming the organization.

Therefore, this research aimed to develop a construction permit application system by applying Agile methodology to enhance local governmental organizations' services to residents. Also, the study aimed to assess user satisfaction with the efficiency of the construction permit application system. System development using Agile methodology will pave the way to gather and store data systematically, access government data, track the status of applications via the LINE online messaging platform, etc. In addition, the methodology will increase speed and accuracy in managing, analyzing, storing, and utilizing data by applying digital technologies to manage the organization's affairs and access from the public on every level. The use of Agile methodology in system development provides quick responses to user needs and thorough, continuous engagement from all users in operations management, which will aid in developing a system that meets the user's needs and truly addresses current challenges.

2. Literature Review

2.1 Background of Surat Thani City Municipality

Surat Thani Municipality began as a community in Talat Sub-district, Mueang Surat Thai District, Surat Thani Province, the northernmost province of southern Thailand. It was governed as a sanitary district until 1932 when Thailand changed from absolute monarchy to democracy. The new form of governance brought new legislation in 1933 that converted Surat Thani Province sanitary districts into municipalities on 7 December 1935 with a total area of 2.67 km^2. On 14 October 1958, Surat Thani Province expanded its area, resulting in a total area of 6.95 km^2. Years later, as the province experienced rapid prosperity and development, new communities and commercial regions were established within and surrounding Surat Thani Municipality. Those areas did not differ much in action and had their local governing entity. As the districts and sub-districts increased, those sanitary districts were later assimilated or converted into districts on 22 December 1994, which enlarged Surat Thani province overall size to 68.97 km^2. Currently, Surat Thani Province has a total population of 127,542 inhabitants.

On 19 April 2007, Mr. Aree Wong-araya, Minister of Interior, signed the regulation, which came into force on 4 May 2007, promoting Surat Thani Town Municipality to become the City Municipality. The City Municipality has 8 offices: Office of Education, Office of Finance, Bureau of Mechanics, Office of Public Health and Environment, Office of the Municipal Clerk, Academic and Planning Division, Social Welfare Division, and Tax Information System Division [6]. This research is an extension of the e-tracking system, which is a part of big data management for enhancing the efficiency of serving people in the old town of Surat Thani

Municipality. The municipality once received support from the program management unit on Area-Based Development (PMUA), the Office of National Higher Education Science Research and Innovation Policy Council, and the Ministry of Higher Education, Science, Research and Innovation in 2020. Those supports were mainly given to the Bureau of Mechanics of Surat Thani City Municipality because much data was still stored in folders as hard copies. Searching for files and information was done manually, which was not in line with the government's digitalization policy, where everything had to be fast and meet user's needs. Moreover, the agency was ready to support and accommodate in terms of personnel and information for this research.

2.2 Agile and Scrum

Agile development methodology and Scrum are one of the most widely-used methods thanks to their fast-paced work by reducing hierarchical bureaucracy and paperwork, thus resulting in a more streamlined, straightforward, flexible, and result-oriented working environment [7], [8] [9], [10], [11], [12], [13], [14]. The frameworks focus on collecting feedback through user testing to rapidly adjust and fix any flaws, fostering faster system development and leading to achieving user needs in a timely fashion [7], [8].

Scrum is an implementation of an agile framework proposed for project management to manage the iterative software development process. It focuses on providing the most value at the earliest. Scrum is a team-oriented agile technique that sets a limited-time boxed iteration called 'Sprint' in which the system is incrementally built and produces different artifacts for its work. It is one of the most popular agile methodologies, thanks to its simplicity and concentration on software management challenges rather than technical software development processes, making it broadly applicable to any domain. Three primary phases of the Scrum life cycle are described below [8].

1) The outline planning phase, also known as the pre-sprint phase, is the first step to describe the general objectives for the system being designed and built. The project team, tools, and resources needed are detailed. It is also known as iteration 0.

• A Product Backlog is created and utilized to document client requirements through user stories and features.

• The requirements are then reviewed and prioritized, and implementation effort is estimated by the product owner, whose role is to keep the product backlog visible and transparent.

• As user stories are created gradually, the product backlog can be continuously updated, and the priority of existing stories may change throughout development.

2) Development phase or sprint phase: It comprises sprint cycles, with the outcome of each cycle being incrementally added to the system. A sprint cycle has the following details:

• Sprints are iterative fixed-length cycles that last between 2-4 weeks.

• Each sprint follows the standard software process steps, starting from requirement analysis or sprint planning from the product backlog and finishing in the delivery phase following the sprint review.

In the sprint planning meeting at the beginning of each sprint, which includes the development team and the product owner, works that must be completed will be agreed. Based on their priority, user stories are incrementally moved from the product backlog to the sprint backlog, and features and functionalities to be implemented are determined. A sprint cycle begins once the pre-sprint planning is completed. During a sprint, the Scrum master isolates the team from external distractions, and the features are built and tested daily through a meeting called daily scrum. Daily scrum meetings are limited to 15 minutes long to improve communication, synchronize activities, refocus the team on the common goal shared by all team members, and resolve any difficulties or hurdles that may arise. The sprint concludes with two meetings: the sprint review meeting, in which the sprint output, a potentially shippable increment, is inspected, analyzed, and assessed, and the sprint retrospective meeting, in which possible future improvements are discussed.

• A burn-down chart is used to track the progress of the sprint.

• Increments may be built by multiple teams, i.e., parallel sprints.

3) The project closure phase occurs when the requirements meet the goals agreed upon by the product owner and the team. The most recent version of the product is now ready for release and distribution, and all the paperwork and user manuals are ready.

It is crucial to work on product quality and measure software development projects to get better insight into the project's progress. Agile methodology addresses quality issues continuously and repeatedly, focusing on software quality through customers, minimizing errors, rapid development, and embracing changes.

Thanks to its flexibility, adaptability, and light documentation, local and international researchers have applied Agile and Scrum in new system developments. In Thailand, many researchers have successfully reached their objectives by applying Agile, such as Lertjabok [15], who researches the implementation of Agile to Design and Develop a Visualization System in Digital Living Book: A Case Study of Office of Academic Resources and Information Technology, Raja Mangala University of Technology Isan which applies the agile methodology to design and develop a digital living book. The design and development are conducted in rapid mode as system users require. Users are, on average, well-received.

Another study is Development of Decision Support System for Asset Budget: A Case Study of Krung Thai Bank Training Center, Khao Yai, Nakhon Ratchasima, which applies the agile methodology to designing and building a decision support system [16]. The system receives a very high level of user satisfaction since it serves as a tool for a training center to allocate budget fairly and appropriately. In addition, the system minimizes errors in asset budgeting. Phusri and Kritworakan's research titled Factor Influencing Employee Motivation and Demotivation: A Study of the Siam Cement Group, Songkhla Province [17] has applied Agile methodology and Scrum to speed up website design for a small and medium enterprise. The research also aids daily interactions and communications between customers and team members to notify customers of any work progress and obstacles continuously, and fosters collaboration in creating the solution, ultimately reducing wasted time.

Overseas researchers such as Hossain and Kashem [18] have stated that Agile techniques are applied to minimize risk factors by developing software quickly. Under agile methodology, any changes are welcome in the software development phase. Ultimately, this paper concludes that Agile techniques can increase software quality and customer value. Muhammad et al. [12] research has collected data from different software development companies' employees to compare factors affecting software quality with agile and scrum methods. The main advantage of the agile technique is its emphasis on customer satisfaction and responsiveness to user requirements throughout its development cycle. By adopting the agile method, the software can capture almost all the required qualities.

Therefore, applying agile methodology to rapidly complete the system development on time to have a system that meets user's requirements becomes an alternative for developers to choose.

3. Materials and Methods

The research was divided into two parts. The first part focused on developing a construction permit application using agile methodology. The second part focused on stakeholders' or users' satisfaction towards the system efficiency using black-box testing [19], [20] with a 5-point Likert scale, then using statistical computation including average (x-bar) and standard deviation (S.D.) to derive the results [21]. Details are shown as follows.

3.1 Development of construction permit application system by applying Agile methodology

Agile methodology was used along with Scrum as shown in Figure 1, to carry out this plan.

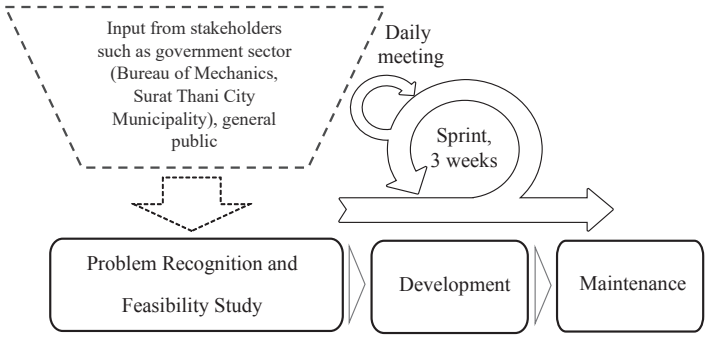

Figure 1. System Development by applying Agile and Scrum.

1) Problem recognition and feasibility study or pre-sprint phase: This step was the most crucial process to understand the user's needs to see the feasibility of changing the system to achieve satisfactory results while

minimizing costs and time to establish clear objectives. The development started with meetings between all stakeholders, such as the government sector (Bureau of Mechanics, Surat Thani City Municipality), the general public, and academics to collect issues, current situations, and organizational needs, to check human resource readiness, to exchange opinions, to collect requirements and expectations to set a scope of work and an operation plan, and to create user stories. The user stories can be summarized as shown in Table 1. For each user story, acceptance criteria were determined to build feasible system capabilities as intended. Each process could be explained as follows:

• Setting up meetings to explain and inquire about user needs: 11 officials (Bureau of Mechanics, Surat Thani City Hall) from various sub-divisions were selected, including Application Form Screening and Evidence Verification Officer, City Planning Auditor, District Monitoring Officer, Engineering Officer, Sanitation Officer, Building Energy Auditor, Chief of Building and City Plan Control Sub-division, Director of Building and City Plan Control Sub-division, Director of Bureau of Mechanics, District Clerk, and Mayor. The public, including owners of local firms, the general public, and academics, were also chosen to understand the responsibilities of all sub-divisions;

• Analyzing related documents, including (1) Application Form for Permission to change the Use of the Building (From Kor.2.), (2) Application Form for Permission to modify or use Parking Spaces, U-turns, and Vehicle Entrances/Exits for Other Purposes (Form Kor.3), (3) Application Form for Renewal of Permit for Construction, Modification, Demolition, or Relocation of Building (Form Kor.4), (4) Application Form for the Substitute of Permit or Substitute of Certificate (Form Kor.5), (5) Summary Report of Application to change the Use of Building (Form Kor.2), (6) Summary Report of Application to modify or use Parking Spaces, U-turns, and Vehicle Entrances/Exits for Other Purposes (Form Kor.3), (7) Summary Report of Application for Renewal of Permit for Construction, Modification, Demolition, or Relocation of Building (Form Kor.4) and (8) Summary Report of Application for the Substitute of Permit or Substitute of Certificate (Form Kor.5);

• A Performing feasibility analysis based on collected data, including assessment of the current information technology system or capital required to install the system, human resources needed to operate the system;

Table 1. User stories.

Step	Stories	Acceptance Criteria
1	As a public user/firm, I want to register and submit an application for different type of construction permit online to register and request a construction permit via the online platform.	1) Register to submit an online application for a construction permit 2) Edit information registered 3) Display a registration result 4) Print out a registration result
2	As a public user/firm, I want to register/save details of construction permit application form to register/save information of construction permit application via an online platform.	1) Register/save details of various construction permit applications 2)Display the result of registration and the information saved 3) Print out the details of the application form
3	As public users/firms, I want to attach and track additional required documents (in case of missing to add) to complete the application.	1) Display required documents (in case of missing to add) 2) Submit additional required documents (in case additional documents are required)
4	As a public user/firm, I want to track an application and approval progress via an online platform and LINE application to check if the application is complete.	1) Display a construction permit application status via an online platform 2) Display the result of the construction permit application via the LINE application

Table 1. User stories. (continue)

Step	Stories	Acceptance Criteria
5	As an official, I want to search and verify applications to approve/deny applications conveniently via an online platform.	1) Search for applications for a construction permit 2) Approve/deny applications 3) Note a reason for denying applications 4) Notify an applicant for additional documents (in case of incomplete application) 5) Display details of approved/denied applications
6	As an officials, I want to see application data online, to manage and print out application data online conveniently.	1) Submit details of different construction permit application forms 2) Display a submission result 3) Print out the information submitted
7	As an official, I want to search for information on construction permit applications submitted with selected conditions to verify information on different types of applications.	1) Print out application documents submitted online. 2) Generate construction permit application letters 3) Generate reports of construction permit application results
8	As an official, I want to specify a level of approvals and centralize the approval permission to delegate approval authority to other officers.	1) Determine a level of approvals to officers 2) Delegate approval authority to officers

2) Development phase or sprint phase: This step was where all stakeholders took part in a meeting to plan the entire system process and then bring user stories to break down into smaller items. Those stories are prioritized based on importance and assigned to sprint cycles. For this system, we assigned 8 sprints for the whole development cycle with a 24-week duration until the completion. For each sprint, user stories were chosen for development, testing, and trial run by a target group to collect user feedback and system functionalities flaws and find a solution to meet user's needs. Details of the development were as follows.

2.1) System Architecture

From data collection and analysis, the development team designed the system architecture by facilitating users or stakeholders, including officials from several sub-divisions of the Bureau of Mechanics and ordinary users, to use the system as a responsive web application on various devices via the internet [22]. Programming languages included PHP and HTML with Bootstrap Framework, jQuery Framework, and LINE Messaging API to accommodate all types of devices. As for storing user data and construction permit applications, MySQL was chosen, as shown in Figure 2 of the system architecture.

2.2) Database Design

The development team and stakeholders designed a database using MySQL to systematically store and display data, as shown in Figure 3 (Entity Relationship Diagram). The diagram consisted of 29 tables with details as follows: user control (syst_avl), API to notify users (syst_avl_api), levels of approval (syst_avl_control), main application submissions (pvs_req), types of application (pvs_req_type), officials' note (pvs_req_note), approved applications (pvs_req_approved), building proprietor form 1 (pvs_req_form1_owner), building proprietor's agent form 1 (pvs_req_form1_agent), land dimensions detail form 1 (pvs_req_form1_land), building proprietor form 6 (pvs_req_form6_owner), building proprietor's agent form 6 (pvs_req_form6_agent), permit application form 6 (pvs_req_form6_land), building proprietor form 7 (pvs_req_form7_owner), building proprietor's agent form 7 (pvs_req_form7_agent), permit transfer details form 7 (transferer) (pvs_req_form7_land_pass), permit transfer details form 7 (transferee) (pvs_req_form7_land_receive), building proprietor form 2 (pvs_req_form2_owner), building proprietor's agent form 2 (pvs_req_form2_agent), land dimensions detail form 2 (pvs_req_form2_land), building proprietor form 3 (pvs_req_form3_owner), building

proprietor's agent form 3 (pvs_req_form3_agent), land dimensions detail form 3 (pvs_req_form3_land), building proprietor form 4 (pvs_req_form4_owner), building proprietor's agent form 4(pvs_req_form4_agent), land dimensions detail form 4 (pvs_req_form4_land), building proprietor form 5 (pvs_req_form5_owner), building proprietor's agent form 5 (pvs_req_form5_agent), land dimensions detail form 5 (pvs_req_form5_land).

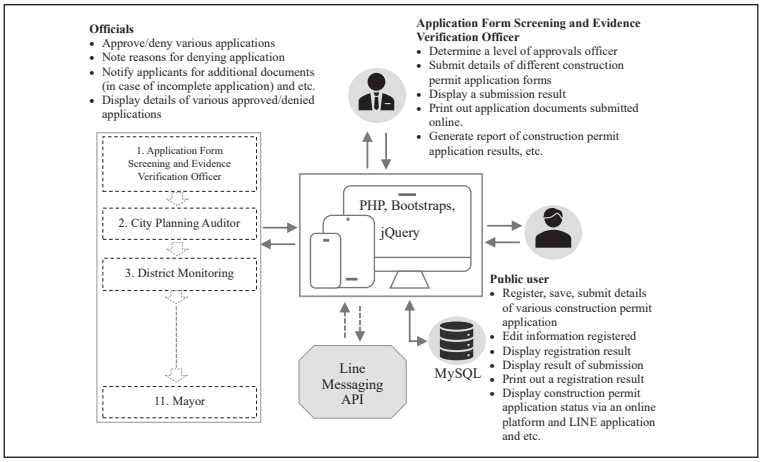

Figure 2. System architecture.

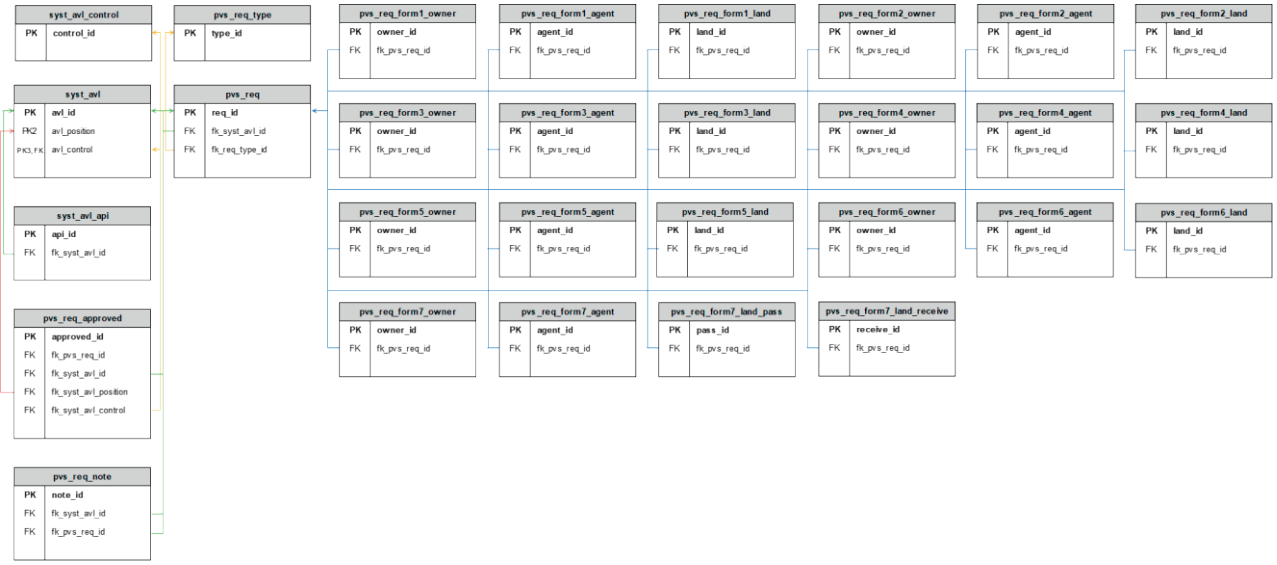

Figure 3. Entity-Relationship Diagram.

3) Maintenance and Project closure phase: This process was divided into two parts. Each part could be explained as follows.

3.1) Maintenance phase: This phase was about testing, fixing, and adjusting the system, which involved users' direct interaction. After system development was complete in each development sprint, the system would be tested to gather inputs from different users, such as the Bureau of Mechanics, ordinary citizens, and the development team. In other words, we conducted a sprint review and then fixed all the bugs and flaws in the system functionalities. With the sprint retrospective for every sprint, we sought solutions to improve the system developed. Also, when an additional fix in each sprint was required, the development team would select works with lower priority from the product backlog or change the priority of each work to run a sprint backlog for each function until the development was complete.

3.2) Project closure phase: This phase is about the requirements that could achieve the development of the operational system as per user stories designed, given the needs met and the goals set as agreed upon

by the system owner and the team. The most recent version of the system was now ready for release and distribution, and at the same time, all the paperwork and user manuals were ready.

3.2 Designing a survey questionnaire to gather data on user satisfaction with the Construction Permit Application System by applying Agile methodology

1) Design a questionnaire to measure the system to validate its accuracy, comprehensiveness, security, and quality, whether it met specifications or objectives, using the black-box testing method [19-20]. The survey comprised 25 questions in 5 dimensions: 1) Function Test, 2) Functional Requirement Test, 3) Usability Test, 4) Security Test and 5) Performance Test. Details of each test are as follows:

- First dimension: The function test was composed of 5 questions measuring the system's ability to search for public user applications, set the level of approval, centralize the approval permission, ability to print application documents submitted, and the ability to generate reports on user applications.
- Second dimension: Functional Requirement Test was composed of 5 questions measuring the system's ability to record the application (officials), verify information and approve applications online (officials), submit applications online (public users), track each application status (public users), and send notification through LINE application.
- Third Dimension: The usability Test was composed of 5 questions measuring the system's user interface design, size of the user interface components, consistency of user interface, font size, and design, icon, and image to convey messages.
- Fourth Dimension: The security Test was composed of 5 questions measuring the system's ability to differentiate types of authorized users, protect users with a username and password, allow users to change the password, protect any technical error when retrieving documents submitted by users, and prevent data breach.
- Fifth dimension: Performance Testing was composed of 5 questions measuring the speed of computation and display of submitted applications, ability to support simultaneous, multiple user access, stability to tolerate heavy continuous usage, stability to store simultaneous, multiple applications and information submitted, and ability to recover data in case of system crash.

2) The questionnaire survey was measured by 3 experts using item objective congruence (IOC) to assess its validity and quality before testing in real situations [23].

3) After the experts reviewed the questionnaire survey, a 5-level Likert rating scale [21] was used to measure user satisfaction with system performance. There were 30 evaluators, including government officials from the Bureau of Mechanics and ordinary citizens.

4. Results and Discussion

4.1 Results of the development of construction permit application system by applying Agile methodology

With a user-friendly design, the system was in the form of responsive web application designed for two main types of users: officials (government sector) and the general public. Details of the development outcome are shown in Figures 4 and 5:

1) Officials (government sector): Officials included officers and personnel of the Bureau of Mechanics, Surat Thani City Municipality, including the Application Form Screening and Evidence Verification Officer, City Planning Auditor, District Monitoring Officer, Engineering Officer, Sanitation Officer, Building Energy Auditor, Chief of Building and City Plan Control Sub-division, Director of Building and City Plan Control Sub-division, Director of Bureau of Mechanics, District Clerk, and Mayor. The system allowed officials to search, review, approve, and deny applications. Also, the system could keep records of approved/denied applications, display details of approved/denied applications, and manage types of applications (Form Kor.2, 3, 4, 5) via an online system (https://etracking.sru.ac.th/login.php). The system was able to authorize and assign different levels of approval. Besides, the system could display reports of different application statuses. Details of the development outcome for officials are shown in Figure 4.

2) Public: Users, including residents, communities, and local firms, were allowed to submit and revise applications (Form Kor.2, 3, 4, 5), and check their application and approval status through the online system and LINE application. Details of the development outcome for the public are shown in Figure 5.

(a) Screen of application form screening and evidence verification officer.

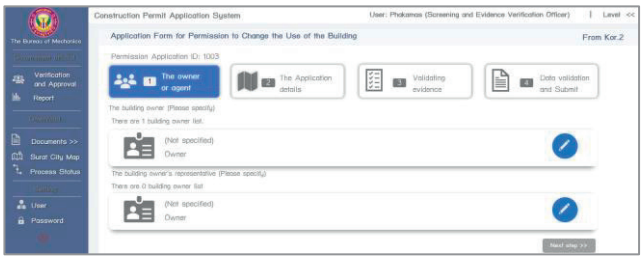

(b) Input screen of form Kor. 2.

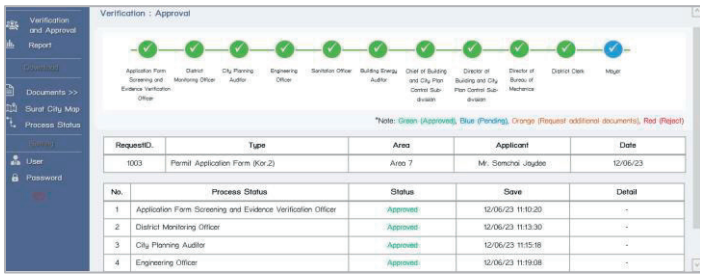

(c) Screen of approval status.

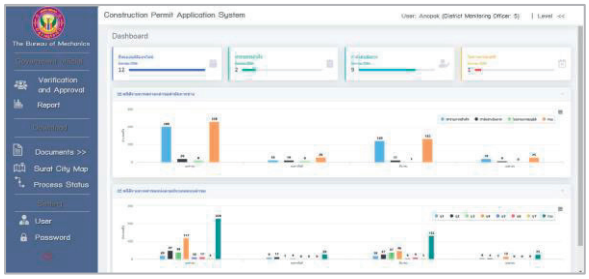

(d) Screen of summary reports.

Figure 4. (a)-(d) Results of system development for officials (government sector users).

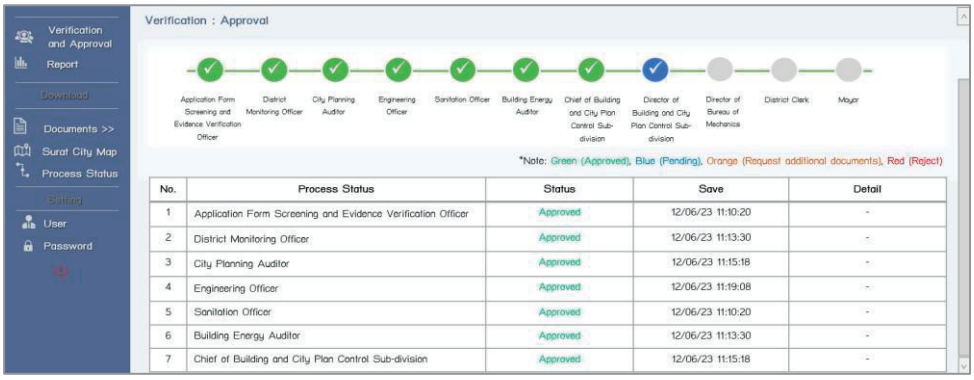

(a) Screen of approval status through the online system.

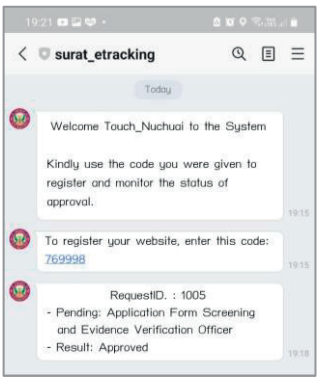

(b) Screen of approval status through LINE application.

Figure 5. (a)-(b) System development results for the public (general public users).

4.2 Results of user satisfaction in the efficiency of the construction permit application system by applying the methodology of Agile

1) The results of designing a tool for assessing user satisfaction are shown below.

Table 2 displays the results of the average IOC score of each item calculated by 3 experts' ratings. The survey comprised 25 questions in 5 dimensions: 1) Function Test, 2) Functional Requirement Test, 3) Usability Test, 4) Security Test, and 5) Performance Test. The average IOC score for the questions was 1.00, within the standard limit of not less than 0.50. Therefore, it can be concluded that all the assessment items of the satisfaction assessment are accurate and can be utilized for evaluation.

2) The results of user satisfaction in developing the construction permit application system. The results are shown below.

Table 2. The results of Item-Objective Congruence (IOC) scores from experts.

Questions	Experts			Total score	IOC	Result
	1	2	3			
Functional Testing						
The ability to search for public user applications	+1	+1	+1	3	1.00	Congruent
The ability to set the level of approval	+1	+1	+1	3	1.00	Congruent
The ability to centralize the approval permission	+1	+1	+1	3	1.00	Congruent
The ability to print application documents submitted	+1	+1	+1	3	1.00	Congruent
The ability to generate reports on user's applications	+1	+1	+1	3	1.00	Congruent
Functional Requirement Testing						
The ability to record the application	+1	+1	+1	3	1.00	Congruent
The ability to verify information and approve applications online	+1	+1	+1	3	1.00	Congruent
The ability to submit applications online	+1	+1	+1	3	1.00	Congruent
The ability to track each application status	+1	+1	+1	3	1.00	Congruent
The ability to send notifications through the LINE application	+1	+1	+1	3	1.00	Congruent
Usability Testing						
User interface design	+1	+1	+1	3	1.00	Congruent
Suitable size of the user interface components	+1	+1	+1	3	1.00	Congruent
Consistency of user interface	+1	+1	+1	3	1.00	Congruent
Font size and design	+1	+1	+1	3	1.00	Congruent
Icon and image to convey messages	+1	+1	+1	3	1.00	Congruent
Security Testing						
The ability to differentiate types of authorized users	+1	+1	+1	3	1.00	Congruent
Protecting users with a username and password	+1	+1	+1	3	1.00	Congruent
Allowing users to change the password	+1	+1	+1	3	1.00	Congruent
Protecting any technical error when retrieving documents submitted by users	+1	+1	+1	3	1.00	Congruent
Preventing data breaches	+1	+1	+1	3	1.00	Congruent
Performance Testing						
The speed of computation and display of submitted applications	+1	+1	+1	3	1.00	Congruent
The ability to support simultaneous multiple-user access	+1	+1	+1	3	1.00	Congruent
The stability to tolerate heavy continuous usage	+1	+1	+1	3	1.00	Congruent
The stability to store simultaneous multiple applications and information submitted	+1	+1	+1	3	1.00	Congruent
The ability to recover data in case of system crash	+1	+1	+1	3	1.00	Congruent

Table 3. User satisfaction in the development of the construction permit application system.

Feature Tested	$\overline{x}$	S.D.	Level
Functional Testing	4.55	.59	Highest
Functional Requirement Testing	4.67	.51	Highest
Usability Testing	4.54	.53	Highest
Security Testing	4.47	.63	Highest
Performance Testing	4.53	.58	Highest
Total	**4.55**	**.57**	Highest

Table 3 displays user satisfaction with developing the construction permit application system, ranging from least to most satisfied. Regarding efficiency in meeting the user's needs (Functional Requirement Testing), it was at the highest level with an average and standard deviation of 4.67 and .51, respectively, followed by the ability to operate according to functionalities designed (Functional Testing), which scored at the highest level with an average and standard deviation of 4.55 and .59 respectively, user-friendliness (Usability Testing) which scored at the highest level with an average and standard deviation of 4.54 and .53 respectively, system performance (Performance Testing) which scored an average and standard deviation of 4.53 and .58 respectively, and satisfaction in security features (Security Testing) which scored at the highest level with an average and standard deviation of 4.47 and .63 respectively.

This research aimed to develop a construction permit application system to enhance local governmental organizations' efficiency in providing services to residents and assess users' satisfaction with the system efficiency. The Methodology was carried out in 2 parts. The first part focused on system development by applying agile methodology, which included 3 main phases: problem recognition and feasibility study or pre-sprint phase, development phase, and maintenance phase. The second part focused on stakeholders' or users' satisfaction with the system efficiency. The result of system development was divided into two main sections: officials (government sector) and the general public. There were various functionalities of the system to use depending on the demands of the users, such as approving or denying various applications, notifying applications for additional documents, displaying details of various approved or denied applications, determining a level of approval officers, submitting details of different construction permit application forms, display construction permit application status via an online platform and LINE application, etc. The developed system is conducted rapidly and flexibly as required by system users and supports user involvement, resulting in a successful mission according to its goals. This is consistent with Muhammad et al. [12], Hossain [18], and Lertjabok [15], who found that the system is fast and meets the needs of users. Moreover, Phusri and Kritworakan [17] found that applying Agile methodology could speed up web application design and aid daily interactions and communications between customers and team members to continuously notify customers of any work progress and obstacles, and foster collaboration in creating the solution which ultimately reduced time wasted. Moreover, the result of assessing user satisfaction showed that user satisfaction with the efficiency of the construction permit application system was at a very high level, scoring an average of 4.55 and a standard deviation of .57. The system also met the standard criteria, which include the ability to operate according to functionalities designed, user-friendliness, system performance and satisfaction in security features. Since the average score for users' overall satisfaction with the system was at a high level, it shows that the developed system by applying agile led to the practical construction permit application system that effectively meets users' needs and could enhance local administrative organizations' efficiency in providing services to residents and help the mission successful according to its standard criteria.

5. Conclusions

In this study, the research team designed the system in a responsive web application accessible via the internet by using PHP language storing data in the MySQL database. The system was developed by applying Agile methodology and Scrum with the participation of all stakeholders, including the government and general public sectors. The result of user satisfaction analysis, which was obtained via a tool developed by black-box testing in conjunction with a 5-level rating scale, concluded that users had a high level of

satisfaction with the efficiency of the system adopted Agile with an average score of 4.55 and a standard deviation of .57. The system was functional and could facilitate users very well. This was consistent with Muhammad et al. [12], Hossain [18], and Lertjabok [15], meaning that the system was fast and met the needs of users. Although the agile approach is popular and effective in developing a system that delivers value to users. However, it also comes with its own set of challenges and some limitations that can affect the speed and collaboration of the research, such as adding new requirements to a system that was not planned initially. To prevent this, it's important to define and prioritize the user stories, involve the user and stakeholders in the planning and review process, and get their feedback regularly.

6. Acknowledgements

This research is an extension to the sub-system under Big Data Management for Enhancing the Efficiency of Serving People in the Old Town of Surat Thani Municipality. The research team wishes to thank the Bureau of Mechanics of Surat Thani City Municipality for its support with personnel and data for system improvement. Also, the research team wishes to extend their sincere gratitude to the development team and Institute of Research and Development, Surat Thani Rajabhat University, for their support and seamless coordination.

Author Contributions: D.P. conducted the research, analyzed the data, and wrote the paper; T.K., K. P., and N.P. were in charge of validating, reviewing a paper; A.P. and S. S. reviewed the manuscript and original draft preparation; all authors had approved the final version.

Funding: This research received no external funding.

Conflicts of Interest: The authors declare no conflicts of interest regarding the publication of this paper.

References

[1] Government Gazette. *National Strategy 2018-2037*. **2018**, *135*(82). 1–22. https://www.sme.go.th/upload/mod_download/download-20201012111719.pdf

[2] Smart City Thailand. Depa. **2022**. https://www.depa.or.th/en/smart-city-plan/smart-city-office

[3] Smart cities through smart concept. *Office of the Council of State.* **2021**, https://lawforasean.krisdika.go.th/File/files/Smart%20City.pdf (In Thai)

[4] United Nations E-Government Survey 2020. *UN E-Government Knowledgebase*. **2022**, https://publicadministration.un.org/egovkb/en-us/Data/City/id/73-Bangkok/dataYear/2022

[5] Digital Government Development Agency. *UN E-Government Survey 2020*. **2020**, https://www.dga.or.th/wp-content/uploads/2020/07/DGA_EGDI2020.pdf

[6] Municipality Office. *Bureau of Mechanics*. **2022**, https://www.suratcity.go.th/web/index.php/en/home-en (In Thai)

[7] Petcharat, W.; Sutthirak, T.; Janwichian, K.; Khamkhow, A.; Artitung, P. The Information System Development for Management of Professional Experience Training Department of Management Science, Faculty of Management Science, Nakhon Si Thammarat Rajabhat University. *Rajapark Journal*. **2021**, *15*, 39, 109-123.

[8] Samar, A.; Samar, S.; Heba, A-N. Agile Software Development: Methodologies and Trends. *International Journal of Interactive Mobile Technologies*, **2001**, *14*(11), 246-269. https://doi.org/10.3991/ijim.v14i11.13269

[9] Pusri, N.; Kritworakarn, C. Applying Agile Project Management to Website Development. (Extended Abstract) *The 2nd Seminar on Industrial Engineering and Industrial Management*. **2018**, https://imcmu.eng.cmu.ac.th/pdf/590632068.pdf

[10] Andy, B.; Martinson, O.; Chrie, N.; Dave, B. A systematic literature review: how agile is agile project management?. *Issues in Information System*, **2021**, *22*, 278-296. https://iacis.org/iis/2021/3_iis_2021_298-316.pdf

[11] Shahbaz, G. A. K.; Salman, A.; Mukhtar, A.; Adnan, N.; Abdul, R.; Naveed, A. A Systematic Literature Review of Success Factors and Barriers of Agile Software Development. *International Journal of Advanced Computer Science and Applications*. **2018**, *9*, 278-291.

[12] Muhammad, S. A.; Babur, M. H.; Imran, M.; Izaz-ul, H.; Usman, A.; Tamoor, W.; Wajid, A.; Amina, Y.; Bilal-b, Ijaz.; Hadiqa, N.; Muhammad, S. Comparison of Agile Method and Scrum Method with Software Quality Affecting Factors. *International Journal of Advanced Computer Science and Applications*. **2019**, *10*, 531-535.

[13] Srisura, R.; Wayalun, S.; Salee, R.; Sinjungreed, W. Use of the Agile Concept in the Development of an Online Platform to Empower Ban Tha Kor Community Enterprised in Ubon Ratchathani. *Industrial Technology Journal*. **2022**, *7*, 67-79.

[14] Hoy, A.; Xu, M. Agile Software Requirements Engineering Challenges-Solutions-A Conceptual Framework from Systematic Literature Review. *Information*. **2023**, *14*, 1-19. https://doi.org/10.3390/info14060322

[15] Lertjabok, C.; Janruang, J. Implementation of Agile to Design and Develop Visualization System in Digital Living Book: A Case Study of Office of Academic Resources and Information Technology, Rajamangala University of Technology Isan. *National & International Conference on Global Goals, Local Actions: Looking Back and Moving Forward*. *2020*, **2020**, 1002-1013. http://journalgrad.ssru.ac.th/index.php/8thconference/article/view/2260

[16] Maneesuriya, E.; Janruang, J. Development of Decision Support System for Asset Budget: A case Study of Krung Thai Bank Training Center Khaoyai, Nakhonratchasima. *National & International Conference on Global Goals, Local Actions: Looking Back and Moving Forward 2020*. **2020**, *1*, 1200-1210. http://journalgrad.ssru.ac.th/index.php/8thconference/article/view/2288

[17] Phusri, N. Application of Agile project management for website development. *Graduate School*. **2020**, https://cmudc.library.cmu.ac.th/frontend/Info/item/dc:161532

[18] Hossain, A.; Kashem, A.; Sultana, S. Enhancing Software Quality Using Agile Techniques. *IOSR Journal of Computer Engineering*. **2013**, *10*, 87-93.

[19] Khan, M. E.; Khan, F. A Comparative Study of White Box, Black Box and Grey Box Testing Techniques. *International Journal of Advanced Computer Science and Applications*. **2012**, *3*, 12-15.

[20] Felderer, M.; Buchler, M.; Johns, M.; Brucker, A. D.; Breu, R.; Pretschner, A. Security Testing: A Survey. *Advances in Computer*. **2016**, *101*, 1-51. https://doi.org/10.1016/bs.adcom.2015.11.003

[21] Jebb, A. T.; Ng, V.; Tay, L. A Review of Key Likert Scale Development Advances:1995-2019, *Front. Psychol*. **2021**, *12*, 1-14. https://doi.org/10.3389/fpsyg.2021.637547

[22] Kharat, A.; Bhosal, P.; Gupta, S.; Barshe, S. Responsive Web Design. *International Research Journal of Engineering and Technology (IRJET)*. **2018**, *5*, 1888-1892.

[23] Turner, Y R. C.; Carlson, L. Indexes of Item-Objective Congruence for Multidimensional Items. *International Journal of Testing*. **2009**, *3*, 163-171.

ASEAN
Journal of Scientific and Technological Reports
Online ISSN:2773-8752

Research article

Germinated Sang Yod Brown Rice as a Novel Prebiotic for Synbiotic Dietary Supplement Development

Nattakan Dangmanee[1*]

[1] Faculty of Agro and Bio-Industry, Thaksin University, Phatthalung, 93210, Thailand; nattakan.d@tsu.ac.th
* Correspondence: nattakan.d@tsu.ac.th

Citation:
Dangmanee, N. Germinated sang yod brown rice as a novel prebiotic for synbiotic dietary supplement development. *ASEAN J. Sci. Tech. Report.* **2024**, *27*(1), 37-43 https://doi.org/10.55164/ajstr.v27i1.249850.

Article history:
Received: June 13, 2023
Revised: October 7, 2023
Accepted: November 7, 2023
Available online: December 29, 2023

Abstract: This study aimed to investigate the prebiotic properties of germinated Sang Yod brown rice in supporting the growth of the probiotic bacteria *Lactobacillus pentosus* GP6. Germinated brown rice was dried, ground into powder, and mixed with De Man Rogosa and Sharpe (MRS) broth at 1%, 3%, and 5%. Bacterial cells were counted at 0, 3, 6, 9, 12, and 24 h after incubation at 37°C. The results showed that the concentration of germinated Sang Yod brown rice powder that exhibited the highest bacterial growth was 3% (10.97 log cfu/ml), followed by 5% (10.85 log cfu/ml) and 1% (10.42 log cfu/ml), respectively. The 3% germinated Sang Yod brown rice powder produced a synbiotic dietary supplement with *L. pentosus* GP6. The results showed that *L. pentosus* GP6 survived with 10.00-10.30 log cfu/ml cell numbers at 4°C for 6 months. This study demonstrated that germinated Sang Yod brown rice could be implemented as a prebiotic and component of synbiotic dietary supplement products.

Keywords: Germinated Sang Yod brown rice; Prebiotic; Synbiotic dietary supplement

1. Introduction

Consumers increasingly demand healthy and safe foods like functional foods to improve overall health and well-being and reduce the risk of specific diseases [1]. Prebiotics are one of the fastest-growing sectors within functional foods. Many food products can consume these compounds as supplements or functional ingredients [2]. Prebiotics are substrates selectively utilized by probiotics, conferring a health benefit. Probiotics are "harmless live normal flora/microorganisms dietary food supplements which provide a health benefit on the host when administered in adequate amounts, and it also leads to having nutritional advantages" [3]. Different prebiotics will stimulate the growth of indigenous gut bacteria. Prebiotics have enormous potential for modifying gut microbiota. These substances are not digested in the stomach. Consequently, they reach the colon, selectively fermented by potentially beneficial bacteria [4]. Fruit, vegetables, cereals, and other edible plants are sources of carbohydrates constituting potential prebiotics. The following may be mentioned as such potential sources: bananas, corncob, sweet potato, barley, wheat, and rice [5-11].

Rice is one of the basic components of the daily diet for nearly half of the world's population. Nutritionally, it is an important source of carbohydrates, protein, iron, calcium, thiamine, riboflavin, and niacin [12]. Rice, especially non-white rice, is considered a good source of prebiotic compounds. The Sang Yod red rice (*Oryza sativa*, L., var. indica) is a unique red rice, initially planted in Phatthalung, a

province in the south of Thailand, for a hundred years. It has been proposed as the protected rice variety under the law and registered as a good associated with geographical indications called Sang Yod rice of Muang Phatthalung since 2006 [13]. Sang Yod rice contains minerals, vitamin B complex, and bioactive compounds. The germinated brown rice contains biofunctional components like dietary fibers, phytic acids, vitamins, and γ-aminobutyric acid (GABA) [14,15]. Prebiotics are called dietary carbohydrates and soluble fiber that can stimulate the growth of potentially beneficial bacteria [16].

Finding optimal use of dietary fibers becomes increasingly imperative. Germinated rice is also a source of resistant starch, but its prebiotic properties have not been evaluated directly. In this respect, the exploration of the prebiotic effect of germinated brown rice and its application for the production of the synbiotic dietary supplement is lacking. Therefore, we investigate the prebiotic properties of germinated Sang Yod brown rice to support the growth of probiotic bacteria and the production of synbiotic dietary supplements.

2. Materials and Methods

2.1 Preparation of germinated Sang Yod brown rice

Sang Yod brown rice was obtained from a local polishing mill in Phatthalung, in southern Thailand. The germinated Sang Yod brown rice was prepared by washing brown rice with water and repeated twice with water. The washed brown rice was soaked with water at room temperature (28-30 °C) for 4 h. The soaked brown rice was put in a container for germination. The germination process was performed at 35 °C for 36-40 h. The germinated brown rice was washed with water and used for further experiments.

2.2 Preparation of germinated Sang Yod brown rice powder

Germinated Sang Yod brown rice was dried in a hot air oven at 60 °C for 13 h (the final moisture content was 5%), then ground with a blender to make a fine powder. All samples were finely ground to obtain the 100-mesh powder. The samples were stored at -20 °C and used for further experiments.

2.3 Preparation of probiotic microorganisms

The probiotic microorganism used in the experiment, *Lactobacillus pentosus* GP6, was cultured in De Man Rogosa and Sharpe (MRS) broth at 37°C in an anaerobic condition for 48 h [17]. This bacterial culture was adjusted to 0.5 McFarland standard (microbial concentration was approximately 1.5×10^8 cfu/ml) with 0.85% normal saline solution (NSS). The bacterial suspension was diluted with MRS broth to obtain an initial microbial concentration of approximately 1×10^6 cfu/ml for further experiments.

2.4 Study on prebiotic properties

The prepared germinated Sang Yod brown rice powder was mixed in the MRS broth by adding the powder at 1, 3, and 5% (w/v) concentration. The sample without the germinated Sang Yod brown rice powder was used as a control sample. All samples were autoclaved at 121 °C for 15 min. *L. pentosus* GP6 (5%) was added to each sample and incubated at 37 °C under anaerobic conditions. Throughout the incubation period, samples were collected at 0, 3, 6, 9, 12, and 24 h to count microbial cells.

2.5 Prebiotc index

Prebiotic index (I_{preb}) is the ratio of probiotic growth in the prebiotic to probiotic growth in a control (0% prebiotic). A prebiotic index higher than 1 means that tested carbohydrates positively affect the probiotic growth. If the prebiotic index is near 1, it indicates a low effectiveness of the tested carbohydrate. The prebiotic index was calculated using the equation: log cfu/ml of probiotic in tested carbohydrate/log cfu/ml of probiotic in control.

2.6 Statistical analysis

All experiments were conducted in triplicate and the results were expressed as mean ± SD. The statistical examination of the data was performed using the SPSS version 16.0 program. The probiotic growth

data (24 h of incubation) at different concentrations of Sang Yod germinated brown rice powder was compared to the control (0% prebiotic) using an analysis of the variance (ANOVA) test. These means were compared using the Duncan two-way Test at a 95 percent confidence level.

3. Results and Discussion

3.1 Germinated Sang Yod brown rice powder

This study used germinated Sang Yod brown rice powder to study prebiotic properties. The yield of germinated Sang Yod brown rice soaked with water for 4 h following incubation at 35 °C was 85.70%. The germinated Sang Yod brown rice was dried at 60 °C, homogenized, and sifted through a 100-mesh sieve to generate the germinated Sang Yod brown rice powder (Figure 1). The mass of powder was 35.31 g or a yield of 8.31%. Germination can alter brown rice's physicochemical, nutritional, and nutraceutical value. These changes in brown rice characteristics during germination are valuable information for developing functional rice-based food products [18].

Figure 1. Germinated Sang Yod brown rice powder.

3.2 Prebiotic property of Germinated Sang Yod brown rice powder

In this study, we examined the prebiotic capacity of germinated Sang Yod brown rice to increase the growth of the probiotic strain. The growth promotion of *L. pentosus* GP6 by germinated Sang Yod brown rice is shown in Figure 2. The result found that all the concentrations of germinated Sang Yod brown rice powder increased the growth of *L. pentosus* GP6 compared to the control group (MRS broth without the germinated Sang Yod brown rice powder). The concentration of germinated Sang Yod brown rice powder that exhibited the highest bacterial growth was 3% (10.97 log cfu/ml) followed by 5% (10.85 log cfu/ml) and 1% (10.42 log cfu/ml), respectively. Based on these experimental results, the germinated Sang Yod brown rice expressed prebiotic properties. This finding was consistent with the previous study [19].

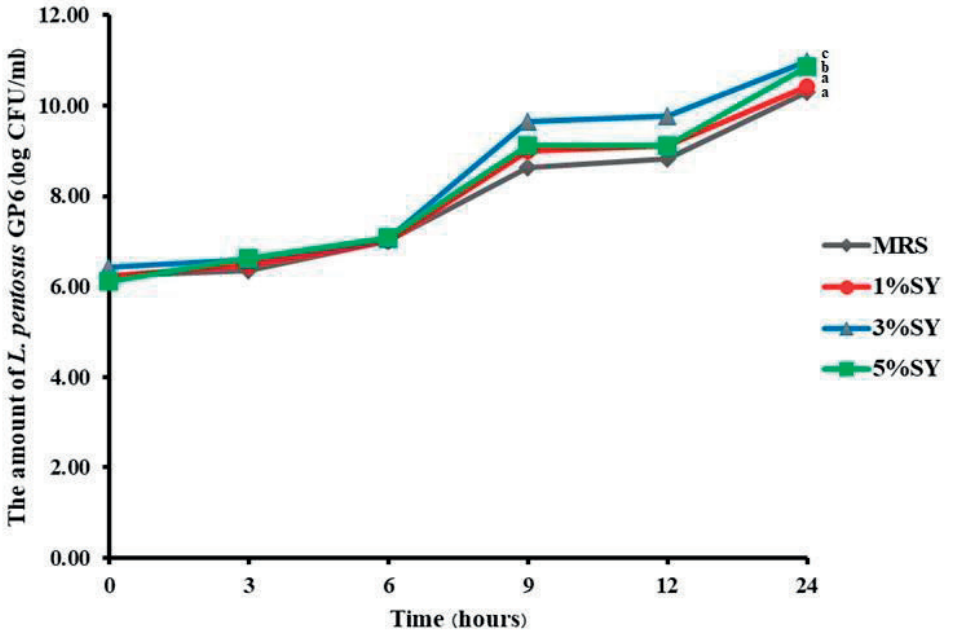

Figure 2. The growth of *L. pentosus* GP6 in MRS broth mixed with germinated Sang Yod brown rice powder at concentrations of 1, 3, and 5%, for which the various letters showed a significant mean difference ($p < 0.05$) in each added concentration of germinated Sang Yod brown rice powder.

The results obtained in this study showed that the probiotics could grow using the prebiotic as a carbon source. Several quantitative approaches have been devised to determine the functional activity of prebiotics under in vitro fermentation conditions. The previous research reported maximum Lactobacillus plantarum TISTR 875 growth in germinated Hang rice (3 and 5% w/v) of 4.5 log cfu/ml and 4.10 log cfu/ml, respectively [20]. Banana starch from Kluai Namwa Luang possessed the significantly highest probiotic growth promotion ability [21]. Moreover, to evaluate the prebiotic capacity of three commercial prebiotics, i.e., Frutafit, Oligomate 55, and lactulose, mostly probiotic bacteria isolated from commercial products grew faster on Frutafit and Oligomate 55 than on lactulose [22]. Another study reported that the fermentation of instant Sang-Yod rice porridge mixed with isomaltooligosaccharides produced from rice starch showed a good preference for prebiotic properties [23]. The growth and viability of *Lactobacillus rhamnosus* GR-1 in fermented rice pudding samples supplemented with one type of prebiotic were investigated. The results showed that adding short-chain inulin, long-chain inulin, and oat had no adverse supplementation effects on the viability of *L. rhamnosus* GR-1. There was the potential for producing a novel functional food [24].

The number of bacterial cells at all concentrations of germinated Sang Yod brown rice powder was higher than that of probiotics at the minimum therapeutic dose (at least 10^6 cfu/ml or 6 log cfu/ml [25-26]. However, germinated Sang Yod brown rice powder added to MRS broth at concentrations of 1, 3 and 5%, respectively, after incubation at 37 °C for 24 h, *L. pentosus* GP6 did not differ in the early fermentation period compared to the control. Inoculation growth was inversely proportional to the amount of germinated Sang Yod brown rice powder used. This may be due to the addition of germinated Sang Yod brown rice powder, causing an increase in the amount of nutrients or the concentration of the solution. The viscosity of the food, especially macromolecules such as biopolymers, increases the viscosity of the food, which may impede its transmission into cells. This causes the cells to take time to adapt early. However, over time, the macromolecule compounds were degraded and promoted inoculation thus at the end of the fermentation process, the count in MRS broth mixed with germinated Sang Yod brown rice powder was higher than in MRS broth control unit at 24 h of curing. In addition, the different concentrations of germinated Sang Yod brown rice powder showed a significantly different effect on the growth promotion of *L. pentosus* GP6 ($p < 0.05$). Thus, 3% of germinated Sang Yod brown rice powder was used as a prebiotic to produce a synbiotic dietary supplement product.

3.3 Production of synbiotic dietary supplements

The synergistic combination of probiotics and prebiotics leads to the formation of synbiotics. Synbiotics are the future-proof solution for novel and functional food [27]. Creating appropriate combinations of probiotic strains and nutraceutical mixtures remains key to developing multi-benefits synbiotic products because little information is known on nutraceuticals' effect on probiotics' viability [28]. In this study, we used 3% of germinated Sang Yod brown rice powder as the component of a synbiotic dietary supplement product. This product examined the amount of bacterial cells during storage conditions at 4 °C for 6 months. The result showed that *L. pentosus* GP6 survived and grew from 10.00-10.30 log cfu/ml (Figure 3). Moreover, the survival bacteria cells exhibited more than 10.00 log cfu/ml, or 97.09% survival rates compared with the amount of *L. pentosus* GP6 cells at the start period.

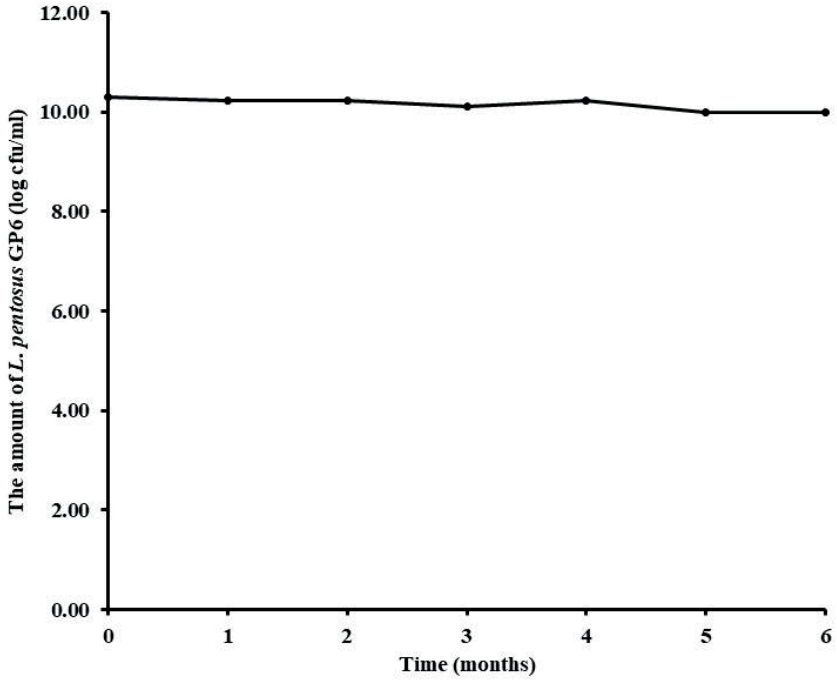

Figure 3. The amount of bacterial cells in synbiotic dietary supplement product during storage at 4 °C for 6 months.

4. Conclusions

The present study deals with the prebiotic property evaluation of germinated Sang Yod brown rice to support the growth of *L. pentosus* GP6 and the production of synbiotic dietary supplements. The germinated Sang Yod brown rice powder increased the growth of *L. pentosus* GP6; thus, germinated Sang Yod brown rice exhibited prebiotic properties. The 3% germinated Sang Yod brown rice powder was also used as a prebiotic to produce a synbiotic dietary supplement in conjunction with the probiotic *L. pentosus* GP6 strain.

5. Acknowledgements

The author would like to thank the Faculty of Agro and Bio-Industry, Thaksin University, for providing laboratory facilities. Office of National Higher Education Science Research and Innovation Policy Council, Thailand, supported this research.

Author Contributions: Conceptualization, methodology, testing, data curation, and writing—original draft preparation, N.D.

Funding: This work was supported by The Thailand Research Fund, Grant No.: 64A105000007.

Conflicts of Interest: The author declares no conflict of interest.

References

[1] Saman, P.; Fuciños, P.; Vázquez, J. A.; Pandiella, S. S. Fermentability of brown rice and rice bran for growth of human *Lactobacillus plantarum* NCIMB 8826. *Food Technology and Biotechnology*. **2011**, *49*(1), 128-132.

[2] Davani-Davari, D.; Negahdaripour, M.; Karimzadeh, I.; Seifan, M.; Mohkam, M.; Masoumi, S. J.; Berenjian, A.; Ghasemi, Y. Prebiotics: definition, types, sources, mechanisms, and clinical applications. *Foods*. **2019**, *8*(3), 92. https://doi.org/10.3390/foods8030092

[3] Abatenh, E.; Gizaw, B.; Tsegay, Z.; Tefera, G.; Aynalem, E. Health benefits of probiotics. *Journal of Bacteriology and Infectious Diseases*. **2018**, *2*(1), 8-27.

[4] Markowiak, P.; Śliżewska, K. Effects of probiotics, prebiotics, and synbiotics on human health. *Nutrients*. **2017**, *9*(9), 1021. https://doi.org/10.3390/nu9091021

[5] Sun, H.; Zhang, P.; Zhu, Y.; Lou, Q.; He, S. Antioxidant and prebiotic activity of five peonidin-based anthocyanins extracted from purple sweet potato (*Ipomoea batatas* (L.) *Lam.*). *Scientific Reports*. **2018**, *8*, 5018. https://doi.org/10.1038/s41598-018-23397-0.

[6] Suman, D.; Sreeja, V. Barley: A cereal with potential for development of functional fermented foods. *International Journal of Fermented Foods*. **2019**, *8*(1), 1-13. https://doi.org/10.30954/2321-712X.01.2019.1

[7] Rajendran, M.; Chandran, K. R. Grain dimension, nutrition and nutraceutical properties of black and red varieties of rice in India. *Current Research in Nutrition and Food Science*. **2020**, *8*(3), 903-923. https://dx.doi.org/10.12944/CRNFSJ.8.3.20

[8] Powthong, P.; Jantrapanukorn, B.; Suntornthiticharoen, P.; Laohaphatanalert, K. Study of prebiotic properties of selected banana species in Thailand. *Journal of Food Science and Technology*. **2020**, *57*(7), 2490-2500. https://doi.org/10.1007/s13197-020-04284-x

[9] Albuquerque, M. T. R.; Borges, C. W. P.; Cavalcanti, M. T.; Lima, M. S.; Magnani, M.; Souza, E. L. Potential prebiotic properties of flours from different varieties of sweet potato (*Ipomoea batatas* L.) roots cultivated in Northeastern Brazil. *Food Bioscience*. **2020**, *36*, 100614. https://doi.org/10.1016/j.fbio.2020.100614

[10] Harris, S.; Powers, S.; Monteagudo-Mera, A., Kosik, O.; Lovegrove, A.; Shewry, P.; Charalampopoulos, D. Determination of the prebiotic activity of wheat arabinogalactan peptide (AGP) using batch culture fermentation. *European Journal of Nutrition*. **2020**, *59*, 297-307. https://doi.org/10.1007/s00394-019-01908-7

[11] Boonchuay, P.; Wongpoomchai, R.; Jaturasitha, S.; Mahatheeranont, S.; Watanabe, M.; Chaiyaso, T. Prebiotic properties, antioxidant activity, and acute oral toxicity of xylooligosaccharides derived enzymatically from corncob. *Food Bioscience*. **2021**, *40*, 100895. https://doi.org/10.1016/j.fbio.2021.100895

[12] Juliano, B. O. *Rice in human nutrition*. Rome: FAO. 1993.

[13] Department of Intellectual Property. *Sangyod Muang Phatthalung Thailand rice (Geographical Indications: GI)*. Thailand: Ministry of Commerce. **2011**.

[14] Banchuen, J.; Thammarutwasik, P.; Ooraikul, B.; Wuttijumnong, P.; Sirivongpaisal, P. Increasing the bio-active compounds contents by optimizing the germination conditions of Southern Thai Brown Rice. *Songklanakarin Journal of Science and Technology*. **2010**, *32*(3), 219-230. http://rdo.psu.ac.th/sjstweb/index.php

[15] Subhasree, R.S.; Bhakyaraj, R.; Dinesh Babu, P. Evaluation of brown rice and germinated brown rice as an alternative substrate for probiotic food formulation using *Lactobacillus* spp. isolated from goat milk. *International Food Research Journal*. **2013**, *20*(5), 2967-2971.

[16] Mohamed, L. H.; Kabeir, B. M.; Mustafa, S. E.; Ibraheem, S. E. Prebiotic effect of different cereal bran (sorghum, barely and Millet) on growth of *Bifidobacterium longum* BB536 during fermentation of goat milk. *International Journal of Current Microbiology and Applied Sciences*. **2020**. *9*(10), 625-634. https://doi.org/10.20546/ijcmas.2020.910.074

[17] Dangmanee, N. Probiotic properties of *Lactobacillus pentosus* GP6 isolated from fermented ground pork. *Journal of Current Science and Technology*. **2018**, *8*(1), 41-49.

[18] Munarko, H.; Sitanggang, A. B.; Kusnandar, S.; Budijanto, S. Germination of five Indonesian brown rice: evaluation of antioxidant, bioactive compound, fatty acids, and pasting properties. *Food Science and Technology*. **2022**, *42*, e19721. https://doi.org/10.1590/fst.19721

[19] Soodpakdee, K.; Nacha, J.; Rattanachart, N.; Owatworakit, A.; Chamyuang, S. Fermentation with *Pleurotus ostreatus* enhances the prebiotic properties of germinated riceberry rice. *Frontiers in Nutrition*. **2022**. *9*, 839145. https://doi.org/10.3389/fnut.2022.839145

[20] Tayuan, C.; Ruksagul, N.; Sriputhong, R. Effect of germinated Hang rice on growth and viability of probiotic *Lactobacillus* during refrigerated storage. *International Food Research Journal*. **2016**, *23*(2), 889-893.

[21] Jaiturong, P.; Laosirisathian, N.; Sirithunyalug, B.; Eitssayeam, S.; Sirilun, S.; Chaiyana, W.; Sirithunyalug, J. Physicochemical and prebiotic properties of resistant starch from *Musa sapientum* Linn., ABB group, cv. Kluai Namwa Luang. *Heliyon*. **2020**, *6*, e05789. https://doi.org/10.1016/j.heliyon.2020.e05789

[22] Figueroa-González, I.; Rodríguez-Serrano, G.; Gómez-Ruiz, L.; García-Garibay, M.; Cruz-Guerrero, A. Prebiotic effect of commercial saccharides on probiotic bacteria isolated from commercial products. *Food Science and Technology*. **2019**, *39*(3), 747-753. https://doi.org/10.1590/fst.07318

[23] Plongbunjong, V.; Graidist, P.; Knudsen, K. E. B.; Wichienchot, S. Isomaltooligosaccharide synthesised from rice starch and its prebiotic properties in vitro. *International Journal of Food Science & Technology*. **2017**, *52*(12), 2589-2595. https://doi.org/10.1111/ijfs.13545

[24] Williams, M.; Hekmat, S. *Lactobacillus rhamnosus* GR-1 in fermented rice pudding supplemented with short chain inulin, long chain inulin, and oat as a novel functional food. *Fermentation*. **2017**, *3*(4), 55. https://doi.org/10.3390/fermentation3040055

[25] Dave, R. I.; Shah, N. P. Ingredient supplementation effects on viability of probiotic bacteria in yogurt. *International Journal of Dairy Science*. **1998**, *81*(11), 2804-2816. https://doi.org/10.3168/jds.S0022-0302(98)75839-4

[26] Samona, A.; Robinson, R. K. Effect of yoghurt cultures on the survival of *Bifidobacteria* in fermented milks. *International Journal of Dairy Technology*. **1994**, *47*(2), 58-60. https://doi.org/10.1111/j.1471-0307.1994.tb01273.x

[27] Florowska, A.; Hilal, A.; Florowski, T. Chapter 2 - Prebiotics and synbiotics. *Probiotics*. **2022**, 19-37. https://doi.org/10.1016/B978-0-323-85170-1.00018-X

[28] Awaisheh, S. S.; Haddadin, M.; Robinson, R. K. I. Incorporation of selected nutraceuticals and probiotic bacteria into fermented milk. *International Dairy Journal*. **2005**, *15*, 1184-1190. https://doi.org/10.1016/j.idairyj.2004.11.003

ASEAN
Journal of Scientific and Technological Reports
Online ISSN:2773-8752

Research article

Optimal Wind Power Plant Layout Using Ant Colony Optimization

Pongsak Makhampom[1], Jompob Waewsak[2*], Chana Chancham[3], Somphol Chiwamongkhonkarn[4], and Yves Gagnon[5]

[1] Faculty of Engineering, Thaksin University, Phatthalung, 93210, Thailand; 602995011@tsu.ac.th
[2] Research Center in Energy and Environment, Division of Physics, Faculty of Science, Thaksin University, Phatthalung, 39210, Thailand; jompob@tsu.ac.th
[3] Research Center in Energy and Environment, Division of Physics, Faculty of Science, Thaksin University, Phatthalung, 93210, Thailand; chi_phy_tsu@hotmail.com
[4] Faculty of Engineering, Thaksin University, Phatthalung, 93210, Thailand; dung_ding19@hotmail.com
[5] Université de Moncton Edmundston, New Brunswick, Canada; yves.gagnon@umoncton.ca
* Correspondence: jompob@tsu.ac.th

Citation:
Makhampom, P.; Waewsak, J.; Chancham, C.; Chiwamongkhonkarn, S.; Gagnon Y. Optimal wind power plant layout using ant colony optimization. *ASEAN J. Sci. Tech. Report.* **2024**, *27*(1), 44-57. https://doi.org/10.55164/ajstr.v27i1.250609

Article history:
Received: August 20, 2023
Revised: November 28, 2023
Accepted: November 30, 2023
Available online: December 28, 2023

Abstract: The optimal layout of wind power plants is very important as the arrangement of wind turbine generators (WTGs) profoundly affects the overall energy output of the wind power plant. To address this important issue, this research investigates the best layout for WTGs in wind power plants with different terrain features across three locations in Thailand using the Ant Colony Optimization (ACO) algorithm. The objective functions of maximizing the net annual energy production (AEP) and minimizing the wake losses were used to achieve the optimal wind power plant layout. Using the MERRA-2 database, computational fluid dynamics (CFD) wind flow modeling was performed to create 10x10 km^2 microscale wind resource maps of locations characterized by flat, semi-complex, and complex terrains to install wind power plants. The CFD wind flow modeling yielded wind speeds of 5.00 to 5.76, 4.21 to 8.90, and 3.10 to 4.45 m/s for the flat, semi-complex, and complex terrains, respectively, making them feasible for utility-scale wind power plants. WTGs of multiple blade diameters, ranging from 90 to 126 m, with a nominal capacity of 2.5 MW at 100 m above ground-level hub heights, were used in this study. The Gamesa G126-2.5MW WTG with a 126 m blade diameter produces the highest net AEP of 14.3, 76.1, and 38.9 GWh/yr for the three terrains. Hence, this WTG was used to perform an ACO-based optimization to improve the electricity production of the wind power plants. Such studies are important to improve the efficiency of wind power plants, thus extracting the maximum kinetic energy possible from the winds and improving the economic viability of wind power plants.

Keywords: Wind power plant; wind turbine generator; ant colony optimization; annual energy production; wake loss.

1. Introduction

With growing energy demand, concerns regarding global warming are also rising as most of our energy demand is met by burning greenhouse gas (GHG) emitting fossil fuels. Replacing fossil fuels with renewable sources is one of the most effective methods to combat the rising energy demand without polluting our environment. The adoption of renewable

energy is on the fast track, resulting in sources like wind becoming more common worldwide. The Global Wind Energy Council (GWEC) reports 93.7 GW of new wind energy installation in 2021, bringing the total global wind energy capacity to 837 GW, an increase of 12.4 % from 2020 [1]. For its part, Thailand heavily relies on fossil fuels to meet its rising energy demand [2]. However, the country has ambitious plans to diversify its energy mix by developing renewable energy sources.

Thailand's Alternative Energy Development Plan 2018-2037 (AEDP2018) will be the major roadmap for developing its energy sector. According to this plan, Thailand will have an installed capacity of 29,411 MW of renewable and alternative energy by 2037, of which 2,989 MW must come from wind energy [3]. Throughout the country, Thailand has nominal wind speeds averaging 4 to 5 m/s at 90 m above ground level (agl) [4]. However, specific locations in the country have sufficient wind resources to develop wind power. In parts of the Northeast, particularly near the Korat Plateau's edge and along the coast of Nakhon Si Thammarat Province, the relatively high wind speeds offer good wind energy development opportunities [5–7]. In addition, the central regions of the country along the Gulf of Thailand and the Andaman Sea also have relatively high wind energy development potentials [8-9]. The bay of Bangkok in the Gulf of Thailand has good wind speeds of 5.5-6.5 m/s at multiple heights simulated using CFD and Weather Research and Forecasting (WRF) atmospheric models offering wind energy production capacities ranging from 6,000-80,000 MW using different WTGs [10]. Using CFD wind flow modeling at multiple elevations, the wind potential of the Southernmost region of Thailand is assessed, resulting in a wind potential of 300 MW able to generate 690 GWh/year of electricity [11] A detailed wind resource mapping of the Nakhon Si Thammarat and Songkhla provinces in southern Thailand yielded a wind power generation protentional of 1,374 MW at 80 m agl and a 407 MW of wind energy using small wind turbines [12]. Finally, some studies even estimate the onshore wind energy potential of Thailand between 13 to 17 GW if given the proper regulatory and policy attention [13]. These studies suggest that Thailand has good onshore wind energy potential that can be developed to increase its renewable energy share in energy production. However, considering the social challenges faced by onshore wind energy developments, there should be a high emphasis on increasing the energy output from individual wind power plants and thus minimizing their numbers.

Wind power plants often cause visual and noise disturbances for residents living nearby [14]. Large wind turbines can cause significant visual disturbances and are facing increasing opposition from the public, especially from people living in highly aesthetic-valued areas [15]. With these factors influencing the development of new wind power plants, it is important to increase the energy output from the wind power plant to reduce the need for new wind power plant developments and to extract the maximum energy possible. One way of doing it is to improve the layout of the wind power plant by optimally arranging the WTGs since their wake significantly affects the overall energy output of the wind power plant.

Many studies have used various methods to design wind power plant layouts. Yang et al. [16] optimized the layout of a wind power plant to improve the energy output using the Simulated Annealing algorithm. Chen et al. [17] applied a Greedy algorithm to reduce the wake effect of multiple hub height WTGs on flat and complex terrains. Finally, using the objective function of levelized costs of energy (LCOE), multiple deterministic algorithms have been used to design optimal wind power plant layouts to reduce the LCOE in the presence of wake effects [18].

In this study, the layouts of the Pak Phanang Wind Farm, the Lamtakong Wind Farm, and the Romklao Wind Farm were optimized to increase the net AEP and to reduce the wake effects using the Ant Colony Optimization (ACO) algorithm. This study contributes to developing methodologies to improve the energy outputs from wind power plants and their economic efficiencies.

2. Materials and Methods

2.1 Study area

The terrains in Thailand are classified into five classes by the National Terrain Classification System (NTCS), as summarized in Table 1. This study considers three slope categories: flat, semi-complex, and complex terrains, as shown in Table 2, with their respective slope gradients.

Table 1. Slope classes are defined by the National Terrain Classification System (NTCS) of Thailand.

Slope Class	Gradient (%)
1	0 – 12
2	13 – 20
3	21 – 35
4	36 – 50
5	51+

Table 2. Practical slope descriptions.

Slope Class	Gradient (%)
Flat	0 – 20
Semi-complex	21 – 35
Complex	35+

Three wind power plant sites are studied (Fig. 1) to optimize their layout using the AOC algorithm. The Pak Phanang Wind Farm, located in southern Nakhon Si Thammarat province, has a flat terrain with a 3.73% slope gradient. The Lamtakong Wind Farm, situated in northeastern Nakhon Ratchasima province, has a semi-complex terrain with a 21.2% slope gradient. Finally, the Romklao Wind Farm, located in central Mukdaharn province, has a complex terrain with a 44.63% slope gradient.

2.2 Wind data

The wind data is a key component for the wind energy assessment of an area. This study used the MERRA-2 long-term wind database from 1985–2015 to generate virtual met masts (VMM). The MERRA-2 database presents wind speed and direction 50 m above ground level (agl). The positions of the three VMMs used in this study are given in Table 3. The average wind speeds for these VMM, based on the MERRA-2 wind database, are 4.21 m/s for the Pak Phanang Wind Farm, 4.34 m/s for the Lamthakong Wind Farm, and 4.23 m/s for the Romkhlao Wind Farm. The Weibull distribution analysis, presented in Fig. 2, reveals that the shape parameter (k) and the scale parameter (A) were as follows: Pak Phanang Wind Farm, k=2.686, A=4.738 m/s; Lamthakong Wind Farm, k=2.737, A=4.88 m/s; and Romkhlao Wind Farm, k=2.652, A=4.763 m/s.

2.3 Microscale wind resource map

Microscale wind resource maps are used to evaluate the technical power potential of the wind resources over the areas studied. CFD modeling was performed using the digital elevation model (DEM) presented in Fig. 3, roughness indices, and the wind data from the VMM for each site to determine the wind speeds within the domain of the three areas studied. These microscale wind resource maps were created using ArcGIS V10.2 with a spatial resolution of 90 m.

Table 3. The geographical position of three virtual met masts (VMM).

Wind Power Plant	Positions	Coordinate	
		Latitude	Longitude
Pak Phanang Wind Farm	Pak Phanang District, Nakhon Si Thammarat Province	8° 23' 13.71'' N	100° 14' 5.4'' E
Lamtakong Wind Farm	Sikhio District, Nakhon Ratchasima Province	14° 49' 0.2'' N	101° 33' 33.3'' E
Romkhlao Wind Farm	Nikhom Kham Soi District, Mukdahan Province	16° 22' 49.2'' N	104° 24' 51.1'' E

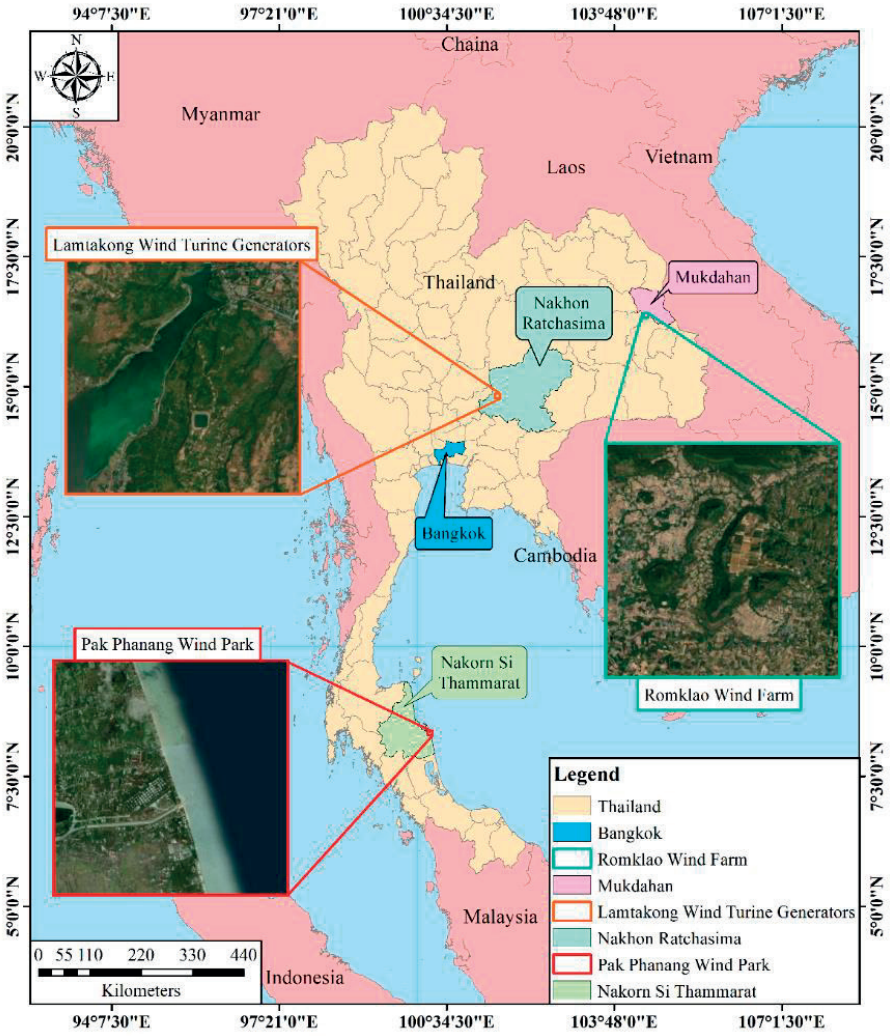

Figure 1. The Pak Phanang Wind Farm, the Lamtakong Wind Farm, and the Romklao Wind Farm.

2.4 Wind turbine generator

Multiple WTGs with a rated power of 2.5 MW and having different rotor diameters were tested in this study to find the optimal WTG to maximize the AEP and minimize the wake losses. The characteristics of the WTGs studied are presented in Table 4. Each WTG has a unique power curve, with power characteristics based on the cut-in wind speed (c_i), the cut-out wind speed (c_o), and the rated wind speed (v_{tated}). It is shown in Fig. 4.

Table 4. Characteristics of the wind turbine generators studied.

Hub Height (m)	Manufacturer/Model	Rated Power (MW)	Rotor Diameter (m)	Cut-in Speed (m/s)	Cut-out Speed (m/s)
100	Nordex N90/2500	2.5	90	3.0	25.0
100	Fuhrländer FL 2500/100	2.5	100	3.5	25.0
100	General Electric GE 2.5-103	2.5	103	3.0	25.0
100	FWT 104/2500	2.5	104	3.0	25.0
100	Gamesa G126-2.5MW	2.5	126	2.0	21.0

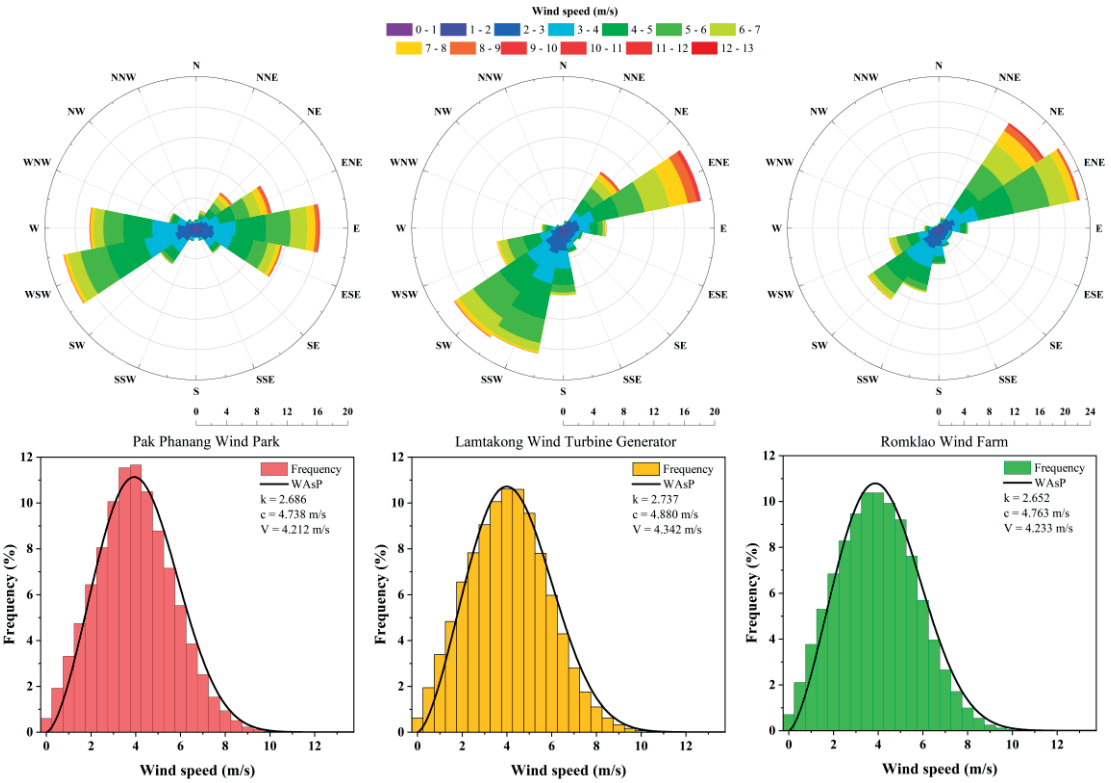

Figure 2. The wind roses and Weibull distributions at an elevation of 50 m agl based on the MERRA-2 database for the three sites studied.

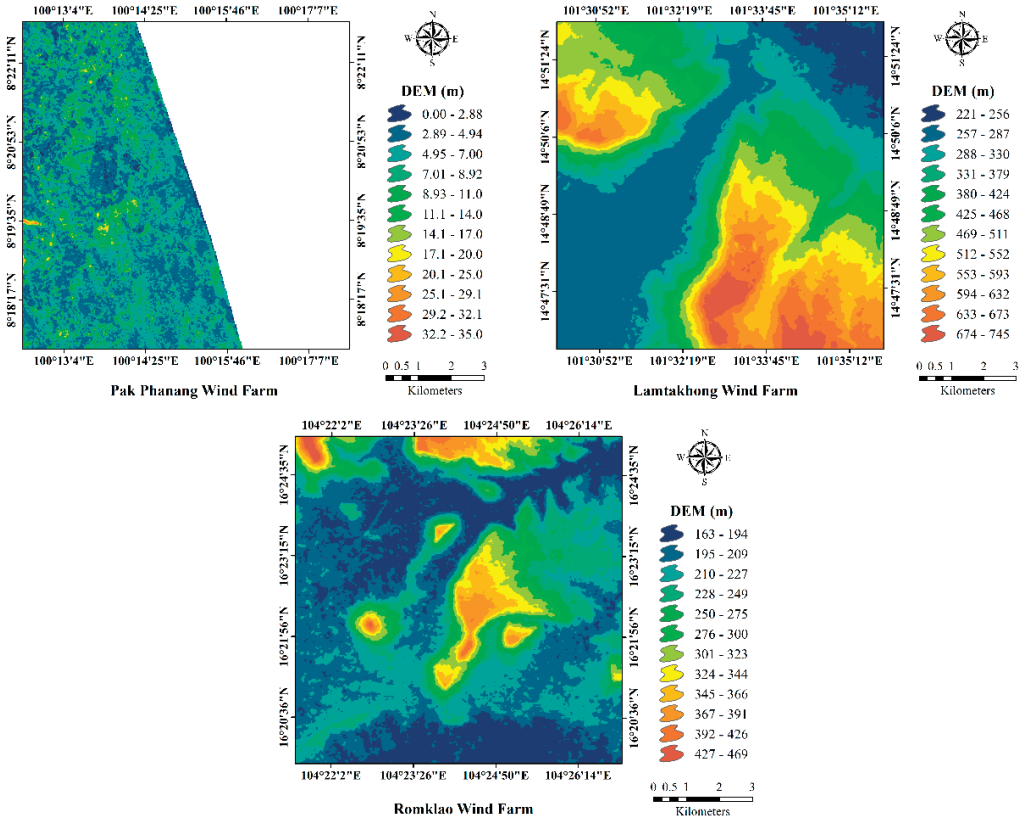

Figure 3. The digital elevation model (DEM) was used in this study.

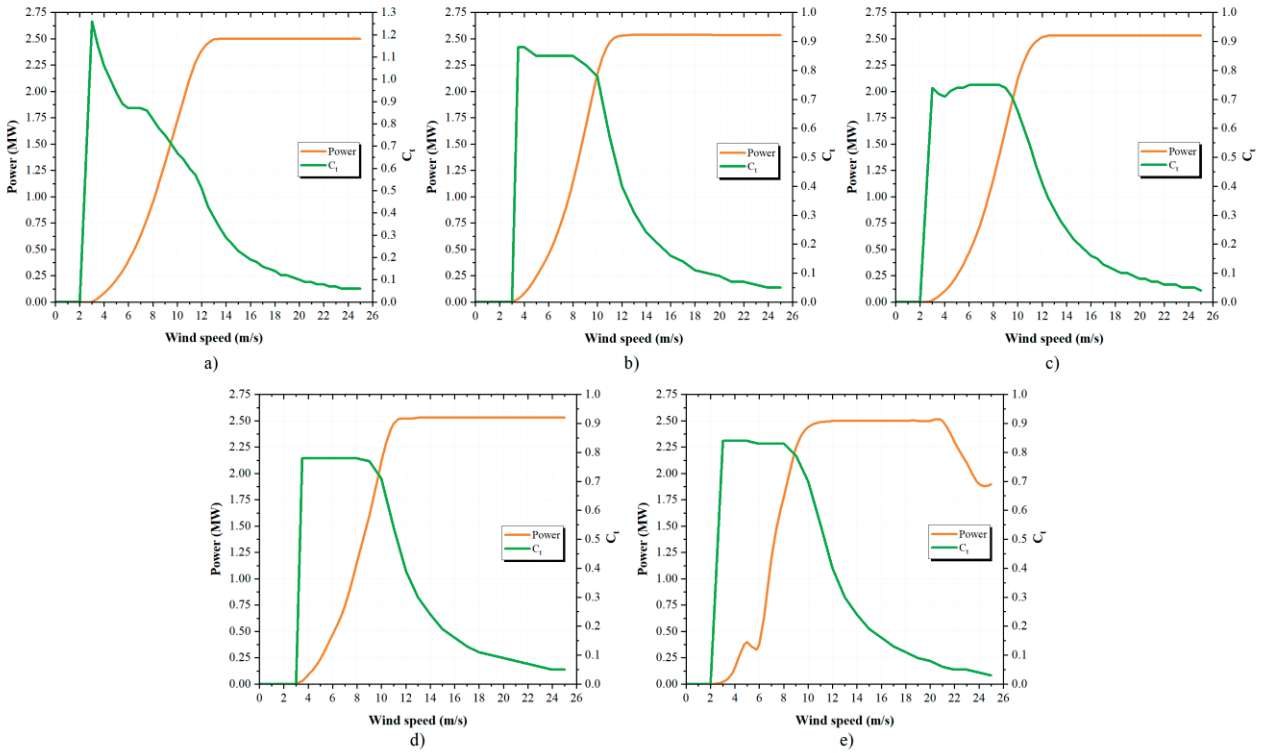

Figure 4. The power curves of the wind turbine generators studied: a) Nordex N90/2500; b) Fuhrländer FL 2500/100; c) General Electric GE 2.5-103; d) FWT 104/2500; and e) Gamesa G126-2.5MW.

2.5 Ant colony optimization algorithm

The Ant Colony Optimization (ACO) algorithm was developed for discrete optimization problems based on the ant colony's food-searching behavior. The ACO is a multistep optimization process, similar to an ant randomly finding food and leaving a chemical trail for its colony to follow to find the food source to bring back to the nest [19].

The ACO algorithm used in this study was performed using a MATLAB code. A study by Eroglu [19] used an objective function to locate the WTG with the x-y coordinate system at the specified distance between the WTG and the total power generated by the WTG.

The energy produced by the WTG is expressed as a linear equation. This shows that the energy produced depends on the wind speed, consisting of three parts, as shown in Eq. 1 [20]. In Part 1 is the wind speed that is less than the cut-in wind speed v_{cutin} which is the lowest wind speed at which the WTG starts to generate electricity, with the electrical power produced equal to 0. In Part 2, a linear equation as a function of the wind speed is applied between v_{cutin} and v_{rated} Which is the speed at which the nominal power of the WTG is determined. This linear equation consists of a slope. (λ) and a constant (η) to define the power curve. In Part 3, the WTG produces power at it nominal capacity (P_{rated}) between the rated wind speed v_{rated} and the cut-out wind speed v_{cutout}.

$$f(v) = \begin{Bmatrix} 0 & v < v_{cutin} \\ \lambda * v + \eta & v_{cutin} \leq v \geq v_{rate} \\ P_{rate,} & v_{cutout} > v > v_{rated} \end{Bmatrix} \quad (1)$$

Considering that the wind characteristics can be described by the Weibull distribution, which depends on the wind speed, the electrical energy produced can be expressed as in Eq. 2.

$$P(\theta) = \int_0^{\infty} f(v) p_v\big(v, k(\theta), c(\theta)\big)\, dv = \int_0^{\infty} f(v) \frac{k(\theta)}{c(\theta)} \left(\frac{v}{k(\theta)}\right)^{k(\theta)-1} e^{-\left(v/c(\theta)\right)^{k(\theta)}} dv \tag{2}$$

Where k is the shape parameter, $c(\theta)$ is the scale parameter at the direction (θ). The Weibull function depends on the wind direction and wind speed (v), whose direction is from 0° to 360°. Eq. 2 can be written as Eq. 3.

$$P(\theta) = \int_0^{360} p\,(\theta) d\theta \int_0^{\infty} f\,(v) \frac{k(\theta)}{c(\theta)} \left(\frac{v}{c(\theta)}\right)^{k(\theta)-1} e^{-\left(v/c(\theta)\right)^{k(\theta)}} dv \tag{3}$$

Eq. 3 shows that the wind speed is continuous. The wind speed is divided into equal ranges, described in terms of $N_v + 1$ from v_{cutin} to v_{rated}, with wind speed starting from $v_1, v_2, v_3, \ldots . v_{N_v}$ and $v_{cutin} < v_1, v_2, v_3, \ldots . , v_{N_v} < v_{rated}$ when $v_0 = v_{cutin}$ and $v_{N_v+1} = v_{rated}$. The energy produced by the WTG can be obtained from Eq. 4.

$$\begin{aligned} P = \lambda \sum_{l=1}^{N_v+1} \left(\frac{v_{j-1} + v_j}{2}\right) \int_0^{360} p_\theta\,(\theta) \left\{ e^{-\left(\frac{v_{j-1}}{c_i(\theta)}\right)^{k\theta}} - e^{-\left(\frac{v_j}{c_i(\theta)}\right)^{k\theta}} \right\} d\theta \\ + P_{rated} \int_0^{360} p_\theta\,(\theta) e^{-\left(\frac{v_{rated}}{c_i(\theta)}\right)^{k\theta}} d\theta \\ + \eta \int_0^{360} p_\theta(\theta) \left\{ e^{-\left(\frac{v_{cutin}}{c_i(\theta)}\right)^{k(\theta)}} - e^{-\left(\frac{v_{rated}}{c_i(\theta)}\right)^{k(\theta)}} \right\} d\theta \end{aligned} \tag{4}$$

where $c_i(\theta)$ is the scale parameter at the wind direction θ after the wake effect is calculated from Eq. 5, while Eq. 6 computes the decreasing speed Vel_def at a distance d of the WTGs.

$$c_i(\theta) = c(\theta) \times (Vel\_def) \tag{5}$$

$$Vel\_def = \left(1 - \frac{\sqrt{1 - C_T}}{(1 + kd/R)^2}\right) \tag{6}$$

In this research, the wind speed range is divided into 16 sectors, where $N_v + 1 = 16$, so the energy generated by the WTG can be calculated from Eqs. 7-9.

$$\begin{aligned} P_\lambda = \lambda \sum_{l=1}^{N_v+1} \left(\frac{v_{j-1} + v_j}{2}\right) \sum_{l=1}^{N\theta+1} (\theta_{l=1} - \theta_l) w_{l-1} \\ \times \left\{ e^{-\left(\frac{v_{j-1}}{c_i\left(\frac{\theta_{l-1}+\theta_l}{2}\right)}\right)^{k\left(\frac{\theta_{l-1}+\theta_l}{2}\right)}} - e^{-\left(\frac{v_j}{c_i\left(\frac{\theta_{l-1}+\theta_l}{2}\right)}\right)^{k\left(\frac{\theta_{l-1}+\theta_l}{2}\right)}} \right\} \end{aligned} \tag{7}$$

$$P_r = P_{rated} \sum_{l=1}^{N\theta+1} (\theta_{l-1} - \theta_l) w_{l-1} e^{-\left(\frac{v_{rated}}{c_i\left(\frac{\theta_{l-1}+\theta_l}{2}\right)}\right)^{k\left(\frac{\theta_{l-1}+\theta_l}{2}\right)}} \tag{8}$$

$$P_\eta = \eta \sum_{l=1}^{N\theta+1} (\theta_{l-1} - \theta_l) w_{l-1} \times \left\{ e^{-\left(\frac{v_{cutin}}{c_i\left(\frac{\theta_{l-1}+\theta_l}{2}\right)}\right)^{k\left(\frac{\theta_{l-1}+\theta_l}{2}\right)}} - e^{-\left(\frac{v_{rated}}{c_i\left(\frac{\theta_{l-1}+\theta_l}{2}\right)}\right)^{k\left(\frac{\theta_{l-1}+\theta_l}{2}\right)}} \right\} \tag{9}$$

where P_λ is the power in relation to the slope in the linear equation of the power curve (kW); P_r is the energy in relation to the maximum power that the wind turbine can produce (kW); and P_η is the power in relation to the constant in the linear equation of the power curve (kW).

From Eqs. 7-9, the electric power of a WTG can be calculated from Eq. 10 and the electricity generated by a wind power plant can be calculated from Eq. 11.

$$P_i = P_\lambda + P_r + P_\eta \tag{10}$$

$$P_f = \sum_{i=l}^{N_t} P_i \tag{11}$$

where P_i is the electric power as the WTG can produce (kW) and P_f is the total electrical energy generated from wind power plants (kW).

2.6 Analysis of electric power produced from wind power

For the electric power analysis, the Gross Annual Energy Production ($Gross\ AEP$), the Net Annual Energy Production ($Net\ AEP$), and the wind power generation efficiency calculated as a capacity factor (CF) was assessed. A higher Net AEP value indicates good wind energy production capacity in the targeted areas and is calculated using Eq 12.

$$Net\ AEP = Gross\ AEP - Wake\ Loss \tag{12}$$

The Gross AEP is calculated using the ACO algorithm, and the wake loss is the electricity production lost due to the wake effects of the WTGs in the wind power plant. The N.O. Jensen wake model was used in this investigation. The optimum layout of a considered wind power plant was simulated to analyze wake loss in WindSim computer software [23].

CF is defined as the availability of a WTG to produce electricity in a year and is given by Eq. 13 [24]. The CF of a WTG also indicates the efficiency of the WTG.

$$CF = \left(\frac{Net\ AEP}{Rated\ Capacity \times 8{,}760}\right) \times 100\% \tag{13}$$

3. Results and Discussion

3.1 Annual and Mean Wind Speeds

Generally, the shear coefficient is used to estimate wind velocity at higher elevations using the measurements from metrological instruments at lower elevations. The Power Law equation is the most well-known equation for calculating the shear coefficient [21,22], and it was used in this study to estimate the wind

speed at 100 m agl based on the VMM reading at 50 m agl. The annual wind speeds of the targeted wind power plants were calculated at 100 m agl. The variation amongst flat, semi-complex, and complex terrain is not significant, with average annual wind speeds of 4.64, 4.79, and 4.67 m/s at Pak Phanang district of Nakhon Si Thammarat province, Sikhio district of Nakhon Ratchasima province and Nikhom Kham Soi District Mukdahan province, respectively. Similarly, the shape parameters in the study areas were 2.69, 2.74, and 2.65, respectively, while the scale parameters were 5.22, 5.38, and 5.25 m/s, respectively.

Using the WindSim tool, microscale wind resource maps, with a size of 10x10 km^2 and a 50 m resolution, were created for the three study areas, as shown in Fig. 5. The average annual wind speeds, at 100 m agl, at the targeted wind power plants of Pak Phanang Wind Farm, Lamtakong Wind Farm, and Romklao Wind Farm ranges from 5.00 to 5.76, 3.1 to 6.45, and 4.21 to 8.90 m/s, respectively.

3.2 Optimal suitability of wind power plants

Using the ACO algorithm in MATLAB, the optimization of the wind power plants was done. With 600 iterations and a processing time of 3.2 to 3.6 hours, the electricity produced in flat terrain Pak Phanang Wind Farm was between 8.6 and 14.3 GWh/yr using multiple WTGs, as shown in Tables 5 and 6. With 14.3 GWh/yr and a CF of 16.31%, the Gamesa G126-2.5MW wind turbine produced the highest AEP, while the Nordex N90/2500 WTG produced the least amount of AEP with 8.6 GWh/yr.

Similarly, with 400 iterations and a processing time of 2.1 hours, the electricity production in the semi-complex Lamtakong Wind Farm was in the range of 52.9 to 72.2 GWh/yr, as shown in Tables 7 and 8. The Gamesa G126-2.5MW WTG produced the highest AEP and CF with 72.2 GWh/yr and 29.0%, respectively, while the Nordex N90/2500 WTG produced the least amount of AEP with 52.9 GWh/yr.

Table 5. AEP of each wind turbine in flat terrain

WTG	HH (m)	No. of WTG	Capacity (MW)	Gross AEP (GWh/y)	V_{avg} (m/s)	Wake Losses (%)	Net AEP (GWh/y)	CF (%)
N90/2500	100	4	10	9.7	4.70	10.9	8.6	9.9
FL 2500/100	100	4	10	11.3	4.68	1.7	11.1	12.6
GE 2.5-103	100	4	10	11.6	4.68	15.1	9.8	11.2
FWT 104/2500	100	4	10	11.3	4.68	4.9	10.7	12.3
G126-2.5MW	100	4	10	15.4	4.70	7.2	14.3	16.3

Note: HH = Hub Height; WTG = Wind Turbine Generator

Table 6. Iteration and time consumption in flat terrain

Turbine	Iterations	Time Consumptions (hr)
N90/2500	600	3.63
FL 2500/100	600	3.22
GE 2.5-103	600	3.20
FWT 104/2500	600	3.23
G126-2.5MW	600	3.18

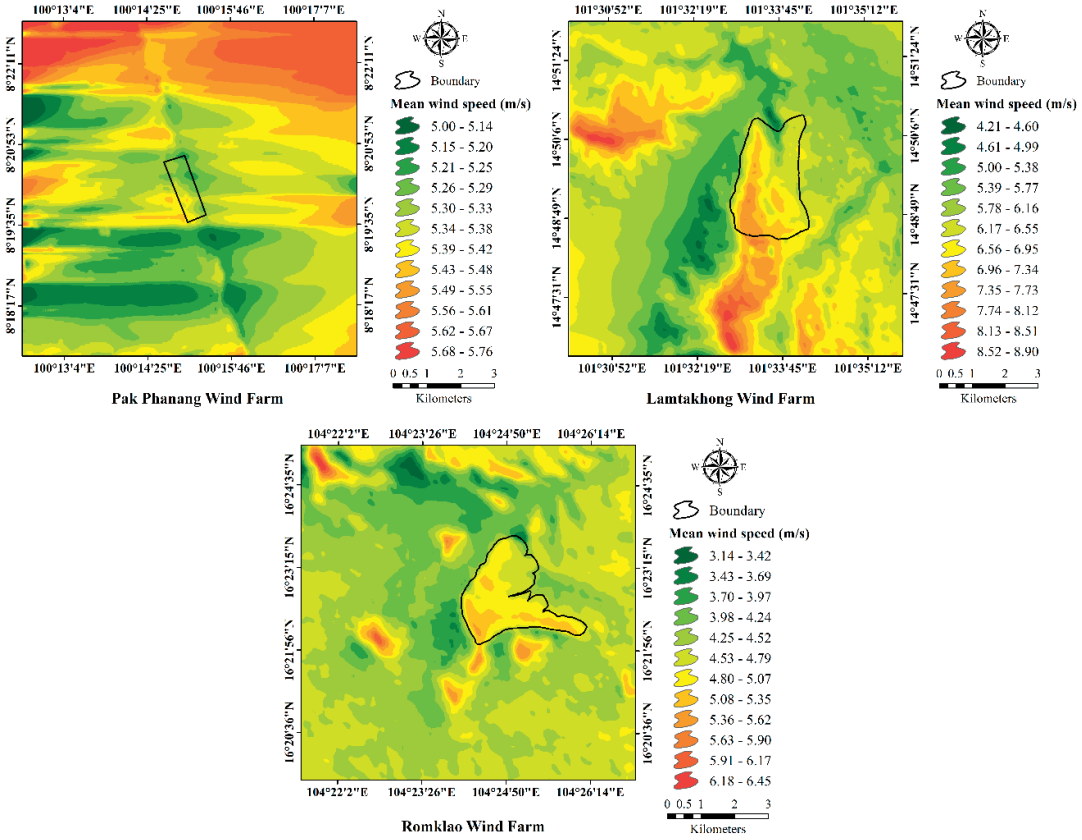

Figure 5. The average annual wind speeds of in the region of the Pak Phanang Wind Farm, the Lamtakong Wind Farm, and the Romklao Wind Farm.

Table 7. AEP of each wind turbine in semi-complex terrain

Turbine	HH (m)	No. of WTG	Capacity (MW)	Gross AEP (GWh/y)	V_{avg} (m/s)	Wake Losses (%)	Net AEP (GWh/y)	CF (%)
N90/2500	100	12	30	55.7	5.8	5.1	52.9	20.11
FL 2500/100	100	12	30	64.3	5.8	6.0	60.4	23.00
GE 2.5-103	100	12	30	65.3	5.8	5.6	61.6	23.46
FWT 104/2500	100	12	30	61.0	5.6	5.1	57.9	22.03
G126-2.5MW	100	12	30	81.5	5.8	6.6	76.1	28.97

Note: HH = Hub Height; WTG = Wind Turbine Generator

Table 8. Iteration and time consumption in semi-complex terrain

Turbine	Iterations	Time Consumptions (hr)
N90/2500	400	2.08
FL 2500/100	400	2.18
GE 2.5-103	400	2.17
FWT 104/2500	400	2.08
G126-2.5MW	400	2.13

In the same way, 800 iterations were performed for the complex terrain of Romklao Wind Farm with a processing time of 4.17-5.02 hours. The electricity production ranged from 22.8 to 38.9 GWh/yr using multiple WTGs, as summarized in Tables 9 and 10. Similarly to the other two wind power plant sites, the

Gamesa G126-2.5MW produced the highest AEP and CF of 38.9 GWh/yr and 13.7%, respectively, while the Nordex N90/2500 produced the least AEP of 22.8 GWh/yr with the lowest CF of 8.0%.

In all three wind power plants with distinct terrains, the Gamesa G126-2.5MW wind turbine performed better, producing the highest AEP and CF with relatively low wake losses. This is due to its larger rotor diameter and lower cut-in speed. Therefore, the final optimization of all three targeted wind power plants was done using this WTG. Using the Gamesa G126-2.5 MW WTG, the ACO-optimized layout of the flat, semi-complex, and complex terrain wind power plants produced net AEP of 14.3, 76.1, and 38.9 GWh/yr, thus improving the electricity production of the wind power plants. The ACO-based optimized wind power plant layouts are presented in Figs 6 - 8. The optimized layouts have significant differences in the positions of WTGs compared to the original layout.

Table 9. AEP of each wind turbine in complex terrain

WTG	HH (m)	No. of WTG	Capacity (MW)	Gross AEP (GWh/y)	V_{avg} (m/s)	Wake Losses (%)	Net AEP (GWh/y)	C.F. (%)
N90/2500	100	13	32.5	25.2	4.32	9.3	22.8	8.0
FL 2500/100	100	13	32.5	32.5	4.46	7.1	30.2	10.6
GE 2.5-103	100	13	32.5	36.7	4.58	2.7	35.7	12.53
FWT 104/2500	100	13	32.5	30.6	4.37	10.0	27.5	9.7
G126-2.5MW	100	13	32.5	42.7	4.38	9.1	38.9	13.7

Note: HH = Hub Height; WTG = Wind Turbine Generator.

Table 10. Iteration and time consumption in complex terrain

Turbine	Iterations	Time Consumptions (hr)
N90/2500	800	5.02
FL 2500/100	800	4.17
GE 2.5-103	800	4.18
FWT 104/2500	800	4.22
G126-2.5MW	800	4.23

4. Conclusions

Wind energy is one of the important renewable energy sources and, along with solar energy, is becoming a primary source. An important challenge in wind power development is optimizing the power production, where wind power plant operators work to maximize the energy output. One way to improve the energy output from wind power plants is by optimizing their layout, as the positions of the WTGs in the wind power plants profoundly affect the overall energy output due to their wake effects. It is, therefore very important to plan an optimal wind power plant layout in the design phase of the development, as the positions of the WTGs cannot be changed after installation.

To achieve this target, this study employed the Ant Colony Optimization (ACO) algorithm to optimize the layout of wind power plants, with the objective functions of increasing the annual energy production (AEP) and the capacity factor (CF) of the plant, while reducing the wake effects. Three wind power plants in different parts of Thailand, i.e., Pak Phanang Wind Farm, Lamtakong Wind Farm, and Romklao Wind Farm, have been studied, having flat, semi-complex, and complex terrains, respectively. Using the MERRA-2 long-term wind database, CFD wind flow modeling was used to map the microscale wind resource maps over the study areas, which revealed acceptable wind speeds for utility-scale wind power plants.

The optimization used multiple commercially available WTGs with different rotor diameters and power characteristics to find the ideal WTG producing the highest AEP and CF with relatively low wake losses. The Gamesa G126-2.5MW WTG performed the best in all three wind power plant locations, producing

the highest AEP of 14.3, 76.1, and 38.9 GWh/y in flat, semi-complex, and complex terrains, respectively, with relatively low wake losses making it the ideal WTG for the layout optimization. Optimizing the layout improved The net AEP for the wind power plants. Such studies are important to improve the efficiency of wind power plants, thus extracting the maximum kinetic energy possible from the winds and improving the economic viability of wind power plants. However, the comparison between metaheuristic algorithms should be performed for further study.

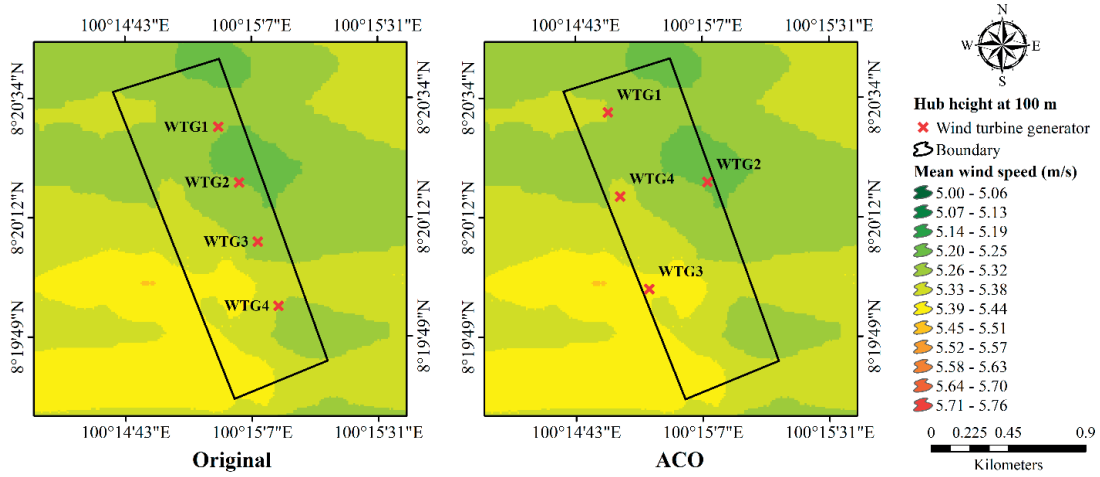

Figure 6. The original (left) and ACO (right) wind turbine locations in the Pak Phanang Wind Farm.

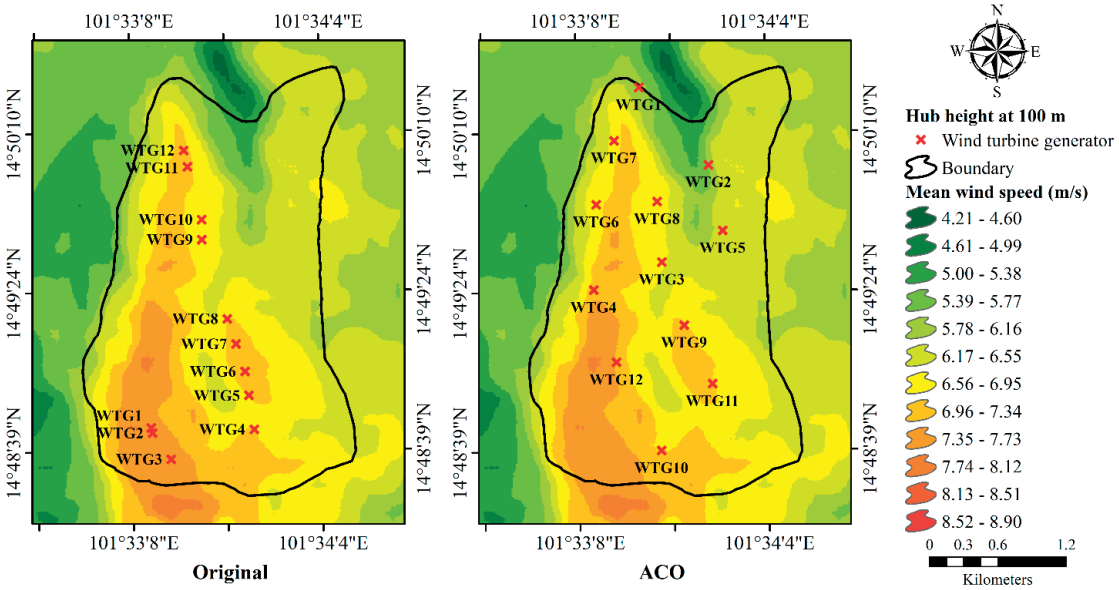

Figure 7. The original (left) and ACO (right) wind turbine locations in the Lamtakong Wind Farm.

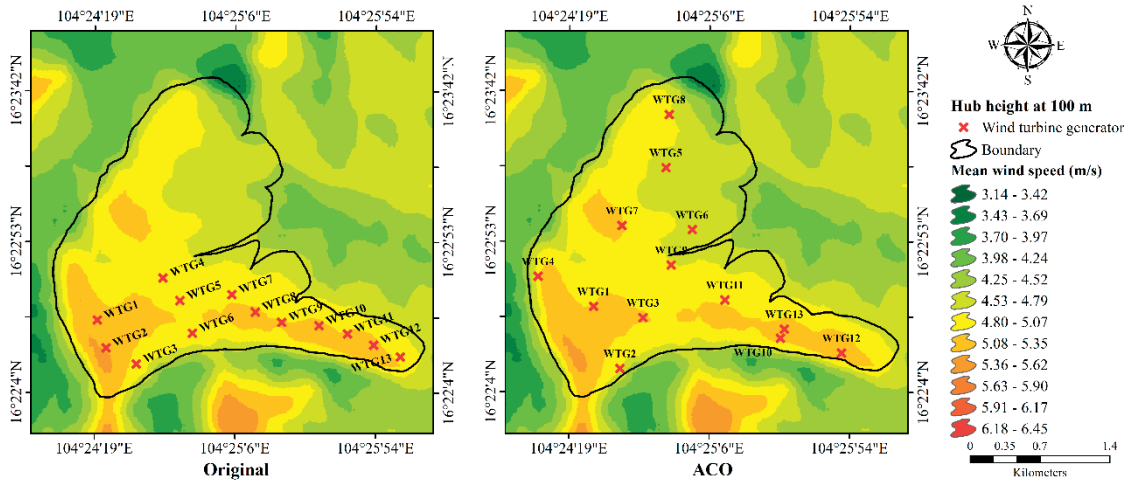

Figure 8. The original (left) and ACO (right) wind turbine locations in the Romklao Wind Farm.

5. Acknowledgements

This study was supported by the Energy Conservation and Promotion Fund Office (ENCON Fund) through graduate research funds. The authors thank the Research Center in Energy and Environment, Thaksin University (Phatthalung Campus), for providing the research tools and assistance.

Author Contributions: Conceptualization, J.W., Investigation. Writing – original draft preparation, P.M.; Project administration. Funding acquisition. Methodology. Visualization, J.W.; Software, C.C., and S.C.; Analysis and validation of results, J.W. and Y.G.; Writing – review & editing J.W. and Y.G. All authors have read and agreed to the published version of the manuscript.

Funding: The Energy Conservation and Promotion Fund Office (ENCON Fund) provided funding for this project on 2019 fiscal year.

Conflicts of Interest: The authors declare no conflict of interest.

References

[1] GWEC, Global Wind Energy Council, Global wind report 2022, Wind Energy Technol. **2022**. 75. https://gwec.net/global-wind-report-2022/.

[2] EGAT, EGAT Report. **2018**. https://www.egat.co.th/en/images/publication/EGAT-Overview-2018_en.pdf (accessed June 8, 2023)

[3] Department of Alternative Energy Development and Efficiency. Percentage of Alternative Energy Consumption. **2023a**. Retrieved from https://www.dede.go.th/download/state_66/Percentage _of_ Alternative_Energy_Consumption_November_2565.pdf (accessed: 20.12.2023)

[4] Department of Alternative Energy Development and Efficiency. The Alternative Energy Development Plan 2018-2037 (AEDP2018). **2023b**. Retrieved from https://www.dede.go.th/download/Plan_62/20201021_ TIEB_AEDP2018.pdf (accessed: 20.12.2023)

[5] Puangkaew, W.; Waewsak, J.; Kongruang, C.; Chancham, C.; Matan, N.; Tirawanichakul, Y.; Tirawanichakul, S. Assessment of Wind Energy Resource and Feasibility of Installing 0.225-0.75 MW Wind Power Plants along the Coast of Nakhon Si Thammarat and Songkhla Provinces. *Thaksin University Journal*. **2010**, *12*, 129–137.

[6] Chiwamongkhonkarn, S.; Waewsak, J.; Chaichana, T. Wind Resource Potential at Pak Phanang and Chian Yai Districts of Nakhon Si Thammarat Province. *Thaksin University Journal*. **2014**, *17*, 13–20.

[7] Chiwamongkhonkarn, S.; Waewsak, J.; Chancham, C. Forecasting of Wind Speed Using Advanced Research-WRF Model. *Thaksin University Journal*. **2020**, *23*, 20–30.

[8] Ranthodsang, M.; Waewsak, J.; Kongruang, C.; Gagnon, Y. Offshore wind power assessment on the western coast of Thailand. *Energy Reports.* **2020**, *6*, 1135–1146. https://doi.org/10.1016/j.egyr.2020.04.036

[9] Waewsak, J.; Niyomtham, L.; Cheewamongkholkarn, S.; Chancham, C. Offshore Wind Resource Assessment of Thailand Using Remote Sensing Technique. *ASEAN Journal of Scientific and Technological Reports*, **2021**, *24*(1), 71–83. https://doi.org/10.55164/ajstr.v24i1.226833

[10] Chancham, C., Waewsak, J., Gagnon, Y., Offshore wind resource assessment and wind power plant optimization in the Gulf of Thailand, *Energy*. **2017**, *139*, 706–731. https://doi.org/10.1016/j.energy.2017.08.026

[11] Waewsak, J., Chancham, C., Chiwamongkhonkarn, S., Gagnon, Y., Wind Resource Assessment of the Southernmost Region of Thailand Using Atmospheric and Computational Fluid Dynamics Wind Flow Modeling. *Energies.* **2019**, *12*(10), 1899. https://doi.org/10.3390/EN12101899

[12] Waewsak, J.; Landry, M.; Gagnon, Y. High-resolution wind atlas for Nakhon Si Thammarat and Songkhla provinces, Thailand, Renew. *Energy*. **2013**, *53*, 101–110. https://doi.org/10.1016/j.renene.2012.11.009

[13] An Industry Perspective on Strengthening Onshore Wind Development in Thailand. https://ec.europa.eu/eurostat/statistics-. (accessed April 29, 2023)

[14] Leung D.Y.C.; Yang, Y. Wind energy development and its environmental impact : A review, Renew. Sustain. *Energy Rev*. **2012,** *16*. 1031–1039. https://doi.org/10.1016/j.rser.2011.09.024

[15] Molnarova, K.; Sklenicka, P.; Stiborek, J.; Svobodova, K.; Salek, M.; Brabec, E. Visual preferences for wind turbines : Location, numbers and respondent characteristics, Appl. *Energy*. **2012**, *92*, 269–278. https://doi.org/10.1016/j.apenergy.2011.11.001

[16] Yang, K.; Kwak, G.; Cho, K.; Huh, J. Wind farm layout optimization for wake effect uniformity. *Energy*. **2019**, *183*, 983–995. https://doi.org/10.1016/j.energy.2019.07.019

[17] Chen, K.; Song, M.X.; Zhang, X.; Wang, S.F. Wind turbine layout optimization with multiple hub height wind turbines using a greedy algorithm, Renew. *Energy*. **2016**, *96*, 676–686. https://doi.org/10.1016/j.renene.2016.05.018

[18] Nagpal, S.V.; Liu, M.V.; Anderson, C.L. A comparison of deterministic refinement techniques for wind farm layout optimization, Renew. *Energy*. **2021**, *168*, 581–592. https://doi.org/10.1016/j.renene.2020.12.043

[19] Eroğlu, Y.; Seçkiner, S.U. Design of wind farm layout using ant colony algorithm, Renew. *Energy*. **2012**, *44*, 53–62. https://doi.org/10.1016/j.renene.2011.12.013

[20] Yunus, E. Wind farm layout optimization using ant colony and particle filtering approaches Wind Farm Layout Optimization using Ant Colony and Particle Filtering Approaches in Industrial Engineering Publication (https://doi.org/10.13140/RG.2.2.11304.26883) [Master Thesis University of Gaziantep]. **2017**.

[21] Werapun, W.; Tirawanichakul, Y.; Waewsak, J. Wind Shear Coefficients and their Effect on Energy Production. *Energy Procedia*. **2017**, *138*, 1061–1066. https://doi.org/10.1016/J.EGYPRO.2017.10.111

[22] Islam, K.D.; Theppaya, T.; Ali, F.; Waewsak, J.; Suepa, T.; Taweekun, J.; Titseesang, T.; Techato, K. Wind energy analysis in the coastal region of bangladesh. *Energies*. **2021**, *14*, 1–18. https://doi.org/10.3390/en14185628

[23] WindSim-CFD wind flow modeling www.windsim.com (Accessed on 28 November 2022).

[24] Waewsak, J.; Kongruang, C.; Gagnon, Y.; Assessment of wind power plants with limited wind resources in developing countries: Application to Ko Yai in southern Thailand. *Sustainable Energy Technologies and Assessments*. **2017**, *19*, 79-93.

ASEAN
Journal of Scientific and Technological Reports
Online ISSN:2773-8752

Research article

Study of Orbit Motion of Hydrogen and Deuterium Beam Ions Toward Neutral Beam Injection Experiment in Thailand Tokamak-1

Pitchayada Wangkhahat[1], Siriyaporn Sangaroon[2*], Apiwat Wisitsorasak[3], Kunihiro Ogawa[4], Nopporn Poolyarat[5], and Mitsutaka Isobe[6]

[1] Faculty of Science, Mahasarakham University, Maha Sarakham, 44150, Thailand; 63010212041@msu.ac.th
[2] Faculty of Science, Mahasarakham University, Maha Sarakham, 44150, Thailand; siriyaporn.s@msu.ac.th
[3] Faculty of Science, King Mongkut's University of Technology Thonburi, Bangkok, 10140, Thailand; apiwat.wis@kmutt.ac.th
[4] National Institute for Fusion Science, National Institutes of Natural Sciences, Toki, 509-5292, Japan and The Graduate University for Advanced Studies, SOKENDAI, Oroshi-cho, Toki, 509-5292, Japan; ogawa.kunihiro@nifs.ac.jp
[5] Thailand Institute of Nuclear Technology, Bangkok, Thailand; nopporn@tint.or.th
[6] National Institute for Fusion Science, National Institutes of Natural Sciences, Toki, 509-5292, Japan and The Graduate University for Advanced Studies, SOKENDAI, Oroshi-cho, Toki, 509-5292, Japan; isobe.mitsutaka@nifs.ac.jp
* Corresponding author: siriyaporn.s@msu.ac.th

Citation:
Wangkhahat, P.; Sangaroon, S.; Wisitsorasak, A.; Ogawa, K.; Poolyarat, N.; Isobe, M. Study of orbit motion of hydrogen and deuterium beam ions toward neutral beam injection experiment in Thailand Tokamak-1. *ASEAN J. Sci. Tech. Report.* **2024**, *27*(1), 58-67. https://doi.org/10.55164/ajstr.v27i1.251121.

Article history:
Received: October 1, 2023
Revised: December 3, 2023
Accepted: December 6, 2023
Available online: December 28, 2023

Abstract: Thailand Tokamak-1 (TT-1) is a small tokamak under the operation of the Thailand Institute of Nuclear Technology. In our future plans, TT-1 has the feasibility of being equipped with external heating systems to achieve high-performance plasma operation and conduct physics associated with fast ions generated by the external heating system. One of the potential external heating systems under consideration is a positive-ion-source-based neutral beam injection (NBI) heating system. The primary source of fast ions for the NBI can be either hydrogen or deuterium-doped hydrogen beams. This study examines how hydrogen and deuterium ions, namely protons and deuterons, respectively, move in orbits, using the Lorentz orbit (LORBIT) code to track their full gyromotion. The energy of the ions has been varied between 200 eV and 40 keV. Three trajectory motions have been characterized, i.e., counter-passing ion, co-passing ion, and trapped ion. The average Larmor radius, dependent on the ion energies, has been investigated. The Larmor radius significantly increases with increasing ion energy in the case of trapped ions, while in the case of counter- and co-passing ions, the Larmor radius exhibits a slight increase with increasing ion energy. Furthermore, the pitch angle range of the lost ion in the TT-1 has been investigated. The results demonstrate the feasibility of utilizing a deuterium-doped hydrogen beam in TT-1 to study fast ion physics. To avoid a large number of lost ions, it is possible to use a deuterium-doped hydrogen beam with an energy not exceeding approximately 10 keV in the TT-1.

Keywords: Thailand Tokamak-1; Neutral Beam Injection; Protons; Deuterons; Lorentz orbit (LORBIT) code

1. Introduction

Fusion energy offers a nearly inexhaustible energy source and very low environmental pollution. To achieve suitable conditions for the fusion reactions on the Earth, plasma must be confined by powerful magnetic fields and

externally heated to multimillion-degree temperatures. One of the most effective external heating is the neutral beam injection (NBI), the primary source of fast ions, including protons and deuterons [1, 2]. Enhancing our understanding of fast ions is one of the important research areas in present-day fusion devices because effective fast ion confinement is essential for achieving high-performance plasmas [3]. In medium-sized fusion devices, such as the Compact Helical System (CHS) with a major radius of 1 m and a minor radius of 0.2 m, a 1% deuterium-doped hydrogen NBI with a beam energy typically ranging from 35 to 40 keV was employed to study fast ion physics [4, 5].

Thailand is well aware of the impact of fusion technology and has a national plan for establishing a fusion research center. With support from the Chinese Academy of Sciences (ASIPP), the Thailand Institute of Nuclear Technology (TINT) is operating Thailand-Tokamak 1 (TT-1), which originated from a former device, HT-6M [6]. The installation of TT-1 at TINT's headquarters in Nakhonnayok province, Thailand, was completed at the beginning of 2023. TT-1 is the small-size tokamak with a major radius of 0.65 m and a minor radius of 0.21 m. It can increase the plasma current (I_p) to 100 kA and the toroidal magnetic field strength (B_t) to 1.52 T. The first plasma was achieved in July 2023. In our plans, TT-1 will be equipped with external heating systems to achieve high-performance plasma operation and conduct physics associated with fast ions generated by external heating systems. One of the planned external heating systems will be a positive-ion-source-based neutral beam injection (NBI) heating system [7, 8]. The first phase will employ an NBI equipped with a hydrogen beam. Deuterium-doped hydrogen beams are considered to enhance high-performance plasma conditions further. The ultimate goal of this work is to conduct a numerical investigation into the behavior of hydrogen and deuterium ions, namely protons and deuterons, respectively, by utilizing the collisionless LORBIT code [9] to track their full gyromotion in TT-1. This analysis will directly support the experimental plan's feasibility for achieving high-performance plasmas in TT-1 using NBI heating utilizing the hydrogen and deuterium-doped hydrogen NBI. This paper is structured as follows: section 2 describes the simulation setup, section 3 presents the results and discussion, and section 4 concludes with a summary.

2. Simulation setup

In this work, the orbit motions of protons and deuterons were tracked using the LORBIT code developed by the National Institute for Fusion Science, Japan [9]. This code has been widely employed for calculating the gyromotion of fast ions in various magnetic confinement systems such as in the LHD [10, 11], EAST [12], KSTAR [13], CFQS [14], Wendelstein 7-X [15], HL-2A and HL-2M [16]. In these works, the deuterons of the NBI source have been tracked to characterize the beam ion motion and study the prompt loss of beam ions for the design of fast ion loss diagnostics [15]. The LORBIT code has also been employed to study the behavior of fusion-born high-energy particles such as tritons and alphas [12]. An overview of the setup used to obtain the orbit motions of protons and deuterons is shown in Figure 1. The calculation in the LORBIT was linked to the magnetic field equilibrium. Here, the magnetic field equilibrium within TT-1 was determined using the FreeGS code, which solves the Grad-Shafranov equation with free boundary conditions [17]. The magnetic field equilibrium was provided for a plasma with ~~an~~ I_p of 100 kA, B_t of 1 T, and magnetic axis position (R_{ax}) of 0.67 m. I_p was clockwise, and B_t was counterclockwise as viewed from the top. It was reported that in the TT-1, the prompt lost beam ion occurs at a time less than approximately 10^{-6} s [7, 8]. Thus, this calculation set the orbit-following time to 10^{-4} s, high enough to track the deposited injected ion. Each ion was launched with the initial position fixed at a cylindrical coordinate of (r_0, ϕ_0, z_0) = (0.72 m, 0, 0) as shown in Figure 2a). The initial velocity along the z-axis (v_z) was assumed to be zero. Additionally, velocity along the x-axis (v_x) and velocity along the y-axis (v_y) were varied for the initial velocity vector ($\boldsymbol{v}$) to allow for the ion's initial pitch angle (χ_0) to range from 0° to 180°. Note that the pitch angle was calculated by determining the angle between the $\boldsymbol{v}$ at the deposition position and the local direction of the $\boldsymbol{B}$, i.e., χ is defined as $\chi = \arccos(v_{\parallel}/v)$, where $v_{\parallel}$ represents the parallel ion velocity concerning the local direction of $\boldsymbol{B}$. In this work, we varied the initial energy of protons and deuterons between 200 eV and 40 keV. In the collisionless motion, the total energy of the ion was constant along the trajectory. Furthermore, we employed the vacuum vessel geometry of TT-1 in the LORBIT calculation to study ion confinement and loss properties. Ions were considered lost when crossing with the last close flux surface (LCFS) and colliding with the vacuum vessel. Ion motion is determined by

solving the equation of motion subjected to the Lorentz force, i.e., $m\mathrm{d}\boldsymbol{v}/dt = q(\boldsymbol{v}\times\boldsymbol{B}+\boldsymbol{E})$, where m is the mass of the proton (m = 1.67377 × 10^{-27} kg) or deuteron (m = 3.34359 × 10^{-27} kg), $\boldsymbol{v}$ is its relative velocity, q is the charge of the proton (q = 1.60219 × 10^{-19} C) or deuteron (q = 1.60219 × 10^{-19} C), $\boldsymbol{B}$ is the magnetic field and $\boldsymbol{E}$ is electric field. Note that $\boldsymbol{E}$ is excluded in the LORBIT calculation because the plasma's potential is usually significantly lower than the beam ions' energy. By tracking the ion's trajectory, we can analyze its motion within the TT-1. To validate the orbit motions of protons and deuterons in the TT-1, we calculated the average Larmor radius along the trajectory of each ion and the guiding center trajectory (see Figure 2b)). Note that the Larmor radius is given by $\rho_L = mv_\perp/ZeB$, where m is the mass of the proton or deuteron, $v_\perp$ is the relative perpendicular velocity, Ze is the charge of the proton (Ze = 1.60219 × 10^{-19} C) or deuteron (Ze = 1.60219 × 10^{-19} C), and B is the magnetic field. The guiding center trajectory was calculated using the MATLAB function called Envelope Extraction [18].

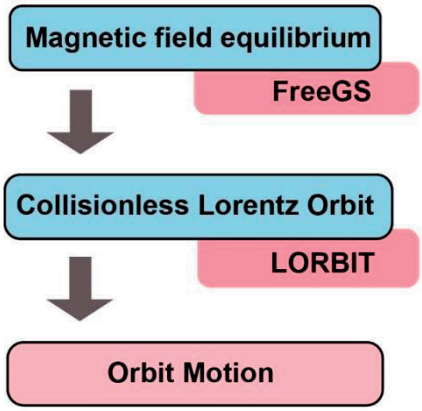

Figure 1. Flowchart to calculate the motion of the hydrogen and deuterium beam ions in orbits using the LORBIT code to track their full gyromotion.

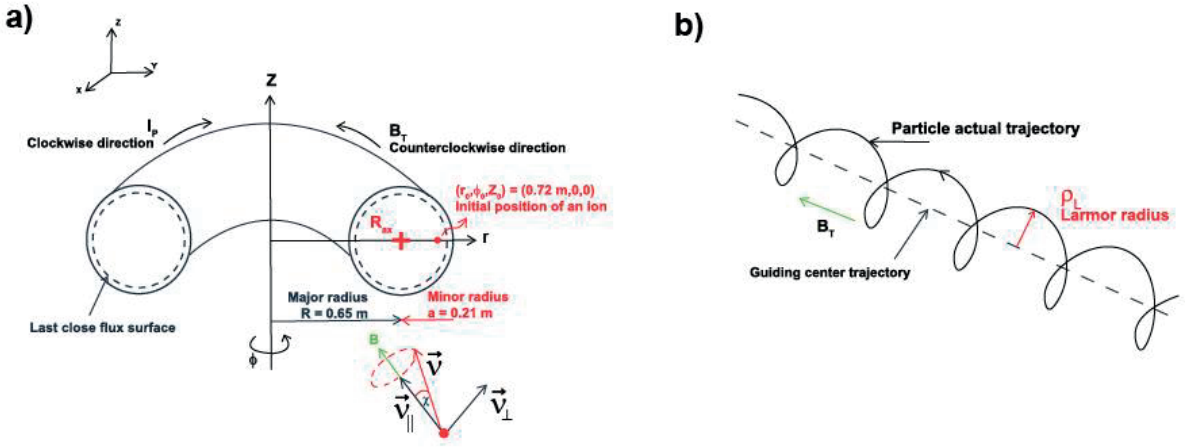

Figure 2. a) The diagram shows the TT-1 torus, vacuum vessel, last close flux surface, initial position of an ion, and its velocity. b) The diagram shows the actual particle and guiding center trajectories where the Larmor radius is defined.

3. Results and Discussion

The results of the averaged Larmor radius along the trajectory and the guiding center trajectory of protons and deuterons in the TT-1 are reported in this section.

3.1 Characterization of ion motion in TT-1

Figure 3a) illustrates the orbit motion of protons, while Figure 3b) depicts the orbit motion of deuterons in a poloidal view. For these calculations, the initial position of the ions was located at (r_0, ϕ_0, z_0) = (0.72 m, 0, 0), and the initial energy of both protons and deuterons was set to 20 keV. In this study, we varied the velocities along the x-axis (v_x) and y-axis (v_y) to allow the ion's initial pitch angle to range from 0° to 180°. We observed that the trajectories of protons and deuterons exhibit four distinct types of motion: counter-passing ion, co-passing ion, trapped ion, and ion loss. The counter-passing ion is classified by shifting inward concerning the magnetic axis of ion motion. In contrast, the co-passing ion is classified by shifting outward concerning the magnetic axis of ion motion. The trapped ion is classified into a banana shape. All trajectories characterized as a counter-passing ion, co-passing ion, and trapped ion remained confined within TT-1 without impacting the vacuum vessel, in other words, without crossing the LCFS, while ion loss occurred when ions crossed the LCFS and hit the vacuum vessel. Enhancing our understanding of fast ion confinement and loss behavior in the TT-1 is one of the important issues for achieving high-performance plasmas in future operations using NBI heating. The motion of ions depends on the pitch angle, and we have summarized the pitch angle range data for protons and deuterons in Table 1. The ion loss ranges for proton and deuteron occurs at angles resulting in the upper region of counter-passing ions, as the ions have high parallel velocity ($v_{||} >> v_{\perp}$) with co-direction with the magnetic field (low pitch angle), and the curvature drift is dominant for the drift orbit. In TT-1, it is found that the lost beam ions move upward due to ion curvature drift, and thus, the lost positions are located on the upper panel of the vacuum vessel (see Figures 3 and 4). It is clear that even though protons and deuterons exhibit the same characteristic motion and pitch angles, their Larmor radius significantly differs due to their mass differences. Deuterons show a wide range of pitch angles, which can result in ion loss. Figure 4a) displays the typical collisionless proton orbits depicting counter-passing ion confinement and ion loss in a three-dimensional view. The lost beam ions are classified into a fat banana orbit and collide with the vacuum vessel. Figure 4b) illustrates the extracted guiding center trajectory of these actual motions in poloidal projection.

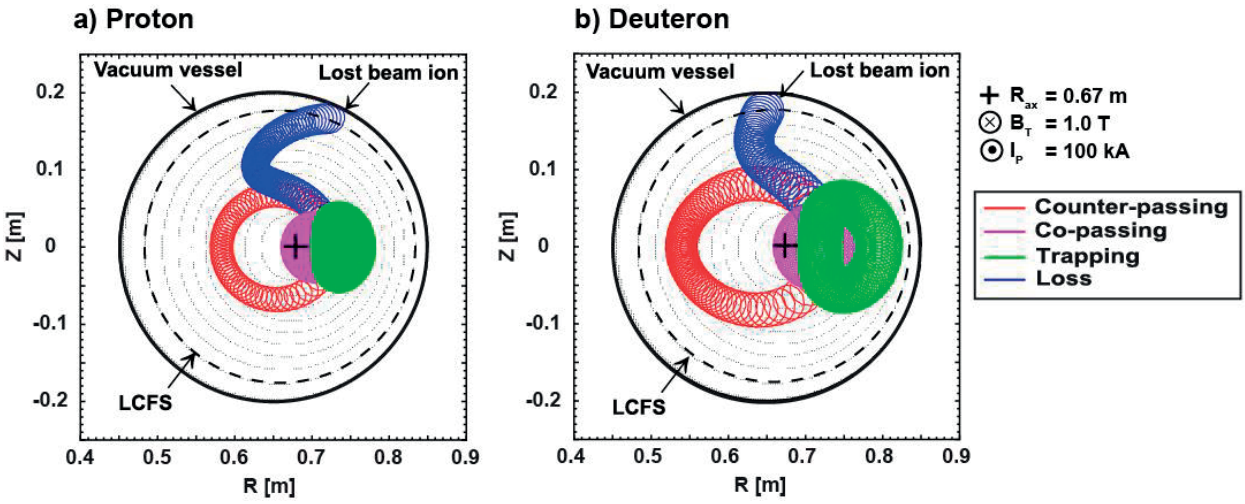

Figure 3. a) Examples of the trajectories of the counter-passing ion (red), co-passing ion (magenta), trapped ion (green), and loss ion (blue) of proton in poloidal view of TT-1 when the initial pitch angles of hydrogen were set to be 50°, 105 °, 89 °, and 66 °, respectively. b) Examples of the trajectories of the counter-passing ion (red), co-passing ion (magenta), trapped ion (green), and loss ion (blue) of the deuteron in the poloidal view of TT-1 when the initial pitch angles of hydrogen were set to be 50°, 105 °, 89 °, and 66 °, respectively. Note that the initial position of the ions was located at (r_0, ϕ_0, z_0) = (0.72 m, 0, 0), and ion energy was 20 keV.

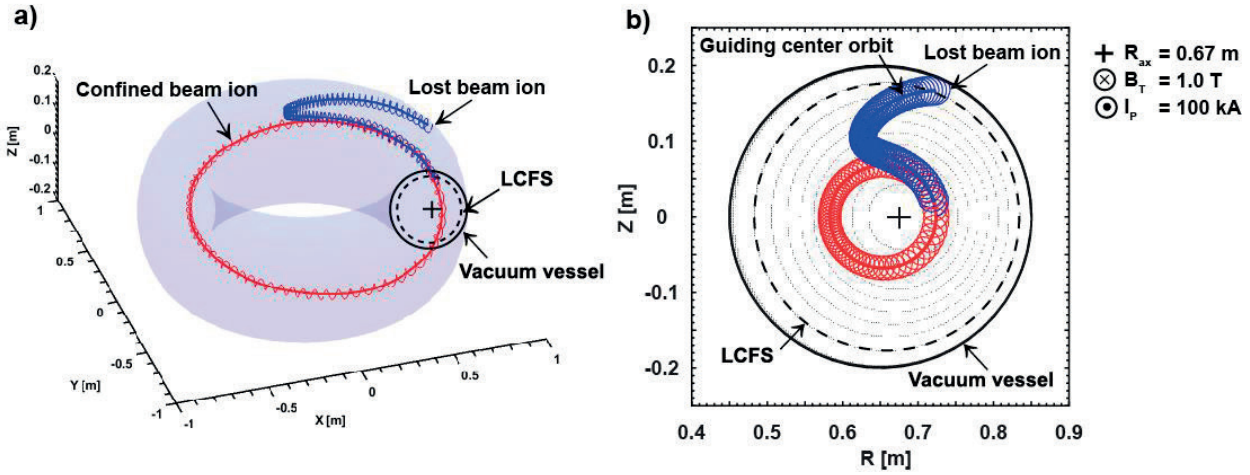

Figure 4. Typical collisionless proton orbits were calculated by the LORBIT code in a) three-dimensional view and b) poloidal projection. The figures show the actual particle and guiding center trajectories (thick lines). Lost beam ions (blue) are classified into a fat banana orbit and hit the vacuum vessel, while confined beam ions (red) exhibit counter-passing ion orbits and are well-confined.

Table 1. Relationship between the motion and pitch angle range of protons and deuterons.

Ion type	Motion type	Range of pitch angle
Proton	counter-passing ion	0˚ - ~ 60˚
	co-passing ion	~ 100˚ - ~ 180˚
	trapped ion	~ 75˚ - ~ 100˚
	loss ion	~ 60˚- ~ 75˚
Deuteron	counter-passing ion	0˚ - ~ 50˚
	co-passing ion	~ 100˚ - ~ 180˚
	trapped ion	~ 85˚ - ~ 100˚
	loss ion	~ 50˚- ~ 85˚

3.2 The impact of energy on confined ion motion

In this study, we varied the energy of protons and deuterons in the range of 200 eV to 40 keV to investigate how energy affects ion confinement motion. Figures 5a) and 5b) depict the trajectories of confined protons when the ion has an energy of 2 keV and 10 keV, respectively. Larmor radius is given by $\rho_\perp = mv_\perp/ZeB$, where $v_\perp$ is proportional to the ion energy. Consequently, as the ion energy increases, the Larmor radius of ions also increases. It is evident in this work that the orbital motion, in other words, Larmor radius, increases with higher energy. Similarly to the proton motion, the confined deuteron trajectories are shown in Figures 5c) and 5d). The results show that the orbital motion of deuterons, in other words, Larmor radius, increases with higher energy. The Larmor radius of protons and deuterons was calculated and is displayed in Figure 6a) for counter-passing ions, Figure 6b) for co-passing ions, and Figure 6c) for trapped ions. In the counter-passing ion case, the Larmor radius slightly increases from 0.04 cm to 0.60 cm for protons and from 0.05 cm to 0.91 cm for deuterons when the ion's energy increases from a few eV to an extremely high energy of 40 keV. It is found that deuterons have almost the same Larmor radius as protons at low energy and are approximately 52 % larger at an extremely high energy of 40 keV. In the co-passing ion case, the Larmor radius slightly increases from 0.04 cm to 0.48 cm for protons and from 0.05 cm to 0.68 cm for deuterons when the ion's energy increases from a few eV to an extremely high energy of 40 keV. It is found that deuterons have almost the same Larmor radius as protons at low energy and are approximately 42 % larger at an extremely high energy of 40 keV. In the trapping case, the Larmor radius significantly increases from 0.21 cm to 3.00 cm for protons

and from 0.30 cm to 4.23 cm for deuterons when the ion's energy increases from a few eV to an extremely high energy of 40 keV. It is found that deuterons' Larmor radius is approximately 42 % larger than a proton's Larmor radius at an ion's energy of 2 keV and approximately 41 % larger than a proton's Larmor radius at an extremely high ion's energy of 40 keV.

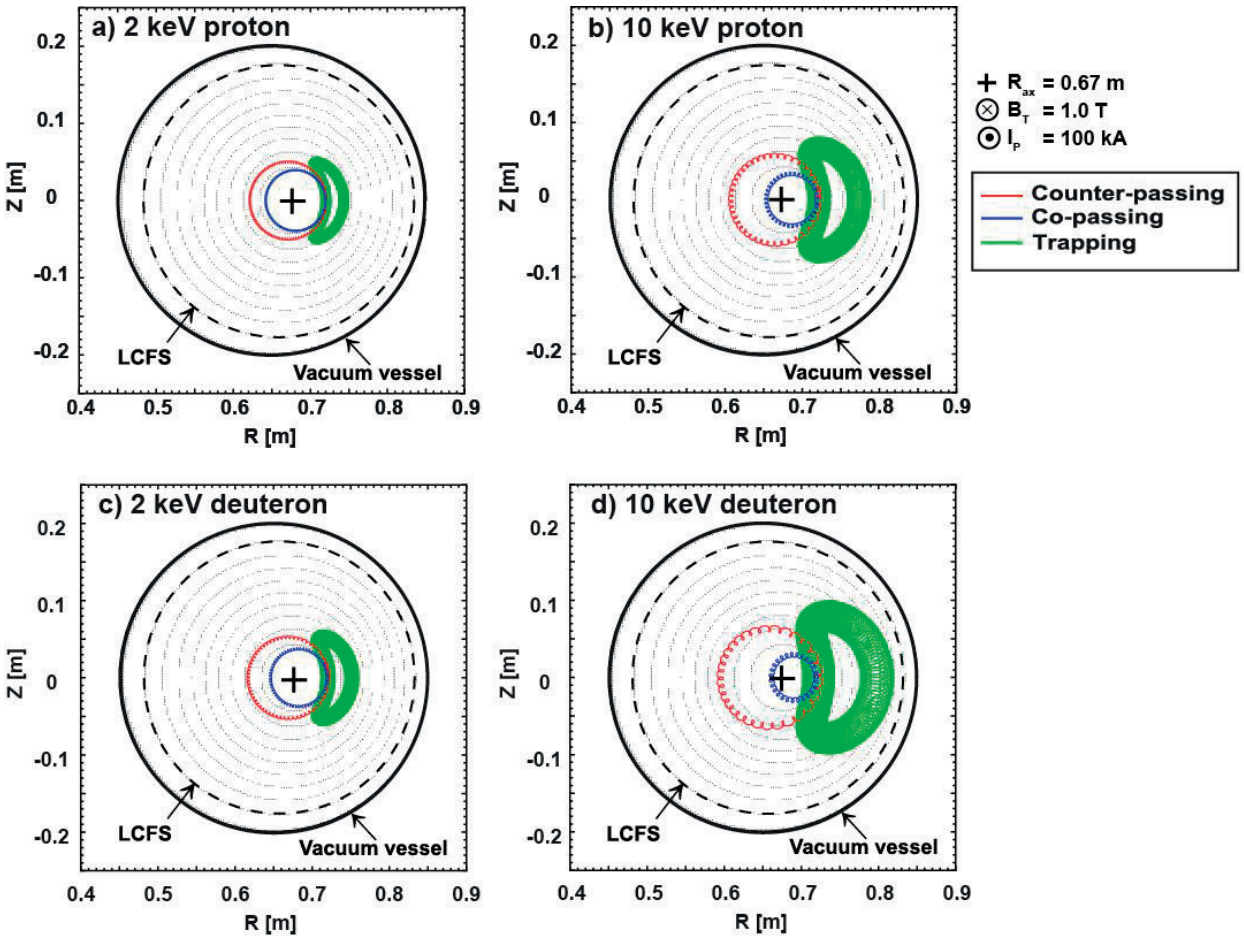

Figure 5. Typical orbit of well-confined ions characterized as counter-passing ion, co-passing ion, and trapped ion of proton with energy of a) 2 keV and b) 10 keV, and deuteron with energy of c) 2 keV and d) 10 keV.

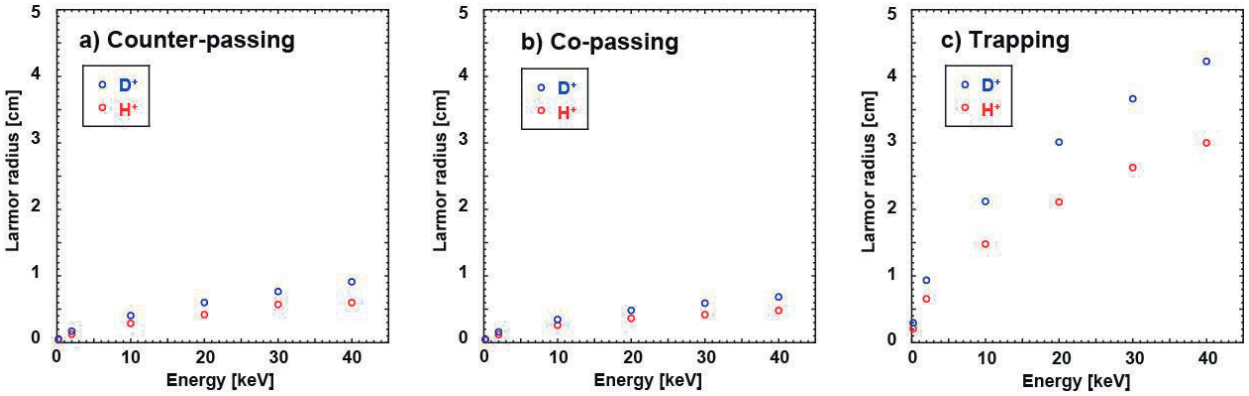

Figure 6. Typical Larmor radius of proton and deuteron characterized by a) counter-passing, b) co-passing, and c) trapping motions.

3.3 The impact of energy on loss ion motion

Most of the lost ions were near the passing and trapped boundary where the trapped ion is classified into a banana shape. The size of the banana orbit can be calculated by considering the motion of a trapped particle in a nonuniform magnetic field. The width of the orbit (W) can be written as $W = 2v_{||}/\omega_{c\theta}$, where $\omega_{c\theta}$ is a gyro-frequency. Since $v_{||}$ is proportional to the ion energy, the size of the banana orbit increases as the ion energy increases. In this evaluation, we assessed the behavior of trapped and lost ions when the pitch angle was fixed at approximately 80° while varying the energy from 200 eV to 40 keV. Figures 7a) and 7b) show the guiding center trajectory of protons and deuterons, respectively. Note that the actual motions were removed for better visibility. As the energy increases, the trajectory width and height of the banana orbit, in other words, the banana shape, become larger. Note that the width of the banana orbit was determined from the maximum trajectory width in the radial direction, and the height of the banana orbit was determined from the maximum trajectory height in the z-axis direction (see Figure 7a)). The protons became lost ions when they had an energy above 20 keV, while the deuterons became lost ions when they had an energy above 10 keV. The width and height of the banana-shaped motion for protons and deuterons, which depended on the ion's energy being lower than the energy that causes the fat banana orbit of a lost ion, were calculated and displayed in Figures 8a) and 8b), respectively. At an ion's energy increased from 200 eV to 10 keV, the results show that the banana shape width significantly increases from 0.01 m to 0.05 m for protons and from 0.01 m to 0.08 m for deuterons. The banana shape width of deuterons was approximately 60 % wider than the banana shape width of protons at an ion's energy of 10 keV. Consequently, the banana shape height significantly increases from 0.08 m to 0.13 m for protons and from 0.08 m to 0.16 m for deuterons. The banana shape height of deuterons was approximately 23 % higher than that of protons.

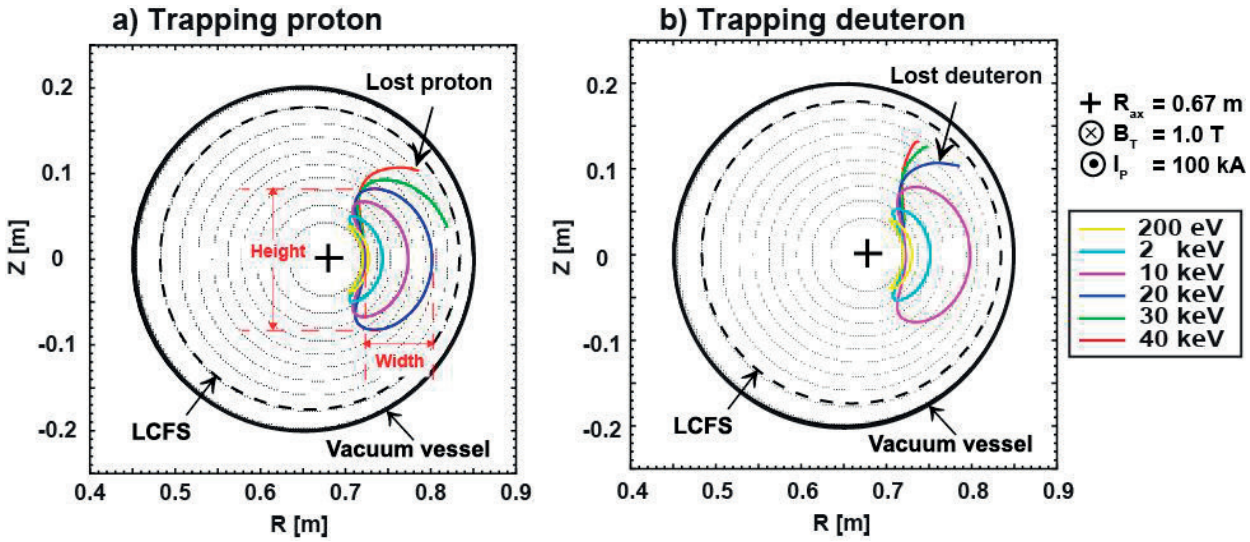

Figure 7. The typical guiding center trajectory of a) protons and b) deuterons was characterized by a banana shape when the pitch angle was fixed at approximately 80° while varying the energy from 200 eV to 40 keV.

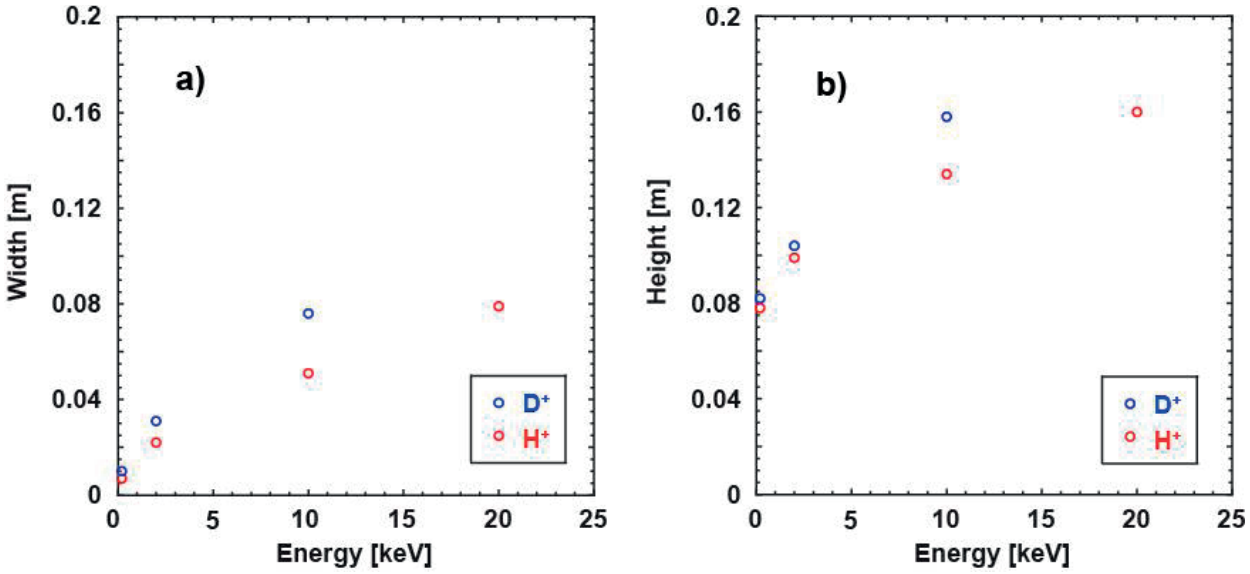

Figure 8. a) The width of the banana orbit, determined from the maximum trajectory width in the radial direction, and b) the height of the banana orbit, determined from the maximum trajectory height in the *z*-axis direction for protons and deuterons versus ion's energy that lower than the energy that causes the fat banana orbit of a lost ion.

4. Conclusions

In our upcoming initiatives, TT-1 is exploring the possibility of integrating external heating systems to enhance plasma performance and investigate the physics associated with fast ions generated by these external heating systems. Among the considered options is a positive-ion-source-based NBI heating system. The NBI plan can utilize hydrogen and deuterium-doped hydrogen beams as its primary ion source. This study focuses on the orbital dynamics of protons and deuterons, employing the collisionless LORBIT code for trajectory tracking. The investigation categorizes three types of confined ion motions: counter-passing ions, co-passing ions, and trapped ions, for both protons and deuterons, which depend on their initial pitch angles. Additionally, we examine how the average Larmor radius, influenced by ion energies, evolves. We observed a significant increase in the Larmor radius with higher ion energy, particularly for trapped ions. In contrast, counter-passing and co-passing ions exhibit a more modest increase in Larmor radius as ion energy rises. The results demonstrate the possibility of using either a hydrogen and/or a deuterium-doped hydrogen NBI in TT-1 to study fast ion physics in plans. In future work, exploring the feasibility and effectiveness of NBI in TT-1 is recommended by utilizing the birth profile of ions computed using the Monte Carlo fast ion module NUBEAM code. The investigation should consider factors such as ion collisions, charge exchange loss and recombination, and the transport of beam ions. The results from this study will directly contribute to shaping the future experimental strategy for achieving high-performance plasmas by utilizing the external heating system, such as the NBI system in TT-1.

5. Acknowledgements

S.S. acknowledged the financial support by the Program Management Unit for Human Resources and Institutional Development, Research and Innovation fiscal year 2023 (Grant No. B37G660016) and by Thailand Science Research and Innovation (TSRI) via Fundamental Fund FY2566 (Contract Number 2589646/4369740). P.W. acknowledged the financial support by the Faculty of Science, Mahasarakham University, in fiscal year 2023 (Grant No. 6601001/2566).

Author Contributions: Conceptualization, S.S., A.W., K.O., M.I.; methodology, P.W.; validation, P.W.; formal analysis, P.W.; investigation, P.W.; data curation, P.W.; writing—original draft preparation, P.W., S.S.;

writing—review and editing, P.W., S.S., A.W., K.O., M.I., N.P; visualization, P.W.; supervision, K.O., M.I.; project administration, N.P.; funding acquisition, S.S., P.W. All authors have read and agreed to the published version of the manuscript.

Funding: Please ensure to include the following statements in your manuscript:

1. "This research was funded by Program Management Unit for Human Resources and Institutional Development, Research and Innovation fiscal year 2023, grant number B37G660016, and by Thailand Science Research and Innovation (TSRI) via Fundamental Fund FY2566, grant number 2589646/4369740, and by Faculty of Science, Mahasarakham University fiscal year 2023, grant number 6601001/2566."
2. "The Article Processing Charges (APC) were funded by the Program Management Unit for Human Resources and Institutional Development, Research, and Innovation for fiscal year 2023, grant number B37G660016."

Conflicts of Interest: The authors declare no conflict of interest. The funders had no role in the design of the study, in the collection, analyses, or interpretation of data, in the writing of the manuscript, or in the decision to publish the results.

References

[1] Sergei Sharapov. *Energetic Particles in Tokamak Plasmas*. CRC Press. **2021.**

[2] Moseev, D.; Salewski, M.; Garcia-Munoz, M.; Geiger, B.; Nocente, M. Recent progress in fast-ion diagnostics for magnetically confined plasmas. *Reviews of Modern Plasma Physics*. **2018**, *2*(7), 1-68. https://doi.org/10.1007/s41614-018-0019-4

[3] Fasoli, A.; Gormenzano, C.; Berk, H. L.; Breizman, B.; Briguglio, S.; Darrow, D. S.; Gorelenkov, N.; Heidbrink, W.W.; Janu, A.; Konovalov, S.V.; Nazikian, R.; Noterdaeme, J.-M.; Sharapov, S.; Shinohara, K.; Testa, D.; Tobita, K.; Todo, Y.; Vlad, G.; Zonca, F. *Chapter 5: Physics of energetic ions*. **2007**, *47*(6), S264-S284. https://doi.org/10.1088/0029-5515/47/6/s05

[4] Isobe, M.; Okamura, S.; Nagaoka, K.; Osakabe, M.; Toi, K.; Yoshimura, Y.; Matsuoka, K.; Sasao, M.; Darrow, D.S. Fast-Ion-Diagnostics for CHS Experiment. *Plasma and Fusion Research*. **2007**, *2*, S1076. https://doi.org/10.1585/pfr.2.s1076

[5] Isobe, M.; Sasao, M.; Okamura, S.; Osakabe, M.; Kubo. S.; Minami, T.; Matsuoka, K.; Takahashi, C.; CHS Group. Experimental Study of Fast Ion Confinement in CHS. *J. Plasma Fusion Res. SERIES*. **1998**, *1*. 366-369.

[6] HT-6M TEAM. Engineering Aspects of The HT-6M Tokamak. *Fusion Technology*. **1986**, *9*(3), 476–480. https://doi.org/10.13182/fst86-a24733

[7] Paenthong, W.; Wisitsorasak, A.; Sangaroon, S.; Promping, J.; Ogawa, K.; Isobe, M. Fast-ion orbit analysis in Thailand Tokamak-1. *Fusion Engineering and Design*. **2022**, *183*, 113254. https://doi.org/10.1016/j.fusengdes.2022.113254

[8] Sangaroon, S.; Ogawa, K.; Isobe, M.; Wisitsorasak, A.; Paenthong, W.; Promping, J.; Poolyarat, N.; Tamman, A.; Ploykrachang, K.; Dangtip, S.; Onjun, T. Feasibility study of neutral beam injection in Thailand Tokamak-1. *Fusion Engineering and Design*. **2023**, *188*, 113419. https://doi.org/10.1016/j.fusengdes.2023.113419

[9] Mitsutaka, I.; Dan, F.; Mamiko, S. Lorentz alpha orbit calculation in search of position suitable for escaping alpha particle diagnostics in ITER. *J. Plasma Fusion Res. SERIES*. **2009**, *43*(4). https://inis.iaea.org/search/search.aspx?orig_q=RN:43003775

[10] Ogawa, K.; Isobe, M.; Nishitani, T.; Murakami, S.; Seki, R.; Nuga, H; Pu, N.; Osakabe, M.; LHD Experiment Group. Study of first orbit losses of 1 MeV tritons using the Lorentz orbit code in the LHD. *Plasma Science & Technology*. **2019**, *21*(2), 025102. https://doi.org/10.1088/2058-6272/aaeba8

[11] Ogawa, K.; Isobe, M.; Nuga, H.; Seki, R.; Ohdachi, S.; Osakabe, M. Evaluation of Alpha Particle Emission Rate Due to the p-^{11}B Fusion Reaction in the Large Helical Device. *Fusion Science and Technology*. **2022**, *78*(3), 175–185. https://doi.org/10.1080/15361055.2021.1973294

[12] Ogawa, K.; Zhong, G.; Zhou, R.; Li, K.; Isobe, M.; Hu, L. 1 MeV Triton Orbit Analysis in EAST Plasmas. *Plasma and Fusion Research*. **2020**, *15*, 2402022. https://doi.org/10.1585/pfr.15.2402022

[13] Jun Young Kim; Rhee, T.; Kim, J.-H.; Yoon, S. W.; Park, B. H.; Isobe, M.; Ogawa, K.; Ko, W. H. Prompt loss of beam ions in KSTAR plasmas. *AIP Advances*. **2016**, *6*, 105013. https://doi.org/10.1063/1.4966588

[14] Ogawa, K.; Isobe, M.; Seki, R.; Nuga, H.; Yamaguchi, H.; Sangaroon, S.; Shimizu, A.; Okamura, S.; Takahashi, H.; Oishi, T.; Kinoshita, S.; Murase, T.; Nakagawa, S.; Tanoue, H.; Osakabe, M.; Liu, H. F.; Xu, Y. Feasibility study of fast ion loss diagnostics for CFQS by beam ion loss calculation on vacuum vessel. *Journal of Instrumentation*. **2021**, *16*(9), C09029. https://doi.org/10.1088/1748-0221/16/09/c09029

[15] Ogawa, K.; Bozhenkov, S. A.; Äkäslompolo, S.; Killer, C.; Grulke, O.; Nicolai, D.; Satheeswaran, G.; Isobe, M.; Osakabe, M.; Yokoyama, M.; Wolf, R. C. Energy-and-pitch-angle-resolved escaping beam ion measurements by Faraday-cup-based fast-ion loss detector in Wendelstein 7-X. *Journal of Instrumentation*. **2019**, *14*(9), C09021. https://doi.org/10.1088/1748-0221/14/09/c09021

[16] Ogawa, K.; Zhang, Y.; Zhang, J.; Sangaroon, S.; Isobe, M.; Liu, Y. Predictive analysis for triton burnup ratio in HL-2A and HL-2M plasmas. *Plasma Physics and Controlled Fusion*. **2021**, *63*(4), 045013. https://doi.org/10.1088/1361-6587/abe054

[17] Dudson, B. (n.d.). *Welcome to FreeGS's documentation! — FreeGS 0.2.0 documentation*. Freegs.readthedocs.io. Retrieved September 25, 2023, from https://freegs.readthedocs.io/en/latest/

[18] The MathWorks, Inc. (n.d.). *Envelope Extraction - MATLAB & Simulink*. www.mathworks.com. Retrieved September 25, 2023, from https://www.mathworks.com/help/signal/ug/envelope-extraction-using-the-analytic-signal.html

ASEAN
Journal of Scientific and Technological Reports
Online ISSN:2773-8752

Research article

Molecular Docking of Bioactive Compounds from Thai Medicinal Plants Against Xanthine Oxidase for Gout Treatment

Apiradee Pothipongsa[1], Thanakorn Damsud[2], and Surachet Burut-Archanai[3, 4]*

[1] Faculty of Science and Technology, Rajamangala University of Technology Srivijaya, Nakhon Si Thammarat, 80110, Thailand; apiradee.p@rmutsv.ac.th
[2] Faculty of Science and Technology, Rajamangala University of Technology Srivijaya, Nakhon Si Thammarat, 80110, Thailand; thanakorn.d@rmutsv.ac.th
[3] Faculty of Science, Chulalongkorn University, Bangkok, 10330, Thailand; surachet.bur@biotec.or.th
[4] Marine Biotechnology Research Team, Integrative Aquaculture Biotechnology Research Group, National Center for Genetic Engineering and Biotechnology (BIOTEC), Pathum Thani, 12120, Thailand
* Correspondence: surachet.bur@biotec.or.th

Citation:
Pothipongsa, A.; Damsud, T.; Burut-Archanai, S. Molecular docking of bioactive compounds from Thai medicinal plants against xanthine oxidase for gout treatment. *ASEAN J. Sci. Tech. Report.* **2024**, *27*(2), 68-72. https://doi.org/10.55164/ajstr.v27i1.250948.

Article history:
Received: September 18, 2023
Revised: December 3, 2023
Accepted: December 6, 2023
Available online: December 28, 2023

Abstract: Xanthine oxidase (XO) is a crucial enzyme of the purine catabolism pathway, which catalyzes the reaction of hypoxanthine to xanthine and xanthine to uric acid. The high level of uric acid leads to gout, kidney disease, and several disorders. In this study, molecular docking was performed to investigate potential bioactive compounds from Thai medicinal plants that acted as XO inhibitors compared to commercial drugs. Among 30 bioactive compounds tested, 16 were classified as strong XO inhibitors. These compounds include asiatic acid, benzyl glucosinolate, beta-sitosterol, chlorogenic acid, curcumin, eupatorin, gamma-mangostin, hibiscitrin, lutein, nimbolide, piperine, quercetin, rosmarinic acid, rutin, sesamin, and vitexin. They exhibited binding affinity values ranging from -8.5 to -10.6 kcal/mol. Moreover, moderate XO inhibitors were identified with binding affinity of -6.2 to -8.0 kcal/mol, consisting of the 7 compounds of gallic acid, garcinia acid, gingerol, limonene, linalyl acetate, panduratin A, and scopoletin. As a result, Thai medicinal plants could serve as potential sources of bioactive compounds for further drug design for treating gout patients.

Keywords: Molecular docking; Xanthine oxidase; Gout; Thai medicinal plants

1. Introduction

Gout is an inflammatory arthritis that can affect anyone, regardless of gender and age. It has been reported to increase rapidly worldwide [1]. Gout is a prolonged presence of high uric acid levels (hyperuricemia) in the bloodstream. This condition leads to the formation of monosodium urate crystals, which can accumulate in synovial fluid or surrounding tissue, causing acute and chronic inflammation, tissue damage, and pain [2]. Moreover, gout patients are at risk of developing chronic conditions such as hypertension, chronic kidney disease, cardiovascular diseases, diabetes, or metabolic syndrome, which can impact their quality of life [3].

Gout is an inherited purine metabolism disorder involving xanthine oxidase (XO, EC 1.17.3.2), an enzyme responsible for breaking down purine nucleotides to uric acid. Excess uric acid can then crystallize and trigger the symptoms characteristic of gout. The XO-catalyzed reaction produces reactive oxygen species (ROS), causing oxidative damage to tissues and other diseases

linked to oxidative stress [4-5]. The XO inhibitors have been investigated as potential drugs to block the biosynthesis of uric acid and have shown promise in anti-cancer therapies [6]. Allopurinol is a common drug for gout treatment, mainly included as an XO inhibitor to reduce uric acid levels. However, it has been reported on side effects, such as hypersensitivity reactions, Stevens–Johnson syndrome, hepatotoxicity, and nephrotoxicity [7]. Febuxostat is a recommended drug for gout patients beyond allopurinol, with superior antioxidant and anti-inflammatory effects [8]. However, febuxostat has fewer effects on skin reactions than allopurinol but increases the risk of gout in patients with cardiovascular diseases [9]. Both drugs function as XO inhibitors by stably binding the XO active sites, preventing the conversion of xanthine to uric acid.

Many bioactive compounds were recently studied for their anti-oxidative, antibacterial, antiviral, and anti-mutagenic activities *in vitro* and *in vivo* experiments, including XO inhibitors from plants [10-11] and fungi [12]. To avoid these adverse side effects of drugs for gout treatment, bioactive compounds with fewer or no side effects are known to be investigated in medicinal plants. Traditional medicine in Asian countries showed several potential lead compounds for XO inhibition, such as cordauvarin A from Vietnamese *Uvaria cordata* [13], quercetin from Indonesian *Sonchus arvensis* [14], and quercetin, quinic acid and rutin from *Plumeria rubra* or Malaysian Red [10].

Molecular docking is a computational tool that predicts the interaction between a small molecule and a protein based on energy complementation at the atomic level. Widely used for identifying potential drug candidates, molecular docking predicts the binding affinity of small molecules to a protein or receptor of interest, offering a time- and cost-saving technique for screening interesting molecules from a large database [15]. Numerous studies have employed molecular docking for xanthine oxidase research [5, 16-19]. However, only a few studies have investigated XO activities *in vitro* in Thai medicinal plants [20-22]. Therefore, we aimed to screen the potential bioactive compounds as XO inhibitors using the molecular docking technique to investigate their function based on the interactions between proteins and ligands from Thai medicinal plants for gout treatment. The other identified XO inhibitors may serve as valuable candidates for further development into potential lead compounds.

2. Materials and Methods

2.1 Collection of structures

The three-dimensional structure of proteins was carried out from the Protein Data Bank (PDB) [23]. This study's PDB ID of xanthine oxidase (XO) was 1N5X. This structure was obtained through X-ray diffraction techniques with a resolution of 2.80 angstroms, R-value free of 0.275, and R-value work of 0.244 [24].

For the three-dimensional structure of ligands, 30 of 72 different biologically active compounds from Thai medicinal plants with potential XO binding affinity were selected. These ligands were sourced from the PubChem database and have associated PubChem Compound Identifiers (CIDs), as shown in Figure 1. Allopurinol and febuxostat were used as references for XO inhibitors. The 30 structures of bioactive compounds and 2 reference ligands of XO inhibitor were structurally drawn using the online tool chem-space.com (https://chem-space.com/search).

2.2 Molecular docking

The molecular docking was conducted between the mammalian XO protein (PDB ID: 1N5X) and ligands, as mentioned in Figure 1, using the CB-Dock2 web server, https://cadd.labshare.cn/cb-dock2/php/index.php, which executed based on the AutoDock Vina algorithm [25]. The docking process employs template-independent blind docking techniques to calculate the pockets and binding sites of the protein-ligand complexes with initial parameters with five possible coupling cavities. Subsequently, the best-performing cavity was selected and the binding affinity values for the interaction between protein and ligands were calculated. Docking scores were reported as binding energy to the Vina score (kcal/mol). The binding energy of ligands lower than their controls was chosen for further analysis to determine the positions of amino acids in the binding interaction with the XO. The protein-ligand interaction was visualized using BIOVIA Discovery Studio 2021 [26].

3. Results and Discussion

3.1 Molecular docking

Based on the results of protein-ligand interaction, 30 different bioactive compounds were assessed against XO using molecular docking methods, comparing them to two control ligands. It was observed that the binding affinity values for all ligands ranged from -1.5 to -10.6 kcal/mol (Figure 2). The binding affinities of both control ligands to the XO were consistent with previous studies, ranging from -5.6 to -7.1 for allopurinol [13-14] and -8.7 to -10.1 for febuxostat [27-28]. Variations in XO templates and analytical parameters may result in value discrepancies between studies.

From this calculated binding affinity, it can be inferred that two groups of bioactive compounds have different abilities to bind to XO protein. The first group exhibited a high potential for XO inhibitors, with binding affinity values ranging from -8.5 to -10.6 kcal/mol. This group includes 16 different compounds:rutin (-10.6 kcal/mol); quercetin and gamma-mangostin (-10.2 kcal/mol); rosmarinic acid (-10.1 kcal/mol); eupatorin (-10.0 kcal/mol); chlorogenic acid and lutein (-9.7 kcal/mol); sesamin and beta-sitosterol (-9.6 kcal/mol); curcumin, benzyl glucosinolate and nimbolide (-9.4 kcal/mol); vitexin and hibiscitrin (-9.3 kcal/mol); piperine (-9.2 kcal/mol); and asiatic acid (-8.5 kcal/mol). These compounds exhibited better binding affinities than control ligands, allopurinol, and febuxostat, which showed binding affinities of -6.1 and -8.1 kcal/mol, respectively. These results, according to the XO binding activity, were found in natural extracts from medicinal plants of *Thunbergia laurifolia* [29], *Carissa carandas* [30], Vietnamese *Uvaria cordata* [13], and *Garcinia mangostana* [31]. Rutin, quercetin, and gamma-mangostin emerged as this study's top XO-binding bioactive compounds. *In silico* and *in vitro* investigations of quercetin [14] and rutin [32] demonstrated that both compounds were more effective than allopurinol in binding to XO and inhibiting its activity. Furthermore, crude extracts containing quercetin and rutin from *Plumeria rubra* exhibited superior XO inhibition activity compared to allopurinol [10]. Additionally, quercetin supplementation effectively reduced uric acid levels in obese males with gout, with no observed side effects on kidney and liver function when consumed at a dose of 500 milligrams daily for 4 weeks [33]. Gamma-mangostin, extracted from *Garcinia mangostana*, demonstrated the potential to maintain blood uric acid levels in rats [31]. Molecular docking studies revealed that piperine exhibited slightly better binding affinity to the XO enzyme than allopurinol, as it does not directly bind to the enzyme's active site [34]. Moreover, the binding affinity of other compounds involved in XO inhibitors, such as cordauvarin A (-8.8 kcal/mol) [13], has been reported.

In addition, the second group of compounds had a lower binding affinity for XO than the first group, with binding affinity values ranging from -6.2 to -8.0 kcal/mol. These compounds also exhibited good binding capabilities compared to allopurinol (-6.1 kcal/mol) but not febuxostat. In this group, there were 7 compounds: pandurate A (-8.0 kcal/mol); gingerol (-7.8 kcal/mol); scopoletin (-7.7 kcal/mol); gallic acid (-6.7 kcal/mol); limonene (-6.5 kcal/mol); linalyl acetate (-6.3 kcal/mol); and garcinia acid (-6.2 kcal/mol). Shaik and colleagues reported the ability of gallic acid to inhibit the activity of the XO enzyme and prevent the occurrence of acute myocardial ischemia in experimental mice [35]. Based on the binding affinity score of allopurinol to XO of -6.1 kcal/mol (Figure 2), it could be pointed out that the 16 compounds in the first group have a higher potential for binding to XO and may be of greater interest for further investigation in the context of XO inhibitors compared to the compounds in the second group.

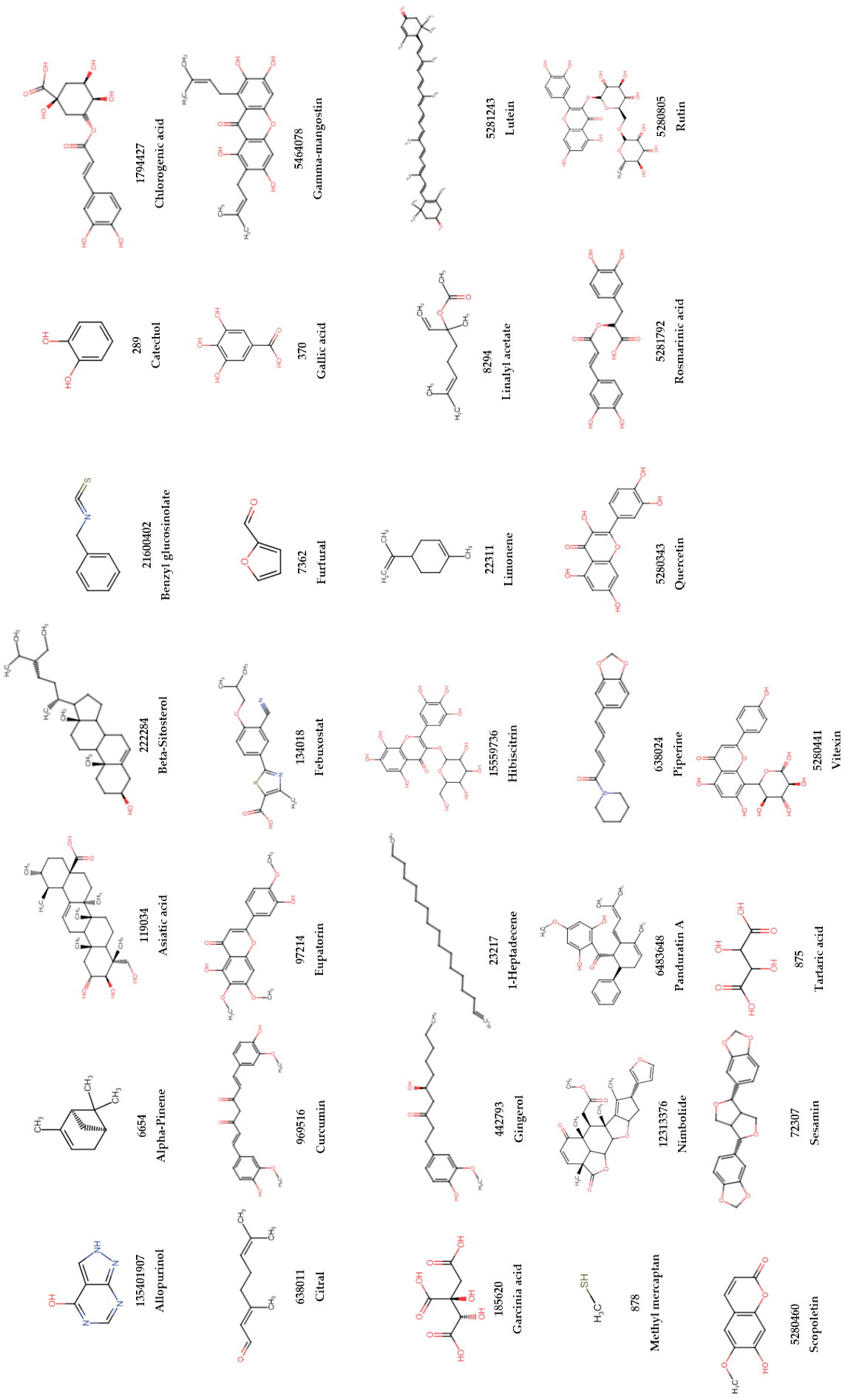

Figure 1. The structures of 30 bioactive compound ligands from Thai medical plants and (*) the two reference ligands of XO inhibitor. The PubChem CIDs are shown in number as mentioned.

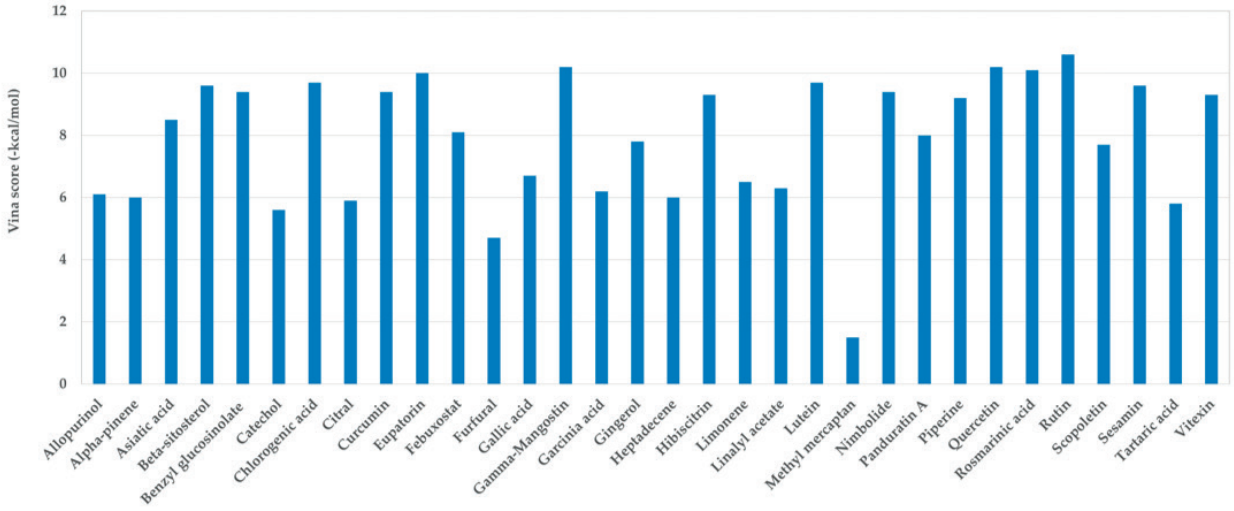

Figure 2. Binding affinities of various ligands found in Thai medicinal plants against XO.

Based on the 3D-structural interaction between ligands and XO, the amino acid residues involved in the binding interaction between XO and the 16 biologically active compounds from the first group (strong potential compounds as XO inhibitors) were further analyzed. The binding interaction between the ligands and the XO was found to involve amino acids from chains A and B of the protein. These interactions are mediated by hydrogen bonds, hydrophobic, ionic, and cation-π interactions (Figure 3 – 4). The specific amino acids involved in the binding interactions vary depending on the type of ligand. From this study, the bioactive compounds of rutin, chlorogenic acid, sesamin, beta-sitosterol, nimbolide, vitexin, hibiscitrin and asiatic acid were observed to interact with important amino acids Ala28, Arg32, Leu41, Cys73, Arg606, Pro675, Glu676, Glu679, and Asp828 in the XO structure. These amino acids also play a significant role similar to the binding interaction between febuxostat and the XO protein (Figure 3). Therefore, these compounds might inhibit the XO enzyme via a non-competitive inhibition mechanism such as febuxostat, a non-purine analog that acts as a non-competitive XO inhibitor [36]. The docking results of febuxostat with 1N5X protein showed interacted residues of Glu802, Thr1010, Arg880, Asn768, Leu873 and Leu648 [28]. For simulating an interaction between XO and ligands quercetin, gamma-mangostin, rosmarinic acid, eupatorin, curcumin, lutein, benzyl glucosinolate and piperine, it was found that the interaction of Glu332, Trp336, Lys422, Gln423, Arg427, Asp430, and Asp1170 was similar to the positions in the XO with allopurinol (Figure 4). From the virtual screening analysis of cordauvarin A from Vietnamese *Uvaria cordata*, the Glu802, Ala910, Gly913, and Phe914 were found as main amino acids that were responsible for the interaction at the active site of XO, whereas the Glu802, Thr1010, Arg880, Ala1079, Phe1009, and Phe914 of XO interacted with allopurinol [13]. These results suggested that the inhibition mechanism of these bioactive compounds might function similarly to allopurinol, a competitive inhibitor of XO [37].

According to XO sequences, bovine XO shares a 90% similarity with human XO in the overall sequence [38]. This conservation of amino acids should reveal a role of binding pattern and activity in both [24]. As a result, the predicted binding sites using molecular docking suggested that binding should correspond to configurations of the human XO.

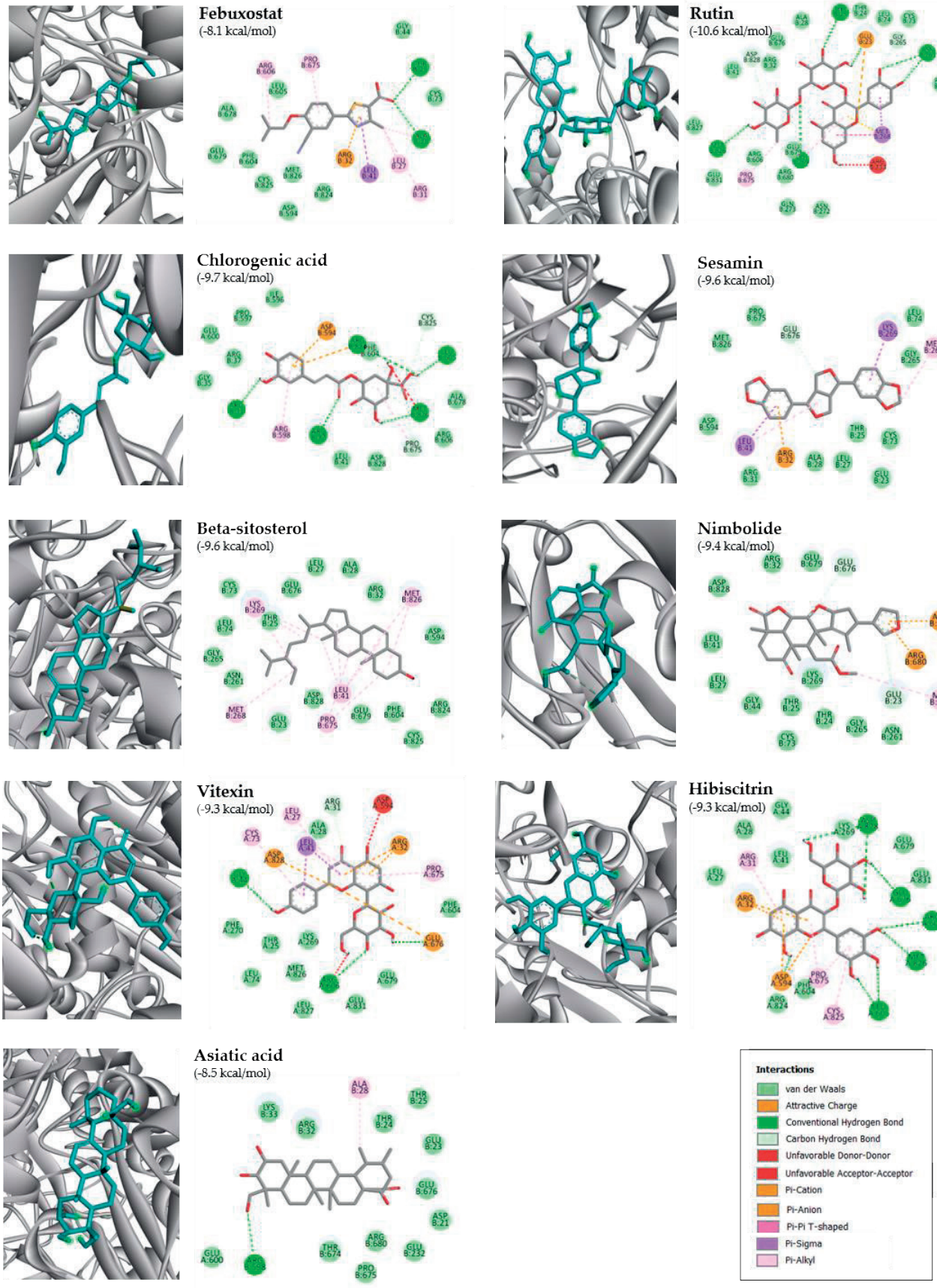

Figure 3. Visualization of XO with strong potential XO inhibitors, which interact with febuxostat.

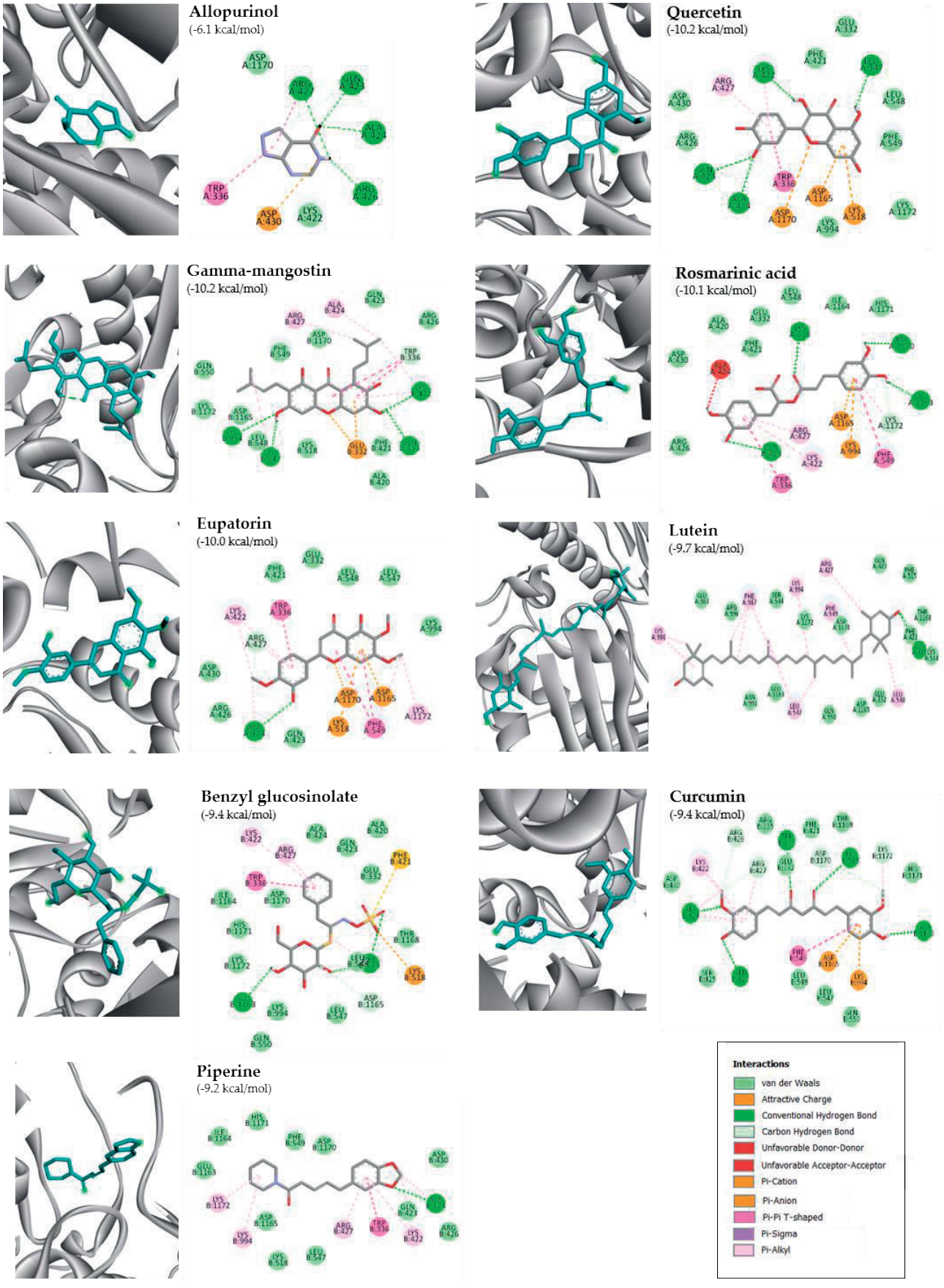

Figure 4. Visualization of XO with strong potential of XO inhibitors, which interacts with allopurinol.

Currently, gout treatment guidelines are to control uric acid levels in the blood using medication. Although allopurinol is often the first-line choice for reducing blood uric acid levels by inhibiting the XO activity, its use is limited by severe skin rashes. Therefore, febuxostat is preferred, especially in gout patients with impaired kidney function. However, it is not recommended to use febuxostat in patients with allergic reactions to allopurinol or in those with coronary artery disease [9]. Uric acid is primarily eliminated through the kidneys, and other treatment approaches involve using medications to enhance the excretion of uric acid through urine.

Table 1. Bioactive compounds and their sources from Thai medicinal plants

	Binding affinity (kcal/mol)	Bioactive compounds	Thai medicinal plants	References
Strong potential XO inhibitors	-10.6	Rutin	*Moringa stenopetala*	[39]
	-10.2	Gamma-mangostin	*Garcinia mangostana*	[31]
	-10.2	Quercetin	*Allium ascalonicum*	[40]
	-10.1	Rosmarinic acid	*Ocimum gratissimum*	[40]
	-10.0	Eupatorin	*Orthosiphon aristatus*	[41]
	-9.7	Chlorogenic acid	*Clitoria ternatea*	[40]
	-9.7	Lutein	*Tagetes erecta*	[42]
	-9.6	Sesamin	*Sesamum indicum*	[40]
	-9.6	Beta-sitosterol	*Leucaena leucocephala*	[40]
	-9.4	Curcumin	*Curcuma longa*	[40]
	-9.4	Benzyl glucosinolate	*Carica papaya*	[43]
	-9.4	Nimbolide	*Azadirachta indica*	[40]
	-9.3	Vitexin	*Garcinia cowa*	[44]
	-9.3	Hibiscitrin	*Hibiscus sabdariffa*	[45]
	-9.2	Piperine	*Piper nigrum*	[40]
	-8.5	Asiatic acid	*Centella asiatica*	[40]
Moderate potential XO inhibitors	-8.0	Panduratin A	*Boesenbergia rotunda*	[40]
	-7.8	Gingerol	*Zingiber officinale*	[40]
	-7.7	Scopoletin	*Syzygium cumini*	[40]
	-6.7	Gallic acid	*Azadirachta indica*	[40]
	-6.5	Limonene	*Myristica fragrans*	[40]
	-6.2	Garcinia acid	*Garcinia atroviridis*	[46]
	-6.3	Linalyl acetate	*Citrus aurantium*	[40]
Low potential XO inhibitors	-6.0	Heptadecene	*Cassia siamea*	[47]
	-6.0	Alpha-pinene	*Citrus hystrix*	[40]
	-5.9	Citral	*Citrus aurantifolia*	[40]
	-5.8	Tartaric acid	*Azadirachta indica*	[48]
	-5.6	Catechol	*Sauropus androgynus*	[40]
	-4.7	Furfural	*Cassia siamea*	[47]
	-1.5	Methyl mercaptan	*Paederia foetida*	[49]

Thailand has a large plant biodiversity with various bioactive compounds exhibiting biological and pharmacological activities of antioxidant, anti-inflammatory, and antimicrobial properties. Interestingly, from the molecular docking results, sources of strong and moderate potential bioactive compounds for XO inhibitors were found in many Thai medicinal plants mentioned in Table 1. These results were supported by using *Orthosiphon aristatus* for gout treatment by increasing diuresis [50]. The unripe fruit peels and leaves from *Carica papaya* showed high XO inhibitory activity [51]. As a result, Thai medicinal plants could be potential sources of bioactive compounds for further drug design for treating gout patients. Experimental investigations are imperative to assess the pharmacological efficacy of these compounds in treating gout.

4. Conclusions

In the present study, molecular docking is important in understanding the molecular interaction between bioactive compounds from Thai medicinal plants and XO enzymes. The 30 different bioactive compounds were screened for their potential as XO inhibitors compared to commercial drugs. The docking results showed that the 16 compounds were classified as strong XO inhibitors, including asiatic acid, benzyl glucosinolate, beta-sitosterol, chlorogenic acid, curcumin, eupatorin, gamma-mangostin, hibiscitrin, lutein, nimbolide, piperine, quercetin, rosmarinic acid, rutin, sesamin, and vitexin. The moderate XO inhibitors were identified with the 7 compounds of gallic acid, garcinia acid, gingerol, limonene, linalyl acetate, panduratin A, and scopoletin. The interaction of these ligands against XO protein could provide valuable insights for predicting potential bioactive compounds from Thai medicinal plants for the design and development of natural XO inhibitors. However, further experimental studies, including *in vitro*, *in vivo*, and preclinical tests, are required to evaluate the pharmacological potential of these compounds for gout treatment.

5. Acknowledgements

The authors would like to thank the Center of Excellence for Marine Biotechnology, Department of Marine Science, Faculty of Science, Chulalongkorn University, and the Program of Science, Faculty of Science and Technology, Rajamangala University of Technology Srivijaya, for providing research facilities.

Author Contributions: Conceptualization, A.P., T.D., and S.B.; methodology, A.P.; formal analysis, A.P., and S.B.; investigation, A.P., T.D., and S.B.; resources, A.P., T.D., S.B., and P.K.; data curation, A.P., and S.B.; writing—original draft preparation, A.P., T.D., and S.B.; writing—review and editing, A.P. and S.B.; visualization, A.P, and S.B.; supervision, S.B.

Funding: This research received no external funding.

Conflicts of Interest: The authors declare no conflict of interest.

References

[1] Dehlin, M.; Jacobsson, L.; Roddy, E. Global epidemiology of gout: prevalence, incidence, treatment patterns and risk factors. *Nature Reviews Rheumatology*. **2020**,*16(7)*, 380–390. doi:10.1038/s41584-020-0441-1

[2] Neogi, T.; Jansen, T.L.; Dalbeth, N.; Fransen, J.; Schumacher, H.R.; Berendsen, D.; Brown, M.; Choi, H.; Edwards, N.L.; Janssens, H.J.; Lioté, F.; Naden, R.P.; Nuki, G.; Ogdie,A.; Perez-Ruiz, F.; Saag, K.; Singh, J.A.; Sundy, J.S.; Tausche, A.K.; Vaquez-Mellado, J.; Yarows, S.A.; Taylor, W.J. Gout classification criteria: an American College of Rheumatology/European League Against Rheumatism collaborative initiative. *Annals of the Rheumatic Diseases*. **2015**, *74*(10), 1789–1798. doi:10.1136/annrheumdis-2015-208237

[3] Choi, H.K.; McCormick, N.; Yokose, C. Excess comorbidities in gout: the causal paradigm and pleiotropic approaches to care. *Nature Reviews Rheumatology*. **2022**, *18*(2), 97–111. doi:10.1038/s41584-021-00725-9

[4] Miric, D.J.; Kisic, B.M.; Filipovic-Danic, S.; Grbic, R.; Dragojevic, I.; Miric, M.B.; Puhalo-Sladoje, D. Xanthine oxidase activity in type 2 diabetes mellitus patients with and without diabetic peripheral neuropathy. *Journal of Diabetes Research*. **2016**, 4370490. doi:10.1155/2016/4370490

[5] Santi, M.D.; Paulino Zunini, M.; Vera, B.; Bouzidi, C.; Dumontet, V.; Abin-Carriquiry, A.; Grougnet, R.; Ortega, M.G. Xanthine oxidase inhibitory activity of natural and hemisynthetic flavonoids from *Gardenia oudiepe* (Rubiaceae) *in vitro* and molecular docking studies. *European Journal of Medicinal Chemistry*. **2018**, 143, 577–582. doi:10.1016/j.ejmech.2017.11.071

[6] Battelli, M.G.; Polito, L.; Bortolotti, M.; Bolognesi, A. Xanthine oxidoreductase-derived reactive species: physiological and pathological effects. *Oxidative Medicine and Cellular Longevity*. **2016**, Article 3527579. doi:10.1155/2016/3527579

[7] Wang, Y.; Zhu, J.X.; Kong, L.D.; Yang, C.; Cheng, C.H.; Zhang, X. Administration of procyanidins from grape seeds reduces serum uric acid levels and decreases hepatic xanthine dehydrogenase/oxidase activities in oxonate-treated mice. *Basic and Clinical Pharmacology & Toxicology*. **2004**, *94*(5), 232–237. doi:10.1111/j.1742-7843.2004.pto940506.x

[8] Sezai, A.; Soma, M.; Nakata, K.; Osaka, S.; Ishii, Y.; Yaoita, H.; Hata, H.; Shiono, M. Comparison of febuxostat and allopurinol for hyperuricemia in cardiac surgery patients with chronic kidney disease (NU-FLASH trial for CKD). *Journal of Cardiology*. **2015**, *66*(4), 298–303. doi:10.1016/j.jjcc.2014.12.017

[9] Wang, M.; Zhang, Y.; Zhang, M.; Li, H.; Wen, C.; Zhao, T.; Xie, Z.; Sun, J. The major cardiovascular events of febuxostat versus allopurinol in treating gout or asymptomatic hyperuricemia: a systematic review and meta-analysis. *Annals of Palliative Medicine*. **2021**, *10*(10), 10327–10337. doi:10.21037/apm-21-1564

[10] Mohamed Isa, S.S.P.; Ablat, A.; Mohamad, J. The antioxidant and xanthine oxidase inhibitory activity of *Plumeria rubra* flowers. *Molecules*. **2018**, *23*(2), 1-18. doi:10.3390/molecules23020400

[11] Liang, H.; Deng, P.; Ma, Y.F.; Wu, Y.; Ma, Z.H.; Zhang, W.; Wu, J.D.; Qi, Y.Z.; Pan, X.Y.; Huang, F.S.; Lv, S.Y.; Han, J.L.; Dai, W.D.; Chen, Z. Advances in experimental and clinical research of the gouty arthritis treatment with traditional Chinese medicine. *Evidence-Based Complementary and Alternative Medicine*. **2021**, Article 8698232. doi:10.1155/2021/8698232

[12] Kumar, S.; Pagar, A.D.; Ahmad, F.; Dwibedi, V.; Wani, A.; Bharatam, P.V.; Chhibber, M.; Saxena, S.; Singh, I.P. Xanthine oxidase inhibitors from an endophytic fungus *Lasiodiplodia pseudotheobromae*. *Bioorganic Chemistry*. **2019**, 87, 851-856. doi:10.1016/j.bioorg.2018.12.008

[13] Tran, L.T.T.; Le, T.N.; Ho, D.V.; Nguyen, T.H.; Pham, V.P.T.; Pham, K.T.V.; Nguyen, T.K.; Tran, M.H. Virtual screening and *in vitro* evaluation to identify a potential xanthine oxidase inhibitor isolated from Vietnamese *Uvaria cordata*. *Natural Product Communications*. **2022**, *17*(2), 1-8. doi:10.1177/1934578X221080339.

[14] Hendriani, R.; Nursamsiar, N.; Tjitraresmi, A. *In vitro* and *in silico* evaluation of xanthine oxidase inhibitory activity of quercetin contained in *Sonchus arvensis* leaf extract. *Asian Journal of Pharmaceutical and Clinical Research*. **2017**, *10*(14), 50-53. doi:10.22159/ajpcr.2017.v10s2.19486

[15] Sicho, M.; Svozil, D. Molecular docking as a tool to virtually develop drugs. *Chemicke Listy*. **2017**, *111*(11), 754-759.

[16] Zafar, H.; Iqbal, S.; Javaid, S.; Khan, K.M.; Choudhary, M.I. Xanthine oxidase inhibitory and molecular docking studies on pyrimidones. *Medicinal Chemistry*. **2018**, *14*(5), 524–535. doi:10.2174/1573406413666171129224919

[17] Pan, Y.; Lu, Z.; Li, C.; Qi, R.; Chang, H.; Han, L.; Han, W. Molecular dockings and molecular dynamics simulations reveal the potency of different inhibitors against xanthine oxidase. *ACS omega*. **2021**, *6*(17), 11639–11649. doi:10.1021/acsomega.1c00968

[18] Hou, C.; Shi, C.; Ren, J. Xanthine oxidase targeted model setup and its application for antihyperuricemic compounds prediction by in silico methods. *eFood*. **2021**, 2, 296-306. doi:10.53365/efood.k/147019

[19] Choudhary, D.K.; Chaturvedi, N.; Singh, A.; Mishra, A. Investigation of hypoglycemic effects, oxidative stress potential and xanthine-oxidase activity of polyphenols (gallic acid, catechin) derived from faba bean on 3T3-L1 cell line: insights into molecular docking and simulation study. *Toxicology Research*. **2020**, *9*(3), 308–322. doi:10.1093/toxres/tfaa025

[20] Pongpiriyadacha, Y.; Nuansrithong, P.; Sirintharawech, N. Antioxidant activity and xanthine oxidase inhibitor from Thai medicinal plants used for tonic and longevity. Proceedings of 47th Kasetsart University Annual Conference: Science. (pp 94-102). The Thailand Research Fund, Bangkok, Thailand, **2009**.

[21] Taejarernwiriyakul, O.; Buasai, M.; Rattanatranurak, I.; Sriyod, P.; Chanluang, S. Xanthine oxidase inhibitory activity of medical plants. *Thai Pharmaceutical and Health Science Journal*. **2011**, *6*(1), 1-6.

[22] Seephonkai, P.; Mongkolsiri, N.; Thiabphet, W.; Traisathit, R.; Sedlak, S.; Wongpakam, K.; Dhammaraj, T.; Sangdee, A. Antioxidant, xanthine oxidase inhibitory and antibacterial activities of selected galactogogue Thai medicinal plant water and ethyl acetate extracts. *Journal of Research in Pharmacy*. **2021**, *25*(4), 519-530. doi:10.29228/jrp.42

[23] Bernstein, F.C.; Koetzle, T.F.; Williams, G.J.; Meyer, E.F.; Brice, J.M.D.; Rodgers, J.R.; Kennard, O.; Shimanouchi, T.; Tasumi, M. The Protein Data Bank: a computer-based archival file for macromolecular structures. *Journal of Molecular Biology*. **1977**, *112*(3), 535–542. doi:10.1016/s0022-2836(77)80200-3

[24] Okamoto, K.; Eger, B.T.; Nishino, T.; Kondo, S.; Pai, E. F.; Nishino, T. An extremely potent inhibitor of xanthine oxidoreductase. Crystal structure of the enzyme-inhibitor complex and mechanism of inhibition. *The Journal of Biological Chemistry*. **2003**, *278*(3), 1848–1855. doi:10.1074/jbc.M208307200

[25] Liu, Y.; Yang, X.; Gan, J.; Chen, S.; Xiao, Z.X.; Cao, Y. CB-Dock2: improved protein-ligand blind docking by integrating cavity detection, docking and homologous template fitting. *Nucleic Acids Research*. **2022**, *50(W1)*, W159–W164.doi:10.1093/nar/gkac394

[26] Biovia, D.S. Discovery Studio Visualizer. **2021**, San Diego.

[27] Thangathirupathi, A.; Ali, N.; Natarajan, P.; Kumar, R.D. Molecular docking studies of andrographolide with xanthine oxidase. *Asian Journal of Pharmaceutical and Clinical Research*. **2013**, 6, 295-297.

[28] Yang, Y.; Chen, Q.; Ruan, S.; Ao, J.; Liao, S.-G. Insights into the inhibitory mechanism of viniferifuran on xanthine oxidase by multiple spectroscopic techniques and molecular docking. *Molecules*. **2022**, 27, 7730. doi:10.3390/molecules27227730

[29] Jiwajinda, S.; Santisopasri, V.; Murakami, A.; Kim, O.K.; Kim, H.W.; Ohigashi, H. Suppressive effects of edible Thai plants on superoxide and nitric oxide generation. *Asian Pacific Journal of Cancer Prevention*. **2002**, *3*(3), 215–223.

[30] Peamaroon, N.; Moonrungsee, N.; Boonmee, A.; Suwancharoen, S.; Kasemsuk, T.; Jakmunee, J. Phytochemical and xanthine oxidase inhibitory activity of *Carissa carandas* L. Fruit Extract. *RMUTP Research Journal*. **2020**, *13*(2), 106-118.

[31] Niu, Y.; Li, Q.; Tu, C.; Li, N.; Gao, L.; Lin, H.; Wang, Z.; Zhou, Z.; Li, L. Hypouricemic actions of the pericarp of mangosteen *in vitro* and *in vivo*. *Journal of Natural Products*. **2023**, *86*(1), 24-33. doi: 10.1021/acs.jnatprod.2c00531.

[32] Malik, N.; Dhiman, P.; Khatkar, A. *In silico* design and synthesis of targeted rutin derivatives as xanthine oxidase inhibitors. *BMC Chemistry*. **2019**, *13*, 71. doi:10.1186/s13065-019-0585-8

[33] Pathomweepisut, N.; Thetsana, P.; Tengumnuay, P. Effect of quercetin supplementation on serum uric acid in obese male patients. *Journal of Medicine and Health Sciences*. **2022**, *29*(1), 15-25.

[34] Fitria, L.; Widyananda, M.H.; Sakti, S.P. Analysis of allopurinol, cucurbitacin b, morindine, and piperine as xanthine oxidase inhibitor by molecular docking. *Journal of Smart Bioprospecting and Technology*. **2019**, *1*(1), 6-11. doi:10.21776/ub.jsmartech.2019.001.01.2

[35] Shaik, A.H.; Shaik, S.R.; Shaik, A.S.; Daoud, A.; Salim, M.; Kodidhela, L.D. Analysis of maslinic acid and gallic acid compounds as xanthine oxidase inhibitors in isoprenaline administered myocardial necrotic rats. *Saudi Journal of Biological Sciences*. **2021**, *28*(4), 2575–2580. doi:10.1016/j.sjbs.2021.01.062

[36] Kikuchi, H.; Fujisaki, H.; Furuta, T.; Okamoto, K.; Leimkühler, S.; Nishino, T. Different inhibitory potency of febuxostat towards mammalian and bacterial xanthine oxidoreductases: insight from molecular dynamics. *Scientific Reports*. **2012**, 2, 331. doi: 10.1038/srep00331.

[37] Yamamoto, T.; Moriwaki, Y.; Suda, M.; Nasako, Y.; Takahashi, S.; Hiroishi, K.; Nakano, T.; Hada, T.; Higashino, K. Effect of BOF-4272 on the oxidation of allopurinol and pyrazinamide *in vivo*. Is xanthine dehydrogenase or aldehyde oxidase more important in oxidizing both allopurinol and pyrazinamide?. *Biochemical Pharmacology*. **1993**, *46*(12), 2277–2284. doi:10.1016/0006-2952(93)90618-7

[38] Berglund, L.; Rasmussen, J.T.; Andersen, M.D.; Rasmussen, M.S.; Petersen, T.E. Purification of the bovine xanthine oxidoreductase from milk fat globule membranes and cloning of complementary deoxyribonucleic acid. *Journal of Dairy Science*. **1996**, *79*(2), 198-204. doi:10.3168/jds.S0022-0302(96)76351-8

[39] Habtemariam, S.; Varghese, G.K. Extractability of rutin in herbal tea preparations of *Moringa stenopetala* leaves. *Beverages*. **2015**, *1*(3), 169-182. doi:10.3390/beverages1030169

[40] Buathong, R.; Duangsrisai, S. Plant ingredients in Thai food: a well-rounded diet for natural bioactive associated with medicinal properties. *PeerJ*. **2023**, 11, e14568. doi:10.7717/peerj.14568

[41] Chriscensia, E.; Arham, A.A.; Wibowo, E.C.; Gracius, L.; Nathanael, J.; Hartrianti, P. Eupatorin from *Orthosiphon aristatus*: A Review of The Botanical Origin, Pharmacological Effects and Isolation Methods. *Current Biocative Compounds*. **2023**, *19*(8), e310323215364. doi: 10.2174/1573407219666230331122318

[42] Alotaibi, H.N.; Anderson, A.K.; Sidhu, J.S. Influence of lutein content of marigold flowers on functional properties of baked pan bread. *Annals of Agricultural Sciences*. **2021**, *66*(2), 162-168. doi:10.1016/j.aoas. 2021.12.002

[43] Li, Z.Y.; Wang, Y.; Shen, W.T.; Zhou, P. Content determination of benzyl glucosinolate and anti-cancer activity of its hydrolysis product in *Carica papaya* L. *Asian Pacific Journal of Tropical Medicine*. **2012**, *5*(3), 231–233. doi:10.1016/S1995-7645(12)60030-3

[44] Yorsin, S.; Sriwiriyajan, S.; Chongsa, W. Vasorelaxing effect of *Garcinia cowa* leaf extract in rat thoracic aorta and its underlying mechanisms. *Journal of Traditional and Complementary Medicine*. **2022**, *13*(3), 219–225. doi:10.1016/j.jtcme.2022.12.001

[45] Da-Costa-Rocha, I.; Bonnlaender, B.; Sievers, H.; Pischel, I.; Heinrich, M. *Hibiscus sabdariffa* L. - a phytochemical and pharmacological review. *Food chemistry*. **2014**, 165, 424–443. doi:10.1016/j.foodchem. 2014.05.002

[46] Mackeen, M.M.; Ali, A.M.; Lajis, N.H.; Kawazu, K.; Kikuzaki, H.; Nakatani, N. Antifungal garcinia acid esters from the fruits of *Garcinia atroviridis*. *Zeitschrift fur Naturforschung. C, Journal of biosciences.* **2002**, *57*(3-4), 291–295. doi:10.1515/znc-2002-3-416

[47] Siriamornpun, S.; Sriket, C; Sriket, P. Phytochemicals of Thai local edible herbs. *International Food Research Journal*. **2014**, *21*(3), 1009-1016.

[48] Muangthai, P; Nookaew, P. Monitoring on some organic acids in fresh and processed rural plant leaves in Thailand. *Asian Journal of Natural and Applied Sciences*. **2015**, *4*(1), 82-89.

[49] *Paederia Foetida* Linn: Phytochemistry, pharmacological and traditional uses. *International Journal of Pharmaceutical Sciences and Research*. **2013**, *4*(12), 4525-4530. doi: 10.13040/IJPSR.0975-8232.4(12).4525-30

[50] Tangjitjareonkun, J.; Yahayo, W.; Supabphol, R. Application of *Orthosiphon stamineus* for diuretic effect. *Journal of Medicine and Health Sciences*. **2017**, *24*(1), 67-78.

[51] Azmi, S.M.N.; Jamal, P.; Amid, A. Xanthine oxidase inhibitory activity from potential Malaysian medicinal plant as remedies for gout. *International Food Research Journal*. **2012**, *19*(1), 159-165.

ASEAN
Journal of Scientific and Technological Reports
Online ISSN:2773-8752

Research article

Impacts of Climate Change and Regional Variations on Future Rainfall Patterns in Thailand by Downscaling Method

Supanee Maichandee[1], Prachaya Namwong[2], Onuma Methakeson[3]*

[1] Faculty of Sciences and Agricultural Technology, Rajamangala University of Technology Lanna, 50300, Thailand; supanee_j@rmutl.ac.th
[2] Faculty of Sciences and Agricultural Technology, Rajamangala University of Technology Lanna, 50300, Thailand; prachaya@rmutl.ac.th
[3] Faculty of Sciences and Agricultural Technology, Rajamangala University of Technology Lanna, 50300, Thailand; pookonuma_k@rmutl.ac.th
* Correspondence: pookonuma_k@rmutl.ac.th

Citation:
Maichandee, S.; Namwong, P.; Methakeson, S. Impacts of climate change and regional variatons on future rainfall patterns in Thailand by downscaling method. *ASEAN J. Sci. Tech. Report.* **2024**, *27*(1), 80–91. https://doi.org/10.55164/ajstr.v27i1.250817.

Article history:
Received: September 4, 2023
Revised: December 11, 2023
Accepted: December 12, 2023
Available online: December 28, 2023

Abstract: In this study, we investigated the impacts of climate change on rainfall patterns in Thailand using the downscaling method. The simulation data was obtained from the Weather Research and Forecasting (WRF) model, using the Community Earth System Model (CCSM) as a boundary condition. The characteristics of rainfall were analyzed in terms of the total annual rainfall, rainfall intensity, the number of days with heavy rain, and the total amount of rainfall in each season in the future compared to the base periods. It was found that the simulation of the climate in upper Thailand was consistent with the reanalysis values, with TCC ranging from 0.6 to 0.9. The simulated annual rainfall amount is underestimated throughout the country. There are indications that rainfall will increase in average and extreme terms in some regions, including the eastern region of the Northeast, the western side of the North, and the upper part of the West. In the southern part of the country, the overall rainfall indices are expected to decrease with low confidence in almost the entire region.

Keywords: WRF model; CCSM; Climate simulation; Rainfall in Thailand; Dynamical downscaling

1. Introduction

Nowadays, many studies provide evidence to support the conclusion that the global climate is changing [1-3]. Numerous studies confirm that global temperatures have risen from the past to the present, and this trend is expected to continue in the future [4–7]. A rise in temperature increases the air's ability to hold water, increasing atmospheric water vapor. The higher storm moisture content results in stronger storms and more severe flooding. Surface heating increases evaporation, which leads to a drier soil surface. This, in turn, can increase the risk of severe and prolonged drought [8].

One interesting topic is the response of rainfall characteristics to climate change, which can vary from region to region. Simulation of the climate using a climate model is an effective tool for studying future climate change. The capability of climate simulation is often evaluated by comparing the outputs of past simulations with observational data. Global climate changes have been simulated using Global Climate Models (GCMs) by numerous renowned climate research organizations. The outputs from the GCMs are too coarse and unsuitable for regional climate change studies. One commonly used approach to improve the resolution of the output is dynamical downscaling using regional climate models (RCMs). RCM simulation utilizes geographical data and GCM output as lateral boundary data to process and obtain an output with sufficient

resolution for studying climate at a regional scale. GCMs and RCMs are computational models that employ the principles of fluid dynamics and thermodynamics to calculate the rates of change in various physical attributes, including water vapor, heat, cloud water, temperature, and carbon.

The Intergovernmental Panel on Climate Change (IPCC) has released a statement on the projection of carbon dioxide concentrations. In the Fifth Edition of the Climate Report, the projection of greenhouse gas concentrations under various conditions was referred to as the Representative Concentration Pathway (RCP2.6, 4.5, 6.0, and 8.5) [9]. The numbers at the end of each RCP (2.6, 4.5, 6.0, and 8.5) represent the concentrations in 2100 relative to the pre-industrial level. Therefore, RCP8.5 is considered the worst-case scenario. A new set of climate scenarios has been developed concerning the sixth IPCC report [10]. The scenarios are indicated as SSPx-y, where 'SSPx' refers to the shared socio-economic pathway (SSP1, SSP2, SSP3, and SSP5), describing the socio-economic trends underlying the scenario, and 'y' denotes the approximate level of radiative forcing resulting from the scenario in the year 2100. There are five main scenarios (SSP1-1.9, SSP1-2.6, SSP2-4.5, SSP3-7.0, and SSP5-8.5).

Changes in the future climate, as predicted by different models and projection pathways, yield different outputs. The average precipitation may both increase and decrease [11]. The increased heat and humidity results in more precipitation under the RCP4.5 and RCP8.5 projections [12]. An increase in precipitation was observed in both intensity and frequency in almost all East Asian areas under the RCP4.5 projection [13]. Long-term climate projection at high resolution for Southeast Asia at 20x20 km resolution up to the end of the 21st century using a regional climate model from the Hadley Centre based on datasets from the ECHAM4 under the A2 GHG emission scenario was simulated by Chinvanno et al. [14]. Results show that precipitation tends to fluctuate in the first half of the century but shows an increasing trend with higher intensity, which will be seen in the latter half. Maijandee et al. [15] studied the extreme rainfall index in Thailand using the output from the MM5-RCM model. The raw outputs from the MM5-RCM were adjusted using the direct method to reduce biases. The study results suggest that most regions in the North, West, and Northeast will experience an increase in rainfall during the rainy season and a decrease in rainfall during the dry season. The central and eastern regions may experience decreased rainfall during the rainy season and increased rainfall during the dry season. The number of consecutive rainy days for the southern region tends to decrease on the Andaman side and increase on the southeast coast. The predicted extreme precipitation during 2020–2029 relative to 1990–1999 in Thailand under RCP8.5 has been examined using the simulation of the NRCM based on the WRF model forced by the Community Climate System Model version 4 (CCSM4) [16]. The study indicates an increasing pattern of annual precipitation levels in northern Thailand, while significant decreasing trends are projected for the eastern region. A remarkable rising trend in the simple daily intensity index (SDII) is predicted, with statistically significant increases ranging from 5% to 20%. Projected changes in the means and extremes of precipitation over Thailand were discussed under the A2, A1B, and B1 emission scenarios [17]. There is a prediction of a shift to drier conditions over the Central-East and South sub-regions in every season under all scenarios. The projected changes in rainfall over Thailand for the early (2011–2040), middle (2041–2070), and late (2071–2099) periods under the RCP4.5 and RCP8.5 were examined using the high-resolution multi-model simulations from the Coordinated Regional Climate Downscaling Experiment (CORDEX) [18]. The ensemble means of rainfall changes for both RCPs during dry months reveal a clear contrast between the northern-central-eastern and southern parts of Thailand, which generally experience wetter and drier conditions, respectively. In contrast, it is projected that generally drier conditions will prevail throughout the country during the wet season (June to September) for both RCPs. Masud et al. [19] analyzed 24 extreme weather indices in Northern Thailand. The observation data used included the maximum and minimum temperatures and the daily precipitation data from 1960 to 2010. HadCM3 and PRECIS were used as GCM and RCM models, respectively. Climate modeling for 1960–2100 was conducted using the statistical downscaling method. The result shows an insignificant decrease in total annual rainfall, but it is anticipated that annual rainfall will increase in the future compared to the base period. Based on the findings of the Intergovernmental Panel on Climate Change (IPCC) Sixth Assessment Report (AR6), there is anticipated to be an elevation in precipitation levels in regions situated at high latitudes, the equatorial Pacific, and certain areas within the monsoon regions. Conversely, a reduction in precipitation is expected in certain parts of the subtropics and the limited regions within the tropics [10].

Rainwater is an important source of water in Thailand. It is important for agriculture, especially crops that rely on rainfall for growth. The country's agriculture is predominantly seasonal. Variations in rainfall patterns can lead to decreased quantities and quality of agricultural products. Dramatic changes in rainfall patterns, such as increased or decreased rainfall, might lead to more frequent and severe floods and droughts. Drought has resulted in farmers being unable to grow crops effectively. Flooding has caused significant damage to the country. These incidents result in losses that harm the economy, national development, quality of life, population health, and ecological balance. Rainfall change data is valuable for planning in various sectors, including agriculture, water management, tourism, public health, and business development.

In this research, we simulated the responses of rainfall characteristics to climate change in Thailand. The downscaling method was used. The regional climate model used is the WRF model. The GCM output is obtained from CCSM4 as boundary data.

2. Materials and Methods

The simulation domain is Thailand, and double-nested domain experiments were conducted. The two domains are indicated in Figure 1. Two periods were selected for simulation to study the changes in rainfall: the base year (1990-1999) and the future years (2020-2029). The simulation was obtained from the Weather Research and Forecasting Model (WRF) version 3.8.1, developed by the National Center for Atmospheric Research (NCAR). The forcing data is from the Community Climate System Model (CCSM), a coupled climate model for simulating the Earth's climate system with components representing the Earth's atmosphere, ocean, land surface, and sea ice [20]. CCSM4 is a subset of CESM1 (The Community Earth System Model). The dataset is also available from NCAR's CISL Research Data Archive (http://rda.ucar.edu/datasets/ds316.0).

The CESM dataset. CESM data has an intermediate file format ready to be imported into the model. The projection used to simulate future rainfall is RCP6.0. The physics options used in WRF include the Kain-Fritsch (new Eta) scheme [21–22] for the Cumulus option, the Monin-Obukhov Similarity scheme [23] for the Surface-layer option, the Noah Land-Surface Model [24] for the Land-surface option, the WRF Single-Moment (WSM) 3-class simple ice [25] for the Microphysics Schemes, the YSU scheme [26] for the Boundary-layer option, the RRTM Radiation [27] for Longwave Radiation, and the Dudhia scheme [28] for Shortwave Radiation.

Most of the parameters chosen for analysis, except the cumulus option, are commonly employed in climate simulations in Southeast Asia [29–32]. For the cumulus option, the author selected the Kain-Fritsch (new Eta) scheme for this study to present an alternative simulation perspective, as several studies have shown that this scheme is also suitable as a good option and has been used in Thailand climate simulation as well [33–34].

The initial 3-month (October–December of 1898) period is designated a spin-up period, and the outputs during this period are not included in the analysis. To evaluate the performance of the WRF simulation, the output with a 20 km grid spacing resolution for the base-year period was compared to the reanalysis data. The temporal correlation coefficients (TCC) between observations and simulations are calculated and used to quantify the performance of RCMs [35]. The correlation coefficient is a quantity that gives the quality of a least squares fit to the original data. This operator correlates each gridpoint of two fields over all timesteps [36].

The characteristics of Thailand's rainfall are analyzed in terms of the total annual rainfall, rainfall intensity (the amount of rainfall per rainy day), the number of days with heavy rain (the days with rainfall exceeding 20 mm in a year), and the average total rainfall in each season. The changes in rainfall are indicated by the annual average percentage change in the future year compared to the base year.

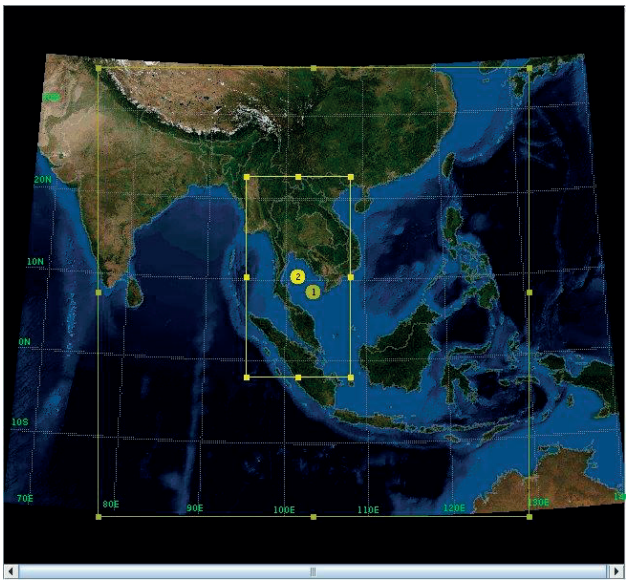

Figure 1. Shows the study domain.

3. Results and Discussion

3.1 Evaluation of the model

3.1.1 Temporal Correlation Coefficient (TCC) between simulation and reanalysis data

Figure 2. shows the temporal correlation coefficient, which is a variable that indicates the temporal relationship between the model results and the reanalysis values in the base year. The model results were correlated with the observational values, with TCC ranging from 0.18–0.9. The climate simulation in upper Thailand yielded consistent results with the reanalysis data, showing TCC values ranging from 0.6 to 0.9. The simulation revealed temporal inconsistency in the model values, particularly in the southern region and certain parts of the eastern region, specifically Chonburi and Rayong province, with low TCC values ranging from 0.18 to 0.5. Temporal inconsistencies in Southern Thailand are not unexpected due to the region's climate, characterized by high temporal and spatial variability, particularly regarding rainfall.

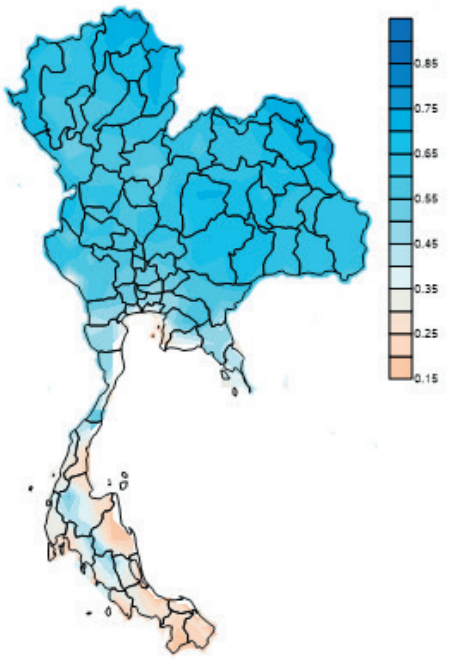

Figure 2. Shows TCC Between simulation and reanalysis data.

3.1.2 Rainfall Distribution from Simulation and Reanalysis Data

Figure 3 shows that the model can simulate high rainfall areas well, especially in the southern, western, and eastern regions of the Northeast. However, the simulated rainfall is significantly lower than the observed values for the entire country, especially in the Southern region.

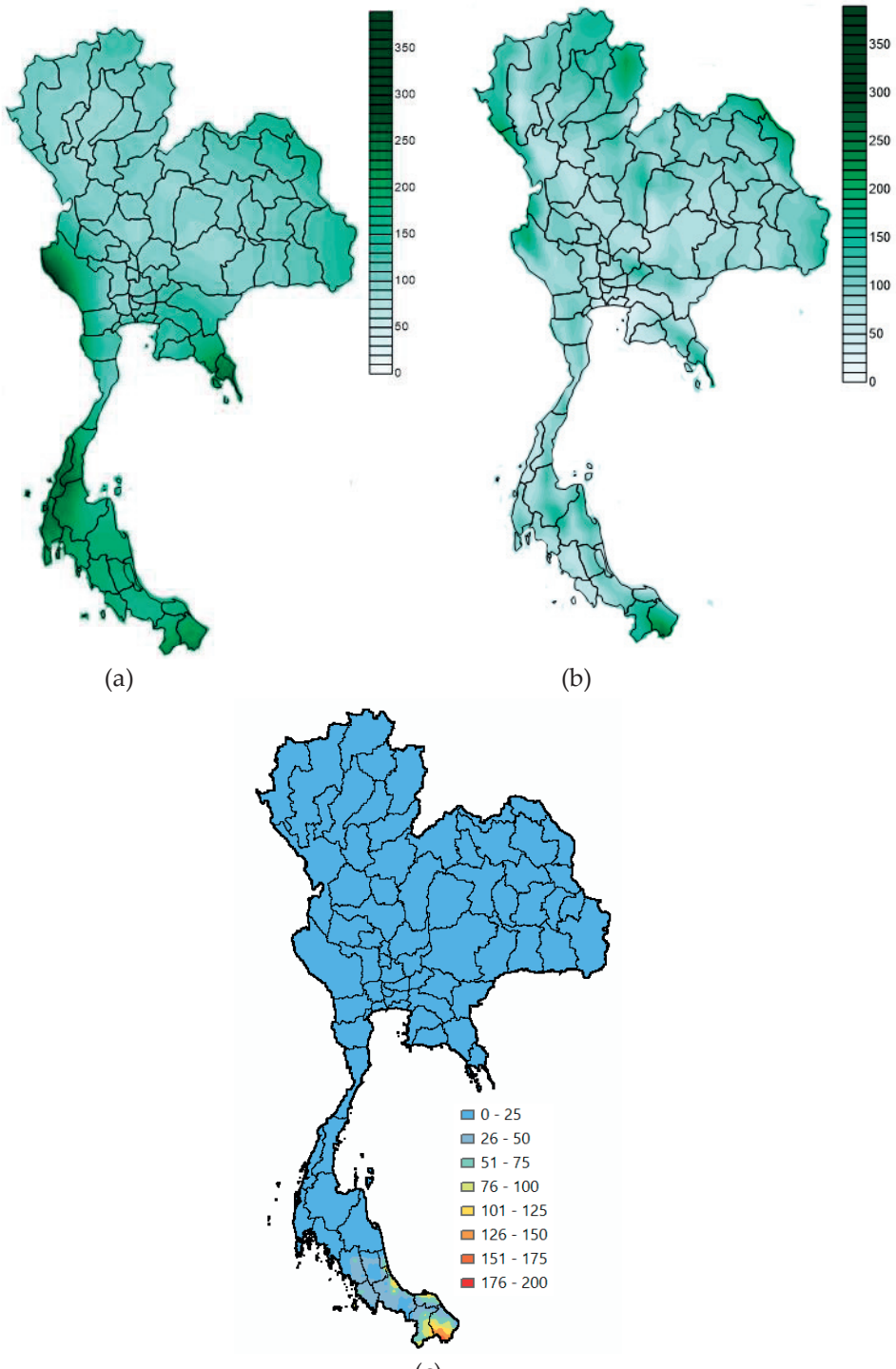

Figure 3. Shows the average annual rainfall (in cm) during the base-year period of 1990–1999, derived from reanalysis data (a) and the output of the WRF simulation (b), and (c) the difference between the two datasets utilizing the IDW technique.

3.2 Projection of Future Rainfall Changes

3.2.1 Projection of changes in the average total annual rainfall.

As shown in Figure 4., more annual rainfall is expected in the lower central, upper West, and eastern regions of the Northeast. Most areas in the Northeast, East, and South may experience a decrease in rainfall. There is an expectation that the northern part of the western region and the western part of the North, which are adjacent to the Thongchai mountain range, will experience an increase in average annual rainfall in the future.

3.2.3 Projection Changes in Rainfall Intensity on a Rainy Day

Figure 5. shows the intensity of rainfall on rainy days. The index is frequently analyzed to assess extreme climate conditions. According to the simulation results, it can be seen that most areas in the upper part of Thailand are likely to experience heavier rainfall. The eastern part of the Northeast and the western and northwestern regions are expected to experience an increase in both total annual rainfall and rainfall intensity. In the future, it is predicted that almost all regions in the south, which currently receive a particularly large amount of rainfall, will experience a decrease in rainfall intensity.

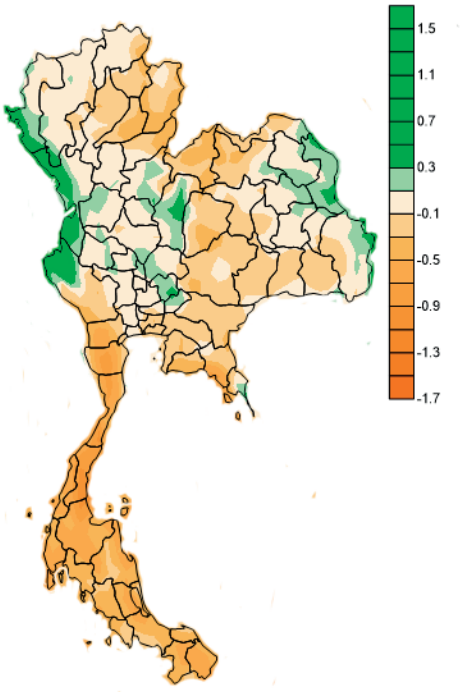

Figure 4. Shows the projected changes in average total annual rainfall in percentage.

As shown in Figure 4, it is evident that most regions in the country are expected to experience decreased precipitation. This could be attributed to the elevated average rainfall during the reference period (1990-1999). There was a noticeable rise in summer rainfall after the mid-1990s. According to the study by Faikrua et al. [37], most of Thailand experienced increased summer precipitation after 1994. The possible causes of this phenomenon are cyclonic anomalies over the Indochina Peninsula in the lower troposphere and the stronger ascending motion of local Hadley circulation over eastern Thailand after 1994.

The increase in rainfall intensity on a rainy day in upper Thailand follows Teerachai's result, in which a remarkable rising trend of annual SDII in 2020–2029 relative to 1990–1999 is observed in the simulation using RCP 8.5 [16].

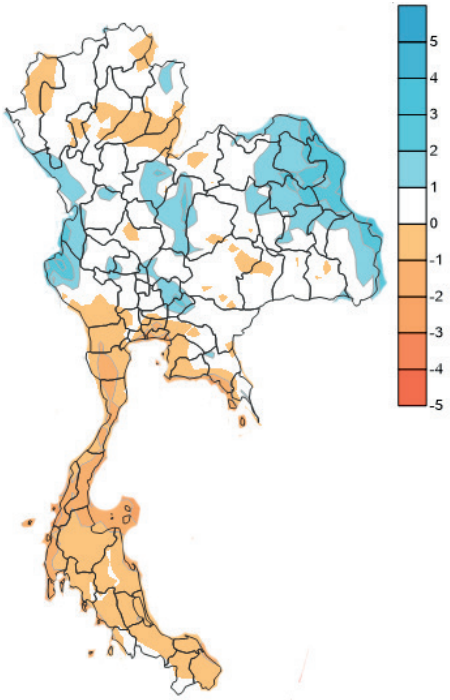

Figure 5. Shows the projected changes in average rainfall intensity on a rainy day in percentage.

3.2.3 Projection changes in the number of days of heavy rain

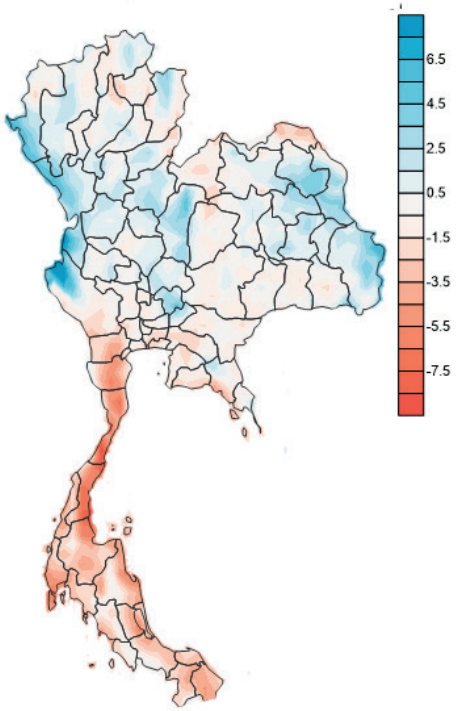

Figure 6. Shows the projected changes in the number of days with heavy rainfall in percentage.

Figure 6 shows that the number of heavy rainfall days is generally increasing in most parts of the upper country, especially in the northern, northeastern, and central regions. On the contrary, the southern region is expected to experience a decreasing trend in the number of days with heavy rainfall. The change in the number of heavy rain days ranges from -8 to 7 percent.

3.2.4 Changes in Seasonal Rainfall

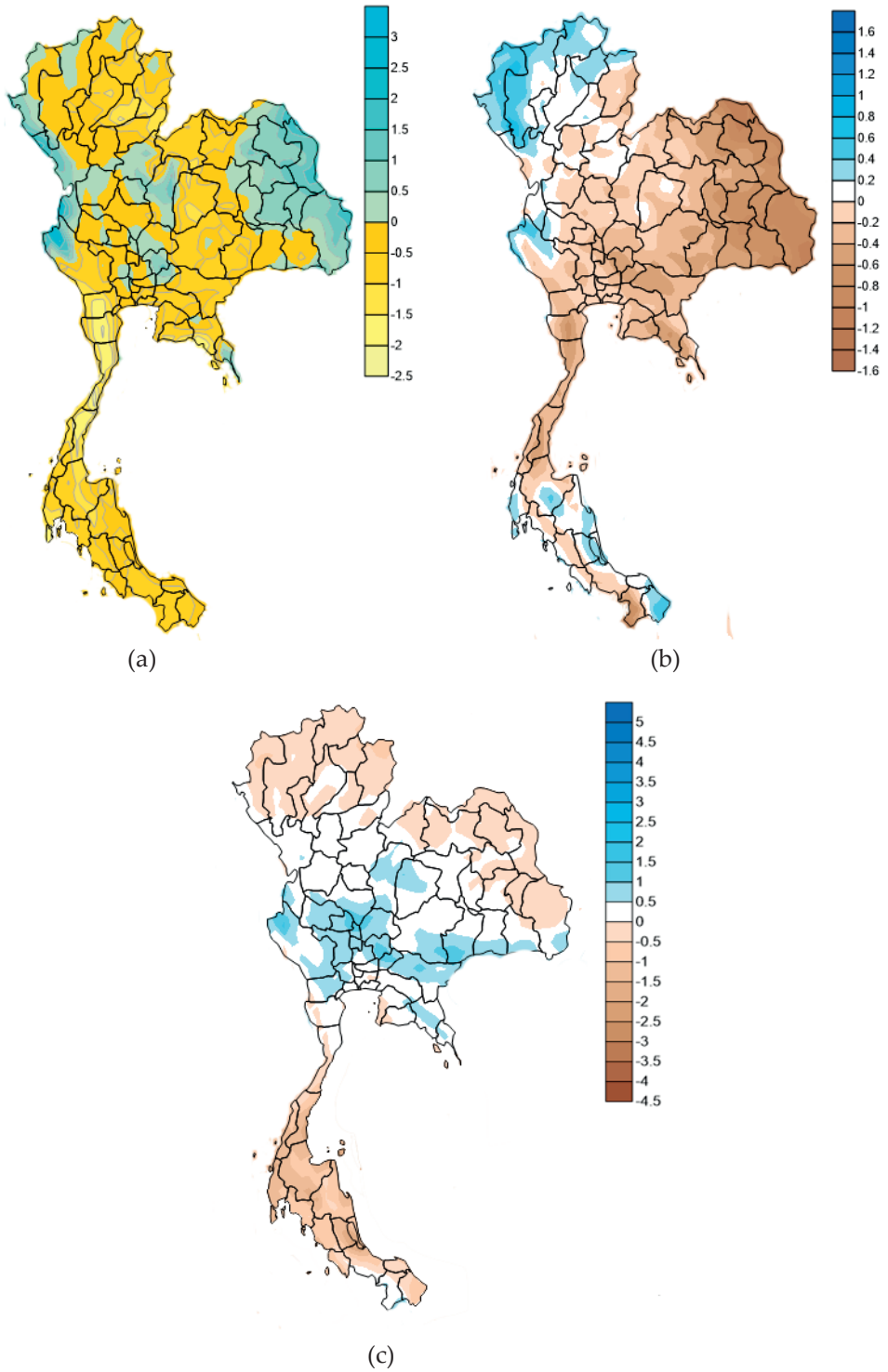

(a) (b)

(c)

Figure 7. Shows the projected changes in seasonal rainfall in percentage during (a) the rainy season (June to September), (b) summer (March to May), and (c) winter (October to February).

The average rainfall pattern during the rainy season is similar to yearly rainfall. This season's rainfall increase is expected in some parts of the North, West, Central, and Northeast regions. Figure 7(b) shows that most areas will receive less summer rainfall, especially in the Northeast and east. An increase in summer rainfall is also observed in some parts of the northern, western, and southern regions. A projected change in

winter rainfall in most areas in the upper part of the country ranges from -0.5 to 1 percent. The southern part of the country has experienced a more significant decrease in rainfall than other regions.

Some of the findings from this study are consistent with the research conducted from the ensemble means of projected changes in rainfall for RCP4.5 and RCP8.5 by Tangang et al. [18]. The results show a distinct contrast between the northern-central-eastern parts and the southern parts of Thailand, with generally wetter and drier conditions, respectively (during dry months), while generally drier conditions are projected during the wet season (June to September) throughout the country.

In general, there is a decrease in rainfall across most regions of Thailand. This finding may differ from the results in earlier research. For example, according to Arpornrat et al. [33], the average southwest monsoon rainfall in Thailand is expected to increase by the end of the century. Chotamonsak et al. [29] suggested that there will be overall increases in precipitation, with some local decreases during the dry season. Additionally, Chinvanno et al. [14] stated that precipitation will likely fluctuate in the first half of the century, with higher rainfall expected across the region in the latter half. However, the experiments are climate simulations under different conditions (models, periods, RCP, etc.). The decrease in rainfall has also been published in several studies. For example, an annual precipitation total decline (PRCPTOT index) has been observed in eastern Thailand in WRF simulation under RCP 8.5 [16]. Additionally, CORDEX-SEA simulations at 25 km spatial resolution under RCP4.5 and 8.5 have shown a decrease in annual precipitation over most of the SEA region by the end of the 21st century [18]. According to Manomaiphiboon et al. [38], while there are no substantial changes in average precipitation in the upper sub-regions, less rain is expected for the South in most seasons in the mid-21st century years simulation under IPCC A2, A1B, and B1 scenarios.

4. Conclusions

Climate change is a phenomenon that affects many different fields and has been investigated for decades. Many studies have found that this phenomenon affects rainfall characteristics in various regions. This research analyzed the response of rainfall to climate change in Thailand. The results of the CESM model with RCP 6.0 emission assumptions were used. The output from the CESM model was dynamically downscaled using the WRF regional climate model to increase the resolution. Two periods were selected for simulation to study the changes in rainfall: the base year (1990-1999) and the future years (2020-2029). Results from the simulation in the base year are evaluated by comparing them to the reanalysis data, which represents the observed data. The evaluation found that the simulation of the climate in upper Thailand was consistent with the reanalysis values. The TCC values indicate low temporal consistency with the reanalysis, ranging from 0.18 to 0.5 in the South, a region characterized by high rainfall variability. WRF can simulate rainy areas well, but the amount of rainfall is underestimated compared to the observed value. However, lower values may not impact the projected changes in rainfall because the simulated changes are based on comparing two data sets, both of which have underestimated values.

The projections indicate that some parts of the upper and most parts of the south of the country will probably experience a decrease in rainfall annually and seasonally, particularly during the summer. There are indications that rainfall will increase in both average and extreme conditions, such as total annual rainfall, rainfall intensity, and the number of days with heavy rainfall, in some regions, including the eastern region of the Northeast, the western side of the North, and the upper part of the West. These regions receive more rainfall than other parts of the country, and there will likely be an increase in both the frequency and intensity of rainfall. The area of interest is the southern part of the country, where the overall rainfall indices are expected to decrease annually and seasonally, except for some areas where summer rain is expected to increase. However, considering the evaluation, confidence in the simulations in this area is low.

The results from this simulation are quite different from those of our previous research [15]. This difference may be attributed to the utilization of different models and options. Multiple studies indicate that in the future, rainfall in Thailand is likely to fluctuate, with both increases and decreases. The results depend on the simulation conditions, the model used, the different model options, and the study period. The numerous factors that affect rainfall simulation make it really challenging to obtain accurate simulation values. To utilize the simulation data, users must be aware that the output of simulations inevitably contains

discrepancies. The application of simulation results should be studied through extensive research and requires prior knowledge and understanding before implementation.

5. Acknowledgements

The authors express their gratitude to the funding entities. (Thailand Science Research and Innovation (TSRI) through University of Technology Lanna).

Author Contributions: Conceptualization, S.M.; Data processing, O. M.; Evaluation and Projection analysis, all authors.; Paper writing, S. M.; Editing, P.N.; Corresponding author, O. M. All authors have read and agreed to the published version of the manuscript.

Funding: Thailand Science Research and Innovation (TSRI) through Rajamangala University of Technology *Lanna*

Conflicts of Interest: The authors declare no conflict of interest.

References

[1] Dore, M. H. Climate change and changes in global precipitation patterns: what do we know?. *Environment international*. **2005**, *31*(8), 1167-1181.

[2] Pachauri, R. K.; Allen, M. R.; Barros, V. R.; Broome, J.; Cramer, W.; Christ, R.; ... & van Ypserle, J. P. (2014). *Climate change 2014: synthesis report. Contribution of Working Groups I, II and III to the fifth assessment report of the Intergovernmental Panel on Climate Change* (p. 151). Ipcc. **2014**.

[3] Adedeji, O. Global climate change. *Journal of Geoscience and Environment Protection*. **2014**, *2*(2), 114.

[4] Hansen, J.; Sato, M.; Ruedy, R.; Lo, K.; Lea, D. W.; Medina-Elizade, M. Global temperature change. *Proceedings of the National Academy of Sciences*. **2006**, *103*(39), 14288-14293.

[5] IPCC, I. (2014). Climate change 2014: Synthesis report. Contribution of working groups I, II and III to the fifth assessment report of the intergovernmental panel on climate change.

[6] Lindsey, R.; Dahlman, L. Climate change: Global temperature. *Climate. Gov*. **2020**, 16.

[7] Sentian, J., Payus, C. M., Herman, F., & Kong, V. W. Y. (2022). Climate change scenarios over Southeast Asia. *APN Science Bulletin*.

[8] Trenberth, K.E. Changes in precipitation with climate change. *Climate research*. **2011**, 47(1-2),123-138.

[9] Nurse, L. A.; McLean, R. F.; Agard, J.; Briguglio, L. P.; Duvat-Magnan, V.; Pelesikoti, N.; ... & Webb, A. Small islands Climate Change 2014: Impacts, Adaptation, and Vulnerability. Part B: Regional Aspects. Contribution of Working Group II to the Fifth Assessment Report of the Intergovernmental Panel on Climate Change ed VR Barros et al. **2014**.

[10] Masson-Delmotte, V. P.; Zhai, P.; Pirani, S. L.; Connors, C.; Péan, S.; Berger, N.; ... & Scheel Monteiro, P. M. Ipcc, 2021: Summary for policymakers. in: Climate change 2021: The physical science basis. contribution of working group i to the sixth assessment report of the intergovernmental panel on climate change. **2021**.

[11] Chong-Hai, X. U.; Ying, X. The projection of temperature and precipitation over China under RCP scenarios using a CMIP5 multi-model ensemble. *Atmospheric and Oceanic Science Letters*. **2012**, *5*(6), 527-533.

[12] Oh, S. G.; Park, J. H.; Lee, S. H.; Suh, M. S. Assessment of the RegCM4 over East Asia and future precipitation change adapted to the RCP scenarios. *Journal of Geophysical Research: Atmospheres*. **2014**, *119*(6), 2913-2927.

[13] Chen, H.; Sun, J. Projected change in East Asian summer monsoon precipitation under RCP scenario. *Meteorology and Atmospheric Physics*. **2013**, *121*, 55-77.

[14] Chinvanno, S.; Luang-aram, V.; Sangmanee, C.; Thanakitmetavut, J. Future Climate Projection for Mainland Southeast Asia Countries: Climate Change Scenario of 21st Century. APN, 36. **2011**.

[15] Maijandee, S.; Kreasuwun, J.; Komonjinda, S.; Promnopas, W. Effects of climate change on future extreme rainfall indices over Thailand. *Global NEST Journal*. **2014**, *16*(2), 306-315.

[16] Amnuaylojaroen, T. Projection of the precipitation extremes in Thailand under climate change scenario RCP8. 5. *Frontiers in Environmental Science*. **2021**, *9*, 657810.

[17] Manomaiphiboon, K.; Octaviani, M.; Torsri, K.; Towprayoon, S. Projected changes in means and extremes of temperature and precipitation over Thailand under three future emissions scenarios. *Climate research*. **2013**, *58*(2), 97-115.

[18] Tangang, F.; Santisirisomboon, J.; Juneng, L.; Salimun, E.; Chung, J.; Supari, S.; ... & Yang, H. Projected future changes in mean precipitation over Thailand based on multi-model regional climate simulations of CORDEX Southeast Asia. *International Journal of Climatology*. **2019**, *39*(14), 5413-5436.

[19] Masud, M. B.; Soni, P.; Shrestha, S.; Tripathi, N. K. Changes in climate extremes over North Thailand, 1960–2099. *Journal of Climatology*. **2016**.

[20] Gent, P. R.; Danabasoglu, G.; Donner, L. J.; Holland, M. M.; Hunke, E. C.; Jayne, S. R.; ... & Zhang, M. The community climate system model version 4. *Journal of climate*. **2011**, *24*(19) , 4973-4991.

[21] Kain, J. S.; Fritsch, J. M. Convective parameterization for mesoscale models: *The Kain-Fritsch scheme. In The representation of cumulus convection in numerical models* (pp. 165-170). Boston, MA: American Meteorological Society. **1993**.

[22] Kain, J. S. The Kain–Fritsch convective parameterization: an update. *Journal of applied meteorology*. **2004**, *43*(1), 170-181.

[23] Jiménez, P. A.; Dudhia, J.; González-Rouco, J. F.; Navarro, J.; Montávez, J. P.; García-Bustamante, E. A revised scheme for the WRF surface layer formulation. *Monthly weather review*. **2012**, *140*(3), 898-918.

[24] Chen, F.; Dudhia, J. Coupling an advanced land surface–hydrology model with the Penn State–NCAR MM5 modeling system. Part I: Model implementation and sensitivity. *Monthly weather review*. **2001**, *129*(4), 569-585.

[25] Hong, S. Y.; Dudhia, J.; Chen, S. H. A revised approach to ice microphysical processes for the bulk parameterization of clouds and precipitation. *Monthly weather review*. **2004**, *132*(1), 103-120.

[26] Hong, S. Y.; Noh, Y.; Dudhia, J. A new vertical diffusion package with an explicit treatment of entrainment processes. *Monthly weather review*. **2006**, *134*(9), 2318-2341.

[27] Mlawer, E. J.; Taubman, S. J.; Brown, P. D.; Iacono, M. J.; Clough, S. A. Radiative transfer for inhomogeneous atmospheres: RRTM, a validated correlated-k model for the longwave (Paper 97JD00237). *Journal of geophysical research-all series*. **1997**, *102*, 16-663.

[28] Dudhia, J. Numerical study of convection observed during the winter monsoon experiment using a mesoscale two-dimensional model. *Journal of Atmospheric Sciences*. **1989**, *46*(20), 3077-3107.

[29] Chotamonsak, C.; Salathé Jr, E. P.; Kreasuwan, J.; Chantara, S.; Siriwitayakorn, K. Projected climate change over Southeast Asia simulated using a WRF regional climate model. Atmospheric Science Letters. **2011**, *12*(2), 213-219.

[30] Amnuaylojaroen, T.; Barth, M. C.; Pfister, G.; Bruyere, C. Simulations of emissions, air quality, and climate contribution in Southeast Asia for March and December. *Land-atmospheric research applications in South and Southeast Asia*. **2018**, 233-254.

[31] Kaewmesri, P.; Archevarapuprok, B.; Sooktawee, S. The performance rainfall during rainy seasonal over thailand by using preliminary regional coupled atmospheric and oceanic (wrf-roms) model. *GEOMATE Journal*. **2018**, *14*(45), 109-115.

[32] Ratjiranukool, P.; Ratjiranukool, S. Projection of Extreme Temperature over Northern Thailand by WRF Model. *Applied Mechanics and Materials*. **2017**, *866*, 104-107.

[33] Arpornrat, T.; Ratjiranukool, S.; Ratjiranukool, P.; Sasaki, H. Evaluation of southwest monsoon change over Thailand by high-resolution regional climate model under high RCP emission scenario. *In Journal of Physics: Conference Series*. **2018**, *1144*(1), 012112.

[34] Kirtsaeng, S.; Kreasuwun, J.; Chantara, S.; Kirtsaeng, S.; Sukthawee, P.; Masthawee, F. Weather Research and Forecasting (WRF) model performance for a simulation of the 5 November 2009 heavy rainfall over southeast of Thailand. *Chiang Mai J Sci*. **2012**, *39*(3), 511-523.

[35] Yu, K.; Hui, P.; Zhou, W.; Tang, J. Evaluation of multi-RCM high-resolution hindcast over the CORDEX East Asia Phase II region: Mean, annual cycle and interannual variations. *International Journal of Climatology*. **2020**, *40*(4), 2134-2152.

[36] Schulzweida, U.; Kornblueh, L.; Quast, R. CDO user guide. **2019**.

[37] Faikrua, A.; Pimonsree, S.; Wang, L.; Limsakul, A.; Singhruck, P.; Dong, Z. Decadal increase of the summer precipitation in Thailand after the mid-1990s. *Climate Dynamics*. **2020**, *55*, 3253-3267.

[38] Manomaiphiboon, K.; Octaviani, M.; Torsri, K.; Towprayoon, S. Projected changes in means and extremes of temperature and precipitation over Thailand under three future emissions scenarios. Climate research. **2013**, *58*(2), 97-115.

ASEAN
Journal of Scientific and Technological Reports
Online ISSN:2773-8752

Research article

Carbon Footprint Assessment Based on Life Cycle Assessment of Biomass Power Plant

Jutamas Kaewmanee[1]*, Piyaruk Pradabphetrat[2], and Vichit Rangpan[3]

[1] Program in Management of Natural Resources and Environment, Yala Rajabhat University, Yala, 95000, Thailand; jutamas.k@yru.ac.th
[2] Faculty of Science Technology and Agriculture, Yala Rajabhat University, Yala, 95000, Thailand; Piyaruk.p@yru.ac.th
[3] Faculty of Science Technology and Agriculture, Yala Rajabhat University, Yala, 95000, Thailand; Vichit.r@yru.ac.th
* Correspondence: jutamas.k@yru.ac.th

Citation:
Kaewmanee, J.; Pradabphetrat, P.; Rangpan, V. Carbon Footprint Assessment Based on Life Cycle Assessment of Biomass Power Plant. *ASEAN J. Sci. Tech. Report.* **2023**, *27*(1), 92-101. https://doi.org/10.55164/ajstr.v27i1.250754.

Article history:
Received: August 31, 2023
Revised: December 1, 2023
Accepted: December 6, 2023
Available online: December 28, 2023

Abstract: This research aims to study the carbon footprint based on the life cycle assessment of biomass power plants. Covering the acquisition of raw materials to the end of the production process in biomass power plants (cradle to grave: C2G). The study proposes constructive ways to reduce the carbon footprint of biomass power plants. Conducted research consisting of 3 phases: phase 1, the rubber plantation process; phase 2, the rubber wood processing plant; and phase 3, the biomass power plant. Assessment of carbon footprint: following the principle of life cycle assessment, the results of the carbon footprint assessment found that in Phase 1, the process of growing rubber trees throughout the life cycle calculated the carbon footprint of the sample group as average greenhouse gas emissions from fresh rubber wood and combined with the average greenhouse gas emissions from rubber wood timbers of 1.1186 kgCO_2eq per day. In phase 2, rubber wood processing plants throughout the life cycle have average greenhouse gas emissions of 15,319.11 kgCO_2eq per day. In phase 3, biomass power plants electricity capacity is 9.9 MW per day, and their greenhouse gas emissions are 44,753.60 kg CO_2eq per day. The result found that greenhouse gas emissions from biomass power plants per 1 kWh accounted for a carbon dioxide equivalent of 4.52 kgCO_2eq. Calculate the predictor factors affecting the amount of greenhouse gases in biomass power plants in raw score form as Y = 373.516 +.082 (raw material quantity), where Y is the greenhouse gas emission (kgCO_2eq), using the forecast equation in standard score form. With Z =.983$_{\text{raw material quantity3}}$, It was found that the quantity of raw materials had a positive correlation with the quantity of greenhouse gases at a statistical significance of .01 with a correlation coefficient of .983, which could explain the variability of the variables of the quantity of greenhouse gases with 96.70 percent accuracy.

Keywords: Carbon Footprint; Biomass Power Plants; Rubberwood; Life Cycle Assessment

1. Introduction

According to the global greenhouse gas emissions scenario for 2021, carbon dioxide (CO_2) emissions are projected to grow by 4.8 percent as the economic recovery increases. Due to the coronavirus disease 2019 (COVID-19) situation as well as global emissions in 2021 of approximately 400 million tons of carbon dioxide equivalent (MtCO_2eq), there will be an increase of 1,500 MtCO_2eq of CO_2 [1].

The emission of carbon dioxide in Thailand in 2018 also increased by an average of 3 percent per year, in line with the country's energy consumption, which increased by an average of 3.7 percent per year. However, in 2019, carbon dioxide from energy use was 250.6 $MtCO_2eq$, a 4.8 percent decrease compared to the previous year. The increasing use of renewable energy, according to the government's renewable energy promotion policy, is reducing the emission of carbon dioxide from energy use. Carbon emissions from energy use in the first 6 months of 2020 were 113.9 $MtCO_2eq$, which decreased in all economic sectors, including electricity generation, transportation, industrial, and other economic sectors [2].

The Electricity Generating Authority of Thailand found that the southern electricity generating system in 2020 was at risk because the consumption demand for electricity in the southern region in 2017 was equal to 2,642 MW, while the main power plants, Chana Power Plant and Khanom Power Plant, could only produce 2,024 MW. The remaining 460 MW had to be drawn from the central region, which produced another 140 MW from dams, biomass, and wind. Until now, electricity consumption in the southern region averaged 3.4 percent every year [3]. In Songkhla province, it was found that the total production capacity of biomass power plants amounted to 7 plants, equal to 60 MW [4]. There are also biomass power plants with a capacity of 3 MW, each in the three southern border provinces of Yala, Pattani, and Narathiwat. The Pracharath power plant also allows people to participate in developing the power plant and the community and gain more income from selling fuel to the power plant. This causes community interest in the project to produce more biomass power in the future, which is in line with the policy of the Ministry of Energy, which emphasizes promoting the use of renewable energy in an increasing proportion to create energy security and reduce energy imports from foreign countries [5]. As mentioned above, biomass power plants, which use biomass as fuel to generate electricity, are another cause of greenhouse gas emissions. The technology used to create electricity, such as heat, gasification, and fermentation [6], also uses electricity that emits the most carbon dioxide in the process [7]. Various fuels that generate electricity emit varying amounts of greenhouse gases [8]. Resulting in different levels of impact on the environment.

A life cycle assessment (LCA) application is a tool used to analyze and evaluate the environmental impacts associated with a product throughout its life cycle. The amount of resource use, pollution that results, and environmental impacts resulting from the production of products or services Considering the entire life cycle includes acquiring raw materials, Production, transportation, product use, and processing, including reuse, recycling, and disposal after end-of-life. It can be said that it is a product of birth. Cradle to Grave life cycle assessment Process: Life cycle assessment of any product or process according to ISO 14040 – 14043. The life cycle assessment process can be divided into four steps: Setting goals and scope of study, preparing environmental impact assessment items, and interpreting study results. Therefore, there is interest in applying life cycle assessment principles to assess the carbon dioxide emissions of biomass power plants.

2. Materials and Methods

This research is a data analysis using the life cycle assessment principle as a guideline for assessing the carbon footprint of electricity generation from biomass fuels. It collects and assesses the environmental impact caused by products, production systems, or services throughout their life cycle. Starting from obtaining raw materials and energy production processes to transportation, use, maintenance, and removal. This study assessed the carbon footprint of biomass power generation, starting with planting rubber trees. The use of fuel is wood chips, sawdust, and wood flakes from the rubber wood processing plant transported to the power plant by truck, and the conveyor system into the fuel storage building into the fuel granulator is conveyed to the furnace into the electrical production process to burn such fuel to produce heat. This heat turns the water in the steam generator into steam. This high-pressure steam turns the turbines for the machines that generate electricity and ends at the landfill with the ash from biomass fuel combustion (wood chips). And finally, the project wastewater treatment system. The details, according to the conceptual framework based on life cycle assessment principles, are as follows:

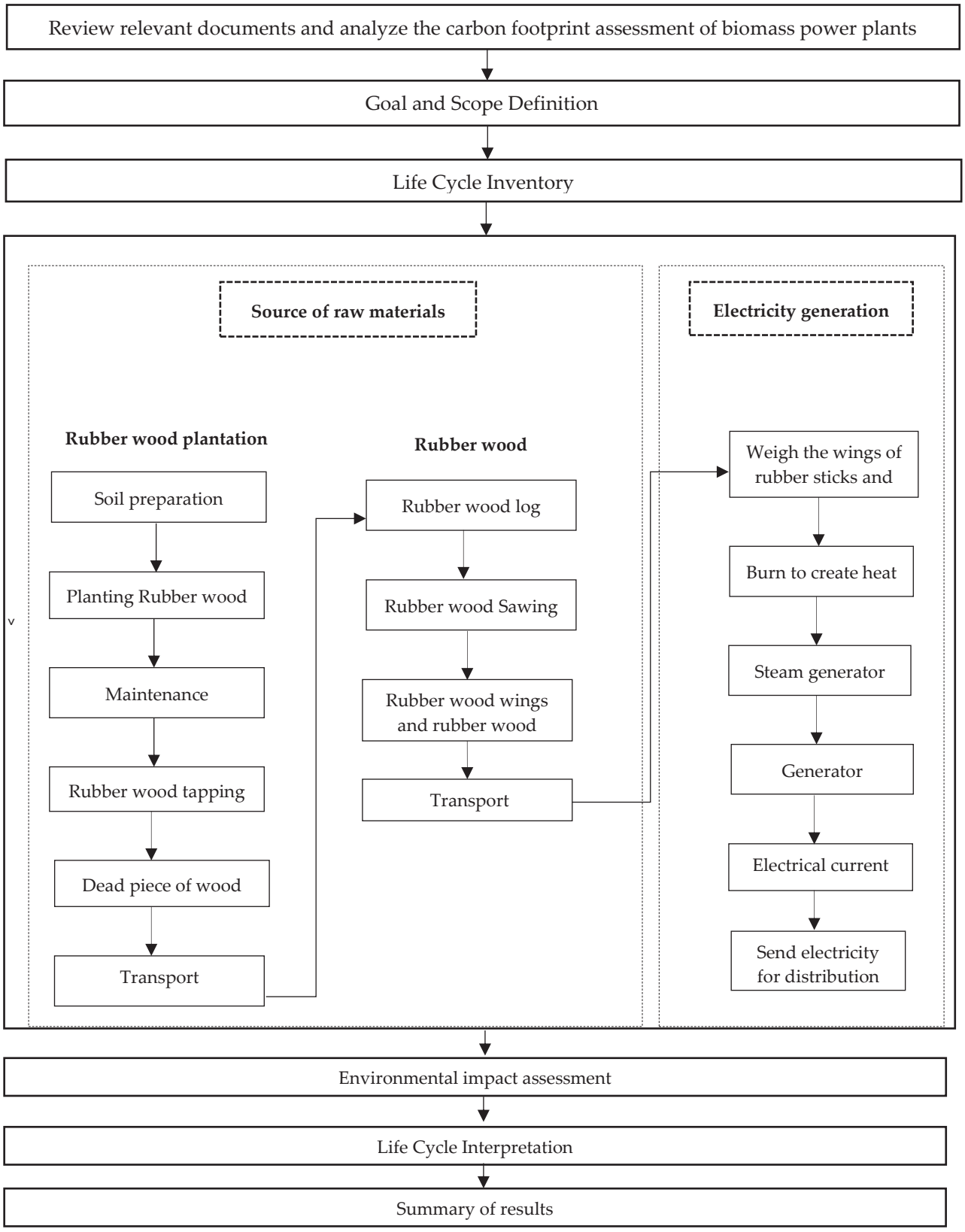

Figure 1. The conceptual framework is based on life cycle assessment principles

2.1 Data collection

Data was collected from rubber farmers, rubber wood processing plant operators, and biomass power plant operators. The data survey includes general information on biomass power plants, environmental inventory, greenhouse gas emission sources, and resource consumption.

2.2 The data collection procedure is as follows

2.2.1. Make a letter requesting information from the biomass power plant to interview the opinions of the executives or stakeholders of the biomass power plant.

2.2.2 Gather information on electricity production from power plants, which produce electricity equal to 9.9 MW. To determine the value of greenhouse gas emissions and use the information from the electricity generation process to assess the carbon footprint. From the acquisition of raw materials and energy, the production process, electricity consumption, water consumption, transportation, usage, and maintenance to calculate the value of greenhouse gas emissions.

2.2.3 Data analysis, calculation, and summing up the release value of greenhouse gases from biomass power plants to set guidelines and improve production processes, including the selection of raw materials and technology, to increase the efficiency of electricity generation and reduce the carbon footprint of biomass power plants. The research methods were conducted following the ISO 14040 standard series. The details are as follows:

(1) Setting the goal and scope of the study (goal and scope definition) The goal of the study (goal definition) is to study and evaluate the carbon footprint according to the principles of life cycle assessment of biomass power plants.

(2) Scope Definition: To study greenhouse gas emissions in electricity production from biomass power plants in Songkhla Province. This is an assessment of the carbon footprint covering from the acquisition of raw materials to the end of the production process in a biomass power plant, Cradle to Grave. Factors related to the study include the type and amount of resource use. Type, amount of energy use, and environmental impact or waste from biomass electricity production. It's mainly for The Functional Unit to evaluate the carbon footprint of electricity production from biomass. This can indicate the amount and severity of environmental impacts in terms of greenhouse gas emissions producing 1 kilowatt per hour of electricity.

(3) Environmental inventory preparation (Life Cycle Inventory: LCI) is an analysis and preparation of environmental inventory obtained from collecting data and quantities of substances entering and substances issued from the use of raw materials, energy, and various wastes that occur throughout the life cycle of electricity production from biomass under the LCA operating principles and all information that was used in this study.

2.2.4 Life Cycle Impact Assessment (LCIA): Once the information had been obtained from the accounting preparation, the researcher checked the accuracy of the data obtained from the biomass power plant and calculated it according to the formula. Then, the greenhouse gas emissions (CO_2 Emission Factor) values were collected from various supporting sources. Both domestically and abroad, to find factors and analytical methods suitable for the analysis to be compiled into a list of results for calculating the carbon footprint of biomass power plants and to know the amount of carbon footprint of electricity production from biomass power plants in each process. This includes guidelines for reducing the carbon footprint in producing electricity from biomass power plants, calculated in terms of kg carbon dioxide equivalent ($kgCO_2eq$).

2.2.5 Life Cycle Interpretation: After calculation, the obtained values will transform the data to be consistent with the objectives set. This will translate the results into global warnings or the release of greenhouse gases and compare the impacts occurring in each main activity in producing electricity from biomass using the results. It is obtained from assessing environmental impacts throughout the life cycle of electricity production from biomass. Let's compare the impact of each activity to see which activity has the most significant impact.

2.3 Data analysis

2.3.1 The calculation of data using the life cycle assessment principle from the acquisition of raw materials through the production process in a biomass power plant until the end of waste disposal from the production process cradle to grave Data was collected from interviews and surveys to verify its completeness, then processed using a statistical program to calculate the value of greenhouse gas emissions throughout the life cycle of the biomass power plant.

2.3.2 Quantitative analysis and descriptive statistics were used to analyze general data on rubber farmers, general information on rubber wood processing plant operator areas, and plots of rubber plantations. The analysis will use the value average. Analysis of greenhouse gas emissions to assess the carbon footprint from biomass power plants of the Greenhouse Gas Management Organization (a public organization) [9].

2.3.3 The collected data was analyzed for relationships using Pearson's correlation analysis method and stepwise linear multiple regression using a statistical package. A study of the relationship between the number of raw materials in biomass power plants and greenhouse gas emissions used linear regression multiple analysis to create a model equation for forecasting the amount of greenhouse gas emissions. When there is a change in the number of raw materials for each type of biomass power plant that has a statistically significant influence on the change, it can be calculated from the following equation 1:

$$Y = \beta_0 + \beta_1(X_1) + \cdots + \beta_n(X_n) \quad (1)$$

X_1, X_2, X_n… = The number of raw materials for each type of biomass power plant.
Y = The amount of greenhouse gas emissions.
$\beta 0$ to βn = The regression coefficients.

3. Results and Discussion

According to the study results and the carbon footprint assessment according to the principle of life cycle assessment of biomass power plants, it started with interviews with rubber farmers. Data on the number of rubber trees that have been planted and the amount of area (rai) used for rubber planting, calculated in the form of fresh rubber wood and kilogram (kg) units, was collected. Finally, calculate the amount of greenhouse gas emissions from fresh rubber wood from the rubber tree planting, covering the entire duration of 25 years (LCIA method IPCC 2013 GWP 100a V1.03), and fresh timber from the felling of latex-tapping rubber trees until latex yield is no longer available or is 25 years or more (LCIA method IPCC 2013 GWP 100a V1.03). The details of the research results are as follows:

I was calculating the amount of greenhouse gas emissions. The calculation of greenhouse gas emissions is divided into 3 cycles, calculating the amount of greenhouse gas emissions from acquiring raw materials. The first part will calculate the greenhouse gas emissions from the rubber planting process. Rubberwood processing plant and calculation of greenhouse gas emissions in electricity production.

3.1 List of information on the rubber planting process

Table 1. The amount of greenhouse gas emissions from fresh rubber wood.

List	Unit	Amount	Cost EF ($kgCO_2eq$)	Calculation result ($kgCO_2eq$) 25 years	Calculation result ($kgCO_2eq$) per day
Fresh rubber wood, sample group 1	kg	456,000	0.0363*	16,552.80	1.84
Fresh rubber wood, sample group 2	kg	76,000	0.0363*	2,758.80	0.31
Fresh rubber wood, sample group 3	kg	292,200	0.0363*	10,599.60	1.18
Average fresh rubber wood	kg	274,666.67	0.0363*	9,970.40	1.11

Note: The referenced value of the emission factor (EF) [10]

Data Collected from the interviews with rubber farmers throughout the cycle, the data collection for the carbon dioxide emission coefficients list, and the source of carbon dioxide emission coefficients in each item are shown in Table 1. The total amount of fresh rubber wood was 824,000 kg. Greenhouse gas emissions from fresh rubber trees averaged 9,970.40 kgCO_2eq. And when compared to the amount of carbon footprint per day, it equals 1.11 kgCO_2eq.

Table 2. The volume of greenhouse gas emissions from rubber wood timbers.

List	Unit	Amount	Cost EF (kgCO_2eq)	Calculation result (kgCO_2eq)	Calculation result (kgCO_2eq) per day
Rubberwood timbers, sample group 1	kg	2,280	0.0471*	107.39	0.0119
Rubberwood timbers, sample group 2	kg	1,520	0.0471*	71.59	0.0080
Rubberwood timbers, sample group 3	kg	1,140	0.0471*	53.69	0.0060
Average rubber wood timbers	kg	1,646.67	0.0471*	77.56	0.0086

Note: The referenced value of the emission factor (EF) [10]

Data collected from the interviews with rubber farmers throughout the cycle and the data collection for the list of carbon dioxide emission coefficients and the source of carbon dioxide emission coefficients in each item are shown in Table 2. The total amount of rubber wood timbers was 4,940 kg, the sample mean was 1,646.67 kg, and when multiplied by the CO_2 emission factor, the average greenhouse gas emissions from rubber wood timbers were 77.56 kgCO_2eq. Compared to the amount of carbon footprint per day, it equals 0.0086 kgCO_2eq.

3.2 Data collection list of rubber wood processing factories.

Table 3. Data collection list for rubber wood processing factories No. 1 and No. 2.

List	Unit	Amount No.1	Amount No.2	Cost EF (kgCO_2eq)	Calculation result (kgCO_2eq) per day No.1	Calculation result (kgCO_2eq) per day No.2	Average (kgCO_2eq) per day
Rubber tree wings	kg	150,000	150,000	0.0829*	12,435.00	12,435	12,435.00
Electricity	kwh	3,085.94	3,085.94	0.5956*	1,225.33	1,837.99	1,531.66
Surface water	m^3	1	1	N/A	N/A	N/A	N/A
Diesel fuel	kg	150	150	0.3522*	70.44	52.83	61.64
Sawdust	kg	15,000	15,000	0.0852*	1,278	1,278	1,278.00
Ten wheeler	km	22	22	0.5900*	5.31	12.98	9.15
Trailer Flat Bed	km	22	22	0.2363*	2.13	5.20	3.67
Average rubber wood processing factory					15,016.21	15,622	15,319.11

Note: The referenced value of the emission factor (EF) [10]

Data collected from the interviews with rubber wood processing plant operators throughout the cycle, the data collection for accounting for the carbon dioxide emission coefficient, and the source of the CO_2 emission coefficient in each item are shown in Table 3. It was found that the wood processing plants No. 1 and No. 2, when multiplied by the CO_2 emission factor, had total GHG emissions of 30,638.21 kgCO_2eq, and the mean was 15,319.11 kgCO_2eq.

3.3 Power plant data collection list with a capacity of 9.9 MW

Table 4. Data collection of biomass electric power plant with a total of 9.9 MW.

List	Unit	Amount	Cost EF ($kgCO_2eq$)	Calculation result ($kgCO_2eq$) per day
Rubber tree wings*	kg	400,000	0.0829	33,160
Surface water*	m^3	36.67	N/A	N/A
Electricity	kWh	7,920	0.5986	4,717.15
Amine	kg	1.33	1.8876	2.51
Diethyl hydroxylamine	kg	1.33	N/A	N/A
Trisodium Phosphate	kg	0.44	2.8586	1.26
Sodium hydroxide*	kg	18	1.1148	20.06
Poly Aluminium Chloride	kg	19.17	0.455	8.72
Polymer**	kg	3.33	2.2000	7.33
Biocide**	kg	3.73	1.4600	5.45
Antiscaleh	kg	12.17	1.6700	20.32
Sulfuric acid*	kg	9.33	0.1219	1.14
Hydrochloric acid*	kg	34.27	0.8709	29.85
Chlorine*	kg	115	1.0548	7.98
Sodium Metabisulfite	kg	3.33	1.5×10^{-5}	5.0×10^{-5}
Coolant*	m^3	26.67	3.0985	82.64
Glue*	kg	0.01	0.5922	0.01
Gear oil	kg	0.01	0.8319	0.01
Oil filter***	kg	0.18	2.1300	0.38
Neon lamp	kg	0.38	2.0×10^{-5}	1.0×10^{-5}
Led lamp	kg	0.01	2.0×10^{-5}	3.0×10^{-6}
GEM-S NYLON	kg	0.03	N/A	N/A
Parker	kg	0.03	N/A	N/A
Engine oil***	kg	0.04	0.6740	0.03
UPVC Ball Check Valve	kg	0.01	2.1331	0.02
Nitrile Gloves	kg	0.26	0.1887	0.05
Cloth gloves*	kg	0.19	2.1100	0.40
Ash	kg	6,000	0.8421	5,052.60
Effluent	m^3	2,398	0.6250	1,498.50
Total				**44,753.60**

Note: The referenced value of the emission factor (EF) [10]
: The referenced value of the emission factor (EF) [11]
: The referenced value of the emission factor (EF) [12]

Data collected from interviews with executives or other stakeholders throughout the cycle, the carbon dioxide emission coefficient, and the source of the CO_2 emission coefficient in each item are shown in Table 4. It was found that when the obtained value is multiplied by the CO_2 emission factor, the daily greenhouse gas emissions value from a biomass power plant is equal to 44,753.60 $kgCO_2eq$

3.4 Life cycle assessment of biomass power plants

Determining the scope of the life cycle assessment of a biomass power plant, covering from the acquisition of raw materials to the end of the production process in a biomass power plant cradle to grave, is an environmental impact assessment. The details are as follows:

Phase 1: Emission of greenhouse gases during the rubber wood planting period by activities starting with 1) preparing the area for growing rubber. The area is plowed. Using fuel, 2) adding fertilizer to add nutrients to the soil, and 3) producing fertilizer and fuel during raw material transportation. From related research, it is said that it does not occur in rubber-growing areas at this stage. But it occurs in the production

process of raw materials [13]. It was found that greenhouse gas emissions in the production process of raw materials account for 60 percent.

Phase 2: Emission of greenhouse gases during rubber wood processing. The activities start with 1) sawing rubber wood, 2) moving wood wings and chips, and 3) transporting rubber wood. Fuel is used. From the production process, greenhouse gases are released from wood wings and wood chips, which account for 88.56 percent.

Phase 3: Emission of greenhouse gases in the electric power production phase by activities. That started with 1) burning rubber wood and 2) Turning water into vapor. A turbine drives it. and 3) Take the steam into a machine to convert it into electricity. During the production process, there is a release. Greenhouse gases from wood chips and wood waste accounted for 86.95 percent due to various activities in the electricity production process. Therefore, the activities that cause greenhouse gas emissions are different. It mostly depends on how many wood wings and wood chips are used for burning. Including the use of electrical energy within the factory, fuel combustion for boiling water in the boiler, and chemicals to improve surface water quality. Including activities that cause pollutants that come from the production process for some steps. The waste that occurs will be caused by burning rubber wood and turned into heavy ash and fly ash, which are filled in areas inside the factory. The wastewater generated from the cooling water is reused to boil further in the boiler.

3.5 Multiple regression analysis of factors affecting the greenhouse gas emissions of biomass power plants.

Table 5. Multiple regression analysis of factors affecting the greenhouse gas emissions of biomass power plants.

Variable	B	SE.	Beta	*t*	Sig.
Constant value	373.516	224.789	-	1.662	.109
Raw material quantity	.082	.003	.983	27.692	.000

R= .983, R^2 = .967, Adjusted R Square .966 SE= 1166.21799, F=96.70, P<.01

From Table 5, it can be seen that the equation that will be used in the regression analysis is that.

The R-value shows the relationship between all the predictor variables. What is the relationship with the dependent variables. The table can be translated as variables predicting the number of raw materials per day, which have a very high relationship with the variables of greenhouse gases. With a relationship in the same direction (the R-value is +).

The R square or R^2 value represents the predictive coefficient of this equation or the efficiency of the forecast using predictive variables (independent variables = quantity of raw materials), which are all in the equation. In this regression analysis, the method of bringing variables into the equation is stepwise (criterion: probability-of-F-to-enter < = .0.50, probability-of-F-to-remove > = .100). Which can be translated as

The raw material quantity variable can correctly explain the variation in the criterion variable at 96.70 percent, with statistical significance at the 01 level.

Create an equation to predict factors affecting greenhouse gas emissions. in raw score format

Y = 373.516 + .082 (raw material quantity)

where Y is greenhouse gas emissions ($kgCO_2eq$)

Predictive equations in the form of standard scores

$Z = .983_{\text{Quantity of raw materials}}$

It can be explained if the raw material quantity variable changes by increasing or decreasing. One unit will result in greenhouse gas emissions changing in the same direction, with a correlation (R) value of 0.983 units.

According to data from rubber farmers, there were three sample groups. Discharge value: According to related research, greenhouse gas emissions from fresh rubber wood, including the average daily greenhouse gas emissions from Rubberwood plantation to the average daily greenhouse gas emissions value, is equal to 1.1186 $kgCO_2$ eq, from related research, said throwing areas. However, it occurs in the production of raw materials such as oil, fertilizer, and pesticide chemicals. This accounted for 60 percent, and Greenhouse gas emissions throughout the rubber growing period accounted for only 40 percent before being taken to the rubber wood processing factory [13]. When entering the rubber wood processing work area, the average daily greenhouse gas emissions value equals 15,319.11 $kgCO_2eq$. The activity with the most significant greenhouse

gas emissions is using electricity within the rubber wood processing factory because electric saws are used in sawing rubber wood and the use of electricity within the factory, such as offices, surface water pumps, and lighting at the rubber wood sawing table. According to related research, [14], rubber wood has a carbon component characterized by environmentally friendly materials. On the other hand, the loss of wood when rubber wood is cut during production is considered a carbon loss. This will result in pallet wood products for molding into furniture, decorations, slats, etc., and the remaining parts will be wooden wings and wood scraps to be resold to biomass power plants. A biomass power plant's daily greenhouse gas emissions value equals 44,753.60 $kgCO_2eq$. The use of rubber wood in the wood wings and wood scraps will give a value of the greatest source of greenhouse gas emissions from biomass power plants because they are used to burn fuel. Hot gas that helps water in the steam generator turn into high-pressure steam. To rotate the turbine of the generator, generating electricity. It will send electricity through the transformer to provide an electrical driving force. And enter the provincial electricity authority system further. Part of the wastewater from the process is reused in the boiler process. Ashes from fuel combustion will be used to fill in the area of the power plant. However, carbon dioxide emissions from combustion or decomposition are considered biological carbon dioxide or carbon neutral. This is because the carbon dioxide released into the environment during the combustion or decomposition of wood is reabsorbed during tree growth [15], indicating that wood biomass is normally defined as having zero global warming potential. After all, wood does not theoretically contribute to a carbon footprint. Search results for predictive variables and factors affecting the amount of greenhouse gases in biomass power plants. Predictive variables (the amount of raw materials) have a positive relationship with the amount of greenhouse gases, with a statistical significance of .01 and a correlation coefficient of .983. The ability to explain the variation of criterion variables (the amount of greenhouse gases) was accurate at 96.70 percent, consistent with the research [16]. They are saying that the amount of garbage is large. The amount of carbon footprint released will also be significant. Consistent with [17], research on multiple regression analysis based on carbon emissions from aviation logistics in Henan Province said that the added value of the transportation, warehousing, postal, and telecommunications industries in Henan Province and the total population of Henan Province affect the carbon footprint of Henan Province's aviation logistics and consistent with [18]. Research on analyzing renewable energy and carbon dioxide emission levels is an important part of the European Union. A panel data regression approach found that renewable energy, biofuels, population, and urbanization status affect carbon dioxide emissions in European Union (EU) countries.

4. Conclusions

The carbon footprint evaluation is done according to life cycle assessment principles for biomass power plants by calculating the percentage of greenhouse gas emissions per day. It was found that the process that occurred within the biomass power plant had the highest greenhouse gas emission of 44,753.60 $kgCO_2eq$ or 70 percent, followed by the process that occurred within the rubber wood processing plant, which had a greenhouse gas emission of 15,319.11 $kgCO_2eq$ or equivalent to 22 percent, and the process from the rubber plantation had the lowest emission of greenhouse gases, equal to 1.1186 $kgCO_2eq$ or equivalent to 8 percent respectively.

5. Acknowledgements

The authors would like to thank the Faculty of Science Technology and Agriculture, Yala Rajabhat University. Including the executives and people involved in biomass power plants, rubber wood processing plants, and rubber farmers in Songkhla province who cooperated in providing detail and help in data collection, and Ms.Natrisorn Abdultoleh, the co-author, who provided tremendously help to complete this research.

Author Contributions: Conceptualization, J.K.; methodology J.K. and P.P.; formal analysis, J.K.; investigation, J.K. and P.P.; writing—original draft preparation, J.K.; writing—review and editing, J.K. and P.P.

Funding: This research received no external funding

Conflicts of Interest: The authors declare no conflict of interest.

References

[1] International Energy Agency. (2021, May 5). Global Energy Review, Assessing the effects of economic recoveries on global energy demand and CO_2 emissions in *2021*. https://iea.blob.core.windows.net /assets/c3086240-732b-4f6a-89d7 db01be018f5e/GlobalEnergyReviewCO_2Emissionsin2021.pdf/.

[2] Office of Energy Policy and Planning. (2020). Carbon Dioxide (CO_2) emissions from energy use in the first 6 months of 2020. *Information and Communication Technology Center Ministry of Energy*.

[3] Electricity Generating Authority of Thailand. (2021, April 20). Electricity generation for the southern region. **2017**. https://www.egat.co.th.

[4] Integrated Provincial Executive Committee. (2021, April 25). Songkhla Province. Songkhla Provincial Development Plan 2018-2022,2019. https://dl.parliament.go.th/handle/20.500.13072/589003.

[5] Department of Mineral Fuels. (2021, April 30). Ministry of Energy, *Daily energy news. 2018.* https://dmf.go.th/public/list/data/detail/id/12872/menu/593/page/3.

[6] Chotsuwan, K.; Losuwannarat, T.; Wannanarat, S. Effectiveness of Small Biomass Power Plants in Thailand, *Journal of Public and Private Managemen*t. **2020**, 7(2), 5-46.

[7] Thanarak, P.; Maneechot, P.; Wansungnern. W. (2016) *Journal of Science and Technology Ubon Ratchathani University*. **2016**, *18*(2), 22-31.

[8] Sriwongsa, K.; Pasuwan, P.; Ravangvong, S.; Nisspa, W. *The Sci of Phetchaburi Rajabhat University*. **2019**, *16*(2), 41-48.

[9] Thailand Greenhouse Gas Management Organization. *Calculation requirements and report on the carbon footprint of the organization*. 8th edition, Bangkok. **2022**.

[10] Thailand Greenhouse Gas Management Organization (Public Organization). (2021, May 30). Product Carbon Footprint. 2021. http://thaicarbonlabel.tgo.or.th/admin/uploadfiles/emission/ts_b934985782.pdf

[11] Winning. (2021, May 30). Emission factors in kg CO_2equivalent per unit. **2012**. https://www.winnipeg.ca /finance/findata/matmgt/documents/2012/6822012/6822012_Appendix_HWSTP_South_End_Plant_Process_Selection_Report/Appendix%207.pdf.

[12] Klanarong, S. Carbon footprint evaluation of electricity generation from biogas: a case study of small UASB plant. *Ph.D. Thesis*. Suranaree University of Technology. **2022**.

[13] Jokjit, W. Carbon Footprint for Sustainable Rubber Products.*Thai rubber magazine*. *Bangkok*. **2013**, *4*(1), 51-56.

[14] Martinez-Alonso, C.; Berdasco, L. Carbon footprint of sawn timber products of Castanea sativa Mill. in the north of Spain. *Journal of Cleaner Production*. **2015,** *102*, 127-135.

[15] Munoz, I.; Rigarlsford, G.; Mila i Canals, L.; King, H. Accounting for greenhouse gas emissions from the degradation of chemicals in the environment. *The International Journal of Life Cycle Assessment*. **2012**, *18*(1), 252-262.

[16] Suthiprapha, N.; Thongto, S. The Carbon Footprint Emission of Municipal Waste by Sources Case Study: Trakanpuetpon Municipality, Ubon Ratchathani Province. *EAU Heritage Journal Science and Technology*. **2020**, *14*(3), 161-174.

[17] Lyu, S.; Wei, Z.; Wang, X.; Xu, L. Multiple regression analysis based on carbon emissions from aviation logistics in Henan Province. *IOP Conference Series: Earth and Environmental Science*. **2019**, *310*(5), 1-6. https://doi.org/10.1088/1755-1315/310/5/052029.

[18] Busu, M.; Catalina Nedelcu, A. Analyzing the Renewable Energy and CO_2 Emission Levels Nexus at an EU Level: A Panel Data Regression Approach. *Processes*. **2023**, *9*(1), 130https://doi.org/10.3390 /pr9010130.

ASEAN
Journal of Scientific and Technological Reports
Online ISSN:2773-8752

Research article

Acid Dye Removal from Wastewaters using Rice Husk Ash Functionalized with Organic Amine Groups as Adsorbent

Sasiprapa Radchatawin[1], Dhandheera Paritporndheera[2], Nitithorn Singkram[3], Nutthanon Suntigul[4], and Sakdinun Nuntang[5*]

[1] Faculty of Science, Maejo University, Chiang Mai, 50290, Thailand; Sasiprapa.ra@gmail.com
[2] Montfort College, Chiang Mai, 50000, Thailand; Dhandheera@gmail.com
[3] Montfort College, Chiang Mai, 50000, Thailand; nitithornsingkram@gmail.com
[4] Montfort College, Chiang Mai, 50000, Thailand; nutthanon.suntigul@gmail.com
[5] Faculty of Science, Maejo University, Chiang Mai, 50290, Thailand; Sakdinun.nt@gmail.com
* Correspondence: Sakdinun.nt@gmail.com

Citation:
Radchatawin, S.; Paritporndheera, D.; Singkram, N.; Suntigul, N.; Nuntang, S. Acid dye removal from wastewaters using rice husk ash functionalized with organic amine groups as adsorbent. *ASEAN J. Sci. Tech. Report.* **2024**, *27*(1), 102-109. https://doi.org/10.55164/ajstr.v27i1.250741

Article history:
Received: August 31, 2023
Revised: December 21, 2023
Accepted: December 26, 2023
Available online: December 28, 2023

Abstract: The use of rice husk ash functionalized with organic amine groups (RHA-NH_2) as an adsorbent for acid dye adsorption from wastewater was studied. The RHA–NH_2 was synthesized successfully via the grafting method using (3-Aminopropyl)-triethoxysilane (APTES) as amine group precursors. The synthesized adsorbents were characterized by using X-ray Powder Diffraction (XRD), Fourier Transform Infrared Spectroscopy (FTIR), N_2 adsorption-desorption analysis, and Scanning Electron Microscopy (SEM). The RHA-NH_2 exhibited an amorphous silica structure and possessed the organic amine group functionalized on the silica surface. The adsorption was studied by using Acid Blue 225 as an acid dye. The amount of acid dye remaining in the aqueous solution was measured by ultraviolet-visible spectrophotometer (UV-Vis). The RHA-NH_2 revealed a higher adsorption capacity (~82 mg/g) than RHA because the amine group enhanced the chemisorption energy.

Keywords: Adsorption; adsorbent; rice husk ash; acid dye, organic amine groups

1. Introduction

Acid dyes are used in many industries, such as textile and dye manufacturing. Water pollution caused by industrial wastewater has become a common problem in many countries [1]. Removing dyes from water is very important since color greatly affects water quality. Even very small concentrations of dyes (less than 1 mg L-1) in water are obvious and unpleasant. Moreover, these dyes also cause health problems such as allergic dermatitis, skin irritation, cancer, and human mutation [2].

Many methods, including physical and chemical technologies and biological processes, have been used to remove colored contaminants from wastewater and reduce environmental problems. The main treatment processes are oxidation [3], coagulation and flocculation [4], membrane separation [5] and adsorption [6]. Among these techniques of dye removal, adsorption is the most convenient and effective due to being less expensive than the others. This process transferred dyes from the water effluent to the adsorbents [7]. Over the past years, several adsorbents have been employed for dye removal, such as metal-organic frameworks (MOFs) [8], zeolite [9], and mesoporous silica [10]. However, those adsorbents are expensive, which results in high operating costs.

Recently, the low-cost adsorbent is interesting for use in adsorption and has a higher usage trend. Rice husk (RH) is an agricultural waste that produces about one-fifth of the world's annual rice production, or around 550 million metric tons [11]. It can be applied for several uses, such as energy production and as an adsorbent. RH has the potential to be accounted as an adsorbent because its main components are carbon and silica. In addition, rice husk ash (RHA) produced by heating rice husk at 700 °C possesses a higher amount of silica content (~84.3%) and has been used as an adsorbent for the removal of pollutants in wastewater such as heavy metals ions [12], and dye [13].

To enhance silica adsorbents' adsorption capacity and selectivity for substances, surface modification is useful by utilizing interactions between adsorbents and adsorbates. Therefore, the modified silica surface has been regarded as an effective adsorbent due to its high surface area, allowing many surface groups to be binding. The amine-functionalized silica (SiO_2-NH_2) has received substantial attention because the amine group positively impacts the performance of the adsorption systems of heavy metals, dyes, and other organic compounds [14-16]. In addition, there has been reported using silica or mesoporous silica modified with amine groups applied as adsorbent to remove the dye in aqueous [17,18]. However, preparing commercial silica or mesoporous silica modified with amine groups as adsorbents is quite complicated and expensive, resulting in high operating costs. Therefore, rice husk ash with high silica content is interesting to modify its surface with amine groups to enhance its adsorption performance and applied as a low-cost adsorbent.

This work aimed to study the use of amine-functionalized rice husk ash (RHA-NH_2) as adsorbents for removing acid dye from wastewater. Advanced analyses examined the textural and structural properties of RHA-NH_2 concerning adsorption. The adsorption performance of RHA–NH_2 for removal of acid dye was evaluated by studying the effects of types of adsorbents and initial concentration of acid dye.

2. Materials and Methods

2.1 Chemicals and reagents

3-Aminopropyltriethoxysilane (3-APTES) was purchased from Aldrich. Dichloromethane, Ethanol, HCl, and NaOH were purchased from RCL Labscan Limited. Acid Blue 225 was of commercial grade and obtained from Dystar Thai LTD. Its chemical structure is shown in Figure 1. All the above materials were used without further purification. Deionized water was used throughout this work.

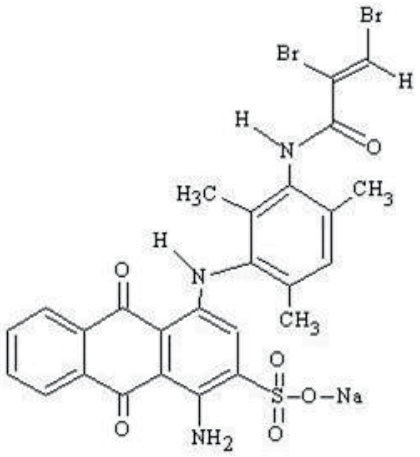

Figure 1. Chemical structure of Acid Blue 225

2.2 Preparation of RHA and RHA-NH_2

The rice husk was immersed in DI water, 1M HCl for 4 h, at a 40 g husk/L ratio. The husks were washed repeatedly with DI water and then dried in an oven at 110 °C for 2 days. Samples of rice husks were converted into adsorbent-rice husk ash (RHA) by heat-treating using ceramic crucibles at 700 °C for 6 h in a muffle furnace. The heated rice husks were crushed to obtain an approximate diameter of < 2mm.

The organic amine functionalized rice husk ash (RHA-NH_2) was prepared by mixing 5 g of RHA with 100 mL of dried toluene. The mixture was refluxed under a nitrogen atmosphere for two hours, and then 4 g of 3-aminopropyltriethoxysilane (3-APTES) was slowly added by a dropper. The mixture was refluxed again for 24 h. The solid was filtered, rinsed with ethanol and dichloromethane 3 times, and then dried at room temperature.

2.3 Characterization of adsorbents

The structures of RHA and RHA-NH_2 materials were analyzed by powder X-ray diffraction (XRD). The XRD analysis was performed on a Bruker D8 Advance X-ray diffractometer with Cu Kα radiation operated at 40 kV and 40 mA. The functional groups of these samples were analyzed FTIR. The FTIR spectra were obtained from a Spectrum 2000 FTIR spectrometer (Perkin-Elmer) with the usual KBr pellet method. The spectral range was chosen from 4000 to 400 cm^{-1}. N_2 adsorption-desorption measurements were carried out at 196 °C using a BEL Japan BELSORP-mini II instrument to determine the material's textural characteristics. SEM analyzed the morphology of these adsorbents. The SEM analysis was carried out using a scanning electron microscope (Model JEOL JEM-2010) at an electron acceleration voltage of 20 kV. Before scanning, the samples were coated with a thin layer of gold using a sputter coater to make them conductive.

2.4 Adsorption study

The adsorption of acid blue 225 over RHA and RHA-NH_2 was investigated in a batch system by adapting from the previous report of Mansoor *et al.* [18]. All batch experiments were carried out in 125 mL glass-stoppered Erlenmeyer flasks containing a fixed amount of adsorbent with 25 mL dye solution at a known initial concentration. The flasks were agitated at a constant speed of 150 rpm for one hour in an incubator shaker at 313 K. The initial dye concentrations were 20, 40, 60, 80, and 100 mg L^{-1}. The solid/liquid ratio was 0.025 g mL^{-1}. The residual amount of dye in each flask was investigated using a UV/VIS spectrophotometer (Model Hitachi-U2001). The amount of dye adsorbed per unit adsorbent (mg dye per g adsorbent) was calculated according to a mass balance on the dye concentration using Eq. (1):

$$q_e = \frac{(C_i - C_e)V}{m} \quad (1)$$

Where C_i is the initial dye concentration (mg L^{-1}), C_e is the equilibrium dye concentration in solution (mg L^{-1}), V is the volume of the solution (L), and m is the weight of adsorbent in g. All the experiments were performed in duplicate, and the average value from the results was taken.

3. Results and Discussion

3.1 Characterization of adsorbents

X-ray patterns for RHA and RHA-NH_2 materials are presented in Figure 2. The XRD patterns of these two materials displayed a broad peak at a diffraction angle (2θ) between 15-30° and a sharp peak at 27°, corresponding to amorphous silica and crystalline silica in quartz form, respectively [11]. However, the RHA-NH_2 materials exhibited a few lower XRD intensities (2θ= 27°) than primary RHA due to functionalized organic amine on RHA surfaces, resulting in a silica structure disorder.

Qualitative identification of functional groups was accomplished by FT-IR spectroscopy. Figure 3 shows the FT-IR spectrum of RHA and organic amine functionalized RHA materials over the 4000-400 cm^{-1} range. A broad band in the range of 3700-3010 cm^{-1} was seen, which can be attributed to the framework of Si-OH group interaction with the defect sites and adsorbed water molecules. The Si-OH peak appeared at about 3172 cm^{-1}. The asymmetric stretching vibrations of Si-O-Si were observed by the absorption bands at 1110 cm^{-1}. The functionalized RHA with amine groups (Figure 3b) generally shows a broad NH_2 stretching at 3424 cm^{-1}, an N-H deformation peak at 1628 cm^{-1}, and C-H stretching of methyl groups at 3064 cm^{-1} [16]. Moreover, the RHA-NH_2 exhibited decreasing peak intensity at 3172 cm^{-1}, implying the loss of surface silanol groups. These results confirmed that the organic amine functionalized on the RHA structure by replacing silanol groups, as seen in the synthesis pathway in Figure 4.

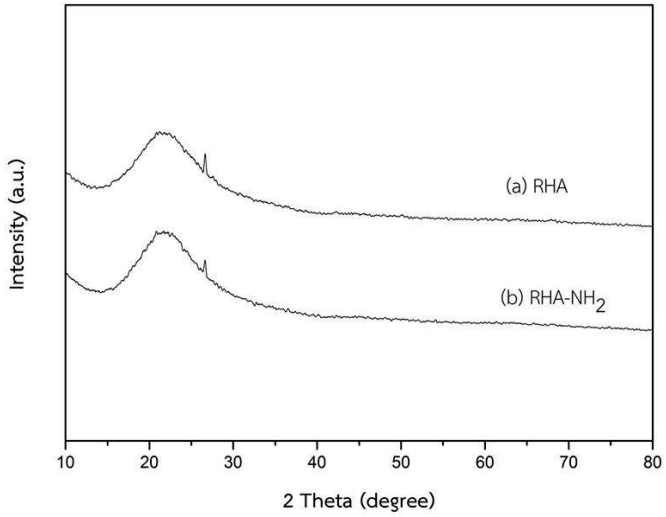

Figure 2. XRD pattern of (a) RHA and (b) RHA-NH_2

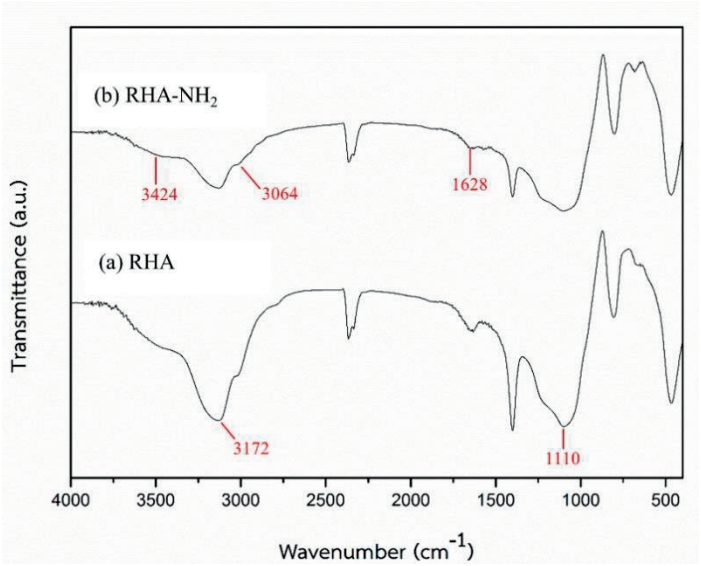

Figure 3. FT-IR spectra of (a) RHA and (b) RHA-NH_2

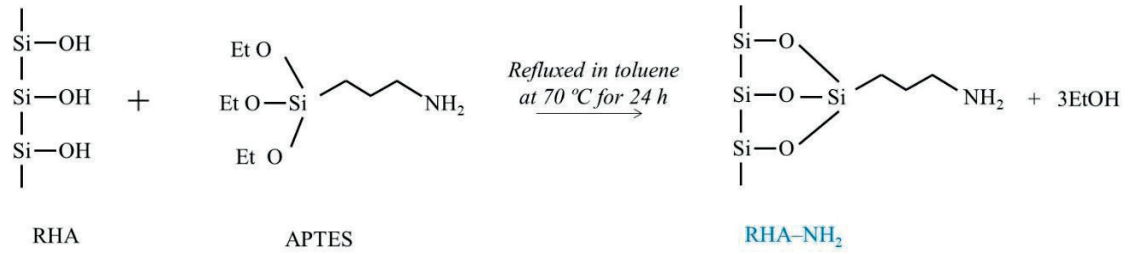

Figure 4. Functionalized with organic amine groups, the replacement of silanol groups on the RHA surface [11].

N_2 adsorption-desorption analysis, as shown in Table 1, determined the textural properties of synthesized materials. Based on its textural properties, RHA is suitable for adsorption due to its highly specific surface area, pore diameter, and pore volume. After the surface of RHA with amino silane was modified, the surface area, pore diameter, and pore volume were reduced compared to pristine RHA. It was probably due to the agglomeration of silica particles after modification of the RHA surface with amino silane. Additionally, the RHA-NH_2 materials exhibited an increase in CHN contents (Table 1). These results suggested that the aminosilane had been incorporated into the pore structure of RHA.

Table 1 Physicochemical properties of the adsorbents

Sample [a]	S_{BET} [b]	D_p [c]	V_t [d]	CHN contents [e]		
	($m^2\ g^{-1}$)	(nm)	($cm^3\ g^{-1}$)	% C	% H	% N
RHA	136	3.71	0.34	0.22 ± 0.01	0.22 ± 0.01	0.08 ± 0.01
RHA-NH_2	44	3.28	0.20	1.63 ± 0.14	0.42 ± 0.04	0.55 ± 0.04

[a] Dried samples
[b] BET surface area
[c] Pore diameter calculated using BJH method
[d] Total pore volume
[e] Determined by CHNS analyzer

SEM analyzed the surface morphology of RHA and RHA-NH2 adsorbents. The micrographs in Figures 5a and c represented the RHA surface in different magnifications. From the SEM images of the RHA adsorbent, it was found that hardly any residual fiber could be observed on its surface. It has been shown that the preparation of silica adsorbent from RHA that had been treated with strong acid and calcination at 700 °C should result in high-purity silica consistent with the CHN result (Table 1). In addition, the prepared adsorbent showed amorphous silica morphology consistent with the XRD result (Figure 2). Moreover, it revealed the agglomeration of silica particles and the surface roughness. However, as seen in Figure 5b and d, the morphology of RHA-NH_2 was quite similar to that of pristine RHA.

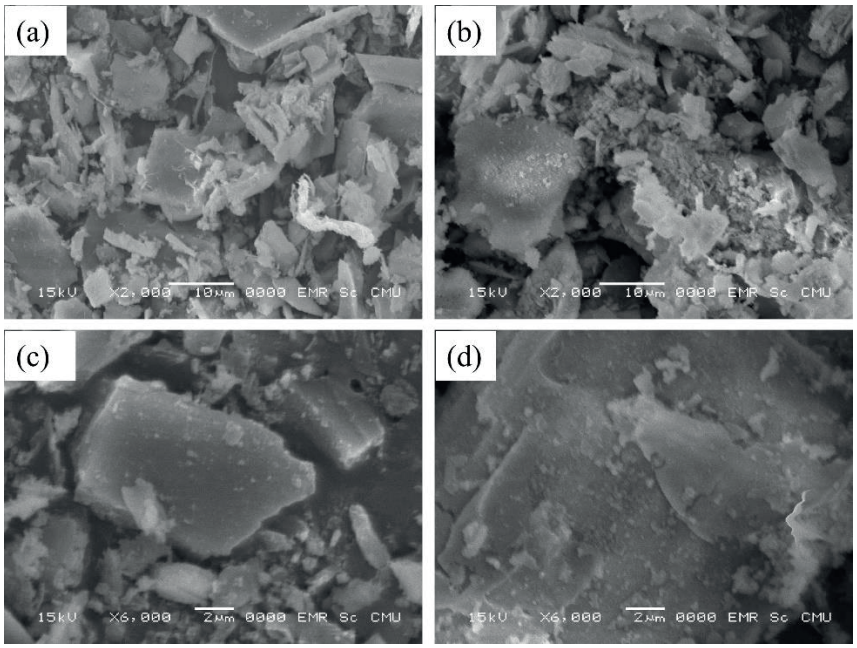

Figure 5. SEM image of (a, c) RHA and (b, d) RHA-NH_2 at a magnification of 2000x and 6000x, respectively.

3.2 Adsorption study

To evaluate the prepared adsorbents' efficacy, the acid dye's equilibrium adsorption was studied as a function of equilibrium concentration. The adsorption isotherms of acid dye on the RHA and RHA-NH_2 adsorbents are shown in Figure 6. By increasing the initial concentration of acid blue 225 from 20 to 100 mg L^{-1}, the adsorption capacity of both adsorbents grew dramatically with a steep slope, resulting in an enhanced rate of adsorption. However, the adsorption order regarding the amount adsorbed (mg/g adsorbent) on the adsorbents is RHA-NH_2 > RHA. The results of this study were consistent with the study of Apichat *et al.*, which reported on the removal of humic acid in wastewater by comparing the RHA and RHA-NH_2 adsorbents [11].

Moreover, RHA-NH_2 exhibited the highest adsorption capacity of the acid dye at 82 mg/g, which is 8 times greater than that of the RHA adsorbent. However, the RHA-NH_2**.** However, the RHA-NH_2 adsorbent showed a lower acid dye adsorption capacity than that of amine-functionalized mesoporous silica (~5-6 times), which was previously reported by Mansoor *et al.* [18]. Since the S_{BET} of RHA-NH_2 was lower than that of amine-functionalized mesoporous silica (~1,092 $m^2\ g^{-1}$), a low amount of organic amine functionalized onto the RHA surface was produced.

In general, the adsorption capacity depends on the chemical and physical properties of the surface of the adsorbent. The RHA with a pure silica surface does not provide strong adsorption sites to interact strongly with acid dyes. The hydroxyl groups on the silica surface fail to induce strong interactions with acid dyes. The adsorption capacity of acid dyes by RHA was enhanced through functionalization with amine groups. The higher adsorption capacity of RHA-NH_2 may be explained to proceed via electrostatic interaction and hydrogen bond formation between the surface of the adsorbent and acid dyes. The sulfonate groups of the acid dye were dissociated and converted to anionic ions in the aqueous solution. Also, in the presence of H^+, the amine groups of RHA-NH_2 become protonated. Then, electrostatic attraction could occur between the positively charged protonated amino groups on the silica surface ($–NH_3^+$) and the negatively charged sulfonate groups ($–SO_3^-$) of the acid dyes. Besides, a simulation of interactions between RHA-NH_2 and acid blue 225 is shown in Figure 7.

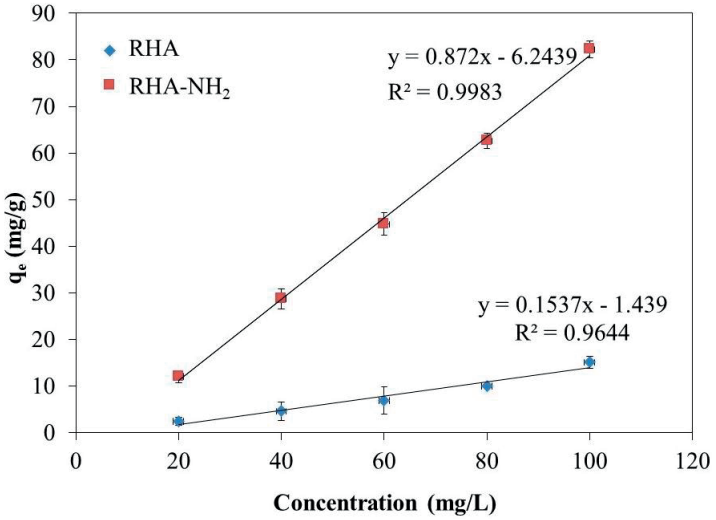

Figure 6. Adsorption isotherm for Acid Blue 225 adsorption on RHA and RHA-NH_2 (solid/liquid ratio = 0.025 g mL^{-1}, agitation speed = 150 rpm, time 60 min, temperature = 40 °C)

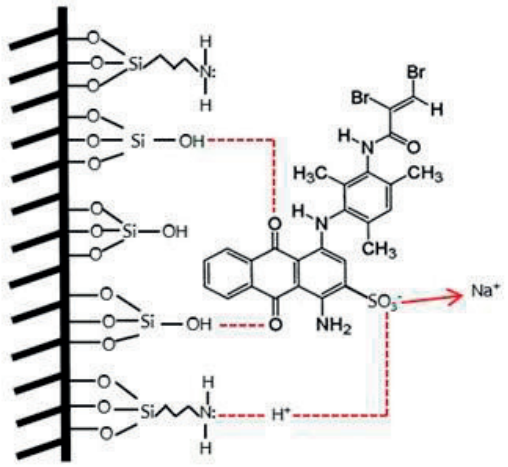

Figure 7. Interactions between Acid blue 225 and RHA-NH_2

4. Conclusions

The adsorption performances of acid dye by rice hush ash (RHA) and organic amine-functionalized rice husk ash (RHA-NH_2) materials were studied in the present work. The RHA-NH_2 could be prepared via the grafting method with 3-APTES. The characteristic results indicated that the RHA-NH_2 exhibited structural properties and morphology similar to pristine RHA. However, the textural properties of RHA-NH_2 were lower than that of RHA adsorbent. In addition, the obtained results showed that the acid dye adsorption capacity of RHA-NH_2 > RHA adsorbent (~ 8 times). Since the adsorption capacity of acid dye by the RHA-NH_2 was enhanced through functionalization with amine groups. Furthermore, the RHA-NH_2 adsorbent exhibited the highest adsorption capacity of the acid blue 225 at 82 mg/g.

5. Acknowledgements

The authors gratefully acknowledge all Applied Chemistry Program and Industrial Chemistry Innovation Program staff, Faculty of Science, Maejo University, for supporting the facilities.

Author Contributions: Conceptualization, S.N.; methodology, S.R. and D.P.; software, N.S..; validation, S.R.. and S.N.; formal analysis, S.R.., D.P., and N.S.; investigation, S.R..; resources, S.N..; data curation, S.N.; writing—original draft preparation, S.R.; writing—review and editing, S.N.; visualization, S.N.; supervision, S.N.; project administration, S.N.; funding acquisition, S.N. All authors have read and agreed to the published version of the manuscript.

Funding: The authors are grateful for the financial support from Maejo University's Disciple Scholarship. The financial support from the Thailand Research Fund (TRF) under the International Research Network: Functional Porous Materials for Catalysis and Adsorption (Grant no. IRN61W0003) is acknowledged.

Conflicts of Interest: The authors declare no conflict of interest.

References

[1] Tiwari, H.; Tripathi, P.; Sonwani, R. K.; Singh, R. S. A synergistic approach combining Adsorption and Biodegradation for effective treatment of acid Blue 113 dye by Klebsiella grimontii entrapped Graphene Oxide-Calcium Alginate Hydrogel Beads. *Bioresource Technology*. **2023**, *387*, 129614. https://doi.org/10.1016/j.biortech.2023.129614

[2] Tiwari, H.; Sonwani, R.; Singh, R. S. Biodegradation and detoxification study of triphenylmethane dye (Brilliant Green) in a recirculating packed-bed bioreactor by bacterial consortium. *Environmental Technology*. **2022**, 1-42. https://doi.org/10.1080/09593330.2022.2131469

[3] Sukhdev, A.; Latha, V.; Bhaskar, P.; Deepthi, P. R.; Kumar, P. M.; Manjunatha, A. S. Use of Cu(II) catalyst assisted oxidative decolorization of dye by chlorinating species in water: A kinetic and mechanistic study with acid red1 dye. *Applied Surface Science Advances*. **2023**, *16*, 100435. https://doi.org/10.1016/j.apsadv.2023.100435

[4] Januário, E. F. D.; Vidovix, T. B.; Bergamasco, R.; Vieira, A. M. S. Performance of a hybrid coagulation/flocculation process followed by modified microfiltration membranes for the removal of solophenyl blue dye. *Chemical Engineering and Processing - Process Intensification*. **2021**, *168*, 108577. https://doi.org/10.1016/j.cep.2021.108577

[5] Zhao, R.; Jin, P.; Zhu, J.; Li, Y.; Li, G.; Volodine, A.; Liu, Y.; Zheng, J.; Van der Bruggen, B. Amino acid-based loose polyamide nanofiltration membrane with ultrahigh water permeance for efficient dye/salt separation. *Journal of Membrane Science*. **2023**, *673*, 121477. https://doi.org/10.1016/j.memsci.2023.121477

[6] Shi, Y.; Chang, Q.; Zhang, T.; Song, G.; Sun, Y.; Ding, G. A review on selective dye adsorption by different mechanisms. *Journal of Environmental Chemical Engineering*. **2022**, *10*(6), 108639. https://doi.org/10.1016/j.jece.2022.108639

[7] Anbia, M.; Lashgari, M. Synthesis of amino-modified ordered mesoporous silica as a new nano sorbent for the removal of chlorophenols from aqueous media. *Chemical Engineering Journal*. **2009**, *150*(2), 555-560. https://doi.org/10.1016/j.cej.2009.02.023

[8] Sağlam, S.; Türk, F. N.; Arslanoğlu, H. Use and applications of metal-organic frameworks (MOF) in dye adsorption: Review. *Journal of Environmental Chemical Engineering*. **2023**, *11*(5), 110568. https://doi.org/10.1016/j.jece.2023.110568

[9] Kiwaan, H. A.; Mohamed, F. S.; El-Ghamaz, N. A.; Beshry, N. M.; El-Bindary, A. A. Experimental and electrical studies of Na-X zeolite for the adsorption of different dyes. *Journal of Molecular Liquids.* **2021**, *332*, 115877. https://doi.org/10.1016/j.molliq.2021.115877

[10] Boukoussa, B.; Mokhtar, A.; El Guerdaoui, A.; Hachemaoui, M.; Ouachtak, H.; Abdelkrim, S.; Addi, A. A.; Babou, S.; Boudina, B.; Bengueddach, A.; Hamacha, R. Adsorption behavior of cationic dye on mesoporous silica SBA-15 carried by calcium alginate beads: Experimental and molecular dynamics study. *Journal of Molecular Liquids*. **2021**, *333*, 115976. https://doi.org/10.1016/j.molliq.2021.115976

[11] Imyim, A.; Prapalimrungsi, E. Humic acids removal from water by aminopropyl functionalized rice husk ash. *J Hazard Mater.* **2010**, *184*(1-3), 775-781. https://doi.org/10.1016/j.jhazmat.2010.08.108

[12] Hossain, N.; Nizamuddin, S.; Ball, A. S.; Shah, K. Synthesis, performance and reaction mechanisms of Ag-modified multi-functional rice husk solvochar for removal of multi-heavy metals and water-borne bacteria from wastewater. *Process Safety and Environmental Protection*. **2024**, *182*, 56-70. https://doi.org/10.1016/j.psep.2023.11.058

[13] Haider, J. B.; Haque, M. I.; Hoque, M.; Hossen, M. M.; Mottakin, M.; Khaleque, M. A.; Johir, M. A. H.; Zhou, J. L.; Ahmed, M. B.; Zargar, M. Efficient extraction of silica from openly burned rice husk ash as adsorbent for dye removal. *Journal of Cleaner Production*. **2022**, *380*, 135121. https://doi.org/10.1016/j.jclepro.2022.135121

[14] Aguado, J.; Arsuaga, J. M.; Arencibia, A.; Lindo, M.; Gascón, V. Aqueous heavy metals removal by adsorption on amine-functionalized mesoporous silica. *J Hazard Mater*. **2009**, *163*(1), 213-221. https://doi.org/10.1016/j.jhazmat.2008.06.080

[15] Chandrashekar Kollarahithlu, S.; Balakrishnan, R. M. Adsorption of pharmaceuticals pollutants, Ibuprofen, Acetaminophen, and Streptomycin from the aqueous phase using amine functionalized superparamagnetic silica nanocomposite. *Journal of Cleaner Production*. **2021**, *294*, 126155. https://doi.org/10.1016/j.jclepro.2021.126155

[16] Abu Rumman, G.; Al-Musawi, T. J.; Sillanpaa, M.; Balarak, D. Adsorption performance of an amine-functionalized MCM–41 mesoporous silica nanoparticle system for ciprofloxacin removal. *Environmental Nanotechnology, Monitoring & Management*. **2021**, *16*, 100536. https://doi.org/10.1016/j.enmm.2021.100536

[17] Beagan, A.; Alotaibi, K.; Almakhlafi, M.; Algarabli, W.; Alajmi, N.; Alanazi, M.; Alwaalah, H.; Alharbi, F.; Alshammari, R.; Alswieleh, A. Amine and sulfonic acid functionalized mesoporous silica as an effective adsorbent for removal of methylene blue from contaminated water. *Journal of King Saud University – Science*. **2022**, *34*(2), 101762. https://doi.org/10.1016/j.jksus.2021.101762

[18] Anbia, M.; Salehi, S. (2012). Removal of acid dyes from aqueous media by adsorption onto amino-functionalized nanoporous silica SBA-3. *Dyes and Pigments*. **2012**, *94*(1), 1-9. https://doi.org/10.1016/j.dyepig.2011.10.016

ASEAN
Journal of Scientific and Technological Reports
Online ISSN:2773-8752

ASEAN
Journal of Scientific and Technological Reports
Online ISSN: 2773-8752

Article type

Type of the Paper (Article, Review, Communication, etc.) *about 8,000 words maximum*

Title (Palatino Linotype 18 pt, bold)

Firstname Lastname[1], Firstname Lastname[2] and Firstname Lastname[2*]

[1] Affiliation 1; e-mail@e-mail.com
[2] Affiliation 2; e-mail@e-mail.com
* Correspondence: e-mail@e-mail.com; (one corresponding authors, add author initials)

Citation:
Lastname, F.; Lastname, F.; Lastname, F. Title. *ASEAN J. Sci. Tech. Report.* **2023**, *26*(X), xx-xx. https://doi.org/10.55164/ajstr.vxxix.xxxxxx

Article history:
Received: date
Revised: date
Accepted: date
Available online: date

Abstract: A single paragraph of about 400 words maximum. Self-contained and concisely describe the reason for the work, methodology, results, and conclusions. Uncommon abbreviations should be spelled out at first use. We strongly encourage authors to use the following style of structured abstracts, but without headings: (1) Background: Place the question addressed in a broad context and highlight the purpose of the study; (2) Methods: briefly describe the main methods or treatments applied; (3) Results: summarize the article's main findings; (4) Conclusions: indicate the main conclusions or interpretations.

Keywords: keyword 1; keyword 2; keyword 3 (List three to ten pertinent keywords specific to the article yet reasonably common within the subject discipline.)

1. Introduction

The introduction should briefly place the study in a broad context and highlight why it is crucial. It should define the purpose of the work and its significance. The current state of the research field should be carefully reviewed and critical publications cited. Please highlight controversial and diverging hypotheses when necessary. Finally, briefly mention the main aim of the work. References should be numbered in order of appearance and indicated by a numeral or numerals in square brackets—e.g., [1] or [2, 3], or [4-6]. See the end of the document for further details on references.

2. Materials and Methods

The materials and methods should be described with sufficient details to allow others to replicate and build on the published results. Please note that your manuscript's publication implicates that you must make all materials, data, computer code, and protocols associated with the publication available to readers. Please disclose at the submission stage any restrictions on the availability of materials or information. New methods and protocols should be described in detail, while well-established methods can be briefly described and appropriately cited.

Interventional studies involving animals or humans, and other studies that require ethical approval, must list the authority that provided approval and the corresponding ethical approval code.

2.1 Subsection

2.1.1. Subsubsection

3. Results and Discussion

This section may be divided by subheadings. It should provide a concise and precise description of the experimental results, their interpretation, as well as the experimental conclusions that can be drawn.Authors should discuss the results and how they can be interpreted from previous studies and the working hypotheses. The findings and their implications should be discussed in the broadest context possible. Future research directions may also be highlighted.

3.1. Subsection

3.1.1. Subsubsection

3.2. Figures, Tables, and Schemes

All figures and tables should be cited in the main text as Figure 1, Table 1, etc.

Figure 1. This is a figure. Schemes follow the same formatting.

Table 1. This is a table. Tables should be placed in the main text near the first time they are cited.

Title 1	Title 2	Title 3
entry 1	data	data
entry 2	data	data [1]

[1] Table may have a footer.

3.3. Formatting of Mathematical Components

This is example 1 of an equation:

$$a = 1, \tag{1}$$

The text following an equation need not be a new paragraph. Please punctuate equations as regular text. This is example 2 of an equation:

$$a = b + c + d + e + f + g + h + i + j + k + l + m + n + o + p + q + r + s + t + u \tag{2}$$

The text following an equation need not be a new paragraph. Please punctuate equations as regular text. The text continues here.

4. Conclusions

Concisely restate the hypothesis and most important findings. Summarize the significant findings, contributions to existing knowledge, and limitations. What are the future directions? Conclusions MUST be well stated, linked to original research question & limited to supporting results.

5. Acknowledgements

Should not be used to acknowledge funders – funding will be entered as a separate. As a matter of courtesy, we suggest you inform anyone whom you acknowledge.

Author Contributions: For research articles with several authors, a short paragraph specifying their individual contributions must be provided. The following statements should be used "Conceptualization, X.X. and Y.Y.; methodology, X.X.; software, X.X.; validation, X.X., Y.Y. and Z.Z.; formal analysis, X.X.; investigation, X.X.; resources, X.X.; data curation, X.X.; writing—original draft preparation, X.X.; writing—review and editing, X.X.; visualization, X.X.; supervision, X.X.; project administration, X.X.; funding acquisition, Y.Y. All authors have read and agreed to the published version of the manuscript." Please turn to the CRediT taxonomy for the term explanation. Authorship must be limited to those who have contributed substantially to the work reported.

Funding: Please add: "This research received no external funding" or "This research was funded by NAME OF FUNDER, grant number XXX" and "The APC was funded by XXX". Check carefully that the details given are accurate and use the standard spelling of funding agency names at https://search.crossref.org/funding. Any errors may affect your future funding.

Conflicts of Interest: Declare conflicts of interest or state "The authors declare no conflict of interest." Authors must identify and declare any personal circumstances or interest that may be perceived as inappropriately influencing the representation or interpretation of reported research results. Any role of the funders in the design of the study; in the collection, analyses or interpretation of data; in the writing of the manuscript, or in the decision to publish the results must be declared in this section. If there is no role, please state "The funders had no role in the design of the study; in the collection, analyses, or interpretation of data; in the writing of the manuscript, or in the decision to publish the results".

References

References must be numbered in order of appearance in the text (including citations in tables and legends) and listed individually at the end of the manuscript. We recommend preparing the references with a bibliography software package, such as EndNote, ReferenceManager to avoid typing mistakes and duplicated references. Include the digital object identifier (DOI) for all references where available.

Citations and references in the Supplementary Materials are permitted provided that they also appear in the reference list here.

In the text, reference numbers should be placed in square brackets [ ] and placed before the punctuation; for example [1], [1–3] or [1, 3]. For embedded citations in the text with pagination, use both parentheses and brackets to indicate the reference number and page numbers; for example [5] (p. 100), or [6] (pp. 101–105).

Using the American Chemical Society (ACS) referencing style

[1] Author 1, A.B.; Author 2, C.D. Title of the article. *Abbreviated Journal Name* Year, *Volume*, page range.

[2] Author 1, A.; Author 2, B. Title of the chapter. In *Book Title*, 2nd ed.; Editor 1, A., Editor 2, B., Eds.; Publisher: Publisher Location, Country. **2007**, Volume *3*, pp. 154–196.

[3] Author 1, A.; Author 2, B. *Book Title*, 3rd ed.; Publisher: Publisher Location, Country, **2008**, pp. 154–196.
[4] Author 1, A.B.; Author 2, C. Title of Unpublished Work. *Abbreviated Journal Name* stage of publication (under review; accepted; in press).
[5] Author 1, A.B. (University, City, State, Country); Author 2, C. (Institute, City, State, Country). Personal communication, 2012.
[6] Author 1, A.B.; Author 2, C.D.; Author 3, E.F. Title of Presentation. In Title of the Collected Work (if available), Proceedings of the Name of the Conference, Location of Conference, Country, Date of Conference; Editor 1, Editor 2, Eds. (if available); Publisher: City, Country, Year (if available); Abstract Number (optional), Pagination (optional).
[7] Author 1, A.B. Title of Thesis. Level of Thesis, Degree-Granting University, Location of University, Date of Completion.
[8] Title of Site. Available online: URL (accessed on Day Month Year).

Reviewers sugestion

1. Name, Address, e-mail
2. Name, Address, e-mail
3. Name, Address, e-mail
4. Name, Address, e-mail

URL link:

Notes for Authors >>
https://drive.google.com/file/d/1r0zegnIVeQqe4iLQyT1xDEIinNggINPD/view?usp=sharing
https://drive.google.com/file/d/1r0zegnIVeQqe4iLQyT1xDEIinNggINPD/view?usp=sharing

Online Submissions >> https://ph02.tci-thaijo.org/index.php/tsujournal/user/register

Current Issue >> https://ph02.tci-thaijo.org/index.php/tsujournal/issue/view/16516

AJSTR Publication Ethics and Malpractice >> https://ph02.tci-thaijo.org/index.php/tsujournal/ethics

Journal Title Abbreviations >> http://library.caltech.edu/reference/abbreviations

ASEAN
Journal of Scientific and Technological Reports
Online ISSN:2773-8752

ASEAN
Journal of Scientific and Technological Reports
Online ISSN:2773-8752

ASEAN Journal of Scientific and Technological Reports (AJSTR)
Institute of Research and Innovation, Thaksin University, Phatthalung Campus
222 Moo. 2, Baan Prao Sub-District, Papayom District, Phatthalung, 93210, Thailand
Tel. +668 1540 7304